



# From Probes to Therapeutics: Chemical Biology Studies of Anaplastic Lymphoma Kinase (ALK) and Cereblon

## Citation

Powell, Chelsea Elizabeth. 2020. From Probes to Therapeutics: Chemical Biology Studies of Anaplastic Lymphoma Kinase (ALK) and Cereblon. Doctoral dissertation, Harvard University, Graduate School of Arts & Sciences.

## Permanent link

<https://nrs.harvard.edu/URN-3:HUL.INSTREPOS:37365125>

## Terms of Use

This article was downloaded from Harvard University's DASH repository, and is made available under the terms and conditions applicable to Other Posted Material, as set forth at <http://nrs.harvard.edu/urn-3:HUL.InstRepos:dash.current.terms-of-use#LAA>

## Share Your Story

The Harvard community has made this article openly available. Please share how this access benefits you. [Submit a story](#).

[Accessibility](#)

**From Probes to Therapeutics:  
Chemical Biology Studies of Anaplastic Lymphoma Kinase  
(ALK) and Cereblon**

A dissertation presented

by

**Chelsea Elizabeth Powell**

to

The Committee on Higher Degrees in Chemical Biology

in partial fulfillment of the requirements

for the degree of

Doctor of Philosophy

in the subject of

Chemical Biology

Harvard University

Cambridge, Massachusetts

September 2019

© 2019 Chelsea Elizabeth Powell  
All rights reserved.

## From Probes to Therapeutics: Chemical Biology Studies of Anaplastic Lymphoma Kinase (ALK) and Cereblon

### Abstract

Although there is still discussion surrounding the exact definition of the field, chemical biology is generally described as the development and deployment of a chemical toolbox to manipulate biological systems. The two major overlapping categories that define these chemical tools are probes and drugs.

The rapid development of the field of chemical biology has contributed to the boom in the use of small molecule kinase inhibitors as targeted cancer therapies. **Chapters 2** and **3** discuss the development of new classes of compounds that target anaplastic lymphoma kinase (ALK), a clinically relevant lung cancer target, that may provide ways of overcoming tumor resistance, either on their own or through combination therapies with previous ALK inhibitors. **Chapter 2** describes published work on the development of the first small molecule degraders that can chemically induce ALK degradation, including in non-small-cell lung cancer (NSCLC), anaplastic large-cell lymphoma (ALCL), and neuroblastoma (NB) cell lines (Powell *et al.*, *J Med Chem* 2018). These degraders were developed through conjugation of known pyrimidine-based ALK inhibitors, TAE684 or LDK378, and the cereblon (CRBN) ligand pomalidomide. **Chapter 3** describes the identification of a potential allosteric ALK inhibitor, which would be the first compound that targets ALK through this mechanism of action. Initial profiling of this compound was promising and indicates that further screening against the theorized allosteric pocket should be performed. Both **Chapters 2** and **3** provide proof of concept that a new class of compounds may be used to therapeutically target ALK-positive cancers.

**Chapters 4 and 5** discuss studies around the biology of the CRBN E3 ligase, the E3 ligase recruited by the ALK degraders described in **Chapter 2**. **Chapter 4** describes a screening strategy for identifying novel CRBN modulators that can induce protein degradation. We generated a thalidomide analog library by introducing kinase inhibitor scaffolds to lenalidomide and screened the library in MM1.s cells for CRBN dependent antiproliferative activity. Through this method we identified 5 hit compounds that can selectively induce the degradation of GSPT1, a previously identified target of CRBN modulators. **Chapter 5** describes the use of small molecule degraders to induce CRBN degradation. We compared degraders that recruited CRBN to itself to degraders that recruited the von-Hippel Lindau (VHL) E3 ligase to CRBN. We determined that a higher degree of selective and potent CRBN degradation could be achieved by recruiting VHL. We present lead selective CRBN degraders, ZXH-4-130 and ZXH-4-137, that may be used as probes to better understand endogenous CRBN biology.

**Chapters 6 and 7** describe kinase inhibitor studies around additional therapeutically relevant targets: dual-specificity tyrosine-(Y)-phosphorylation regulated kinase 1A (DYRK1A) and tyrosine kinase nonreceptor 2 (TNK2, also known as ACK1), respectively. **Chapter 6** describes the identification of the first macrocyclic inhibitors of DYRK1A and **Chapter 7** describes high-throughput efforts to optimize lead TNK2 inhibitors from the benzopyrimidodiazepinone scaffold.

Overall, this work fits squarely under the umbrella of chemical biology by demonstrating the development of small molecules as inhibitors, degraders, and modulators for both therapeutic and probe purposes.

# Table of Contents

<i>Title Page</i> .....	<i>i</i>
<i>Copyright Page</i> .....	<i>ii</i>
<i>Abstract</i> .....	<i>iii</i>
<i>Table of Contents</i> .....	<i>v</i>
<i>List of Figures and Tables</i> .....	<i>vii</i>
<i>Abbreviations</i> .....	<i>ix</i>
<i>Acknowledgements</i> .....	<i>xi</i>
<b>Chapter 1: Introduction</b> .....	<b>1</b>
1.1 Chemical Biology: Probes to Therapeutics.....	2
1.2 Kinase Inhibitors and Cancer .....	3
1.3 Anaplastic Lymphoma Kinase (ALK) Positive Cancer .....	6
1.4 Small Molecule Degraders .....	7
1.5 Chemical Biology Studies of ALK and CRBN .....	10
References.....	11
<b>Chapter 2: Chemically Induced Degradation of Anaplastic Lymphoma Kinase (ALK)</b> .....	<b>16</b>
Attributions.....	17
Abstract .....	19
2.1 Introduction .....	20
2.2 Results and Discussion .....	21
2.3 Conclusion .....	35
2.4 Alectinib-Based ALK Degraders.....	36
2.5 Experimental Methods.....	40
References.....	53
<b>Chapter 3: Discovery and Profiling of Allosteric ALK Inhibitors</b> .....	<b>57</b>
Abstract .....	59
3.1 Introduction .....	60
3.2 Results and Discussion .....	62
3.3 Conclusions .....	66
3.4 Experimental Methods.....	67
References.....	69
<b>Chapter 4: Selective Degradation of GSPT1 by Novel Cereblon Modulators Generated from Kinase Inhibitor Scaffolds</b> .....	<b>72</b>

Attributions.....	73
Abstract .....	75
4.1 Introduction .....	76
4.2 Results and Discussion .....	78
4.4 Experimental Methods.....	85
References.....	112
<b>Chapter 5: Chemically Induced Cereblon (CRBN) Degradation: Efficacy of Recruiting CRBN in Comparison to VHL.....</b>	<b>114</b>
Attributions.....	115
Abstract .....	117
5.1 Introduction .....	118
5.2 Results and Discussion .....	119
5.3 Conclusion .....	127
5.4 Experimental Methods.....	128
References.....	146
<b>Chapter 6: Novel Macrocyclic Inhibitors of DYRK1A.....</b>	<b>149</b>
Attributions.....	150
Abstract .....	152
6.1 Introduction .....	153
6.2 Results and Discussion .....	154
6.3 Conclusion .....	159
6.4 Experimental Methods.....	160
References.....	177
<b>Chapter 7: Benzopyrimidodiazepinone Inhibitors of TNK2.....</b>	<b>179</b>
Attributions.....	180
Abstract .....	182
7.1 Introduction .....	183
7.2 Results and Discussion .....	184
7.3 Conclusion .....	192
7.4 Experimental Methods.....	193
References.....	202
<b>Chapter 8: Conclusions and Future Directions .....</b>	<b>205</b>

# List of Figures and Tables

## Figures

<b>Figure 1.1.</b> Kinases catalyze the phosphorylation of a substrate.....	3
<b>Figure 2.1.</b> Chemical structures and characterization of ALK degraders.....	22
<b>Figure 2.2.</b> Anti-proliferative best fit EC <sub>50</sub> values in NSCLC and ALCL lines .....	23
<b>Figure 2.3.</b> Degradation behavior in H3122 and Karpas 299 cells.....	24
<b>Figure 2.4.</b> Anti-proliferative best fit EC <sub>50</sub> values in NB lines .....	26
<b>Figure 2.5.</b> Recovery of degradation activity after shRNA knockdown of ABCB1.....	27
<b>Figure 2.6.</b> Degradation behavior in Kelly and CHLA20 cells.....	28
<b>Figure 2.7.</b> Expression proteomics in Kelly cells.....	30
<b>Figure 2.8.</b> Proteomics hits dose response: Immunoblots .....	31
<b>Figure 2.9.</b> Proteomics hits time courses: Immunoblots .....	31
<b>Figure 2.10.</b> Anti-proliferative best fit EC <sub>50</sub> values in Ba/F3 lines.....	32
<b>Figure 2.11.</b> Structures of alectinib and JH-VIII-157-02.....	36
<b>Figure 2.12.</b> 200 series degradation behavior.....	37
<b>Figure 2.13.</b> 114 series degradation behavior.....	38
<b>Figure 2.14.</b> JH-XIV-61 degradation behavior .....	39
<b>Figure 3.1.</b> Structural similarity of EGFR and ALK.....	62
<b>Figure 3.2.</b> TR-FRET assay for detecting ALK activity.....	63
<b>Figure 3.3.</b> Biochemical Activity of Screening Hit JBJ-02-017-04.....	64
<b>Figure 3.4.</b> Initial medicinal chemistry efforts .....	65
<b>Figure 3.5.</b> Molecular modeling of JBJ-02-017-04 with ALK.....	66
<b>Figure 4.1.</b> Workflow for identifying new CRBN modulators.....	78
<b>Figure 4.2.</b> Hit compounds from cereblon dependent antiproliferative activity screening and their degradative activity of known cereblon modulator targets.....	81
<b>Figure 4.3.</b> Expression proteomics in MM1.S cells after treatment with <b>29</b> .....	82
<b>Figure 4.4.</b> Expression proteomics in MM1.S cells after treatment with <b>2</b> or <b>51</b> .....	82
<b>Figure 4.5.</b> Molecular modeling of <b>26</b> identifies that the nitrogens in the pyrimidine ring are critical for GSPT1 degradation.....	84
<b>Figure 5.1.</b> Pomalidomide CRBN-CRBN degradation behavior in MM1.s cells.....	120
<b>Figure 5.2.</b> Expression proteomics in MM1.S cells after treatment <b>ZXH-3-159</b> .....	121
<b>Figure 5.3.</b> Tricyclic thalidomide analog CRBN-CRBN degradation behavior in MM1.s cells.....	121
<b>Figure 5.4.</b> Thalidomide-VHL ligand based CRBN-VHL degradation behavior in MM1.s cells .....	123

<b>Figure 5.5.</b> Expression proteomics in MM1.S cells after treatment with pomalidomide, <b>ZXH-4-130</b> , or <b>ZXH-4-137</b> .....	124
<b>Figure 5.6.</b> Comparison of lead CRBN degraders to <b>St-15a</b> .....	125
<b>Figure 5.7.</b> CRBN degraders as probes.....	127
<b>Figure 6.1.</b> Structures of harmine and CX-4945. ....	153
<b>Figure 6.2.</b> Biochemical kinase profiling.....	156
<b>Figure 6.3.</b> Cellular kinase profiling.....	157
<b>Figure 6.4.</b> Antiproliferative activity in HNSCC cell lines.....	158
<b>Figure 6.5.</b> Apoptosis and colony formation in CAL27 cells.....	159
<b>Figure 7.1.</b> Benzopyrimidodiazepinone kinase inhibitors .....	183
<b>Figure 7.2.</b> DiscoverX KinomeScan Treespot interaction maps.....	185
<b>Figure 7.3.</b> Metabolite identification after incubation in mouse liver microsomes. ....	191
<b>Figure 7.4.</b> Antiproliferation IC <sub>50</sub> curves in TNK2 D163E expressing Ba/F3 cells .....	193

## Tables

<b>Table 1.1.</b> 51 FDA approved kinase inhibitors as of August 2019. ....	5
<b>Table 2.1.</b> ALK activity assay IC <sub>50</sub> values.....	23
<b>Table 2.2.</b> Z'LYTE assay IC <sub>50</sub> s (nM).....	32
<b>Table 2.3.</b> Pharmacokinetic data for compound <b>9</b> .....	34
<b>Table 2.4.</b> Pharmacokinetic data for compound <b>11</b> .....	35
<b>Table 3.1.</b> SelectScreen profiling IC <sub>50</sub> s (nM). ....	64
<b>Table 4.1.</b> IC <sub>50</sub> (μM) values of thalidomide analogs .....	79
<b>Table 6.1.</b> Antiproliferative IC <sub>50</sub> values (μM).....	158
<b>Table 7.1.</b> Enzyme and cell data for examples with phenyl substituents. ....	187
<b>Table 7.2.</b> Enzyme and cell data for aniline SAR. ....	188
<b>Table 7.3.</b> Enzyme and cell data for aniline SAR and aniline replacements. ....	189
<b>Table 7.4.</b> Mouse microsome and hepatocyte stability, and <i>in vivo</i> mouse PK data.....	191
<b>Table 7.5.</b> Compound characterization.....	194

## Abbreviations

**ABCB1:** ATP-binding cassette subfamily B member 1

**ALCL:** Anaplastic large-cell lymphoma

**ALK:** Anaplastic lymphoma kinase

**AML:** Acute myeloid leukemia or acute myelogenous leukemia

**ATP:** Adenosine triphosphate

**CK1 $\alpha$ :** Casein kinase 1A1

**CRBN:** Cereblon

**CUL4A:** Cullin-4A

**DDB1:** Damaged DNA binding protein 1

**DMSO:** Dimethyl sulfoxide

**DYRK1A:** Dual-specificity tyrosine phosphorylation-regulated kinase 1A

**EGFR:** Epidermal growth factor receptor

**EML4:** Echinoderm microtubule-associated protein-like 4

**GSPT1:** G1 to S phase transition protein 1

**HNSCC:** Head and neck squamous cell carcinoma

**IKZF1:** Ikaros

**IKZF3:** Aiolos

**IMiDs:** Immunomodulatory drugs

**NB:** Neuroblastoma

**NPM:** Nucleoplasmin

**NSCLC:** Non-small-cell lung cancer

**PROTAC:** Proteolysis targeting chimera

**RBX1:** RING-box protein 1

**ROC1:** RING-box protein 1

**TNK2:** Tyrosine kinase nonreceptor 2

**TR-FRET:** Time-resolved fluorescence energy transfer

**VHL:** von Hippel-Lindau

## **Acknowledgements**

I would like to thank Nathanael Gray for his mentorship and support throughout my graduate education. Thank you for the opportunity to gain the skills and knowledge needed to continue working in this exciting field. I would also like to thank the members of my dissertation advising committee: Michael Eck, Pasi Jänne, and Ralph Mazitschek. Thank you for all of your feedback throughout the years and for demonstrating the value of collaboration in science. I hope to follow your strong example.

I would like to thank all of my scientific mentors leading up to my dissertation. I will start with the Independent Science Research Program at The Spence School run by Scott Godsen. It was invaluable to be exposed to real bench work at such a young age and I will forever be grateful. I would like to thank my first lab, Michael Ward's lab at NYU, for the opportunity to work there during high school. I would especially like to thank my mentor at NYU, Zhihua An, for all of her encouragement as I left for college. I would like to thank my undergraduate lab experiences: Geoffrey Abbott's lab at Weill Cornell Medical College and Matthew Bogyo's lab at Stanford. I would especially like to thank Montse Morell for being a wonderful mentor and friend as I worked towards graduate school.

The Gray lab has been a wonderful environment for pursuing a PhD. I would like to thank everyone for being such great collaborators and colleagues. I would especially like to thank Yang Gao, Hubert Huang, Eric Wang, and Fleur Ferguson for their mentorship as I wrote my first independent grants and papers. I would like to thank the graduate students of the Gray lab for being such a wonderful source of support and friendship: Liv Johannessen, Hubert Huang, Carmen Sivakumaren, Benika Pinch, Zainab Doctor, Theresa Manz, Lara Gechijian, Dennis Dobrovolsky, Inchul You, and Anthony Ayala. I would like to give a special thank you to Benika Pinch for being a valued friend and partner in crime throughout graduate school. Chelsika is heading out into the world!

I would like to thank the Chemical Biology Programs at Harvard and DFCI as well as the Therapeutics Program. Thank you to Dan Kahne, Suzzane Walker, Jason Milberg, Catherine Dubreuil, and Milka Kostic. Thank you as well to Rebecca Clements for being my internship buddy.

Thank you to the sketch comedy community at ImprovBoston, especially Emmy Serviss and all of Mister Bismuth. Making people laugh with you has given me a wonderful creative outlet that has allowed me to be a better scientist and person.

Thank you to all of my chemical biology-plus friends. A special thank you to Doug Kenny for being my Broadway buddy and an amazing friend. Thank you to the rest of the adventuring party: Zack Hauseman, Julie Zar, and Bruce Hua. And to everyone else who completes our crazy group: Jessica Spinelli, Jake Nagy, Eric Fujimura, Holly Rees, Freddy Valencia, and Nathan Schauer.

Thank you to my amazing friends from home who have been with me forever: Jessica Bendes, Anne Hilburn, and Sonam Choedon. I am so incredibly lucky to have you all in my life. Thank you especially to Jessica Bendes for every late-night call and FaceTime that was ever needed to get where we are today. Look at all we've done!

Thank you to all of my extended family for your constant support.

And most of all thank you to my parents, Greg and Paula Powell, my brother Brian Powell, and our furry family, Hudson and Sara. Without all of your support, encouragement, and most importantly love, I would not be here today. You mean the world and stars to me.

## **Chapter 1: Introduction**

## 1.1 Chemical Biology: Probes to Therapeutics

Chemical biology is a rapidly developing and young field. As such there is still much discussion surrounding its exact definition.<sup>1,2</sup> While the journal *Nature Chemical Biology* defines chemical biology as a field that combines “scientific ideas and approaches of chemistry, biology and allied disciplines to understand and manipulate biological systems with molecular precision” under the Aims & Scope of their journal, *Cell Chemical Biology* uses a broader definition of “investigations done at the interface of chemistry and biology.” However, *Cell Chemical Biology* does go on to state that they are especially interested in the “use of chemical tools to perturb, visualize, and measure biological systems and properties and offer unique insights into molecular mechanism or physiology.”

From these two publications’ efforts to define their material, we can see some common themes that we may use to generalize the field: chemical biology is the development and deployment of a chemical toolbox to manipulate biological systems. This manipulation may be used in order to better understand the endogenous functions of biology, to develop therapeutics, or some combination of the two.

The central dogma of biology describes the flow of information from DNA to RNA to proteins. It has been suggested that the small molecules that make up the chemical biologist’s toolbox present a fourth missing source of information.<sup>3</sup> Small molecules are essential for biological signaling and by understanding their endogenous functions as well as their use as probes and therapeutics we may begin to have a more complete picture of how biology functions as a whole, complex system.

As has been suggested by the writing so far, probes and drugs are two major overlapping categories for defining the chemical biologist’s toolbox. As such, chemical biology very naturally leads to drug discovery and the development of lead therapeutic compounds. One specific type of drug discovery that has blossomed over the past two decades alongside the rapid development of chemical biology is the development of kinase inhibitors.

## 1.2 Kinase Inhibitors and Cancer

Kinases are enzymes that catalyze the transfer of a phosphoryl group from adenosine triphosphate (ATP) to a substrate (Figure 1.1). Kinases primarily catalyze the phosphorylation of serine, threonine, or tyrosine residues on a protein substrate. As a post-translational modification, phosphorylation can alter the structural conformation of a protein, which in turn can activate or deactivate a protein. In addition, phosphorylation can affect cellular localization, protein-protein interaction, and the rate at which a protein is degraded.<sup>4</sup> Kinases have complementary enzymes in the cell, phosphatases, that can dephosphorylate proteins, making all of the effects of phosphorylation reversible.

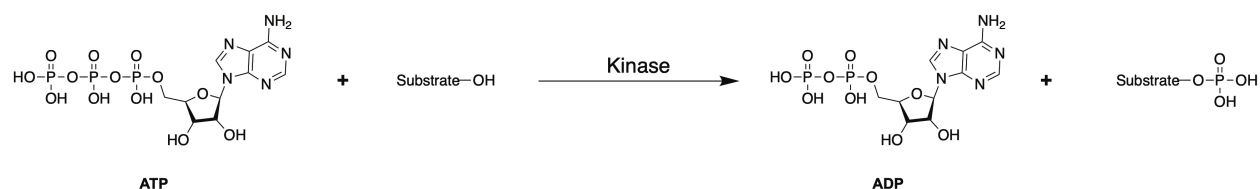


**Figure 1.1.** Kinases catalyze the phosphorylation of a substrate.

Since protein kinase activity was first observed in 1954, kinases have been shown to play an essential role in cell signaling and to be critical for many cellular processes, including metabolism, transcription, cell cycle progression, cell movement, differentiation, and apoptosis.<sup>5,6</sup> Mutations and dysregulation of kinases play causal roles in human disease, including cancer as well as immunological, neurological, metabolic, and infectious diseases.<sup>5,7</sup> The potential for therapeutic intervention has driven the development of small molecule kinase inhibitors. The development of these inhibitors has been particularly impactful in the field of oncology.

Cancer therapy has been revolutionized over the past decade by the ability to treat patients based on genetic mutations specific to their tumor type. Unlike chemotherapies, targeted therapies have a high specificity towards tumor cells, resulting in fewer side effects and a more

predictable clinical response.<sup>8</sup> The large majority of targeted therapies are small molecule kinase inhibitors. Oncogenic kinases that are activated by mutations are attractive targets for cancer therapies because they play essential roles in regulating tumor cell proliferation and survival; this is often referred to as the tumor cells being “addicted” to the oncogenic protein.<sup>7</sup>

The first FDA approved small molecule kinase inhibitor was imatinib (Gleevec), which was approved for the treatment of patients with chronic myelogenous leukemia (CML) that expresses constitutively active breakpoint cluster region-Abelson tyrosine kinase (BCR-ABL) fusion protein.<sup>9</sup> Since this first approval in 2001, the discovery and subsequent approval of small molecule kinase inhibitors has increased rapidly, with 9 new small molecule kinase inhibitors gaining approval last year (2018) and 3 new inhibitors approved this year so far (<http://www.brimr.org/PKI/PKIs.htm>). There are currently 51 approved kinase inhibitors (Table 1.1). Of those 51 kinase inhibitors about 86% are approved as cancer therapeutics.

Kinase inhibitors are categorized into 4 types that describe their binding mode and mechanism of action.<sup>7,10</sup> Type I inhibitors bind the ATP-site of the kinase in the active conformation and are ATP-competitive. The active conformation refers to a “DFG-in” state where the aspartic acid-phenylalanine-glycine (DFG) motif on the activation loop points into the ATP binding site, as well as an “ $\alpha$ C-helix-in” state where the  $\alpha$ C-helix is rotated inward toward the active site.<sup>7,11,12</sup> However, it should be noted that this conformation is not always sufficient for an active state, as a kinase may require additional regulatory elements outside of the kinase domain in order to be active. The majority of kinase inhibitors are type I, which may be due to the fact that many kinase inhibitors have been synthesized to mimic ATP and/or previous kinase inhibitors. Type II inhibitors bind the ATP-site of the kinase in an inactive “DFG-out” conformation, where the shifting of the activation loop exposes a hydrophobic allosteric binding pocket adjacent to the ATP-site. Type II inhibitors span the ATP-site and partially bind this exposed pocket. Type III kinase inhibitors bind allosteric sites outside of the ATP-binding pocket. Type IV inhibitors form an irreversible covalent bond with the kinase.

**Table 1.1.** 51 FDA approved kinase inhibitors as of August 2019. Adapted from the Blue Ridge Institute for Medical Research (<http://www.brimr.org/PKI/PKIs.htm>).

Inhibitor	Year Approved	Known Targets	Disease	Inhibitor	Year Approved	Known Targets	Disease
<b>Sirolimus</b> , Rapamycin	1999*	FKBP/mTOR	Renal transplant; lymphangio-leiomyomatosis	<b>Nintedanib</b> , Vargatef	2014	FGFR1/2/3, PDGFRα/β, VEGFR1/2/3, Flt3	Pulmonary fibrosis, idiopathic
<b>Imatinib</b> , Gleevec	2001	BCR-Abl, Kit, and PDGFR	CML and ALL, Ph <sup>+</sup> aggressive systemic masto-cytosis; CEL; DFSP; HES; GIST; MDS/MDP	<b>Alectinib</b> , CH5424802, Alecensa	2015	ALK and RET	NSCLC, ALK <sup>+</sup>
<b>Erlotinib</b> , Tarceva	2004	EGFR	NSCLC; pancreatic cancer	<b>Cobimetinib</b> , Cotellic	2015	MEK1/2	Melanoma with BRAF mutations together with vemurafenib
<b>Sorafenib</b> , Nexavar	2005	VEGFR1/2/3, B-C-Raf, mutant B-Raf, Kit, Flt3, RET, and PDGFRβ	Thyroid cancer, differen-tiated; hepato-cellular carcinoma; RCC	<b>Lenvatinib</b> , Lenvima	2015	VEGFR1/2/3, PDGFR, FGFR, Kit, RET	Different-iated thyroid cancer
<b>Dasatinib</b> , Sprycel	2006	BCR-Abl, EGFR, Src, Lck, Yes, Fyn, Kit, EphA2, PDGFRβ	CML	<b>Osimertinib</b> , Tagrisso	2015	EGFR T970M	NSCLC
<b>Sunitinib</b> , Sutent	2006	PDGFRα/β, VEGFR1/2/3, Kit, Flt3, CSF-1R, Axl, and RET	RCC; GIST; pancreatic neuro-endocrine tumors	<b>Palbociclib</b> , Ibrance	2015	CDK4/6	Breast cancer, ER <sup>+</sup> and HER2 <sup>+</sup>
<b>Lapatinib</b> , Tykerb	2007	ErbB2, EGFR	Breast cancer	<b>Abemaciclib</b> , Verzenio	2017	CDK4/6	Breast Ca
<b>Nilotinib</b> , Tasigna	2007	BCR-Abl, PDGFR, DDR1	CML, Ph <sup>+</sup>	<b>Acalabrutinib</b> , Calquence	2017	Bruton tyrosine kinase	Mantle cell lymphoma
<b>Temsirolimus</b> , Torisel	2007	FKBP12/mTOR	RCC	<b>Brigatinib</b> , Alunbrig	2017	ALK, ROS1, IGF-1R, Flt3, EGFR	NSCLC, ALK <sup>+</sup>
<b>Everolimus</b> , Afinitor	2009	FKBP12/mTOR	Breast cancer, HER2-negative; PNET; RCC; renal angio-myolipoma; sub-dependymal giant cell astro-cytoma	<b>Midostaurin</b> , Rydapt	2017	Flt3, PDGFR, VEGFR2, PKC	Acute myeloid leukemia, mastocytosis, mast cell leukemia
<b>Pazopanib</b> , Votrient	2009	VEGFR1/2/3, PDGFRα/β, FGFR1/3, Kit, Lck, Fms, Itk	RCC; soft tissue sarcomas	<b>Neratinib</b> , Nerlynx	2017	ErbB2/HER2	HER2 <sup>+</sup> breast cancer
<b>Crizotinib</b> , Xalkori	2011	ALK, MET (HGFR), ROS1, MST1R	NSCLC, ALK <sup>+</sup> or ROS1 <sup>+</sup>	<b>Ribociclib</b> , Kisqali	2017	CDK4/6	Breast cancer
<b>Ruxolitinib</b> , Jakafi	2011	JAK1/2	Myelo-fibrosis; poly-cythemia vera	<b>Baricitinib</b> , Olumiant	2018	JAK1/2	Reumatoid arthritis
<b>Vandetanib</b> , Zactima	2011	RET, EGFRs, VEGFRs, Brk, Tie2, EphRs, and Src family kinases	Thyroid cancer, medullary	<b>Binimetinib</b> , Mektovi	2018	MEK1/2	Melanoma
<b>Vemurafenib</b> , Zelboraf	2011	A/B/C-Raf and B-Raf (V600E)	Melanoma with the <i>BRAF</i> <sup>V600E</sup> mutation	<b>Dacomitinib</b> , Visimpro	2018	EGFR family	EGFR-mutant NSCLC
<b>Axitinib</b> , Inlyta	2012	VEGFR1/2/3, PDGFRβ	RCC	<b>Encorafenib</b> , Braftovi	2018	B-Raf	Melanoma
<b>Bosutinib</b> , BOSULIF	2012	BCR-Abl, Src, Lyn, and Hck	CML	<b>Fostamatinib</b> , Tavalisse	2018	Syk, Spleen tyrosine kinase	thrombo-cytopenia
<b>Cabozantinib</b> , Cometriq	2012	RET, MET, VEGFR1/2/3, Kit, TrkB, Flt3, Axl, Tie2	RCC, HCC, medullary thyroid cancer	<b>Gilteritinib</b> , Xospata	2018	Flt3	AML
<b>Ponatinib</b> , Iclusig	2012	BCR-Abl, BCR-Abl T3151, VEGFR, PDGFR, FGFR, EphR, Src family kinases, Kit, RET, Tie2, Flt3	CML or ALL, Ph <sup>+</sup>	<b>Larotrectinib</b> , Vitkvi	2018	TRK	Solid tumors with NTRK gene fusion proteins
<b>Regorafenib</b> , Stivarga	2012	VEGFR1/2/3, BCR-Abl, B-Raf, B-Raf (V600E), Kit, PDGFRα/β, RET, FGFR1/2, Tie2, and Eph2A	CRC, HCC, GIST	<b>Lorlatinib</b> , Lorbreina	2018	ALK	ALK <sup>+</sup> NSCLC
<b>Tofacitinib</b> , Tasocitinib	2012	JAK3	RA, PA, UC	<b>Netarsudil</b> , Rhopressa	2018	Rho kinase	Glaucoma
<b>Afatinib</b> , Tivantinib	2013	EGFR, ErbB2, ErbB4	NSCLC	<b>Entrectinib</b> , Rozlytrek	2019	TRKA/B/C	NSCLC, NTRK+ solid tumors
<b>Dabrafenib</b> , Tafinlar	2013	B-Raf	Melanoma and NSCLC with <i>BRAF</i> mutations	<b>Erdafitinib</b> , Balversa	2019	FGFR1/2/3/4	Urothelial carcinoma
<b>Ibrutinib</b> , Imbruvica	2013	Bruton tyrosine kinase	Mantle cell lymphoma; CLL; Waldenstrom's macro-globulin-emia; marginal zone lymphoma; graft vs. host disease	<b>Pexidartinib</b> , Turalio	2019	CSF1r,Kit	Tenosynovial giant cell tumors
<b>Trametinib</b> , Mekinist	2013	MEK1/2	Melanoma	<b>Gefitinib</b> , Iressa	2003-2005, 2015	EGFR	NSCLC
<b>Ceritinib</b> , LDK378, Zykadia	2014	ALK, IGF-1R, InsR, ROS1	NSCLC, ALK <sup>+</sup> after crizotinib resistance				

\* Approved as an immunosuppressant without an understood molecular mechanism of action. Kinase inhibitor ability was not reported until 2002.<sup>13</sup>

ALL, acute lymphoblastic leukemia; CEL, chronic eosinophilic leukemia; CLL, chronic lymphocytic leukemia; CML, chronic myelogenous leukemia; CRC, colorectal cancer; DDR1, Discoidin domain receptor family, member 1; DFSP, dermatofibrosarcoma protuberans; GIST, gastrointestinal stromal tumor; HES, hypereosinophilic syndrome, HGFR, hepatocyte growth factor receptor; MDS/MPD, myelodysplastic/myeloproliferative diseases; MST1R, macrophage-stimulating protein receptor aka RON (Recepteur d'Origine Nantais); NSCLC, non-small cell lung cancer; PNET, progressive neuroendocrine tumors of pancreatic origin; Ph<sup>+</sup>, Philadelphia chromosome positive; PA, psoriatic arthritis; RA, rheumatoid arthritis; RCC, renal cell carcinoma; UC ulerative colitis.

Although the development of small molecule kinase inhibitors for the treatment of disease, especially cancer, has rapidly expanded over the past two decades, there are still significant challenges facing the field. The greatest challenge is the issue of drug resistance. The cytotoxic effects of kinase inhibitors against cancer cells create a strong selective pressure for cells to acquire resistance mutations that abrogate drug binding.<sup>7</sup> Additional resistance mechanisms include target kinase amplification and the upregulation of alternative kinase pathways.

### **1.3 Anaplastic Lymphoma Kinase (ALK) Positive Cancer**

Anaplastic lymphoma kinase (ALK) is a receptor tyrosine kinase that was first identified in a chromosomal translocation associated with anaplastic large cell lymphoma (ALCL), a subtype of T-cell non-Hodgkin's lymphoma.<sup>14</sup> Chromosomal translocations involving the kinase domain of ALK are seen in many cancers. In addition to ALCL, ALK fusion proteins are seen in diffuse large B-cell lymphoma (DLBCL), inflammatory myofibroblastic tumor (IMT), breast cancer, colorectal cancer, esophageal squamous cell cancer (ESCC), renal cell cancer (RCC), and non-small-cell lung cancer (NSCLC).<sup>15</sup> ALK fusion partners drive dimerization of the ALK kinase domain, leading to autophosphorylation, which in turn causes the kinase to become constitutively active.<sup>16</sup> Oncogenic ALK may also be expressed due to point mutations as is seen in neuroblastoma (NB), where germline mutations in ALK have been documented to drive the majority of hereditary NB cases.<sup>17,18</sup> Constitutively active oncogenic ALK signals through multiple pathways, including PI3K/AKT, RAS/ERK, and JAK/STAT3, which leads to enhanced cell proliferation and survival.<sup>19</sup>

*ALK* rearranged NSCLC represents ~5% of all NSCLC and is a unique targetable molecular and clinical subset of NSCLC. Patients harboring ALK rearrangements are more likely to be never/limited smokers and such cancers do not typically contain other genomic alterations such as *EGFR* mutations.<sup>20,21</sup> Screening for ALK rearrangements is widely available throughout the US and worldwide and is the standard of care for newly diagnosed advanced NSCLC patients.<sup>22,23</sup> There are currently five FDA approved kinase inhibitors for the treatment of ALK-

positive NSCLC: crizotinib, ceritinib (LDK378), alectinib, brigatinib, and, most recently, lorlatinib. ALK-positive tumors are highly sensitive to ALK inhibition, indicating that these tumors are addicted to ALK kinase activity. However, despite initial dramatic responses of variable median duration (10.9 months for crizotinib; 16.6 months for ceritinib; 25.7 months for alectinib), resistance to therapy typically develops.<sup>24–28</sup>

While next-generation ALK inhibitors such as lorlatinib are an effective next-line therapy for resistant tumors and have shown improvements upon previously approved inhibitors in areas such as potency and overall response rate, patients treated with these agents still eventually acquire resistance, with progression free survival currently at < 12 months.<sup>29–33</sup> The three most prevalent resistance mechanisms are mutation in the ALK kinase domain, upregulation of ALK as a result of gene amplification or copy number gain, and/or activation of ALK-independent signal transduction pathways.<sup>15</sup> Therapeutic strategies that target ALK by employing novel mechanisms of action may provide ways to further delay the emergence of resistance mutations. One such strategy may be the use of small molecule kinase degraders.

#### **1.4 Small Molecule Degradors**

While the vast majority of targeted therapies use small molecule enzyme inhibition, there are drawbacks to the strategy. One of the major drawbacks is that greater than 90% target engagement is often needed for a pharmacological response, which requires large dosing levels that can lead to unwanted off-target effects.<sup>34,35</sup> This has led to a strong interest in methods of directly knocking down cellular protein levels.

There are several knockdown strategies that act at the genetic level, including RNA interference (RNAi), antisense oligonucleotides, and gene editing techniques such as CRISPR/Cas9. Although these techniques have been very useful tools for probing the functional consequences of specific protein loss in biological systems, their efficacy as therapeutics has been significantly hindered by the challenge of delivering nucleic acid therapies.<sup>36</sup> As a result,

there has been a strong push for developing techniques for knocking down protein levels using small molecules that maintain traditional pharmaceutical properties.

Cells contain systems for disposing of unwanted or damaged proteins. The largest of these systems is the ubiquitin-proteasome system (UPS), which consists of a cascade of enzymes that can conjugate the protein ubiquitin onto a target protein in order to mark that protein for degradation by the proteasome.<sup>35</sup> In 2001, Sakamoto et al. published on the rational design of a small molecule that can recruit a target protein to the UPS.<sup>37</sup> They described the design of a heterobifunctional compound composed of one warhead that consisted of a covalent inhibitor of the target protein methionine aminopeptidase-2 (MetAP-2) and a second warhead that consisted of a phosphopeptide that specifically bound to the F-box protein  $\beta$ -TRCP, which is part of the SCF E3 ubiquitin ligase complex. They called this compound proteolysis targeting chimera 1 (PROTAC-1) and demonstrated that this heterobifunctional, chimeric compound could induce the ubiquitination and subsequent proteasomal degradation of MetAP-2 by recruiting MetAP-2 to the SCF E3 ubiquitin ligase complex. PROTAC-1 showed that it is possible to chemically induce protein knockdown, but this first iteration of small molecule induced protein degradation had drawbacks due to the use of the phosphopeptide for E3 ligase recruitment, which led to PROTAC-1, and similar compounds that followed, having poor cell penetration.

The next generation of PROTACs, also called small molecule degraders, abandoned the phosphopeptide in favor of an “all-small molecule” approach that utilized a nonpeptidic E3 ligase binding moiety. In 2008, Schneekloth et al. reported the development of a PROTAC composed of a non-steroidal androgen receptor ligand (SARM) linked to nutlin, a ligand of E3 ubiquitin-protein ligase MDM2.<sup>38</sup> This SARM-nutlin PROTAC successfully recruited the androgen receptor to MDM2, which resulted in ubiquitination and subsequent proteasomal degradation as seen previously. Although this iteration of small molecule degraders had better cell penetration than the first generation of compounds, they still had low cell potency with micromolar doses being needed for target degradation.

In order to improve the potential therapeutic properties of small molecule degraders, researchers sought out ubiquitin E3 ligase binders with more drug-like properties. The solution came from two places: the discovery in 2010 that the immunomodulatory drug thalidomide binds the cereblon (CRBN) E3 ligase and the development of non-peptidic ligands of the von Hippel-Lindau (VHL) E3 ligase in 2012.<sup>39-44</sup> This led to the development of potent small molecule degraders of receptor-interacting protein kinase 2 (RIPK2) that recruited the VHL ligase in 2013, quickly followed by three studies showing the development of potent degraders of members of the BET family of bromodomain-containing proteins that recruited both CRBN and VHL in 2015.<sup>34,45-47</sup>

This latest generation of small molecule degraders were not only potent in cells (effective doses were now in the nanomolar range), but also showed rapid degradation of target proteins, with degradation being seen as early as 1 hour after treatment. These compounds, which used reversible warheads unlike the first iteration of PROTACs, were also shown to act in a catalytic manner with one degrader molecule being able to induce the degradation of multiple protein molecules. This indicated a major potential advantage of using small molecule degraders over inhibitors: effective intracellular concentrations of degraders could be much lower since once a degrader induced the ubiquitination of a protein and it was marked for proteasomal degradation, the compound no longer needed to interact with the protein and was free to act on another target protein. When considering using small molecule degraders to target kinases, another potential advantage includes the ability to address non-kinase, “scaffolding” resistance functions of the kinase protein by degrading the protein entirely, not just inhibiting its enzymatic function. Additionally, *de novo* resistance mutations to selective degraders are less likely to emerge since only transient interaction with the kinase is needed to induce degradation, making mutations that lower binding affinity less effective at abrogating degrader functionality than inhibitor functionality.

In addition to RIPK2, other kinases were soon shown to be amenable to degradation by small molecule degraders including the fusion protein BCR-ABL, as well as CDK9, Aurora A, BTK, FER, PTK2, and EGFR to name a few.<sup>48-52</sup>

## 1.5 Chemical Biology Studies of ALK and CRBN

**Chapter 2** presents the development of the first small molecule degraders that target ALK, demonstrating that it is amenable to chemically induced degradation and that this is a potential new avenue for developing therapeutics that may help delay the emergence of resistance mutations. **Chapter 3** describes efforts to identify the first allosteric ALK inhibitors, as an alternative novel mechanism of action for addressing resistance in ALK-positive cancer. **Chapter 4** discusses the development of a thalidomide analog library by introducing kinase inhibitor scaffolds to another immunomodulatory drug, lenalidomide. This library was screened for antiproliferative activity in order to help identify novel CRBN modulators that could induce protein degradation. **Chapter 5** presents the development of small molecule degraders that induce the degradation of CRBN that may be used as probes to better understand endogenous CRBN biology. Finally, **Chapters 6 and 7** describe efforts to develop and optimize kinase inhibitors for additional clinically relevant kinase targets, dual-specificity tyrosine phosphorylation-regulated kinase 1A (DYRK1A) and tyrosine kinase nonreceptor 2 (TNK2) respectively.

Overall, this work fits squarely under the umbrella of chemical biology by demonstrating the development of small molecules as inhibitors, degraders, and modulators for both therapeutic and probe purposes.

## References

- (1) Ostler, E. L. Chemical Biology Is..... *Chem Cent J* **2007**, 1 (1), 5. <https://doi.org/10.1186/1752-153x-1-5> .
- (2) What's in a Name? *Nat Chem Biol* **2015**, 11 (6), 363–363. <https://doi.org/10.1038/nchembio.1832> .
- (3) Schreiber, S. Small Molecules: The Missing Link in the Central Dogma. *Nature Chemical Biology* **2005**, 1 3.
- (4) Cohen, P. The Regulation of Protein Function by Multisite Phosphorylation – a 25 Year Update. *Trends Biochem Sci* **2000**, 25 (12), 596–601. [https://doi.org/10.1016/s0968-0004\(00\)01712-6](https://doi.org/10.1016/s0968-0004(00)01712-6) .
- (5) Manning, G.; Whyte, D.; Martinez, R.; Hunter, T.; Sudarsanam, S. The Protein Kinase Complement of the Human Genome. *Science* **2002**, 298 (5600), 1912–1934. <https://doi.org/10.1126/science.1075762> .
- (6) Cohen, P. The Origins of Protein Phosphorylation. *Nat Cell Biol* **2002**, 4 (5), ncb0502-e127. <https://doi.org/10.1038/ncb0502-e127> .
- (7) Zhang, J.; Yang, P. L.; Gray, N. S. Targeting Cancer with Small Molecule Kinase Inhibitors. *Nat Rev Cancer* **2009**, 9 (1), 28 39. <https://doi.org/10.1038/nrc2559> .
- (8) Arora, A.; Scholar, E. M. Role of Tyrosine Kinase Inhibitors in Cancer Therapy. *J Pharmacol Exp Ther* **2005**, 315 (3), 971 979. <https://doi.org/10.1124/jpet.105.084145> .
- (9) Jr, R. A Historical Overview of Protein Kinases and Their Targeted Small Molecule Inhibitors. *Pharmacol Res* **2015**, 100, 1 23. <https://doi.org/10.1016/j.phrs.2015.07.010> .
- (10) Müller, S.; Chaikuad, A.; Gray, N. S.; Knapp, S. The Ins and Outs of Selective Kinase Inhibitor Development. *Nat Chem Biol* **2015**, 11 (11), 818 821. <https://doi.org/10.1038/nchembio.1938> .
- (11) Liu, Y.; Gray, N. S. Rational Design of Inhibitors That Bind to Inactive Kinase Conformations. *Nat Chem Biol* **2006**, 2 (7), 358 364. <https://doi.org/10.1038/nchembio799> .
- (12) Vijayan, R.; He, P.; Modi, V.; Duong-Ly, K. C.; Ma, H.; Peterson, J. R.; Jr., R. L.; Levy, R. M. Conformational Analysis of the DFG-Out Kinase Motif and Biochemical Profiling of Structurally Validated Type II Inhibitors. *J Med Chem* **2014**, 58 (1), 466 479. <https://doi.org/10.1021/jm501603h> .
- (13) Hara, K.; Maruki, Y.; Long, X.; Yoshino, K.; Oshiro, N.; Hidayat, S.; Tokunaga, C.; Avruch, J.; Yonezawa, K. Raptor, a Binding Partner of Target of Rapamycin (TOR), Mediates TOR Action. *Cell* **2002**, 110 (2), 177–189. [https://doi.org/10.1016/s0092-8674\(02\)00833-4](https://doi.org/10.1016/s0092-8674(02)00833-4) .
- (14) Chiarle, R.; Voena, C.; Ambrogio, C.; Piva, R.; Inghirami, G. The Anaplastic Lymphoma Kinase in the Pathogenesis of Cancer. *Nat Rev Cancer* **2008**, 8 (1), 11 23. <https://doi.org/10.1038/nrc2291> .

- (15) Jr, R. Anaplastic Lymphoma Kinase (ALK): Structure, Oncogenic Activation, and Pharmacological Inhibition. *Pharmacol Res* **2013**, 68 (1), 68 94.  
<https://doi.org/10.1016/j.phrs.2012.11.007> .
- (16) Bayliss, R.; Choi, J.; Fennell, D. A.; Fry, A. M.; Richards, M. W. Molecular Mechanisms That Underpin EML4-ALK Driven Cancers and Their Response to Targeted Drugs. *Cell Mol Life Sci* **2016**, 73 (6), 1209 1224. <https://doi.org/10.1007/s00018-015-2117-6> .
- (17) George, R. E.; Sanda, T.; Hanna, M.; Fröhling, S.; William, L. I.; Zhang, J.; Ahn, Y.; Zhou, W.; London, W. B.; McGrady, P.; et al. Activating Mutations in ALK Provide a Therapeutic Target in Neuroblastoma. *Nature* **2008**, 455 (7215), 975 978.  
<https://doi.org/10.1038/nature07397> .
- (18) Mossé, Y. P.; Laudenslager, M.; Longo, L.; Cole, K. A.; Wood, A.; Attiyeh, E. F.; Laquaglia, M. J.; Sennett, R.; Lynch, J. E.; Perri, P.; et al. Identification of ALK as a Major Familial Neuroblastoma Predisposition Gene. *Am J Pathology* **2008**, 455 (7215), 930 935.  
[https://doi.org/10.1016/s0002-9440\(10\)65042-0](https://doi.org/10.1016/s0002-9440(10)65042-0) .
- (19) Palmer, R. H.; Vernersson, E.; Grabbe, C.; Hallberg, B. Anaplastic Lymphoma Kinase: Signalling in Development and Disease. *Biochem J* **2009**, 420 (3), 345 361.  
<https://doi.org/10.1042/bj20090387> .
- (20) Sasaki, T.; Rodig, S. J.; Chirieac, L. R.; Janne, P. A. The Biology and Treatment of EML4-ALK Non-Small Cell Lung Cancer. *Eur J Cancer* **2010**, 46 (10), 1773 1780.  
<https://doi.org/10.1016/j.ejca.2010.04.002> .
- (21) Mino-Kenudson, M.; Chirieac, L.; Law, K.; Hornick, J.; Lindeman, N.; Mark, E.; Cohen, D.; Johnson, B.; Janne, P.; Iafrate, A.; et al. A Novel, Highly Sensitive Antibody Allows for the Routine Detection of ALK-Rearranged Lung Adenocarcinomas by Standard Immunohistochemistry. *Clin Cancer Res* **2010**, 16 (5), 1561 1571. <https://doi.org/10.1158/1078-0432.ccr-09-2845> .
- (22) Camidge, R. D.; Theodoro, M.; Maxson, D. A.; Skokan, M.; O'Brien, T.; Lu, X.; Doebele, R. C.; Barón, A. E.; Varella-Garcia, M. Correlations between the Percentage of Tumor Cells Showing an Anaplastic Lymphoma Kinase ( ALK) Gene Rearrangement, ALKsignal Copy Number, and Response to Crizotinib Therapy in ALKfluorescence in Situ Hybridization-Positive Nonsmall Cell Lung Cancer. *Nat Rev Cancer* **2012**, 118 (18), 4486 4494.  
<https://doi.org/10.1038/nrc1165> .
- (23) Kwak, E. L.; Bang, Y.-J.; Camidge, R. D.; Shaw, A. T.; Solomon, B.; Maki, R. G.; Ou, S.-H. I.; Dezube, B. J.; Janne, P. A.; Costa, D. B.; et al. Anaplastic Lymphoma Kinase Inhibition in Non-Small-Cell Lung Cancer. *New Engl J Medicine* **2010**, 363 (18), 1693 1703.  
<https://doi.org/10.1056/nejmoa1006448> .
- (24) Peters, S.; Camidge, R. D.; Shaw, A. T.; Gadgeel, S.; Ahn, J. S.; Kim, D.-W.; Ou, S.-H. I.; Pérol, M.; Dziadziuszko, R.; Rosell, R.; et al. Alectinib Versus Crizotinib in Untreated ALK-Positive Non-Small-Cell Lung Cancer. *New Engl J Medicine* **2017**, 377 (9), 829 838.  
<https://doi.org/10.1056/nejmoa1704795> .
- (25) Katayama, R.; Shaw, A.; Khan, T.; Mino-Kenudson, M.; Solomon, B.; Halmos, B.; Jessop, N.; Wain, J.; Yeo, A.; Benes, C.; et al. Mechanisms of Acquired Crizotinib Resistance in ALK-

Rearranged Lung Cancers. *Sci Transl Med* **2012**, 4 (120), 120ra17 120ra17. <https://doi.org/10.1126/scitranslmed.3003316> .

(26) Cooper, M.; Chim, H.; Chan, H.; Durand, C. Ceritinib: A New Tyrosine Kinase Inhibitor for Non-Small-Cell Lung Cancer. *Ann Pharmacother* **2014**, 49 (1), 107 112. <https://doi.org/10.1177/1060028014553619> .

(27) Sullivan, I.; Planchard, D. ALK Inhibitors in Non-Small Cell Lung Cancer: The Latest Evidence and Developments. *Ther Adv Med Oncol* **2015**, 8 (1), 32 47. <https://doi.org/10.1177/1758834015617355> .

(28) Soria, J.-C.; Tan, D. S.; Chiari, R.; Wu, Y.-L.; Paz-Ares, L.; Wolf, J.; Geater, S. L.; Orlov, S.; Cortinovis, D.; Yu, C.-J.; et al. First-Line Ceritinib Versus Platinum-Based Chemotherapy in Advanced ALK-Rearranged Non-Small-Cell Lung Cancer (ASCEND-4): A Randomised, Open-Label, Phase 3 Study. *Lancet* **2017**, 389 (10072), 917 929. [https://doi.org/10.1016/s0140-6736\(17\)30123-x](https://doi.org/10.1016/s0140-6736(17)30123-x) .

(29) Shaw, A. T.; Felip, E.; Bauer, T. M.; Besse, B.; Navarro, A.; Postel-Vinay, S.; Gainor, J. F.; Johnson, M.; Dietrich, J.; James, L. P.; et al. Lorlatinib in Non-Small-Cell Lung Cancer with ALK or ROS1 Rearrangement: An International, Multicentre, Open-Label, Single-Arm First-in-Man Phase 1 Trial. *Lancet Oncol* **2017**, 18 (12), 1590 1599. [https://doi.org/10.1016/s1470-2045\(17\)30680-0](https://doi.org/10.1016/s1470-2045(17)30680-0) .

(30) Mologni, L. Expanding the Portfolio of Anti-ALK Weapons. *Transl Lung Cancer Res* **2015**, 4 (1), 5 7. <https://doi.org/10.3978/j.issn.2218-6751.2014.07.02> .

(31) Katayama, R.; Friboulet, L.; Koike, S.; Lockerman, E.; Khan, T.; Gainor, J.; Iafrate, A.; Takeuchi, K.; Taiji, M.; Okuno, Y.; et al. Two Novel ALK Mutations Mediate Acquired Resistance to the Next-Generation ALK Inhibitor Alectinib. *Clin Cancer Res* **2014**, 20 (22), 5686 5696. <https://doi.org/10.1158/1078-0432.ccr-14-1511> .

(32) Qin, A.; Gadgeel, S. The Current Landscape of Anaplastic Lymphoma Kinase (ALK) in Non-Small Cell Lung Cancer: Emerging Treatment Paradigms and Future Directions. *Target Oncol* **2017**, 12 (6), 709 718. <https://doi.org/10.1007/s11523-017-0526-1> .

(33) Shaw, A. T.; Friboulet, L.; Leshchiner, I.; Gainor, J. F.; Bergqvist, S.; Brooun, A.; Burke, B. J.; Deng, Y.-L.; Liu, W.; Dardaei, L.; et al. Resensitization to Crizotinib by the Lorlatinib ALKResistance Mutation L1198F. *New Engl J Medicine* **2016**, 374 (1), 54 61. <https://doi.org/10.1056/nejmoa1508887> .

(34) Bondeson, D. P.; Mares, A.; Smith, I. E.; Ko, E.; Campos, S.; Miah, A. H.; Mulholland, K. E.; Routly, N.; Buckley, D. L.; Gustafson, J. L.; et al. Catalytic in Vivo Protein Knockdown by Small-Molecule PROTACs. *Behav Brain Res* **2015**, 11 (8), 611 617. [https://doi.org/10.1016/s0166-4328\(01\)00297-2](https://doi.org/10.1016/s0166-4328(01)00297-2) .

(35) Bondeson, D. P.; Crews, C. M. Targeted Protein Degradation by Small Molecules. *Annu Rev Pharmacol* **2015**, 57 (1), 107–123. <https://doi.org/10.1146/annurev-pharmtox-010715-103507> .

(36) Conde, J.; Artzi, N. Are RNAi and MiRNA Therapeutics Truly Dead? *Trends Biotechnol* **2015**, 33 (3), 141–144. <https://doi.org/10.1016/j.tibtech.2014.12.005> .

- (37) Sakamoto, K. M.; Kim, K. B.; Kumagai, A.; Mercurio, F.; Crews, C. M.; Deshaies, R. J. Protacs: Chimeric Molecules That Target Proteins to the Skp1–Cullin–F Box Complex for Ubiquitination and Degradation. *Proc National Acad Sci* **2001**, *98* (15), 8554–8559. <https://doi.org/10.1073/pnas.141230798> .
- (38) Schneekloth, A. R.; Pucheault, M.; Tae, H.; Crews, C. M. Targeted Intracellular Protein Degradation Induced by a Small Molecule: En Route to Chemical Proteomics. *Bioorg Med Chem Lett* **2008**, *18* (22), 5904–5908. <https://doi.org/10.1016/j.bmcl.2008.07.114> .
- (39) Churcher, I. Protac-Induced Protein Degradation in Drug Discovery: Breaking the Rules or Just Making New Ones? *J Med Chem* **2017**, *61* (2), 444–452. <https://doi.org/10.1021/acs.jmedchem.7b01272> .
- (40) Ito, T.; Ando, H.; Suzuki, T.; Ogura, T.; Hotta, K.; Imamura, Y.; Yamaguchi, Y.; Handa, H. Identification of a Primary Target of Thalidomide Teratogenicity. *Science* **2010**, *327* (5971), 1345–1350. <https://doi.org/10.1126/science.1177319> .
- (41) Buckley, D. L.; Molle, I.; Gareiss, P. C.; Tae, H.; Michel, J.; Noblin, D. J.; Jorgensen, W. L.; Ciulli, A.; Crews, C. M. Targeting the von Hippel–Lindau E3 Ubiquitin Ligase Using Small Molecules To Disrupt the VHL/HIF-1 $\alpha$  Interaction. *J Am Chem Soc* **2012**, *134* (10), 4465–4468. <https://doi.org/10.1021/ja209924v> .
- (42) Buckley, D. L.; Gustafson, J. L.; Van Molle, I.; Roth, A. G.; Tae, H.; Gareiss, P. C.; Jorgensen, W. L.; Ciulli, A.; Crews, C. M. Small-Molecule Inhibitors of the Interaction between the E3 Ligase VHL and HIF1 $\alpha$  . *Angewandte Chemie Int Ed* **2012**, *51* (46), 11463–11467. <https://doi.org/10.1002/anie.201206231> .
- (43) Van Molle, I.; Thomann, A.; Buckley, D. L.; So, E. C.; Lang, S.; Crews, C. M.; Ciulli, A. Dissecting Fragment-Based Lead Discovery at the von Hippel–Lindau Protein:Hypoxia Inducible Factor 1 $\alpha$  Protein-Protein Interface. *Chem Biol* **2012**, *19* (10), 1300–1312. <https://doi.org/10.1016/j.chembiol.2012.08.015> .
- (44) Galdeano, C.; Gadd, M. S.; Soares, P.; Scaffidi, S.; Molle, I.; Birced, I.; Hewitt, S.; Dias, D. M.; Ciulli, A. Structure-Guided Design and Optimization of Small Molecules Targeting the Protein–Protein Interaction between the von Hippel–Lindau (VHL) E3 Ubiquitin Ligase and the Hypoxia Inducible Factor (HIF) Alpha Subunit with in Vitro Nanomolar Affinities. *J Med Chem* **2014**, *57* (20), 8657–8663. <https://doi.org/10.1021/jm5011258> .
- (45) Winter, G.; Buckley, D.; Paulk, J.; Roberts, J.; Souza, A.; Dhe-Paganon, S.; Bradner, J. Phthalimide Conjugation as a Strategy for in Vivo Target Protein Degradation. *Science* **2015**, *348* (6241), 1376–1381. <https://doi.org/10.1126/science.aab1433> .
- (46) Lu, J.; Qian, Y.; Altieri, M.; Dong, H.; Wang, J.; Raina, K.; Hines, J.; Winkler, J. D.; Crew, A. P.; Coleman, K.; et al. Hijacking the E3 Ubiquitin Ligase Cereblon to Efficiently Target BRD4. *Chem Biol* **2015**, *22* (6), 755–763. <https://doi.org/10.1016/j.chembiol.2015.05.009> .
- (47) Zengerle, M.; Chan, K.-H.; Ciulli, A. Selective Small Molecule Induced Degradation of the BET Bromodomain Protein BRD4. *Acs Chem Biol* **2015**, *10* (8), 1770–1777. <https://doi.org/10.1021/acschembio.5b00216> .

- (48) Lai, A. C.; Toure, M.; Hellerschmied, D.; Salami, J.; Jaime-Figueroa, S.; Ko, E.; Hines, J.; Crews, C. M. Modular PROTAC Design for the Degradation of Oncogenic BCR-ABL. *Angew Chem-ger Edit* **2015**, *128* (2), 818 821. <https://doi.org/10.1002/ange.201507634> .
- (49) Huang, H.-T.; Dobrovolsky, D.; Paulk, J.; Yang, G.; Weisberg, E. L.; ctor, Z.; Buckley, D. L.; Cho, J.-H.; Ko, E.; Jang, J.; et al. A Chemoproteomic Approach to Query the Degradable Kinome Using a Multi-Kinase Degradator. *Cell Chem Biol* **2017**, *25* (1), 1 19. <https://doi.org/10.1016/j.chembiol.2017.10.005> .
- (50) Olson, C. M.; Jiang, B.; Erb, M. A.; Liang, Y.; ctor, Z.; Zhang, Z.; Zhang, T.; Kwiatkowski, N.; Boukhali, M.; Green, J. L.; et al. Pharmacological Perturbation of CDK9 Using Selective CDK9 Inhibition or Degradation. *Nat Chem Biol* **2018**, *14* (2), 163 170. <https://doi.org/10.1038/nchembio.2538> .
- (51) Bondeson, D. P.; Smith, B. E.; Burslem, G. M.; Buhimschi, A. D.; Hines, J.; Jaime-Figueroa, S.; Wang, J.; Hamman, B. D.; Ishchenko, A.; Crews, C. M. Lessons in PROTAC Design from Selective Degradation with a Promiscuous Warhead. *Cell Chem Biol* **2017**, *25* (1), 1 34. <https://doi.org/10.1016/j.chembiol.2017.09.010> .
- (52) Burslem, G. M.; Smith, B. E.; Lai, A. C.; Jaime-Figueroa, S.; McQuaid, D. C.; Bondeson, D. P.; Toure, M.; Dong, H.; Qian, Y.; Wang, J.; et al. The Advantages of Targeted Protein Degradation Over Inhibition: An RTK Case Study. *Cell Chem Biol* **2017**, *25* (1), 1 15. <https://doi.org/10.1016/j.chembiol.2017.09.009> .

## **Chapter 2: Chemically Induced Degradation of Anaplastic Lymphoma Kinase (ALK)**

## Attributions

The work in this chapter is adapted from a manuscript published in the *Journal of Medicinal Chemistry* in 2018 titled “Chemically Induced Degradation of Anaplastic Lymphoma Kinase (ALK)” by Powell *et al.*<sup>1</sup> Author contributions, funding sources, and competing interests for this work can be found near the end of the chapter, before the references.

## Chapter 2: Chemically Induced Degradation of Anaplastic Lymphoma Kinase (ALK)

Chelsea E. Powell,<sup>†,◇</sup> Yang Gao,<sup>⊥</sup> Li Tan,<sup>†,◇</sup> Katherine A. Donovan,<sup>†,◇</sup> Radosław P. Nowak,<sup>†,◇</sup>  
Amanda Loehr,<sup>⊥</sup> Magda Bahcall,<sup>‡</sup> Eric S. Fischer,<sup>†,◇</sup> Pasi A. Jänne,<sup>‡,§</sup> Rani E. George,<sup>⊥</sup> Nathanael  
S. Gray<sup>\*,†,◇</sup>

<sup>†</sup>Department of Cancer Biology, <sup>‡</sup>Lowe Center for Thoracic Oncology, and <sup>§</sup>Belfer Center for Applied  
Cancer Science, Dana-Farber Cancer Institute, Boston, Massachusetts 02215, United States

<sup>◇</sup>Department of Biological Chemistry & Molecular Pharmacology, Harvard Medical School, Boston,  
Massachusetts 02115, United States

<sup>⊥</sup>Department of Pediatric Hematology and Oncology, Dana-Farber Cancer Institute and Children's Hospital  
Boston, Harvard Medical School, Boston, Massachusetts 02215, United States

\* Correspondence: [Nathanael\\_Gray@dfci.harvard.edu](mailto:Nathanael_Gray@dfci.harvard.edu) (N.S.G.).

## **Abstract**

We present the development of the first small molecule degraders that can induce anaplastic lymphoma kinase (ALK) degradation, including in non-small-cell lung cancer (NSCLC), anaplastic large-cell lymphoma (ALCL), and neuroblastoma (NB) cell lines. These degraders were developed through conjugation of known pyrimidine-based ALK inhibitors, TAE684 or LDK378, and the cereblon ligand pomalidomide. We demonstrate that in some cell types degrader potency is compromised by expression of drug transporter ABCB1. In addition, proteomic profiling demonstrated that these compounds also promote the degradation of additional kinases including PTK2 (FAK), Aurora A, FER, and RPS6KA1 (RSK1).

## 2.1 Introduction

Anaplastic lymphoma kinase (ALK) is a receptor tyrosine kinase that was first identified in a chromosomal translocation associated with anaplastic large cell lymphoma (ALCL), a subtype of T-cell non-Hodgkin's lymphoma.<sup>2</sup> Chromosomal translocations involving the kinase domain of ALK are seen in many cancers. In addition to ALCL, ALK fusion proteins are seen in diffuse large B-cell lymphoma (DLBCL), inflammatory myofibroblastic tumor (IMT), breast cancer, colorectal cancer, esophageal squamous cell cancer (ESCC), renal cell cancer (RCC), and non-small-cell lung cancer (NSCLC).<sup>3</sup> ALK fusion partners drive dimerization of the ALK kinase domain, leading to autophosphorylation, which in turn causes the kinase to become constitutively active.<sup>4</sup> Oncogenic ALK may also be expressed due to point mutations as is seen in neuroblastoma (NB), where germline mutations in ALK have been documented to drive the majority of hereditary NB cases.<sup>5,6</sup> Constitutively active oncogenic ALK signals through multiple pathways, including PI3K/AKT, RAS/ERK, and JAK/STAT3; this signaling leads to enhanced cell proliferation and survival.<sup>7</sup>

ALK is an attractive target for cancer therapies not only for its prominent role in a number of malignancies, but also for its scant expression in normal adult tissue, which is restricted to a small subset of neural cells, reducing off-target toxicities of ALK-selective agents.<sup>3,8</sup> There are currently five FDA approved kinase inhibitors for the treatment of ALK-positive NSCLC: crizotinib, ceritinib (LDK378), alectinib, brigatinib and, most recently, lorlatinib. ALK-positive tumors are highly sensitive to ALK inhibition, indicating that these tumors are addicted to ALK kinase activity. However, despite initial dramatic responses of variable median duration (10.9 months for crizotinib; 16.6 months for ceritinib; 25.7 months for alectinib), resistance to therapy typically develops.<sup>9-13</sup>

While next-generation ALK inhibitors such as lorlatinib have been able to successfully target resistant tumors and have shown improvements in potency and overall response rates

relative to approved inhibitors, resistance to these inhibitors still consistently arises in patients.<sup>14–17</sup> Therapeutic strategies that target ALK with a novel mechanism of action may provide ways to further delay the emergence of resistance mutations. Here we described the development and characterization of bivalent small molecules that are capable of inducing proteasome-mediated degradation of ALK.

We developed small molecule degraders (also called PROTACs or degronimides) which are hetero-bifunctional small molecules that can induce degradation of a protein by bringing it into proximity of an E3 ligase.<sup>18</sup> When the ternary complex is formed, the E3 ligase ubiquitinates the target protein, leading to its proteasomal degradation. It has recently been shown that this technology may be used to induce both kinase and kinase fusion protein degradation.<sup>19</sup>

Here we present two examples of degraders that can induce ALK degradation in NSCLC cells expressing the fusion protein echinoderm microtubule-associated protein-like 4 (EML4)-ALK, ALCL cells expressing the fusion protein nucleophosmin (NPM)-ALK, and NB cells expressing either ALK F1174L or ALK R1275Q.

## 2.2 Results and Discussion

We designed the degraders **9** and **11** based on known ALK inhibitors TAE684 and LDK378 (ceritinib), respectively, and used the cereblon ligand pomalidomide to recruit the E3 ubiquitin ligase complex (Figure 2.1A). A 2-polyethylene glycol (PEG) linker was selected for these prototypical ALK degraders due to the success of a previously generated TAE684 based multi-kinase degrader.<sup>20</sup> As control compounds to complement the degraders **9** and **11**, we designed the analogs **10** and **12** with des-carbonyl pomalidomide groups that exhibit substantially weakened binding to cereblon, as confirmed by a biochemical cereblon binding assay (Figures 2.1A, 2.1C). Using an ALK activity assay, we validated that both the degraders and their des-

carbonyl counterparts are still able to bind ALK, with  $IC_{50}$ s comparable to their parental kinase inhibitors (Figure 2.1B, Table 2.1).

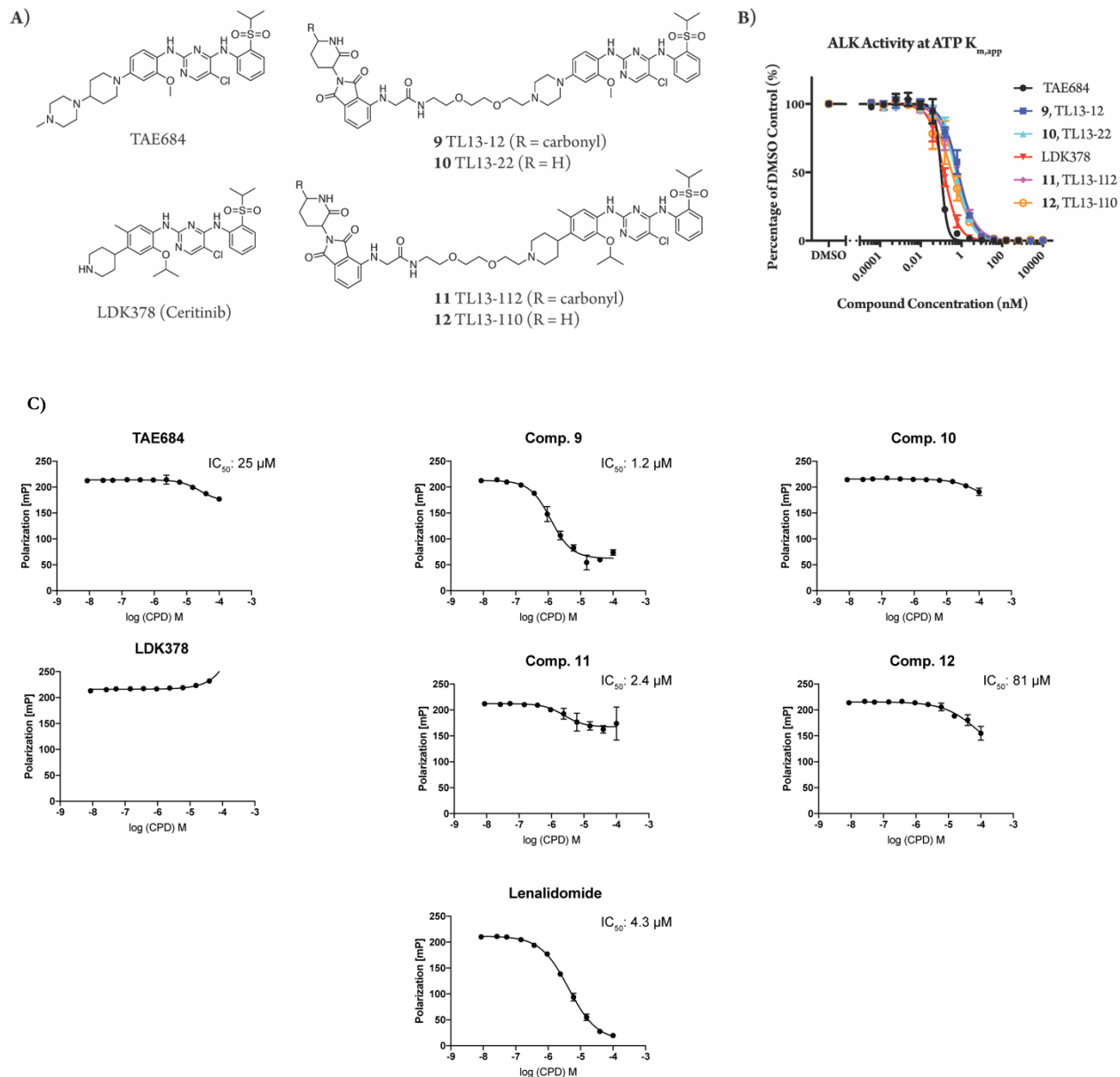


**Figure 2.1.** Chemical structures and characterization of ALK degraders. (A) TAE684 is the parental kinase inhibitor of **9** and **10**. LDK378 is the parental inhibitor of **11** and **12**. **9** and **11** are ALK targeted degraders while **10** and **12** contain des-carbonyl versions of the pomalidomide group, causing them to exhibit substantially weakened binding to cereblon. (B) TR-FRET ALK activity assay, plotted as the mean of three technical replicates  $\pm$  SD. (C) Fluorescence polarization cereblon binding assay  $IC_{50}$  curves  $\pm$  SD ( $n = 4$ ).  $IC_{50}$  values shown when calculated by variable slope equation in GraphPad Prism 7.

**Table 2.1.** ALK activity assay IC<sub>50</sub> values.

	<b>TAE684</b>	<b>Comp. 9</b>	<b>Comp. 10</b>	<b>LDK378</b>	<b>Comp. 11</b>	<b>Comp. 12</b>
<b>IC<sub>50</sub> (nM)</b>	0.10	0.69	0.54	0.14	0.60	0.34
<b>95% CI</b>	0.09273 to 0.1098	0.6263 to 0.7614	0.4994 to 0.5879	0.1243 to 0.1485	0.5421 to 0.6667	0.2797 to 0.4123

We examined the effects of the degraders on cell proliferation in ALK-driven NSCLC line H3122, and ALCL lines Karpas 299 and SU-DHL-1. In both NSCLC and ALCL cell lines the degraders and parental kinase inhibitors were about equipotent, while the des-carbonyl compounds were less active than the inhibitors, indicating that the potent anti-proliferative effects seen with the degraders are due in part to their ability to degrade ALK (Figure 2.2).

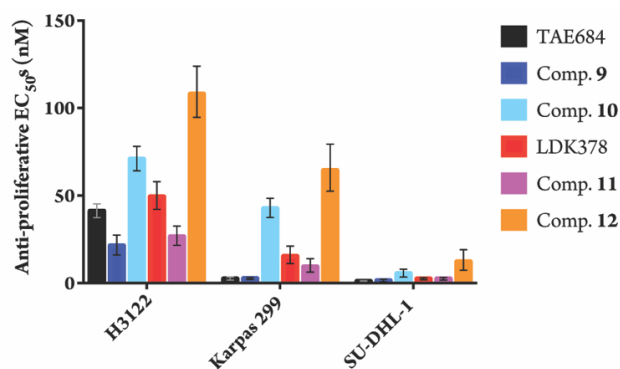


**Figure 2.2.** Anti-proliferative best fit EC<sub>50</sub> values with 95% CI in NSCLC and ALCL cell lines after 72-hr treatments (three biological replicates; Graphpad Prism 7 software).

We next studied the induced degradation of ALK and a known off-target of TAE684 and LDK378, Aurora A kinase, in H3122 and Karpas 299 cells.<sup>21,22</sup> A dose titration of **9** and **11** in each cell line for 16 hours demonstrated that **9** is more selective for degradation of ALK versus Aurora A than **11**, which is consistent with LDK378's higher selectivity for ALK compared to TAE684 (Figure 2.3A).<sup>22</sup> From these dose titrations the DC<sub>50</sub>s of **9** and **11** against ALK were calculated to be the same in H3122 cells (10 nM, two independent experiments), while **11** induced more potent ALK degradation in Karpas 299 than **9** with DC<sub>50</sub>s of 40 nM and 180 nM, respectively (two

independent experiments). Time course treatments with both degraders showed that some ALK degradation is observed at 4 hours of treatment in H3122 cells and at 8 hours of treatment in Karpas 299 cells, and maximum degradation is achieved at 16 hours in both cases (Figure 2.3B).

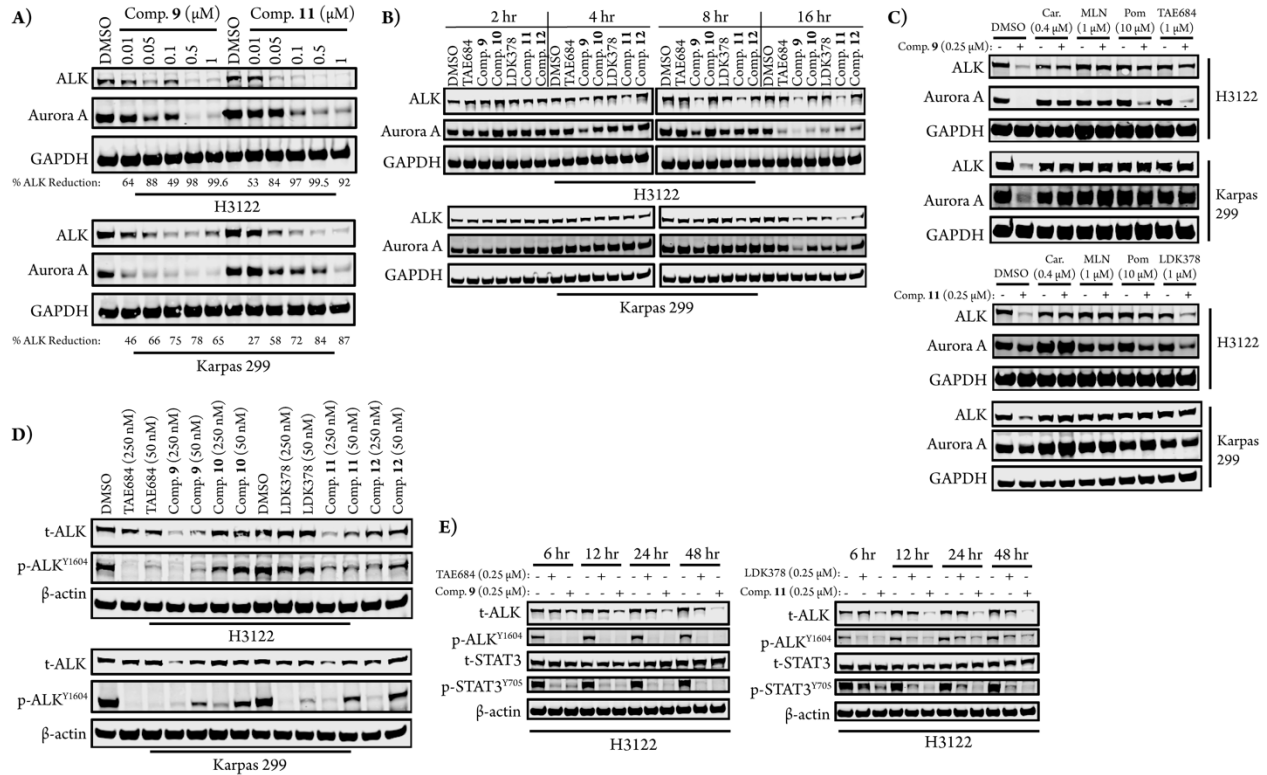


**Figure 2.3.** Degradation behavior in H3122 and Karpas 299 cells. (A) Immunoblots after 16 hours of treatment with dose titrations of **9** and **11**. (B) Immunoblots after treatment with 250 nM of compound for the indicated amount of time. (C) Immunoblots after 2-hour pre-treatments with DMSO, carfilzomib (Car), MLN4924 (MLN), pomalidomide (Pom), TAE684, or LDK378 followed by 16-hour treatments with **9** or **11**. (D) Immunoblots of downstream ALK signaling after 16-hour compound treatments; t-ALK indicates total ALK and p-ALK indicates phosphorylated ALK. (E) Immunoblots of sustained downstream ALK signaling after the indicated treatment times.

Pre-treatment of the cell lines with the proteasome inhibitor carfilzomib prevented degradation of both ALK and Aurora A, validating that the degradation seen is occurring via the proteasome (Figure 2.3C). MLN4924 indirectly inhibits the cereblon E3 ligase by blocking neddylation of the cullin RING ligase, CUL4, in the protein complex, which is required for ligase activity. Pre-treatment with MLN4924 also prevented degradation of ALK and Aurora A,

confirming that the degradation seen is occurring via recruitment of the cereblon E3 ligase complex (Figure 2.3C). Pre-treatment with pomalidomide or the parental kinase inhibitor also prevented ALK degradation, although pre-treatment with LDK378 only showed partial rescue in H3122 cells. This demonstrates that engagement of both ALK and cereblon is required for the observed degradation.

We compared the effects on downstream signaling between the parental kinase inhibitors, the degraders, and their des-carbonyl counterparts by examining ALK phosphorylation by western blot after 16 hours of treatment; this demonstrated that the extent of downstream signaling inhibition by the degraders is cell line dependent (Figure 2.3D). In H3122 cells, **9** inhibits downstream signaling to a similar extent as its parental kinase inhibitor, while **11** shows improved downstream inhibition. In Karpas 299 cells the degraders affect downstream signaling to a lesser extent than the kinase inhibitors. In both cell lines the degraders affect downstream signaling more than their des-carbonyl counterparts, indicating that the degrader downstream effects are due to both degradation and inhibition of ALK.

When observing downstream signaling over a 48-hour time course in H3122 cells, **9** sustains inhibition of ALK and STAT3 phosphorylation to a similar extent as TAE684, while **11** shows a distinct improvement on sustained inhibition compared to LDK378 (Figure 2.3E). This is significant because inhibition of STAT3 signaling leads to significant anti-proliferative effects in EML4-ALK expressing cells and sustained ALK pathway inhibition has been linked to greater anti-tumor efficacy.<sup>23-25</sup>

When we tested the anti-proliferative effects of the degraders in NB cell lines we observed a previously unreported potential obstacle with the degrader technology related to the ATP-binding cassette sub-family B member 1 (ABCB1) drug transporter. We used Kelly and Lan5 lines, which are ABCB1 low expressing cells, and SH-SY5Y and CHLA20 lines, which are ABCB1 high expressing cells. ABCB1 has been shown to efflux hydrophobic and amphipathic compounds.<sup>26</sup> This drug transporter activity can be inhibited by tariquidar.<sup>27</sup> In the ABCB1 high expressing cells

the degraders had low anti-proliferative activity compared to the parental inhibitors. However, when we co-treated with tariquidar we saw an increase in anti-proliferative activity of the degraders with  $EC_{50}$ s comparable to the parental kinase inhibitors (Figure 2.4). In addition, knockdown of ABCB1 using shRNA also increased degrader-mediated ALK degradation and inhibition of proliferation (Figure 2.5). Thus, we concluded that degraders can be substrates of the ABCB1 transporter. Future SAR efforts will need to focus on modifications to the degrader molecules that will prevent them from being effluxed by ABCB1 transporters.

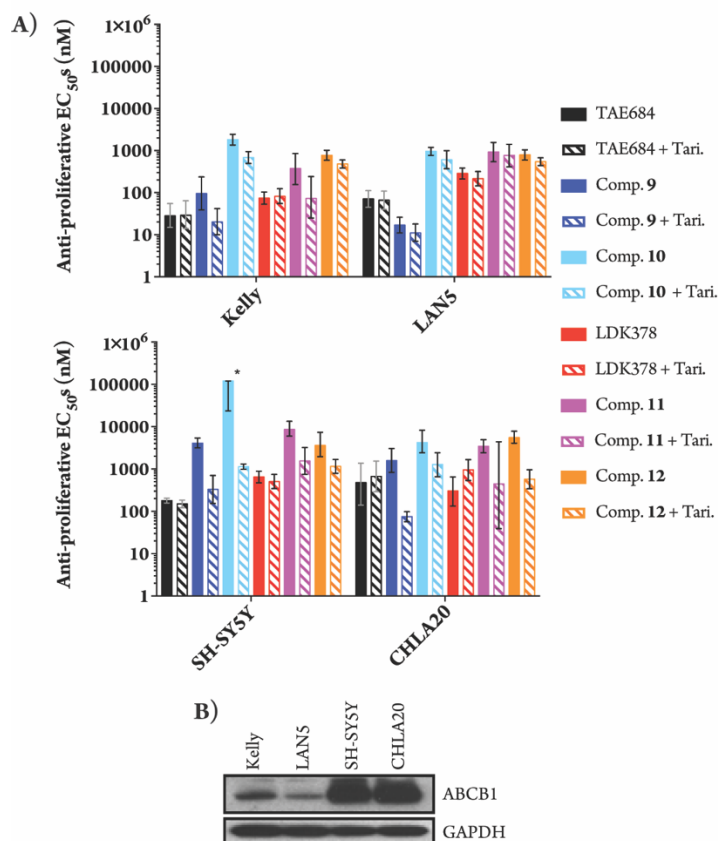


**Figure 2.4.** (A) Anti-proliferative best fit  $EC_{50}$  values with 95% CI in NB cell lines after 72-hr treatments (two biological replicates; Graphpad Prism 7 software: \* = upper CI not calculated by model). 125 nM of tariquidar (Tari.) was used for the indicated co-treatments. (B) Immunoblot of ABCB1 expression in NB lysates.

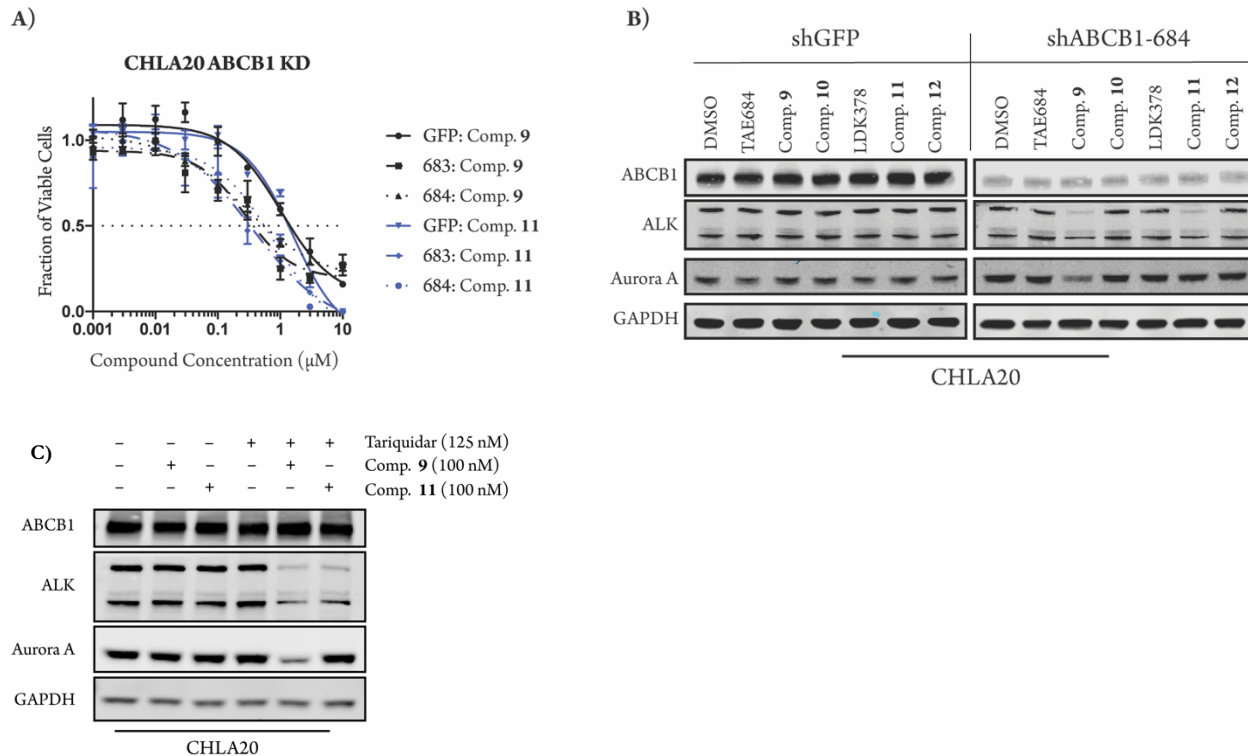


**Figure 2.5.** Recovery of degrader activity after shRNA knockdown of ABCB1. 683 indicates ABCB1 targeting shRNA TRCN0000059683 and 684 indicates ABCB1 targeting shRNA TRCN0000059684. (A) Anti-proliferation EC<sub>50</sub> curves  $\pm$  SD after 72 hr treatment (three biological replicates; Graphpad Prism 7 software). (B) Immunoblot of after shRNA knockdown and 16 hr treatment with 100 nM compound. (C) Tariquidar Controls: Immunoblots after 16 hours of treatment.

We next studied induced ALK degradation by immunoblots using Kelly and CHLA20 cells; CHLA20 cells were always co-treated with 125 nM tariquidar. In Kelly cells **9** and **11** were equipotent ALK degraders, with DC<sub>50</sub>s of 50 nM each as determined by western blot after 16 hr dose titrations (two independent experiments) (Figure 2.6A). As in the NSCLC and ALCL cell lines, **9** was less selective for ALK over Aurora A than **11** in both NB lines (Figure 2.6A). Time courses in the Kelly and CHLA20 cells showed that ALK degradation by the degraders could be observed after 4 hours of treatment in CHLA20 and after 8 hours in Kelly cells (Figure 2.6B). Interestingly, although pre-treatment with carfilzomib, MLN4924, or pomalidomide in both Kelly and CHLA20 cells did prevent Aurora A degradation (Figure 2.6C), only pomalidomide and parental inhibitor pre-treatment prevented ALK degradation. This may be due to carfilzomib and

MLN4924 causing an upregulation of lysosomal degradation by suppressing the ubiquitin-proteasome system.<sup>28</sup>

In Kelly cells **9** is equipotent to TAE684 at inhibiting downstream ALK signaling, while **11** is more potent than LDK378 at 16 hr (Figure 2.6D). In CHLA20 cells both degraders are more potent inhibitors of downstream ALK signaling than their parental inhibitors. **11** shows improved sustained inhibition of ALK phosphorylation compared to LDK378 in both Kelly and CHLA20 cells (Figure 2.6E). In Kelly and CHLA20 cells STAT3 feedback signaling was activated by the parental inhibitors, but not the degraders (Figure 2.6E). This observation indicates that STAT3 was not a downstream player in the anti-proliferative effects observed in these cells and that kinase degraders may have the advantage of preventing feedback activation of STAT3 that has been previously reported as a major drawback of kinase-targeted therapeutics.<sup>29</sup>

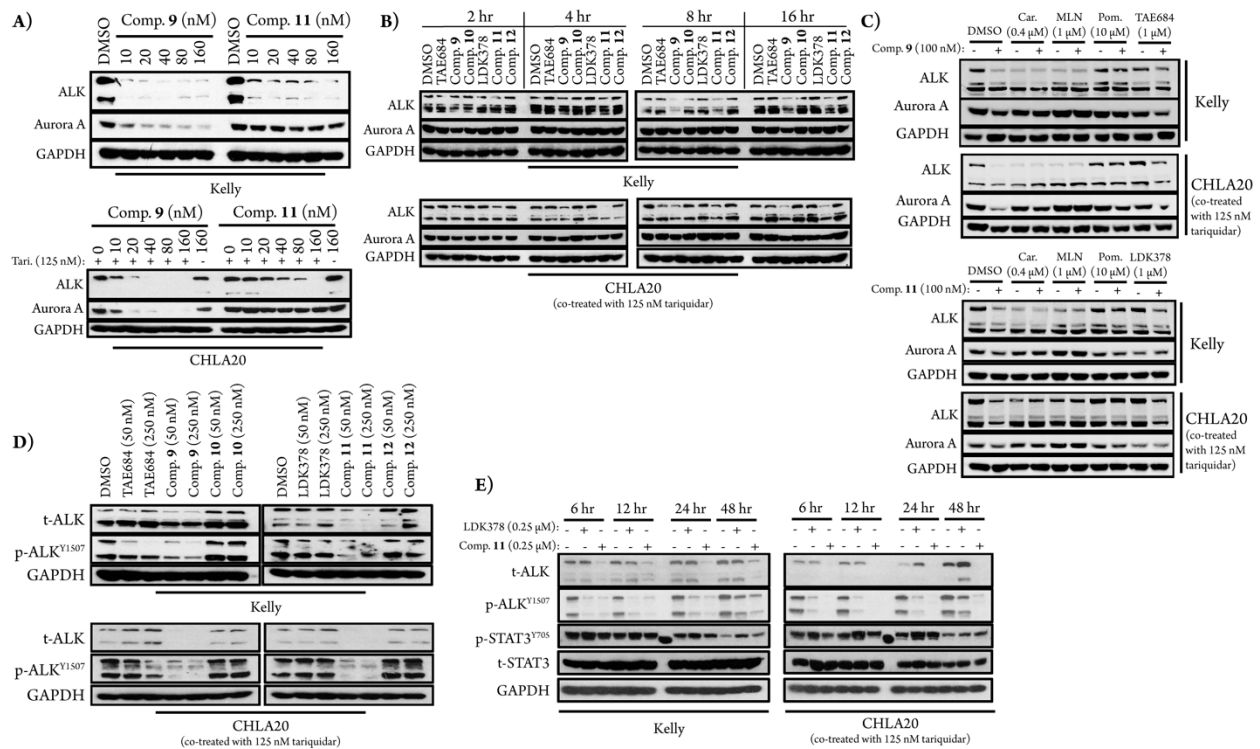
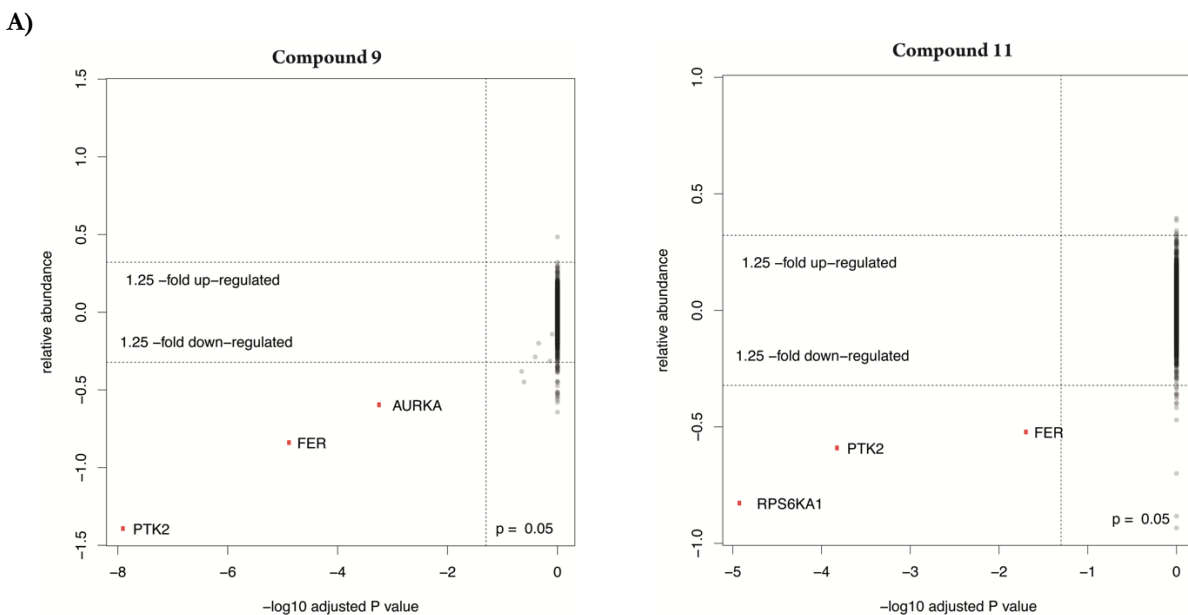


**Figure 2.6.** Degradation behavior in Kelly and CHLA20 cells. (A) Immunoblots after 16 hours of treatment with dose titrations of **9** and **11**. Tari. indicates tariquidar. (B) Immunoblots after treatment with 100 nM of compound for the indicated amount of time.

**Figure 2.6 (continued).**

(C) Immunoblots after 2-hour pre-treatments with DMSO, carfilzomib (Car), MLN4924 (MLN), pomalidomide (Pom), TAE684, or LDK378 followed by 16-hour treatments with **9** and **11**. (D) Immunoblots of downstream ALK signaling after 16-hour compound treatments; t-ALK indicates total ALK and p-ALK indicates phosphorylated ALK. (E) Immunoblots of sustained downstream ALK signaling after the indicated treatment times.

Expression proteomics was performed after 4 hours of treatment with **9** and **11** in Kelly cells; this early time point was selected in order to minimize secondary effects. However, a decrease in ALK abundance was not measured at a significant level for either compound (Figure 2.7). The degradation of targets other than ALK, including PTK2, FER, RPS6KA1, and Aurora A, was measured at significant levels and confirmed by western blot (Figures 2.8, 2.9); the degraded proteins detected by proteomics were shown during time courses to be more rapidly degraded than ALK, which may have resulted in the differences in detection by proteomics. PTK2, FER, and Aurora A have also been previously demonstrated to be very susceptible to kinase targeting degraders.<sup>20</sup> Interestingly, although **9** is a better inhibitor of RPS6KA1 than **11** (Table 2.2), **11** is a better RPS6KA1 degrader (Figures 2.7-9). These results highlight the importance of determining degrader selectivity profiles separately from their parental inhibitors. Since the ability to be degraded may vary for different protein targets, degrader selectivity must be carefully assessed. ALK degraders may be improved upon in the future by using more selective inhibitor scaffolds.



B)

**Compound 9**

Protein	log2FC	Adj. P Value
PTK2	-1.392582392	1.29E-08
AURKA	-0.596254743	0.000587464
FER	-0.839051817	1.35E-05
ALK	-0.381302597	0.2226114
RPS6KA1	-0.287469779	0.39418071
C12orf23; TMEM263	-0.199676432	0.454570329
GAK	-0.141362323	0.802000274
WHSC1; NSD2	0.104188671	0.999965934
CEBPZ	0.094411654	0.999965934
ADNP	0.102147146	0.999965934
ID1	-0.314671313	0.728293042
ZNF692	-0.448653497	0.244950757
UTP20	0.071000261	0.999965934
APOH	0.484537622	0.999965934
MYCN	-0.239175217	0.999965934

**Compound 11**

Protein	log2FC	Adj. P Value
PTK2	-0.590319724	0.000152641
RPS6KA1	-0.82730672	1.21E-05
FER	-0.521893044	0.020570468
RPS6KA3	-0.11103797	0.999887987
UBE2K	0.0774155	0.999887987
AHSA1	0.051315333	0.999887987
LIPE	0.14741429	0.999887987
ALKBH1	-0.205541519	0.999887987
DCX	0.154663879	0.999887987
GYG1	0.13569687	0.999887987
SPC24	0.205051303	0.999887987
B3GAT3	-0.158467869	0.999887987
CLSPN	-0.093161774	0.999887987
MRPL11	0.111227285	0.999887987
ALK	-0.211032794	0.999887987

**Figure 2.7.** Expression proteomics in Kelly cells after 4 hours of treatment with 100 nM of compound or DMSO (triplicate analysis). (A) Fold change in abundance comparing compounds **9** or **11** to **10** and DMSO or **12** and DMSO, respectively, on the y axis. Moderated *t*-test *P* values were calculated using the limma package and shown as  $-\log_{10}$  values on the x axis. (B) Tables of top fifteen proteomics hits (based on B values) for **9** and **11** with ALK highlighted.

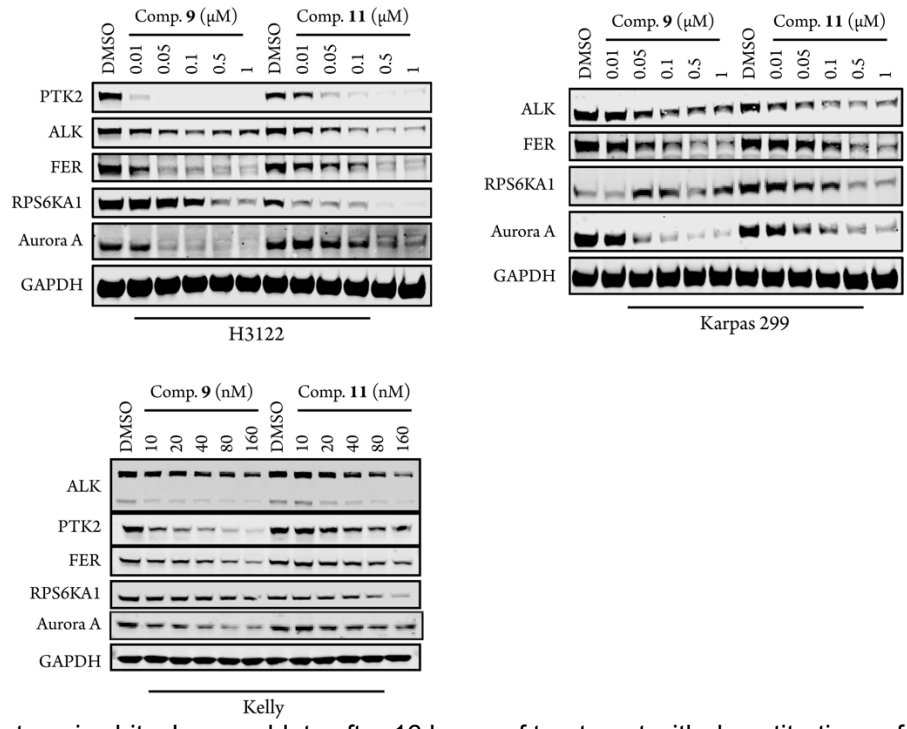


**Figure 2.8.** Proteomics hits: Immunoblots after 16 hours of treatment with dose titrations of compounds 9 and 11.

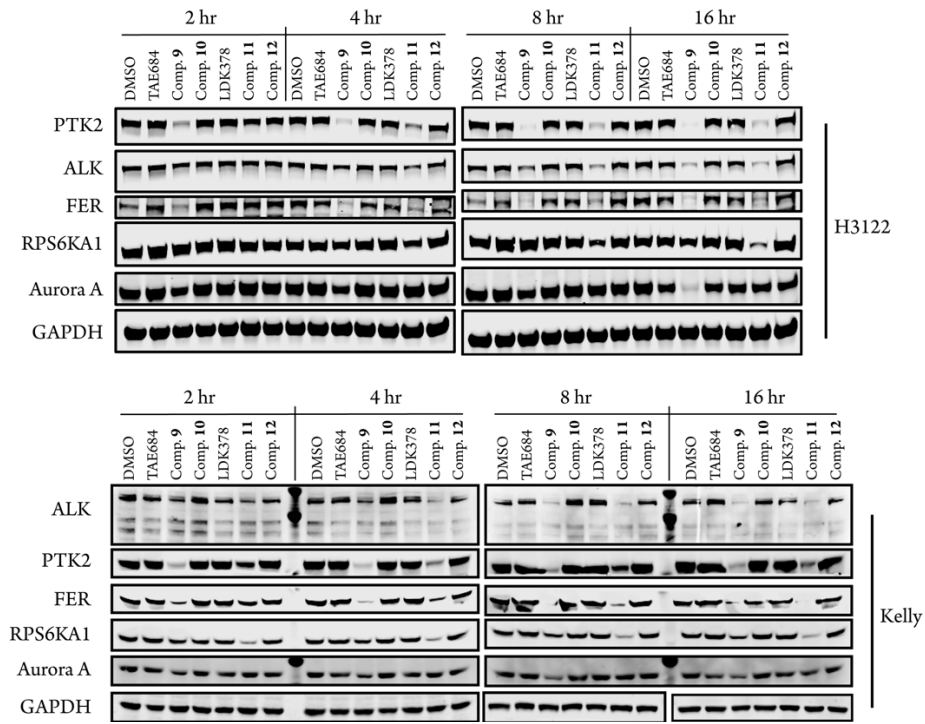


**Figure 2.9.** Proteomics hits time courses: Immunoblots after treatment with 250 nM of compound in H3122 cells or 100 nM of compound in Kelly cells for the indicated amount of time.

**Table 2.2.** Z'LYTE assay IC<sub>50</sub>s (nM)

	Aurora A	FER	PTK2	RPS6KA1
TAE684	9.26	4.18	20.5	15.1
Comp. 9	13.5	8.95	26.6	115
Comp. 10	11.3	5.74	18.4	65.0
LDK378	6550	15.8	27.9	316
Comp. 11	8550	42.4	25.4	677
Comp. 12	9080	23.1	21.2	480

The potential ability of degraders to overcome acquired resistance mutations was assessed using Ba/F3 cells expressing EML4-ALK with the resistant mutations L1196M, C1156Y, or G1202R (Figure 2.10). **9** and **11** both show a drop in anti-proliferative activity similar to the behavior seen with the parental ALK inhibitors when EML4-ALK has a resistant mutation. Since **9** and **11** have demonstrated that ALK is amenable to small molecule induced degradation, it is likely that future ALK targeting degraders based on ALK inhibitors that are able to overcome resistance mutations may have improved pharmacodynamic properties in these resistant mutant cell lines.

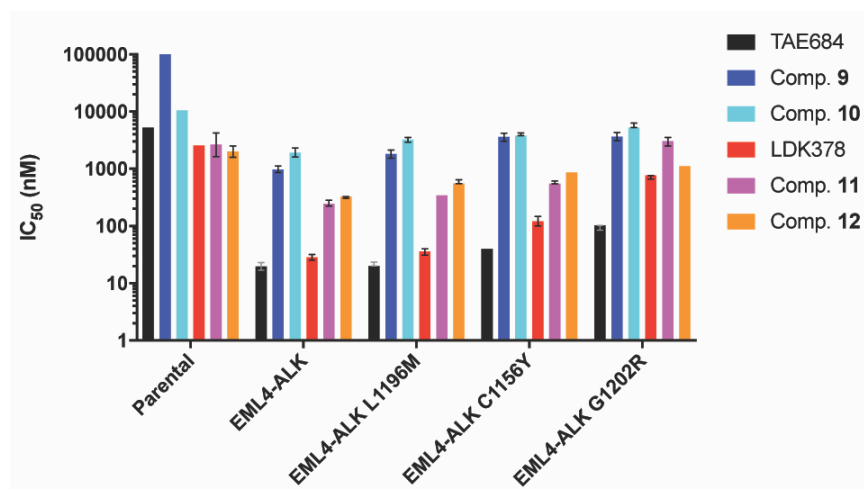


**Figure 2.10.** Anti-proliferative best fit EC<sub>50</sub> values with 95% CI in Ba/F3 parental cells and Ba/F3 cells expressing EML4-ALK and EML4-ALK with secondary mutations (three biological replicates). Cell viability was evaluated using the CellTiter-Glo Luminescent Cell Viability Assay (Promega) after 72 hr. Graphpad Prism 7 software; no error bar indicates that CI was not calculated by model.

While the efficacy of ALK degraders against resistant mutations must be explored further, this work does speak to potential challenges with resistance that may be inherent in the degrader technology since several processes must function together. In addition to the potential resistance by drug transporters demonstrated here, it is possible that factors such as cereblon down-regulation or deubiquitinase upregulation may impact degrader activity.

The pharmacokinetic properties of compounds **9** and **11** were examined at two doses for intraperitoneal (IP) injection (10 mg/kg and 50 mg/kg) and one dose for oral gavage (PO) (50 mg/kg) in male C57Bl/6 mice (Tables 2.3 and 2.4). The plasma exposure for **9** was high for the IP doses, but relatively poor after oral dosing. The  $C_{max}$  and AUC were not dose proportional for the 10 and 50 mg/kg IP doses, but both did increase as the dose was increased from 10 to 50 mg/kg. For **11**,  $C_{max}$  and AUC were dose proportional with IP dosing and there was modest oral bioavailability. Each of the IP groups had one mouse with sharply reduced plasma levels. It was unclear if the cause of the variability was due to precipitation, injection into or near a fat pad or another unknown reason. Notably, after treatment with **11** the mice were difficult to bleed, which is often seen if blood pressure decreases, and the blood had evidence of hemolysis. This was unexpected because the plasma levels of **11** were much higher in the IP groups and this issue was not observed with IP dosing. Therefore, it is possible that this reflects the generation of a metabolite either in the gut or with first-pass metabolism. This potential metabolite generation must be studied further.

**Table 2.3.** Pharmacokinetic data for compound **9**.

<i>Formulation: 1 mg/mL (IP, 10 mg/kg) and 5 mg/ml (IP+PO, 50 mg/Kg) solution in 5/5/90 DMSO/Tween80/10% Captisol</i>									
<b>10 mg/kg IP</b>									
Subject	T <sub>1/2</sub> hr	T <sub>max</sub> hr	C <sub>max</sub> ng/mL	C <sub>max</sub> μM	AUC <sub>last</sub> min*ng/mL	AUC <sub>last</sub> μM.hr	AUC <sub>INF_obs</sub> min*ng/mL	AUC <sub>%Extrap</sub>	Cl <sub>obs</sub> mL/min/kg
10 mg/Kg IP Mouse-1	1.72	0.50	1240	1.29	191210	3.32	199609	4.21	50.10
10 mg/Kg IP Mouse-2	1.45	0.50	1470	1.53	199876	3.47	203839	1.94	49.06
10 mg/Kg IP Mouse-3	1.98	0.25	1280	1.33	194620	3.38	206768	5.88	48.36
<b>Avg.</b>	<b>1.71</b>	<b>0.42</b>	<b>1330</b>	<b>1.38</b>	<b>195235</b>	<b>3.39</b>	<b>203405</b>	<b>4.01</b>	<b>49.17</b>
<b>50 mg/kg IP</b>									
Subject	T <sub>1/2</sub> hr	T <sub>max</sub> hr	C <sub>max</sub> ng/mL	C <sub>max</sub> μM	AUC <sub>last</sub> min*ng/mL	AUC <sub>last</sub> μM.hr	AUC <sub>INF_obs</sub> min*ng/mL	AUC <sub>%Extrap</sub>	Cl <sub>obs</sub> mL/min/kg
50 mg/Kg IP Mouse-4	4.11	0.25	2310	2.41	548970	9.53	741397	25.95	67.44
50 mg/Kg IP Mouse-5	3.77	0.25	2360	2.46	552100	9.58	707415	21.96	70.68
50 mg/Kg IP Mouse-6	3.79	0.08	2330	2.43	588490	10.21	713874	17.56	70.04
<b>Avg.</b>	<b>3.89</b>	<b>0.19</b>	<b>2333</b>	<b>2.43</b>	<b>563187</b>	<b>9.77</b>	<b>720895</b>	<b>21.82</b>	<b>69.39</b>
<b>50 mg/kg PO</b>									
Subject	T <sub>1/2</sub> hr	T <sub>max</sub> hr	C <sub>max</sub> ng/mL	C <sub>max</sub> μM	AUC <sub>last</sub> min*ng/mL	AUC <sub>last</sub> μM.hr	AUC <sub>INF_obs</sub> min*ng/mL	AUC <sub>%Extrap</sub>	Cl <sub>obs</sub> mL/min/kg
50 mg/Kg PO Mouse-7	0.51	6.00	198	0.21	24596	0.43	25175	2.30	1986.09
50 mg/Kg PO Mouse-8	0.45	6.00	166	0.17	20444	0.35	20739	1.43	2410.89
50 mg/Kg PO Mouse-9	1.95	6.00	32	0.03	5786	0.10	8449	31.52	5917.80
<b>Avg.</b>	<b>0.97</b>	<b>6.00</b>	<b>132</b>	<b>0.14</b>	<b>16942</b>	<b>0.29</b>	<b>18121</b>	<b>11.75</b>	<b>3438.26</b>

**Table 2.4.** Pharmacokinetic data for compound **11**. Note: Mice 1 and 4 had sharply reduced plasma levels compared to other members in their experimental groups and were therefore excluded from the averages. Mice 8 and 9 were difficult to bleed with evidence of hemolysis in plasma.

<i>Formulation: 1 mg/mL (IP, 10 mg/kg) and 5 mg/ml (IP+PO, 50 mg/Kg) solution in 5/5/90 DMSO/Tween80/10% Captisol</i>									
<b>10 mg/kg IP</b>									
Subject	T <sub>1/2</sub> hr	T <sub>max</sub> hr	C <sub>max</sub> ng/mL	C <sub>max</sub> μM	AUC <sub>last</sub> min*ng/mL	AUC <sub>last</sub> μM.hr	AUC <sub>INF_obs</sub> min*ng/mL	AUC <sub>%Extrap</sub>	Cl <sub>obs</sub> mL/min/kg
10 mg/Kg IP- Mouse-1	2.4	0.25	435	0.43	27593	0.46	31918	13.6	313
10 mg/Kg IP Mouse-2	2.3	0.25	723	0.72	142994	2.38	158071	9.5	63
10 mg/Kg IP Mouse-3	2.7	0.25	1850	1.85	190285	3.17	222404	14.4	45
<b>Avg.</b>	<b>2.5</b>	<b>0.3</b>	<b>1287</b>	<b>1.3</b>	<b>166639</b>	<b>2.8</b>	<b>190237</b>	<b>12.0</b>	<b>54.1</b>
<b>50 mg/kg IP</b>									
Subject	T <sub>1/2</sub> hr	T <sub>max</sub> hr	C <sub>max</sub> ng/mL	C <sub>max</sub> μM	AUC <sub>last</sub> min*ng/mL	AUC <sub>last</sub> μM.hr	AUC <sub>INF_obs</sub> min*ng/mL	AUC <sub>%Extrap</sub>	Cl <sub>obs</sub> mL/min/kg
50 mg/Kg IP- Mouse-4	24.5	0.25	46	0.05	6027	0.10	49039	87.7	1020
50 mg/Kg IP Mouse-5	3.4	0.50	3600	3.59	672730	11.20	817964	17.8	61
50 mg/Kg IP Mouse-6	2.6	0.25	5330	5.32	676075	11.25	762335	11.3	66
<b>Avg.</b>	<b>3.0</b>	<b>0.38</b>	<b>4465.00</b>	<b>4.46</b>	<b>674403</b>	<b>11.22</b>	<b>790149</b>	<b>14.5</b>	<b>63</b>
<b>50 mg/kg PO</b>									
Subject	T <sub>1/2</sub> hr	T <sub>max</sub> hr	C <sub>max</sub> ng/mL	C <sub>max</sub> μM	AUC <sub>last</sub> min*ng/mL	AUC <sub>last</sub> μM.hr	AUC <sub>INF_obs</sub> min*ng/mL	AUC <sub>%Extrap</sub>	Cl <sub>obs</sub> mL/min/kg
50 mg/Kg PO Mouse-7		0.25	541	0.54	13364	0.22	29020		
50 mg/Kg PO Mouse-8		0.25	117	0.12	12561	0.21	95032		
50 mg/Kg PO Mouse-9		6.00	669	0.67	108901	1.81			
<b>Avg.</b>		<b>2.17</b>	<b>442</b>	<b>0.44</b>	<b>44942</b>	<b>0.75</b>	<b>62026</b>		

## 2.3 Conclusion

By linking known ALK inhibitors TAE684 and LDK378 to pomalidomide we have provided prototypical examples that ALK degradation may be induced by E3 ligase recruitment in three major ALK-positive disease models. These compounds have displayed the ability to improve upon the pharmacodynamic properties of their parental inhibitors, especially sustained inhibition of downstream ALK signaling, indicating that degraders are a promising new avenue for targeted ALK therapies.

## 2.4 Alectinib-Based ALK Degraders

*Attributions:* An additional 7 ALK degraders were tested as part of this thesis work. The data in this section was included in US Patent Application Number 62/737,533, titled “DEGRADERS THAT TARGET ALK AND THERAPEUTIC USES THEREOF,” which was submitted by Dana-Farber Cancer Institute. Inventors included on this patent application were: Chelsea E. Powell, John M. Hatcher, Pasi A. Jänne, and Nathanael S. Gray, who are all affiliated with Dana-Farber Cancer Institute.

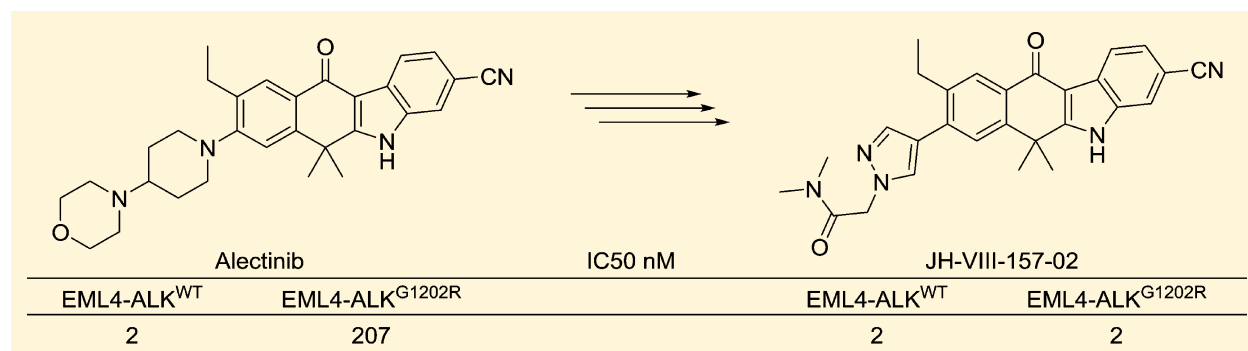


**Figure 2.11.** Structures of alectinib and JH-VIII-157-02. Figure from Hatcher et al, *J Med Chem* (2015).<sup>30</sup>

We have begun further ALK degrader medicinal chemistry efforts based around alectinib and JH-VIII-157-02, an alectinib analog that is able to overcome the G1202R mutation (Figure 2.11).<sup>30</sup> We generated three cereblon-recruiting ALK degraders using alectinib, referred to as the 200 series (Figure 2.12A). 200 series compounds with PEG linkers (JH-XIII-200-1 and JH-XIII-200-2) display anti-proliferative activity in H3122 cells that is comparable to the previously reported ALK degrader TL13-112 (compound 11) (Figure 2.12B); the 200 series compound with a carbon linker, JH-XIII-200-3, displays 10-fold lower activity than TL13-112. Additionally, the 200 series compounds with PEG linkers show activity against EML4-ALK with secondary mutations L1196M, C1156Y, or G1202R that is comparable to the parental inhibitor alectinib. 200 series compounds with PEG linkers display the ability to degrade ALK in a dose dependent manner in

H3122 cells after 16 hr treatments (Figure 2.12C). Off target degradation of Aurora A is also seen. Notably, off target degradation of PTK2 is very low, unlike the previously reported compounds **9** and **11**. The 200 series compound with a carbon linker induces only minimal ALK degradation; this complements the differences in anti-proliferative activity seen with the 200-series in EML4-ALK expressing cell lines. The 200-series is able to degrade ALK around 4 hours with maximum degradation seen around 16 hours (Figure 2.12D). However, the maximum degradation seen is less than what is seen with TL13-112 (compound **11**).

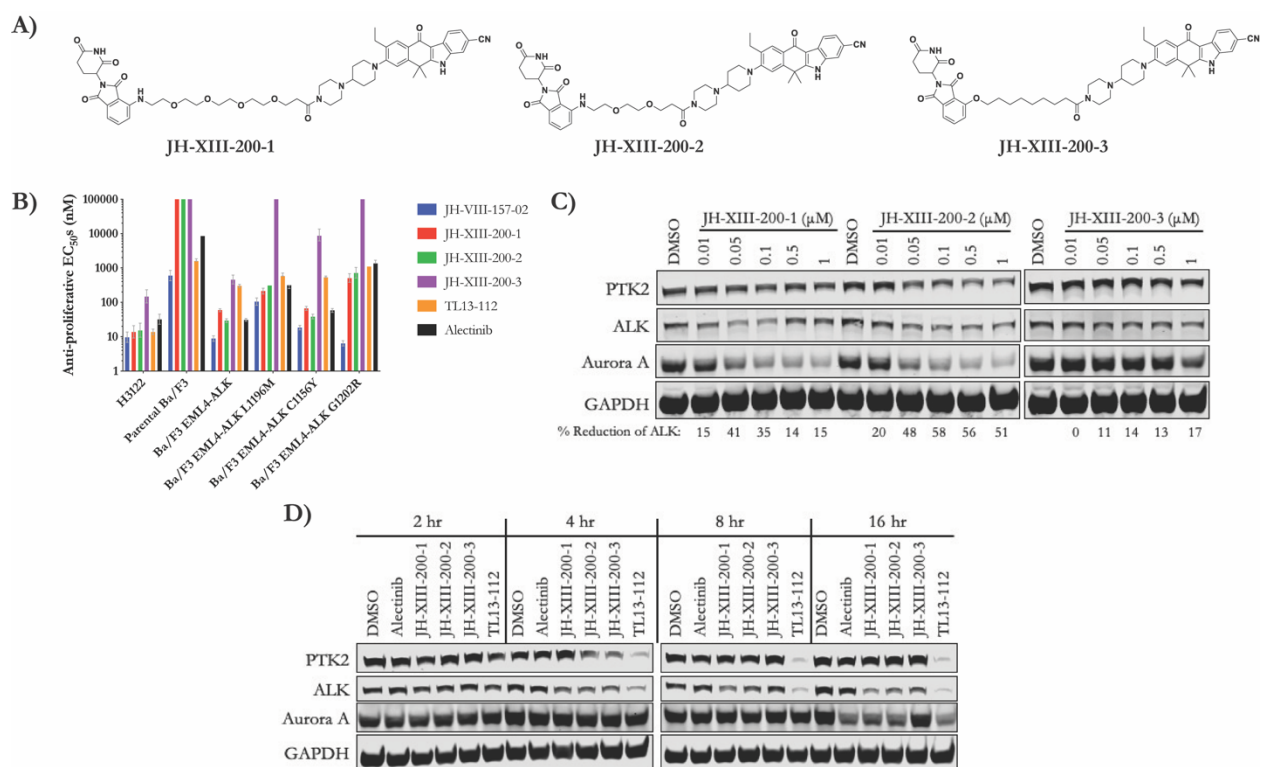


**Figure 2.12.** 200 series degrader behavior. (A) Structures of alectinib-based degraders. (B) Anti-proliferative best fit  $EC_{50}$  values with 95% CI after 72 hr treatments (three biological replicates; Graphpad Prism 7 software; compounds with no activity are indicated by 100,000 nM  $EC_{50}$ s). (C) Immunoblot after 16 hours of treatment in H3122 cells. (D) Immunoblot after treatment with 100 nM of compound for the indicated amount of time in H3122 cells.

We also generated three cereblon-recruiting ALK degraders using JH-VIII-157-02, referred to as the 114 series (Figure 2.13A). Although some anti-proliferative effects are seen with these compounds, their activity is less than that of the previous ALK degrader TL13-112 by an

order of magnitude (Figure 2.13B). Only the compound with the longest linker, JH-XIII-114-2, induced ALK degradation to a measurable extent (Figure 2.13C). JH-XIV-61 was designed with the same warheads as the 114-series for engaging ALK and CRBN, JH-VIII-157-02 and pomalidomide, respectively (Figure 2.14A). However, the 114-series compounds have an N-H amide that can form an intramolecular hydrogen bond with the pyrazole, which may change the trajectory of the warhead. JH-XIV-61 has an N-methyl amide, instead of the N-H amide, with the goal of improving on 114-series activity by preventing the intramolecular hydrogen bond with the pyrazole. However, the anti-proliferative activity shows that JH-XIV-61 has similar activity as a member of the 114 series, and has lower anti-proliferative activity than a member of the 200 series and TL13-112 in EML4-ALK expressing cells (Figure 2.14B). JH-XIV-61 also does not induce measurable ALK degradation (Figure 2.14C).

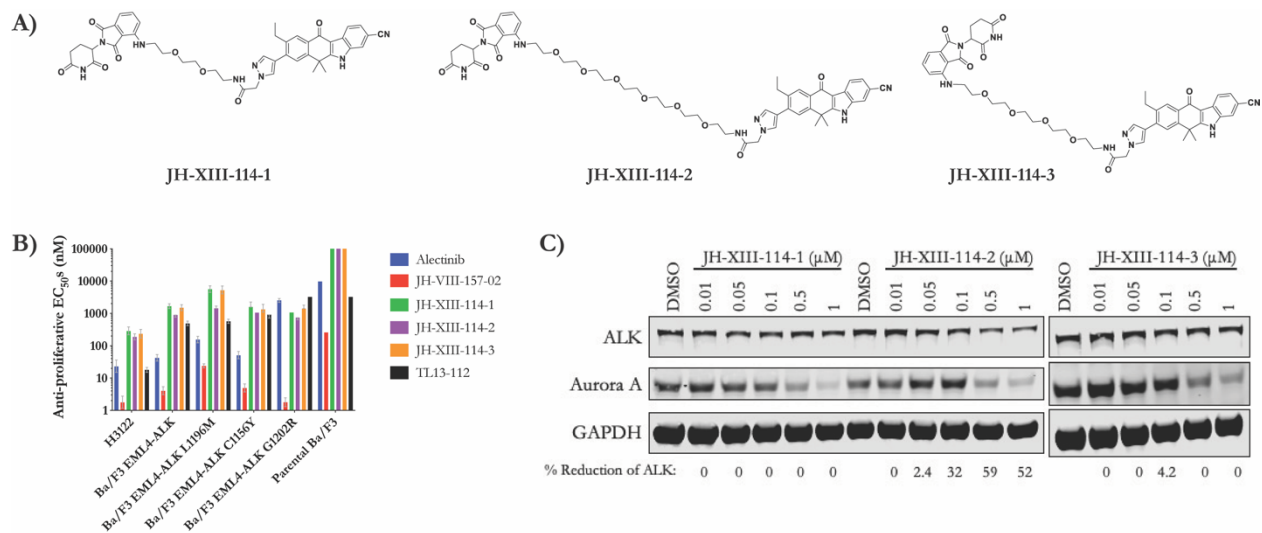


**Figure 2.13.** 114 series degrader behavior. (A) Structures of JH-VIII-157-02-based degraders. (B) Anti-proliferative best fit  $EC_{50}$  values with 95% CI after 72 hr treatments (three biological replicates; Graphpad Prism 7 software; compounds with no activity are indicated by 100,000 nM  $EC_{50}$ s). (C) Immunoblot after 16 hours of treatment in H3122 cells.

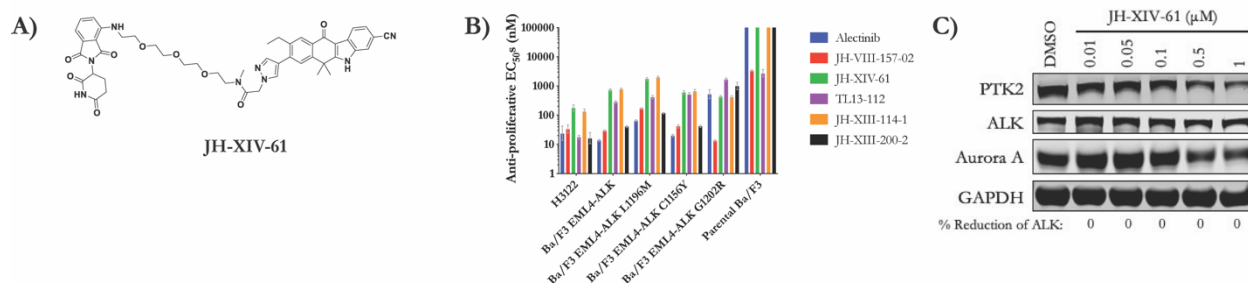


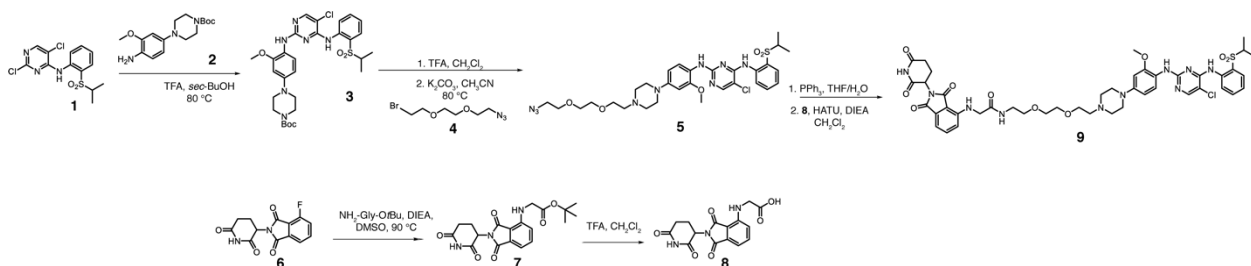
**Figure 2.14.** JH-XIV-61 degrader behavior. (A) Structure of JH-XIV-61. (B) Anti-proliferative best fit  $EC_{50}$  values with 95% CI after 72 hr treatments (three biological replicates; Graphpad Prism 7 software; compounds with no activity are indicated by 100,000 nM  $EC_{50}$ s). (C) Immunoblot after 16 hours of treatment in H3122 cells.

For further examination of the potential of the alectinib scaffold for designing an ALK degrader, we plan to explore the use of alectinib analogs that are weaker ALK binders. We hypothesize that the strong binding of alectinib and JH-VIII-157-02 to ALK may be preventing compound turnover, which is resulting in the lower degradation activity seen with the 200 and 114 series compared to compounds **9** and **11** (TL13-12 and TL13-112). Other major medicinal chemistry routes that we will explore in the future include the use of lorlatinib and its analogs for recruiting ALK, as well as the use of ligands for recruiting the Von Hippel-Lindau (VHL) E3 ligase, which has been shown to be a viable strategy for inducing ALK degradation.<sup>31</sup>

## 2.5 Experimental Methods

Unless otherwise noted, reagents and solvents were obtained from commercial suppliers and were used without further purification.  $^1\text{H}$  NMR spectra were recorded on 500 MHz (Bruker A500), and chemical shifts are reported in parts per million (ppm,  $\delta$ ) downfield from tetramethylsilane (TMS). Coupling constants ( $J$ ) are reported in Hz. Spin multiplicities are described as s (singlet), br (broad singlet), d (doublet), t (triplet), q (quartet), and m (multiplet). Mass spectra were obtained on a Waters Micromass ZQ instrument. Preparative HPLC was performed on a Waters Sunfire C18 column (19 x 50 mm, 5 $\mu\text{M}$ ) using a gradient of 15-95% methanol in water containing 0.05% trifluoroacetic acid (TFA) over 22 min (28 min run time) at a flow rate of 20 mL/min. Purities of assayed compounds were in all cases greater than 95%, as determined by reverse-phase HPLC analysis.

**Scheme 2.1.** Synthesis of **9**



**tert-butyl 4-(4-((5-chloro-4-((2(isopropylsulfonyl)phenyl)amino)pyrimidin-2yl)amino)-3-methoxyphenyl)piperazine-1-carboxylate (3).** Intermediate **1** was prepared according to the literature,<sup>32</sup> while *tert*-butyl 4-(4-amino-3-methoxyphenyl) piperazine-1-carboxylate (**2**) was commercially available. To **1** (693 mg, 2.0 mmol) and **2** (740 mg, 2.4 mmol) in *sec*-butanol (4 mL) was added TFA (185  $\mu\text{L}$ , 2.4 mmol) and the mixture was stirred overnight at 80 °C. The mixture was then concentrated and purified by column chromatography (dichloromethane:methanol = 20:1) to yield 925 mg (75%) of **3** as a white solid.  $^1\text{H}$  NMR (400

MHz, CDCl<sub>3</sub>) δ 9.54 (s, 1H), 8.60 (d, J = 8.4 Hz, 1H), 8.13 (s, 1H), 8.06 (d, J = 7.2 Hz, 1H), 7.91 (d, J 8.0 Hz, 1H), 7.62 (dd, J = 8.8, 8.4 Hz, 1H), 7.33 (s, 1H), 7.25 (dd, J = 8.4, 8.4 Hz, 1H), 6.55 (s, 1H), 6.47 (d, J = 8.8 Hz, 1H), 3.88 (s, 3H), 3.60 (m, 4H), 3.24 (m, 1H), 3.09 (m, 4H), 1.49 (s, 9H), 1.30 (d, J = 7.2 MS (ESI) m/z 617 (M+H)<sup>+</sup>.

**N<sup>2</sup>-(4-(4-(2-(2-(2-azidoethoxy)ethoxy)ethyl)piperazin-1-yl)-2-methoxyphenyl)-5-chloro-N<sup>4</sup>-(2-(isopropylsulfonyl)phenyl) pyrimidine-2,4-diamine (5).** To **3** (620 mg, 1.0 mmol) in dichloromethane (18 mL) TFA was added (1.8 mL) and the mixture was stirred at room temperature (RT) for 2 h, then was concentrated and dried under vacuum. To the obtained crude intermediate in acetonitrile (5 mL) was added commercially available bromide **4** (300 mg, 1.2 mmol) and potassium carbonate (414 mg, 3.0 mmol). The resulted mixture was stirred under 80 °C overnight, then cooled down to RT and diluted with 50 mL of dichloromethane. The precipitation was filtered, and the filtrate was concentrated and purified by column chromatography (dichloromethane:methanol = 10:1) to yield 524 mg (78%) of **11** as a colorless oil. <sup>1</sup>H NMR (400 MHz, DMSO-*d*<sub>6</sub>) δ 9.54 (s, 1H), 8.62 (d, J = 8.4 Hz, 1H), 8.13 (s, 1H), 8.02 (d, J = 8.4 Hz, 1H), 7.91 (d, J = 8.0 Hz, 1H), 7.62 (dd, J = 8.0, 8.0 Hz, 1H), 7.30 (m, 2H), 6.56 (s, 1H), 6.48 (d, J = 8.4 Hz, 1H), 3.88 (s, 3H), 3.70 (m, 10H), 3.25 (m, 1H), 3.41 (t, J = 5.2 Hz, 2H), 3.20 (m, 4H), 2.70 (m, 4H), 1.32 (d, J = 7.2 Hz, 6H). MS (ESI) m/z 674 (M+H)<sup>+</sup>.

**tert-butyl(2-(2,6-dioxopiperidin-3-yl)-1,3-dioxoisindolin-4-yl)glycinate (7).** Intermediate **6** was prepared according to the literature.<sup>33</sup> To **6** (550 mg, 2.0 mmol) and glycine *tert*-butyl ester (260 mg, 2.0 mmol) in anhydrous DMSO (20 mL) was added *N,N*-diisopropylethylamine (DIEA) (700 μL, 4.0 mmol). The reaction mixture was stirred under 90 °C for 1 day, then cooled down. The mixture was diluted with ethyl acetate (200 mL), washed with water and brine, dried with Na<sub>2</sub>SO<sub>4</sub>, then filtered and concentrated, purified by column chromatography (dichloromethane:ethyl acetate = 2:1) to yield 530 mg (68%) of **7** as a yellow oil. <sup>1</sup>H NMR (400 MHz, CDCl<sub>3</sub>) δ 8.06 (s, 1H), 7.51 (dd, J = 8.4, 7.2 Hz, 1H), 7.15 (d, J = 7.6 Hz, 1H),

6.76 (d,  $J = 6.76$  Hz, 1H), 4.93 (dd,  $J = 12.0, 6.4$  Hz, 1H), 3.94 (s, 2H), 2.67-2.92 (m, 2H), 2.12 (m, 1H), 1.93 (m, 1H), 1.50 (s, 9H). MS (ESI)  $m/z$  388 (M+H)<sup>+</sup>.

**2-(2,6-dioxopiperidin-3-yl)-1,3-dioxoisindolin-4-yl glycine (8)**. To **7** (390 mg, 1.0 mmol) in dichloromethane (18 mL) added TFA (1.8 mL). The mixture was stirred at RT overnight, then was concentrated and dried under vacuum to give **8** as a yellow solid, which was used in next step without purification. MS (ESI)  $m/z$  330 (M-H)<sup>-</sup>.

**N-(2-(2-(2-(4-(4-((5-chloro-4-((2-(isopropylsulfonyl)phenyl)amino)pyrimidin-2-yl)amino)-3-methoxyphenyl)piperazin-1-yl)ethoxy)ethoxy)ethyl)-2-((2-(2,6-dioxopiperidin-3-yl)-1,3-dioxoisindolin-4-yl)amino)acetamide (TL-13-12) (9)**. Under a nitrogen atmosphere, to **5** (135 mg, 0.2 mmol) in tetrahydrofuran (18 mL) and water (1.8 mL) was added triphenylphosphine (63 mg, 0.24 mmol). The reaction mixture was stirred overnight, then concentrated and dried under vacuum. To the obtained crude oil in anhydrous dichloromethane (3 mL) was added **8** (73 mg, 0.22 mmol) and (1-[bis(dimethylamino)methylene]-1*H*-1,2,3-triazolo [4,5-*b*]pyridinium 3-oxid hexafluorophosphate) (HATU) and DIEA (110  $\mu$ L, 0.6 mmol). The reaction mixture was stirred for 2 h, then concentrated and purified by column chromatography (dichloromethane:methanol = 10:1) to yield 136 mg (71%) of **9** as a yellow foam. <sup>1</sup>H NMR (500 MHz, DMSO-*d*<sub>6</sub>)  $\delta$  11.10 (s, 1H), 9.76 (br, 1H), 9.57 (s, 1H), 8.56 (br, 1H), 8.41 (H, 1H), 8.19 (s, 1H), 8.18 (m, 1H), 7.81 (d,  $J = 8.0$  Hz, 1H), 7.60 (m, 1H), 7.57 (dd,  $J = 8.0, 7.5$  Hz, 1H), 7.41 (d,  $J = 8.5$  Hz, 1H), 7.30 (dd,  $J = 8.0, 7.5$  Hz, 1H), 7.07 (d,  $J = 7.0$  Hz, 1H), 6.95 (m, 1H), 6.85 (d,  $J = 8.5$  Hz, 1H), 6.71 (d,  $J = 2.5$  Hz, 1H), 6.53 (dd,  $J = 8.5, 2.5$  Hz, 1H), 5.07 (dd,  $J = 13.0, 5.5$  Hz, 1H), 3.94 (d,  $J = 5.0$  Hz, 2H), 3.85 (m, 2H), 3.80 (m, 2H), 3.76 (s, 3H), 3.58 (m, 4H), 3.45 (m, 4H), 3.40 (m, 4H), 3.30 (m, 2H), 3.24 (m, 2H), 3.03 (m, 2H), 2.53-2.63 (m, 2H), 1.16 (d,  $J = 7.0$  Hz, 6H). MS (ESI)  $m/z$  961 (M+H)<sup>+</sup>.

**10**, **11** and **12** were synthesized with similar procedures as **9**.

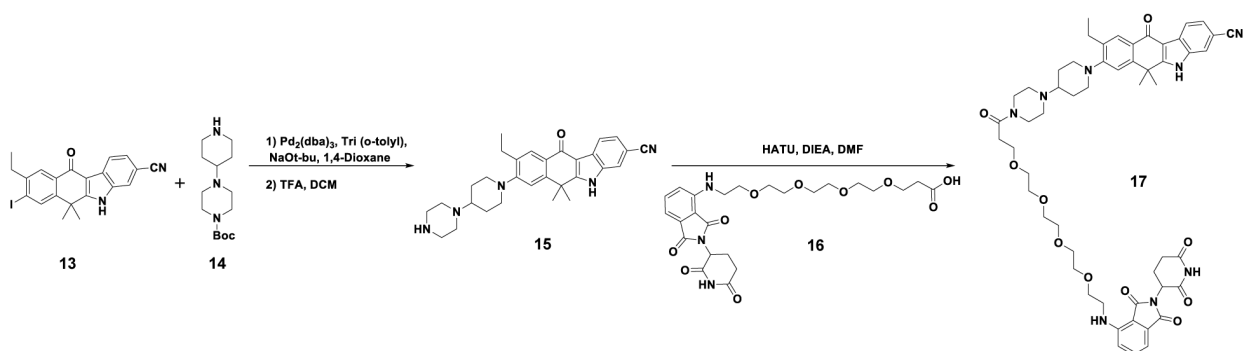
***N*-(2-(2-(2-(4-(4-((5-chloro-4-((2-(isopropylsulfonyl)phenyl)amino)pyrimidin-2-yl)amino)-3-methoxyphenyl)piperazin-1-yl)ethoxy)ethoxy)ethyl)-2-((1,3-dioxo-2-(2-oxopiperidin-3-yl)isoindolin-4-yl)amino)acetamide (TL13-22) (10).** <sup>1</sup>H NMR (500 MHz, DMSO-*d*<sub>6</sub>) δ 9.78 (br, 1H), 9.59 (s, 1H), 8.55 (br, 1H), 8.44 (s, 1H), 8.20 (s, 1H), 8.18 (dd, *J* = 6.0, 5.5 Hz, 1H), 7.82 (s, 1H), 7.81 (d, *J* = 8.0 Hz, 1H), 7.60 (m, 1H), 7.55 (dd, *J* = 8.0, 7.5 Hz, 1H), 7.40 (d, *J* = 8.5 Hz, 1H), 7.31 (dd, *J* = 7.5, 7.5 Hz, 1H), 7.04 (d, *J* = 7.0 Hz, 1H), 6.95 (m, 1H), 6.82 (d, *J* = 8.5 Hz, 1H), 6.71 (d, *J* = 2.5 Hz, 1H), 6.53 (dd, *J* = 8.5, 2.5 Hz, 1H), 4.52 (dd, *J* = 12.0, 6.5 Hz, 1H), 3.93 (d, *J* = 4.5 Hz, 2H), 3.85 (m, 2H), 3.80 (m, 2H), 3.77 (s, 3H), 3.60 (m, 4H), 3.57 (m, 2H), 3.46 (m, 4H), 3.40 (m, 2H), 3.30 (m, 2H), 3.22 (m, 2H), 3.03 (m, 2H), 2.20 (m, 1H), 1.96 (m, 1H), 1.89 (m, 2H), 1.16 (d, *J* = 6.5 Hz, 6H). MS (ESI) *m/z* 947 (M+H)<sup>+</sup>.

***N*-(2-(2-(2-(4-(4-((5-chloro-4-((2-(isopropylsulfonyl)phenyl)amino)pyrimidin-2-yl)amino)-5-isopropoxy-2-methylphenyl)piperidin-1-yl)ethoxy)ethoxy)ethyl)-2-((2-(2,6-dioxopiperidin-3-yl)-1,3-dioxoisoindolin-4-yl)amino)acetamide (TL13-112) (11).** <sup>1</sup>H NMR (500 MHz, DMSO-*d*<sub>6</sub>) δ 11.09 (s, 1H), 9.59 (s, 1H), 9.46 (s, 1H), 8.44 (d, *J* = 8.5 Hz, 1H), 8.38 (br, 1H), 8.25 (s, 1H), 8.18 (dd, *J* = 6.0, 5.5 Hz, 1H), 8.09 (s, 1H), 7.83 (d, *J* = 8.0 Hz, 1H), 7.60 (dd, *J* = 8.5, 8.0 Hz, 1H), 7.57 (dd, *J* = 8.0, 7.5 Hz, 1H), 7.34 (dd, *J* = 8.5, 8.0 Hz, 1H), 7.06 (d, *J* = 6.0 Hz, 1H), 6.93 (dd, *J* = 5.5, 5.5 Hz, 1H), 6.84 (d, *J* = 9.0 Hz, 1H), 6.75 (s, 1H), 5.06 (dd, *J* = 13.0, 5.5 Hz, 1H), 4.48 (m, *J* = 6.0 Hz, 1H), 3.93 (d, *J* = 5.5 Hz, 2H), 3.78 (m, 2H), 3.59 (m, 4H), 3.56 (m, 2H), 3.44 (m, 4H), 3.28 (m, 2H), 3.13 (m, 4H), 2.83-2.99 (m, 2H), 2.52-2.61 (m, 1H), 2.13 (s, 3H), 1.85-2.04 (m, 4H), 1.22 (d, *J* = 6.0 Hz, 6H), 1.15 (d, *J* = 7.0 Hz, 6H). MS (ESI) *m/z* 1002 (M+H)<sup>+</sup>.

***N*-(2-(2-(2-(4-(4-((5-chloro-4-((2-(isopropylsulfonyl)phenyl)amino)pyrimidin-2-yl)amino)-5-isopropoxy-2-methylphenyl)piperidin-1-yl)ethoxy)ethoxy)ethyl)-2-((1,3-dioxo-2-(2-oxopiperidin-3-yl)isoindolin-4-yl)amino)acetamide (TL13-110) (12).** <sup>1</sup>H NMR (500 MHz, DMSO-*d*<sub>6</sub>) δ 9.46 (s, 1H), 8.46 (d, *J* = 8.5 Hz, 1H), 8.25 (s, 1H), 8.16 (dd, *J* = 5.5, 5.0 Hz, 1H),

8.07 (s, 1H), 7.84 (d,  $J = 8.0$  Hz, 1H), 7.81 (s, 1H), 7.61 (dd,  $J = 8.5, 8.0$  Hz, 1H), 7.55 (dd,  $J = 8.0, 7.5$  Hz, 1H), 7.52 (s, 1H), 7.35 (dd,  $J = 8.5, 8.0$  Hz, 1H), 7.03 (d,  $J = 6.0$  Hz, 1H), 6.93 (dd,  $J = 6.0, 5.5$  Hz, 1H), 6.83 (d,  $J = 8.5$  Hz, 1H), 6.78 (br, 1H), 4.52 (dd,  $J = 12.0, 6.0$  Hz, 1H), 3.92 (d,  $J = 5.5$  Hz, 2H), 3.54 (m, 6H), 3.45 (m, 4H), 3.29 (m, 4H), 3.21 (m, 4H), 2.20 (m, 3H), 2.12 (s, 3H), 1.81-2.00 (m, 6H), 1.22 (d,  $J = 6.0$  Hz, 6H), 1.16 (d,  $J = 6.5$  Hz, 6H). MS (ESI)  $m/z$  988 (M+H)<sup>+</sup>.

**Scheme 2.2.** Synthesis of JH-XIII-200-1 (17).



**9-ethyl-8-iodo-6,6-dimethyl-11-oxo-6,11-dihydro-5H-benzo[b]carbazole-3-carbonitrile (13)** and **tert-butyl 4-(piperidin-4-yl)piperazine-1-carboxylate (14)** are commercially available.

**9-ethyl-6,6-dimethyl-11-oxo-8-(4-(piperazin-1-yl)piperidin-1-yl)-6,11-dihydro-5H-benzo[b]carbazole-3-carbonitrile (15)**. Compound **15** was prepared according to literature procedure<sup>30</sup> followed by treatment with 10% TFA in DCM (10 mL) for 1 hour. The solvent was then removed under vacuum and the product used without further purification. MS (ESI)  $m/z$  482.47 (M+H)<sup>+</sup>.

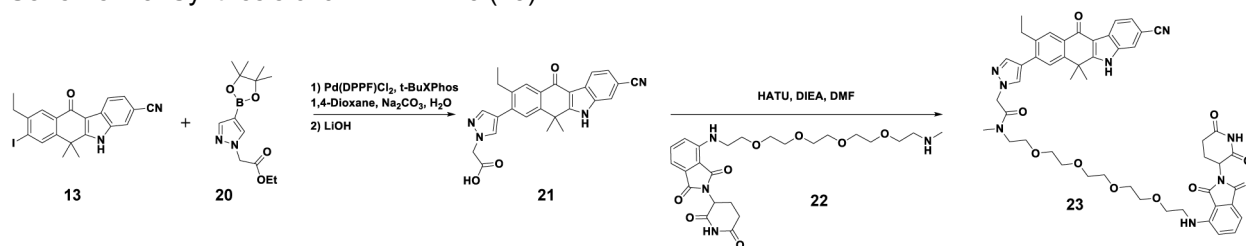
**8-(4-(4-(1-((2-(2,6-dioxopiperidin-3-yl)-1,3-dioxoisindolin-4-yl)amino)-3,6,9,12-tetraoxapentadecan-15-oyl)piperazin-1-yl)piperidin-1-yl)-9-ethyl-6,6-dimethyl-11-oxo-6,11-dihydro-5H-benzo[b]carbazole-3-carbonitrile (JH-XIII-200-1) (17)**. To a stirred solution of 9-ethyl-6,6-dimethyl-11-oxo-8-(4-(piperazin-1-yl)piperidin-1-yl)-6,11-dihydro-5H-

benzo[b]carbazole-3-carbonitrile (**15**) (20 mg, 0.04 mmol), 1-((2-(2,6-dioxopiperidin-3-yl)-1,3-dioxoisindolin-4-yl)amino)-3,6,9,12-tetraoxapentadecan-15-oic acid (**16**) (22 mg, 0.04 mmol), HATU (30 mg, 0.08 mmol) was added DIEA (35  $\mu$ L, 0.2 mmol). The mixture was stirred for 15 minutes and then purified by reverse phase HPLC using a gradient of 1% to 70% ACN in H<sub>2</sub>O to give the desired product as a yellow solid (22mg, 56% yield). MS (ESI) m/z 986.38 (M+H)<sup>+</sup>.

**8-(4-(4-(3-(2-(2-((2-(2,6-dioxopiperidin-3-yl)-1,3-dioxoisindolin-4-yl)amino)ethoxy)ethoxy)propanoyl)piperazin-1-yl)piperidin-1-yl)-9-ethyl-6,6-dimethyl-11-oxo-6,11-dihydro-5H-benzo[b]carbazole-3-carbonitrile (JH-XIII-200-2) (18)**. Prepared using the same procedure for **17** and 3-(2-(2-((2-(2,6-dioxopiperidin-3-yl)-1,3-dioxoisindolin-4-yl)amino)ethoxy)ethoxy)propanoic acid. MS (ESI) m/z 898.29 (M+H)<sup>+</sup>.

**8-(4-(4-(9-((2-(2,6-dioxopiperidin-3-yl)-1,3-dioxoisindolin-4-yl)amino)nonanoyl)piperazin-1-yl)piperidin-1-yl)-9-ethyl-6,6-dimethyl-11-oxo-6,11-dihydro-5H-benzo[b]carbazole-3-carbonitrile (JH-XIII-200-3) (19)**. Prepared using the same procedure for **17** and 9-((2-(2,6-dioxopiperidin-3-yl)-1,3-dioxoisindolin-4-yl)amino)nonanoic acid. MS (ESI) m/z 894.09 (M+H)<sup>+</sup>.

**Scheme 2.3.** Synthesis of JH-XIII-114-3 (**23**).



**2-(4-(3-cyano-9-ethyl-6,6-dimethyl-11-oxo-6,11-dihydro-5H-benzo[b]carbazol-8-yl)-1H-pyrazol-1-yl)-N-(14-((2-(2,6-dioxopiperidin-3-yl)-1,3-dioxoisindolin-4-yl)amino)-3,6,9,12-tetraoxatetradecyl)-N-methylacetamide (JH-XIV-61) (23)**. 2-(4-(3-cyano-9-ethyl-6,6-dimethyl-11-oxo-6,11-dihydro-5H-benzo[b]carbazol-8-yl)-1H-pyrazol-1-yl)acetic acid (**21**) was

prepared according to the literature.<sup>30</sup> To a stirred solution of **21** (15 mg, 0.034 mmol), 4-((5,8,11,14-tetraoxa-2-azahexadecan-16-yl)amino)-2-(2,6-dioxopiperidin-3-yl)isoindoline-1,3-dione (**22**) (17 mg, 0.034 mmol) and HATU (26 mg, 0.068 mmol) was added DIEA (30  $\mu$ L, 0.17 mmol). The mixture was stirred for 15 minutes and then purified by reverse phase HPLC using a gradient of 1% to 70% ACN in H<sub>2</sub>O to give the desired product as a yellow solid (14mg, 41% yield). MS (ESI) m/z 928. 61 (M+H)<sup>+</sup>.

**2-(4-(3-cyano-9-ethyl-6,6-dimethyl-11-oxo-6,11-dihydro-5H-benzo[b]carbazol-8-yl)-1H-pyrazol-1-yl)-N-(2-(2-(2-((2-(2,6-dioxopiperidin-3-yl)-1,3-dioxoisoindolin-4-yl)amino)ethoxy)ethoxy)ethyl)acetamide (JH-XIII-114-1) (24)**. Prepared using the same procedure for **23** and 4-((2-(2-(2-aminoethoxy)ethoxy)ethyl)amino)-2-(2,6-dioxopiperidin-3-yl)isoindoline-1,3-dione. MS (ESI) m/z 825.73 (M+H)<sup>+</sup>.

**2-(4-(3-cyano-9-ethyl-6,6-dimethyl-11-oxo-6,11-dihydro-5H-benzo[b]carbazol-8-yl)-1H-pyrazol-1-yl)-N-(20-((2-(2,6-dioxopiperidin-3-yl)-1,3-dioxoisoindolin-4-yl)amino)-3,6,9,12,15,18-hexaoxaicosyl)acetamide (JH-XIII-114-2) (25)**. Prepared using the same procedure for **23** and 4-((20-amino-3,6,9,12,15,18-hexaoxaicosyl)amino)-2-(2,6-dioxopiperidin-3-yl)isoindoline-1,3-dione. MS (ESI) m/z 1002.46 (M+H)<sup>+</sup>.

**2-(4-(3-cyano-9-ethyl-6,6-dimethyl-11-oxo-6,11-dihydro-5H-benzo[b]carbazol-8-yl)-1H-pyrazol-1-yl)-N-(14-((2-(2,6-dioxopiperidin-3-yl)-1,3-dioxoisoindolin-4-yl)amino)-3,6,9,12-tetraoxatetradecyl)acetamide (JH-XIII-114-3) (26)**. Prepared using the same procedure for **23** and 4-((14-amino-3,6,9,12-tetraoxatetradecyl)amino)-2-(2,6-dioxopiperidin-3-yl)isoindoline-1,3-dione. MS (ESI) m/z 913.79 (M+H)<sup>+</sup>.

***in vitro* Kinase Assays.** ALK kinase activity was measured using ALK<sub>1058-1620</sub> (Carna Biosciences) and a biotinylated gastrin peptide (Carna Biosciences) in PerkinElmer's LANCE Classic assay format. In brief, 0.4 nM of ALK protein and 250 nM of gastrin peptide are incubated with compound at ATP K<sub>m,app</sub> (18  $\mu$ M) in a buffer of 15 mM Tris-HCl (pH 7.5), 0.01% Tween-20, 5

mM MgCl<sub>2</sub>, and 2 mM DTT at a volume of 20 μL in a 384-well plate (White OptiPlate-384, PerkinElmer) for 1 hour at room temperature. 20 μL of detection mixture containing 50 nM of allophycocyanin (APC)-streptavidin (PerkinElmer) and 0.8 nM of europium (Eu) labeled anti-phosphotyrosine antibody (Eu-W1024-anti-phosphotyrosine (PT66); PerkinElmer) in 15 mM Tris-HCl (pH 7.5) and 0.01% Tween-20 is then added to each well and incubated for 1.5 hours at room temperature. Plates are read on an Envision 2104. Z'LYTE kinase assays were conducted for Aurora A, PTK2, FER, and RPS6KA1 at Life Technologies using Km ATP concentrations.

***in vitro* Cereblon Binding Assay.** Compounds in Atto565-Lenalidomide displacement assay were dispensed in a 384-well microplate (Corning, 4514) using D300e Digital Dispenser (HP) and normalized to 1% DMSO into 10 nM Atto565-Lenalidomide, 100 nM DDB1ΔB-CRBN, 50 mM Tris pH 7.5, 200 mM NaCl, 0.1% Pluronic F-68 solution (Sigma). The change in fluorescence polarization was monitored using a PHERAstar FS microplate reader (BMG Labtech) for 30 cycles of 187s each. Data from four independent measurements (n = 4) was plotted and IC<sub>50</sub> values estimated using variable slope equation in GraphPad Prism 7.

**Cell Culture.** H3122 cells were originally obtained as described previously.<sup>34</sup> Karpas 299 cells were obtained from the European Collection of Authenticated Cell Cultures (ECACC) through purchase from Sigma-Aldrich. SU-DHL-1 cells were generously provided by A. Thomas Look (DFCI, Boston, MA) and genotyped at the DFCI Core Facility by standard methods. Kelly, LAN5, SH-SY5Y, and CHLA20 cell lines were obtained from the Children's Oncology Group (COG) cell line repository and genotyped at the DFCI Core Facility by standard methods. Ba/F3 EML4-ALK expressing cells were generated as described previously.<sup>34</sup>

H3122, SU-DHL-1, Kelly, LAN5, SH-SY5Y, CHLA20, and Ba/F3 cell lines were cultured in RPMI-1640 media containing L-glutamine, supplemented with 10% fetal bovine serum (FBS) and 1% penicillin/streptomycin. Parental Ba/F3 cells were cultured with an additional 1 ng/mL recombinant mouse IL-3 (Prospec). Karpas 299 cells were cultured in RPMI-1640 media

containing L-glutamine, supplemented with 20% FBS and 1% penicillin/streptomycin. Mycoplasma testing was performed on a 6-monthly basis and all lines were negative.

**Cell Viability Assays.** Cell viability was evaluated using the CellTiter-Glo Luminescent Cell Viability Assay (Promega) following the manufacturer's standards.

**Immunoblotting.** Cells were washed with PBS before being lysed with Cell Lysis Buffer (Cell Signaling) supplemented with protease and phosphatase inhibitor cocktails (Roche) at 4°C for 15 minutes. The cell lysate was briefly sonicated at a low amplitude (XL-2000, QSonica) before being centrifuged at 14,000 x g for 15 min at 4°C. Protein in cell lysate was quantified by BCA assay (Pierce). Primary antibodies used in this study include ALK (Cell Signaling Technology, C26G7 and D5F3), phospho-ALK (Cell Signaling Technology, Tyr1604, and Abcam, Tyr1507), Aurora A (Cell Signaling Technology, 1F8),  $\beta$ -actin (Cell Signaling Technology, 8H10D10), FAK (PTK2) (Cell Signaling Technology, #3285), FER (Cell Signaling Technology, 5D2), GAPDH (Cell Signaling Technology, 14C10), RSK1 (RPS6KA1) (Cell Signaling Technology, D6D5), STAT3 (Cell Signaling Technology, #9132), and phospho-STAT3 (Cell Signaling Technology, Tyr705). Blot quantification was performed using Image Studio 4.0 software, normalizing to loading controls.  $DC_{50}$ s were modeled using GraphPad Prism 7 software.

**Sample Preparation TMT LC-MS3 Mass Spectrometry.** Kelly cells were treated with DMSO or 100 nM of compounds **9**, **10**, **11**, or **12** in biological triplicates for 4 hours and cells harvested by centrifugation. Lysis buffer (8 M Urea, 50 mM NaCl, 50 mM 4-(2hydroxyethyl)-1-piperazineethanesulfonic acid (EPPS) pH 8.5, Protease and Phosphatase inhibitors from Roche) was added to the cell pellets and homogenized by 20 passes through a 21 gauge (1.25 in. long) needle to achieve a cell lysate with a protein concentration between 1 – 4 mg mL<sup>-1</sup>. A micro-BCA assay (Pierce) was used to determine the final protein concentration of protein in the cell lysate. 200  $\mu$ g of protein for each sample were reduced and alkylated as previously described.<sup>35</sup>

Proteins were precipitated using methanol/chloroform. In brief, four volumes of methanol were added to the cell lysate, followed by one volume of chloroform, and finally three volumes of water. The mixture was vortexed and centrifuged to separate the chloroform phase from the aqueous phase. The precipitated protein was washed with one volume of methanol, centrifuged and the resulting washed precipitated protein was allowed to air dry. Precipitated protein was resuspended in 4 M Urea, 50 mM HEPES pH 7.4, followed by dilution to 1 M urea with the addition of 200 mM EPPS, pH 8. Proteins were first digested with LysC (1:50; enzyme:protein) for 12 hours at room temperature. The LysC digestion was diluted down to 0.5 M Urea with 200 mM EPPS pH 8 and then digested with trypsin (1:50; enzyme:protein) for 6 hours at 37 °C. Tandem mass tag (TMT) reagents (Thermo Fisher Scientific) were dissolved in anhydrous acetonitrile (ACN) according to manufacturers instructions. Anhydrous ACN was added to each peptide sample to a final concentration of 30% v/v, and labeling was induced with the addition of TMT reagent to each sample at a ratio of 1:4 peptide:TMT label. The 10-plex labeling reactions were performed for 1.5 hours at RT and the reaction quenched by the addition of hydroxylamine to a final concentration of 0.3% for 15 minutes at RT. The sample channels were combined at a 1:1:1:1:1:1:1:1:1:1 ratio, desalted using C<sub>18</sub> solid phase extraction cartridges (Waters) and analyzed by LC-MS for channel ratio comparison. Samples were then combined using the adjusted volumes determined in the channel ratio analysis and dried down in a speed vacuum. The combined sample was then resuspended in 1% formic acid, and acidified (pH 2–3) before being subjected to desalting with C18 SPE (Sep-Pak, Waters). Samples were then offline fractionated into 96 fractions by high pH reverse-phase HPLC (Agilent LC1260) through an aeris peptide xb-c18 column (phenomenex) with mobile phase A containing 5% acetonitrile and 10 mM NH<sub>4</sub>HCO<sub>3</sub> in LC-MS grade H<sub>2</sub>O, and mobile phase B containing 90% acetonitrile and 10 mM NH<sub>4</sub>HCO<sub>3</sub> in LC-MS grade H<sub>2</sub>O (both pH 8.0). The 96 resulting fractions were then pooled in a non-continuous manner into 24 fractions and 12 of these fractions were used for subsequent mass spectrometry analysis.

Data were collected using an Orbitrap Fusion Lumos mass spectrometer (Thermo Fisher Scientific, San Jose, CA, USA) coupled with a Proxeon EASY-nLC 1200 LC pump (Thermo Fisher Scientific). Peptides were separated on an EasySpray ES803 75  $\mu\text{m}$  inner diameter microcapillary column (ThermoFisher Scientific). Peptides were separated using a 3 hr gradient of 6–27% acetonitrile in 1.0% formic acid with a flow rate of 400 nL/min.

Each analysis used an MS3-based TMT method as described previously.<sup>36</sup> The data were acquired using a mass range of  $m/z$  340 – 1350, resolution 120,000, AGC target  $1 \times 10^6$ , maximum injection time 100 ms, dynamic exclusion of 70 seconds for the peptide measurements in the Orbitrap. Data dependent MS2 spectra were acquired in the ion trap with a normalized collision energy (NCE) set at 35%, AGC target set to  $1.8 \times 10^4$  and a maximum injection time of 120 ms. MS3 scans were acquired in the Orbitrap with a HCD collision energy set to 55%, AGC target set to  $1.5 \times 10^5$ , maximum injection time of 150 ms, resolution at 50,000 and with a maximum synchronous precursor selection (SPS) precursors set to 10.

**LC-MS Data Analysis.** Proteome Discoverer 2.1 (Thermo Fisher) was used to for .RAW file processing and controlling peptide and protein level false discovery rates, assembling proteins from peptides, and protein quantification from peptides. MS/MS spectra were searched against a Uniprot human database (September 2016) with both the forward and reverse sequences. Database search criteria are as follows: tryptic with two missed cleavages, a precursor mass tolerance of 10 ppm, fragment ion mass tolerance of 0.6 Da, static alkylation of cysteine (57.02146 Da), static TMT labelling of lysine residues and N-termini of peptides (229.16293 Da), and variable oxidation of methionine (15.99491 Da). TMT reporter ion intensities were measured using a 0.003 Da window around the theoretical  $m/z$  for each reporter ion in the MS3 scan. Peptide spectral matches with poor quality MS3 spectra were excluded from quantitation (summed signal-to-noise across 10 channels  $< 200$  and precursor isolation specificity  $< 0.5$ ).

Reporter ion intensities were normalised and scaled using in-house scripts in the R framework.<sup>37</sup> Statistical analysis was carried out using the limma package within the R framework.<sup>38</sup>

**shRNA Knockdown.** pLKO.1 plasmids containing shRNAs targeting *ABCB1* (TRCN0000059683 and TRCN0000059684) were obtained from the RNAi Consortium of the Broad Institute of MIT and Harvard and knockdown performed as described previously.<sup>39</sup>

**Pharmacokinetic Studies.** Pharmacokinetic studies were performed by The Scripps Research Institute, Jupiter, Florida on a fee for service basis. Scripps Florida has a PHS Approved Animal Welfare Assurance (# A4460-01). Pharmacokinetics was assessed in male C57Bl/6 mice. Approximately 25  $\mu$ L of blood was collected at 0.08, 0.25, 0.5, 1, 2, 4, 6, and 8 hours. Plasma was generated by centrifugation and plasma concentrations were determined by LC-MS/MS. Pharmacokinetic parameters were calculated using Phoenix WinNonlin® to determine peak plasma concentration ( $C_{max}$ ), exposure (AUC), half-life ( $t_{1/2}$ ), and clearance (CL). All procedures are approved by the Scripps Florida IACUC and Scripps vivarium is fully AAALAC accredited.

## **Author Contributions**

C.E.P conducted the experiments and analyzed the data. Y.G. and A.L. conducted and analyzed experiments with NB cells. L.T. and J.M.H. developed the chemically induced degradation strategies and synthesized compounds. K.A.D. ran and analyzed expression proteomics. R.P.N ran CRBN binding assay. M.B. provided H3122 and Ba/F3 cell lines, and advised on related experimental procedures. E.S.F., P.A.J., R.E.G., and N.S.G advised on project directions. C.E.P. wrote the paper. All authors read, revised, and approved the manuscript.

## **Funding Sources**

Funding for this work was received from the National Institutes of Health (NIH): Grant R01 CA136851-08 to P.A.J. and N.S.G.; Grant R01 CA148688 to R.E.G.; Grant R01 CA214608-01 to E.S.F. This work was also supported by NIH Grant Numbers 5 T32 GM095450-04, 2 T32 GM007306-40, and 5 F31 CA210619-02 (C.E.P.), and a Friends for Life Neuroblastoma Fellowship (Y.G.).

## **Notes**

The authors declare no competing financial interest.

## References

- (1) Powell, C. E.; Gao, Y.; Tan, L.; Donovan, K. A.; Nowak, R. P.; Loehr, A.; Bahcall, M.; Fischer, E. S.; Jänne, P. A.; George, R. E.; et al. Chemically Induced Degradation of Anaplastic Lymphoma Kinase (ALK). *J Med Chem* 2018, 61 (9), 4249–4255. <https://doi.org/10.1021/acs.jmedchem.7b01655> .
- (2) Chiarle, R.; Voena, C.; Ambrogio, C.; Piva, R.; Inghirami, G. The Anaplastic Lymphoma Kinase in the Pathogenesis of Cancer. *Nat Rev Cancer* 2008, 8 (1), 11 23. <https://doi.org/10.1038/nrc2291> .
- (3) Jr, R. Anaplastic Lymphoma Kinase (ALK): Structure, Oncogenic Activation, and Pharmacological Inhibition. *Pharmacol Res* 2013, 68 (1), 68 94. <https://doi.org/10.1016/j.phrs.2012.11.007> .
- (4) Bayliss, R.; Choi, J.; Fennell, D. A.; Fry, A. M.; Richards, M. W. Molecular Mechanisms That Underpin EML4-ALK Driven Cancers and Their Response to Targeted Drugs. *Cell Mol Life Sci* 2016, 73 (6), 1209 1224. <https://doi.org/10.1007/s00018-015-2117-6> .
- (5) George, R. E.; Sanda, T.; Hanna, M.; Fröhling, S.; William, L. I.; Zhang, J.; Ahn, Y.; Zhou, W.; London, W. B.; McGrady, P.; et al. Activating Mutations in ALK Provide a Therapeutic Target in Neuroblastoma. *Nature* 2008, 455 (7215), 975 978. <https://doi.org/10.1038/nature07397> .
- (6) Mossé, Y. P.; Laudenslager, M.; Longo, L.; Cole, K. A.; Wood, A.; Attiyeh, E. F.; Laquaglia, M. J.; Sennett, R.; Lynch, J. E.; Perri, P.; et al. Identification of ALK as a Major Familial Neuroblastoma Predisposition Gene. *Am J Pathology* 2008, 455 (7215), 930 935. [https://doi.org/10.1016/s0002-9440\(10\)65042-0](https://doi.org/10.1016/s0002-9440(10)65042-0) .
- (7) Palmer, R. H.; Vernersson, E.; Grabbe, C.; Hallberg, B. Anaplastic Lymphoma Kinase: Signalling in Development and Disease. *Biochem J* 2009, 420 (3), 345 361. <https://doi.org/10.1042/bj20090387> .
- (8) Morris, S. W.; Naeve, C.; Mathew, P.; James, P. L.; Kirstein, M. N.; Cui, X.; Witte, D. P. ALK, the Chromosome 2 Gene Locus Altered by the t(2;5) in Non-Hodgkin's Lymphoma, Encodes a Novel Neural Receptor Tyrosine Kinase That Is Highly Related to Leukocyte Tyrosine Kinase (LTK). *Oncogene* 1997, 14 (18), 2175 2188. <https://doi.org/10.1038/sj.onc.1201062> .
- (9) Peters, S.; Camidge, R. D.; Shaw, A. T.; Gadgeel, S.; Ahn, J. S.; Kim, D.-W.; Ou, S.-H. I.; Pérol, M.; Dziadziuszko, R.; Rosell, R.; et al. Alectinib Versus Crizotinib in Untreated ALK-Positive Non-Small-Cell Lung Cancer. *New Engl J Medicine* 2017, 377 (9), 829 838. <https://doi.org/10.1056/nejmoa1704795> .
- (10) Soria, J.-C.; Tan, D. S.; Chiari, R.; Wu, Y.-L.; Paz-Ares, L.; Wolf, J.; Geater, S. L.; Orlov, S.; Cortinovis, D.; Yu, C.-J.; et al. First-Line Ceritinib Versus Platinum-Based Chemotherapy in Advanced ALK-Rearranged Non-Small-Cell Lung Cancer (ASCEND-4): A Randomised, Open-Label, Phase 3 Study. *Lancet* 2017, 389 (10072), 917 929. [https://doi.org/10.1016/s0140-6736\(17\)30123-x](https://doi.org/10.1016/s0140-6736(17)30123-x) .
- (11) Katayama, R.; Shaw, A.; Khan, T.; Mino-Kenudson, M.; Solomon, B.; Halmos, B.; Jessop, N.; Wain, J.; Yeo, A.; Benes, C.; et al. Mechanisms of Acquired Crizotinib Resistance in ALK-

Rearranged Lung Cancers. *Sci Transl Med* 2012, 4 (120), 120ra17 120ra17. <https://doi.org/10.1126/scitranslmed.3003316> .

(12) Cooper, M.; Chim, H.; Chan, H.; Durand, C. Ceritinib: A New Tyrosine Kinase Inhibitor for Non-Small-Cell Lung Cancer. *Ann Pharmacother* 2014, 49 (1), 107 112. <https://doi.org/10.1177/1060028014553619> .

(13) Sullivan, I.; Planchard, D. ALK Inhibitors in Non-Small Cell Lung Cancer: The Latest Evidence and Developments. *Ther Adv Med Oncol* 2015, 8 (1), 32 47. <https://doi.org/10.1177/1758834015617355> .

(14) Mologni, L. Expanding the Portfolio of Anti-ALK Weapons. *Transl Lung Cancer Res* 2015, 4 (1), 5 7. <https://doi.org/10.3978/j.issn.2218-6751.2014.07.02> .

(15) Katayama, R.; Friboulet, L.; Koike, S.; Lockerman, E.; Khan, T.; Gainor, J.; Iafrate, A.; Takeuchi, K.; Taiji, M.; Okuno, Y.; et al. Two Novel ALK Mutations Mediate Acquired Resistance to the Next-Generation ALK Inhibitor Alectinib. *Clin Cancer Res* 2014, 20 (22), 5686 5696. <https://doi.org/10.1158/1078-0432.ccr-14-1511> .

(16) Qin, A.; Gadgeel, S. The Current Landscape of Anaplastic Lymphoma Kinase (ALK) in Non-Small Cell Lung Cancer: Emerging Treatment Paradigms and Future Directions. *Target Oncol* 2017, 12 (6), 709 718. <https://doi.org/10.1007/s11523-017-0526-1> .

(17) Shaw, A. T.; Friboulet, L.; Leshchiner, I.; Gainor, J. F.; Bergqvist, S.; Brooun, A.; Burke, B. J.; Deng, Y.-L.; Liu, W.; Dardaei, L.; et al. Resensitization to Crizotinib by the Lorlatinib ALK Resistance Mutation L1198F. *New Engl J Medicine* 2016, 374 (1), 54 61. <https://doi.org/10.1056/nejmoa1508887> .

(18) Winter, G.; Buckley, D.; Paulk, J.; Roberts, J.; Souza, A.; Dhe-Paganon, S.; Bradner, J. Phthalimide Conjugation as a Strategy for in Vivo Target Protein Degradation. *Science* 2015, 348 (6241), 1376 1381. <https://doi.org/10.1126/science.aab1433> .

(19) Lai, A. C.; Toure, M.; Hellerschmied, D.; Salami, J.; Jaime-Figueroa, S.; Ko, E.; Hines, J.; Crews, C. M. Modular PROTAC Design for the Degradation of Oncogenic BCR-ABL. *Angew Chem-ger Edit* 2015, 128 (2), 818 821. <https://doi.org/10.1002/ange.201507634> .

(20) Huang, H.-T.; Dobrovolsky, D.; Paulk, J.; Yang, G.; Weisberg, E. L.; ctor, Z.; Buckley, D. L.; Cho, J.-H.; Ko, E.; Jang, J.; et al. A Chemoproteomic Approach to Query the Degradable Kinome Using a Multi-Kinase Degradator. *Cell Chem Biol* 2017, 25 (1), 1 19. <https://doi.org/10.1016/j.chembiol.2017.10.005> .

(21) Davis, M. I.; Hunt, J. P.; Herrgard, S.; Ciceri, P.; Wodicka, L. M.; Pallares, G.; Hocker, M.; Treiber, D. K.; Zarrinkar, P. P. Comprehensive Analysis of Kinase Inhibitor Selectivity. *Nat Biotechnol* 2011, 29 (11), 1046 1051. <https://doi.org/10.1038/nbt.1990> .

(22) Marsilje, T. H.; Pei, W.; Chen, B.; Lu, W.; Uno, T.; Jin, Y.; Jiang, T.; Kim, S.; Li, N.; Warmuth, M.; et al. Synthesis, Structure–Activity Relationships, and in Vivo Efficacy of the Novel Potent and Selective Anaplastic Lymphoma Kinase (ALK) Inhibitor 5-Chloro- N2-(2-Isopropoxy-5-Methyl-4-(Piperidin-4-Yl)Phenyl)- N4-(2-(Isopropylsulfonyl)Phenyl)Pyrimidine-2,4-Diamine (LDK378) Currently in Phase 1 and Phase 2 Clinical Trials. *J Med Chem* 2013, 56 (14), 5675 5690. <https://doi.org/10.1021/jm400402q> .

- (23) Takezawa, K.; Okamoto, I.; Nishio, K.; Janne, P.; Nakagawa, K. Role of ERK-BIM and STAT3-Survivin Signaling Pathways in ALK Inhibitor-Induced Apoptosis in EML4-ALK-Positive Lung Cancer. *Clin Cancer Res* 2011, 17 (8), 2140-2148. <https://doi.org/10.1158/1078-0432.ccr-10-2798> .
- (24) Ott, G. R.; Tripathy, R.; Cheng, M.; McHugh, R.; Anzalone, A. V.; Underiner, T. L.; Curry, M. A.; Quail, M. R.; Lu, L.; Wan, W.; et al. Discovery of a Potent Inhibitor of Anaplastic Lymphoma Kinase with in Vivo Antitumor Activity. *ACS Med Chem Lett* 2010, 1 (9), 493-498. <https://doi.org/10.1021/ml100158s> .
- (25) Zhang, S.; Anjum, R.; Squillace, R.; Nadworny, S.; Zhou, T.; Keats, J.; Ning, Y.; Wardwell, S. D.; Miller, D.; Song, Y.; et al. The Potent ALK Inhibitor Brigatinib (AP26113) Overcomes Mechanisms of Resistance to First- and Second-Generation ALK Inhibitors in Preclinical Models. *Clin Cancer Res* 2016, 22 (22), 5527-5538. <https://doi.org/10.1158/1078-0432.ccr-16-0569> .
- (26) Yu, D. M.; Huynh, T.; Truong, A. M.; Haber, M.; Norris, M. D. ABC Transporters and Neuroblastoma. *Adv Cancer Res* 2015, 125, 139-170. <https://doi.org/10.1016/bs.acr.2014.10.005> .
- (27) Roe, M.; Folkes, A.; Ashworth, P.; Brumwell, J.; Chima, L.; Hunjan, S.; Pretswell, I.; Dangerfield, W.; Ryder, H.; Charlton, P. Reversal of P-Glycoprotein Mediated Multidrug Resistance by Novel Anthranilamide Derivatives. *Bioorg Med Chem Lett* 1999, 9 (4), 595-600. [https://doi.org/10.1016/S0960-894X\(99\)00030-X](https://doi.org/10.1016/S0960-894X(99)00030-X) .
- (28) Korolchuk, V. I.; Menzies, F. M.; Rubinsztein, D. C. Mechanisms of Cross-Talk Between the Ubiquitin-Proteasome and Autophagy-Lysosome Systems. *FEBS Lett* 2010, 584 (7), 1393-1398. <https://doi.org/10.1016/j.febslet.2009.12.047> .
- (29) Lee, H.-J.; Zhuang, G.; Cao, Y.; Du, P.; Kim, H.-J.; Settleman, J. Drug Resistance via Feedback Activation of Stat3 in Oncogene-Addicted Cancer Cells. *Cancer Cell* 2014, 26 (2), 207-221. <https://doi.org/10.1016/j.ccr.2014.05.019> .
- (30) Hatcher, J. M.; Bahcall, M.; Choi, H.; Gao, Y.; Sim, T.; George, R.; Janne, P. A.; Gray, N. S. Discovery of Inhibitors That Overcome the G1202R Anaplastic Lymphoma Kinase Resistance Mutation. *J Med Chem* 2015, 58 (23), 9296-9308. <https://doi.org/10.1021/acs.jmedchem.5b01136> .
- (31) Kang, C.; Lee, D.; Lee, C.; Ha, J.; Park, C.; Hwang, J. Induced Protein Degradation of Anaplastic Lymphoma Kinase (ALK) by Proteolysis Targeting Chimera (PROTAC). *Biochem Biophys Res Commun* 2018, 505 (2), 1-6. <https://doi.org/10.1016/j.bbrc.2018.09.169> .
- (32) Galkin, A. V.; Melnick, J. S.; Kim, S.; Hood, T. L.; Li, N.; Li, L.; Xia, G.; Steensma, R.; Chopiuk, G.; Jiang, J.; et al. Identification of NVP-TAE684, a Potent, Selective, and Efficacious Inhibitor of NPM-ALK. *PNAS* 2006, 104 (1), 270-275.
- (33) Lu, J.; Qian, Y.; Altieri, M.; Dong, H.; Wang, J.; Raina, K.; Hines, J.; Winkler, J. D.; Crew, A. P.; Coleman, K.; et al. Hijacking the E3 Ubiquitin Ligase Cereblon to Efficiently Target BRD4. *Chem Biol* 2015, 22 (6), 755-763. <https://doi.org/10.1016/j.chembiol.2015.05.009> .

(34) Sasaki, T.; Koivunen, J.; Ogino, A.; Yanagita, M.; Nikiforow, S.; Zheng, W.; Lathan, C.; Marcoux, P. J.; Du, J.; Okuda, K.; et al. A Novel ALK Secondary Mutation and EGFR Signaling Cause Resistance to ALK Kinase Inhibitors. *Cancer Res* 2011, 71 (18), 6051-6060. <https://doi.org/10.1158/0008-5472.can-11-1340> .

(35) An, J.; Ponthier, C. M.; Sack, R.; Seebacher, J.; Stadler, M. B.; Donovan, K. A.; Fischer, E. S. PSILAC Mass Spectrometry Reveals ZFP91 as IMiD-Dependent Substrate of the CRL4CRBN Ubiquitin Ligase. *Nat Commun* 2017, 8 (1), 1-11. <https://doi.org/10.1038/ncomms15398> .

(36) McAlister, G. C.; Nusinow, D. P.; Jedrychowski, M. P.; Wühr, M.; Huttlin, E. L.; Erickson, B. K.; Rad, R.; Haas, W.; Gygi, S. P. MultiNotch MS3 Enables Accurate, Sensitive, and Multiplexed Detection of Differential Expression across Cancer Cell Line Proteomes. *Anal Chem* 2014, 86 (14), 7150-7158. <https://doi.org/10.1021/ac502040v> .

(37) Team, C. R. R: A Language and Environment for Statistical Computing. *R Foundation for Statistical Computing* 2014.

(38) Ritchie, M. E.; Phipson, B.; Wu, D.; Hu, Y.; Law, C. W.; Shi, W.; Smyth, G. K. Limma Powers Differential Expression Analyses for RNA-Sequencing and Microarray Studies. *Nucleic Acids Res* 2015, 43 (7), e47-e47. <https://doi.org/10.1093/nar/gkv007> .

(39) Chipumuro, E.; Marco, E.; Christensen, C. L.; Kwiatkowski, N.; Zhang, T.; Hatheway, C. M.; Abraham, B. J.; Sharma, B.; Yeung, C.; Altabef, A.; et al. CDK7 Inhibition Suppresses Super-Enhancer-Linked Oncogenic Transcription in MYCN-Driven Cancer. *Cell* 2014, 159 (5), 1126-1139. <https://doi.org/10.1016/j.cell.2014.10.024> .

## **Chapter 3: Discovery and Profiling of Allosteric ALK Inhibitors**

### Chapter 3: Discovery and Profiling of Allosteric ALK Inhibitors

Chelsea E. Powell,<sup>†,◇</sup> Jaebong Jang,<sup>†,◇</sup> Dries J. H. De Clercq,<sup>†,◇</sup> Eunyoung Park,<sup>†,◇</sup> Magda Bahcall,<sup>‡</sup> Pasi A. Jänne,<sup>‡,§</sup> Michael J. Eck,<sup>†,◇</sup> Nathanael S. Gray<sup>\*,†,◇</sup>

†Department of Cancer Biology, ‡Lowe Center for Thoracic Oncology, and §Belfer Center for Applied Cancer Science, Dana-Farber Cancer Institute, Boston, Massachusetts 02215, United States

◇Department of Biological Chemistry & Molecular Pharmacology, Harvard Medical School, Boston, Massachusetts 02115, United States

\* Correspondence: [Nathanael.Gray@dfci.harvard.edu](mailto:Nathanael.Gray@dfci.harvard.edu) (N.S.G.).

## **Abstract**

Treatment of patients with anaplastic lymphoma kinase (ALK)-positive non-small-cell lung cancer (NSCLC) has been greatly improved over the past decade through the use of small molecule kinase inhibitors to target ALK. Although these treatments have drastic initial responses, patients on average develop resistance to these inhibitors within a year of treatment. All current ALK targeted therapies, both approved and in clinical trials, are ATP-competitive kinase inhibitors. A new class of compounds that target ALK may provide ways of overcoming tumor resistance, either on its own or through combination therapies with ATP-competitive inhibitors. In the following work we performed a screen with the goal of identifying and profiling allosteric ALK inhibitors, based on the hypothesis that ALK contains an allosteric site similar to that of the epidermal growth factor receptor (EGFR). From our screen we identified a compound with an allosteric EGFR inhibitor scaffold that is active against ALK, but inactive against EGFR. Initial profiling of this compound was promising and indicates that further screening against the theorized allosteric pocket should be performed.

### 3.1 Introduction

The development of targeted therapies for tumors driven by activating mutations in tyrosine kinases has rapidly improved cancer therapy over the past decade.<sup>1</sup> However, the dramatic initial response that small molecule kinase inhibitors have in the clinic leads to a strong selective pressure for the outgrowth of tumor cells expressing kinases with mutations that make them resistant to binding by the inhibitor. Finding ways to overcome resistance is a recurring obstacle in the use of small molecule kinase inhibitors as cancer therapies, and compounds that are effective against resistant tumors are crucial for lengthening the time that a patient may be effectively treated.

Anaplastic lymphoma kinase (ALK) is a receptor tyrosine kinase that has been shown to form fusion proteins that play a driving role in several cancers, including non-small cell lung cancer (NSCLC).<sup>2,3</sup> ALK-positive NSCLC is notable because of its sizable patient population and the use of FDA approved ALK inhibitors in its treatment. Lung cancer is the leading cause of cancer-related deaths worldwide;<sup>4</sup> 85-95% of lung cancers are NSCLC and about 5% of NSCLC are ALK-positive, meaning that there are approximately 11,300 new cases of ALK-positive NSCLC in the United States each year.<sup>2</sup> ALK-positive tumors are highly sensitive to ALK inhibition, making small molecule inhibitors of ALK a powerful tool for the clinical treatment of this subset of patients with NSCLC.<sup>5</sup>

There are currently five FDA approved kinase inhibitors for the treatment of ALK-positive NSCLC: crizotinib, ceritinib, alectinib, brigatinib, and most recently, lorlatinib. Although these compounds can induce potent tumor regression in patients, resistance to these inhibitors develops rapidly, resulting in relapse.<sup>6-10</sup> Several mutations have been identified in crizotinib-resistant tumors, including L1196M, L1152R, G1269A, C1156Y, F1174L, S1206Y, 1151Tins and G1202R.<sup>11</sup> L1196M is the most common mutation after first-line treatment with crizotinib and is sometimes referred to as the “gatekeeper mutation;” L1196M is sensitive to inhibition by ceritinib,

alectinib, brigatinib, and lorlatinib.<sup>11-14</sup> G1202R is notable because it is resistant to inhibition by all approved ALK inhibitors.

There exists an urgent need to develop novel ALK inhibitors that can surmount resistance mutations. Since all current ALK inhibitors, both approved and in clinical trials, bind the ATP site of the kinase, therapeutic strategies that target ALK with different mechanisms of action may provide ways to further delay the emergence of resistance mutations. Additionally, compounds with novel mechanisms of action could work synergistically with approved ALK inhibitors in combination therapies to prevent resistance development in a way that is analogous to the “triple-cocktail” therapy used to overcome resistance mutations in HIV.

While ATP site kinase inhibitors have had clinical success as cancer treatments, they have several notable limitations, including cross-reactivity with other kinases due to the highly conserved nature of the ATP-binding pocket, competition with intracellular ATP (which is present intracellularly at millimolar concentrations), and resistance mutations developing at the ATP-binding site.<sup>15</sup> Kinase inhibitors that bind to allosteric sites overcome the issue of non-specific kinase binding because allosteric pockets tend to be more unique, resulting in allosteric inhibitors having fewer off-target toxicities. Most allosteric kinase inhibitors are also non-competitive with ATP, thus avoiding interference from intracellular ATP. Importantly, allosteric inhibitors can overcome mutations in the ATP site by nature of binding to an alternate location.

Our group has previously identified allosteric epidermal growth factor receptor (EGFR) inhibitors.<sup>16</sup> EGFR is a receptor tyrosine kinase that is active in many human cancers. Activating EGFR mutations are a major cause of NSCLC, appearing in about 15% of tumors.<sup>17</sup> EGFR-positive NSCLC and ALK-positive NSCLC are dependent on their respective mutations due to the key roles that the activated kinases play in cell proliferation and anti-apoptotic signaling pathways.<sup>18,19</sup> In addition to having similar functions in NSCLC, EGFR and ALK are structurally similar, especially in regards to the orientation of the  $\alpha$ C-helix relative to the ATP site (Figure 3.1).

The previously identified EGFR allosteric pocket is created in part by the outward displacement of the  $\alpha$ C-helix in the inactive conformation of the kinase. Another allosteric kinase pocket, for the kinase p38 $\alpha$ , is created by a DFG-out and  $\alpha$ C-helix-out conformation.<sup>20</sup> Crystal structures of ALK kinase domain bound to various orthosteric inhibitors (type I and II) have shown both  $\alpha$ C-helix and DFG motif in both in- and out- conformations.<sup>21-23</sup> We hypothesize that ALK has a similar allosteric pocket and, as is seen with EGFR, inhibitors of this pocket will be non-ATP-competitive and able to overcome resistance mutations.

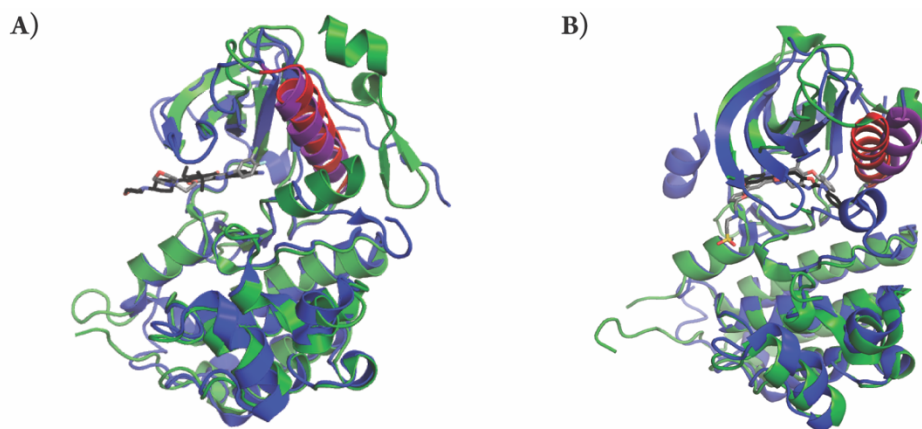


**Figure 3.1.** Structural similarity of EGFR and ALK. (A) Structural alignment of active conformations of EGFR (blue; PDB ID: 2ITY) and ALK (green; PDB ID: 3AOX), using PyMOL (RMSD = 1.013 over 1196 atoms). Gefitinib (gray) is bound to the ATP site of EGFR and alectinib (black) is bound to the ATP site of ALK. The  $\alpha$ C-helix of EGFR is in pink, while the  $\alpha$ C-helix of ALK is in red. (B) Structural alignment of DFG-out,  $\alpha$ C-helix shifted conformations of EGFR (PDB ID: 1XKK) and ALK (PDB ID: 4FNY), using PyMOL (RMSD = 1.342 over 1255 atoms). Type II inhibitors are shown bound to EGFR in gray and ALK in black.

### 3.2 Results and Discussion

We optimized a time-resolved fluorescence energy transfer (TR-FRET) kinase activity assay based on the PerkinElmer Classic LANCE TR-FRET assay; ALK activity is measured in this assay format based on the phosphorylation of a biotinylated gastrin peptide (Figure 3.2). There are two major advantages to using a TR-FRET based assay. First, the “time-gated” nature of TR-FRET means that emission is measured 100-900  $\mu$ s after the initial excitation frequency,

which results in less background fluorescence from the plate, buffer, and compounds. Second, TR-FRET measurements are reported as an emission ratio of signal from the donor fluorophore to the signal from the acceptor fluorophore, which can help account for small variations in liquid transfer since the amount of signal from the acceptor fluorophore is in part dependent on the amount of donor fluorophores being excited. This results in TR-FRET assays having less variation between wells compared to other enzyme assay systems.<sup>24</sup>

Using commercial recombinant ALK kinase (residues 1058 – 1620; Carna Biosciences), we performed a screen of this assay against the ~5,000 compounds in our own group's kinase inhibitor library, which includes allosteric EGFR inhibitors. This screen was run at a high ATP concentration of 1 mM to bias the screen against weak ATP site inhibitors.

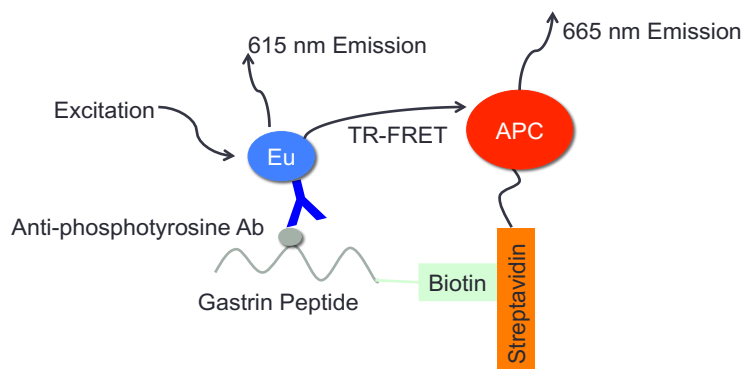


**Figure 3.2.** TR-FRET assay for detecting ALK activity. When ALK is active it will phosphorylate the gastrin peptide, allowing the anti-phosphotyrosine antibody to bind, which in turn will bring the fluorophores, Eu and APC, in close enough proximity for TR-FRET to occur. When ALK is inhibited, it does not phosphorylate the substrate, which means that the antibody no longer binds and TR-FRET does not occur.

From this screen an allosteric EGFR inhibitor scaffold, JBJ-02-017-04, registered as a hit (Figure 3.3A). This hit is exciting because not only is it a novel scaffold for an ALK inhibitor with known allosteric kinase inhibitor moieties, but this compound is also not active against EGFR, which is consistent with our hypothesis that ALK has a similar, but still unique, allosteric pocket (Table 3.1).

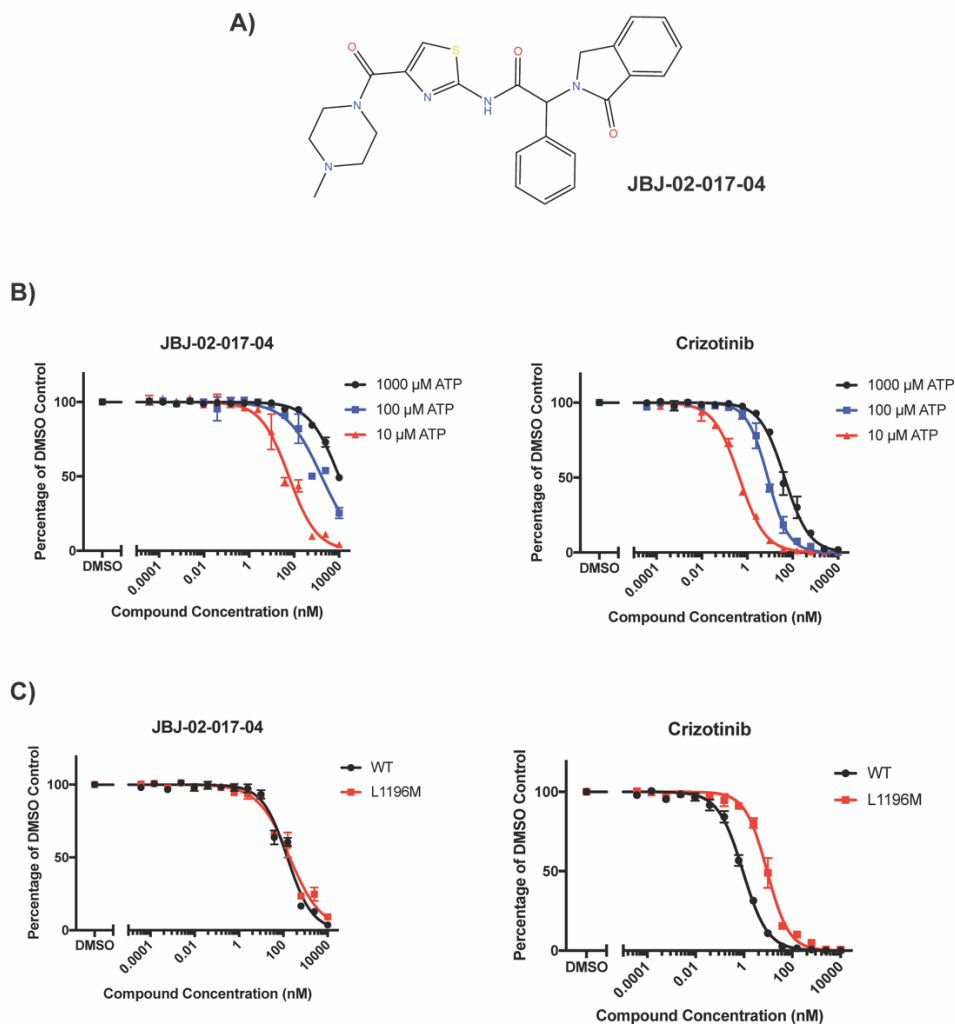


**Figure 3.3.** Biochemical Activity of Screening Hit JBJ-02-017-04. (A) Structure of ALK screening hit, JBJ-02-017-04. (B) The activity of JBJ-02-017-04 and crizotinib against ALK wild-type in the TR-FRET assay at varying ATP concentrations (3 biological replicates). (C) The activity of JBJ-02-017-04 and crizotinib against ALK wild-type and ALK L1196M in the TR-FRET assay (3 biological replicates).

**Table 3.1.** SelectScreen profiling IC<sub>50</sub>s (nM). NA = no activity. \* = ATP concentration is ATP K<sub>m,app</sub> for the assay. All assays were Z'-Lyte activity assays except for ALK L1196M, which was a LanthaScreen binding assay. The LanthaScreen does not use ATP, but had an ATP-site binding tracer concentration of 10 nM.

	EGFR WT	EGFR T790M	ALK WT	ALK WT	ALK L1196M
<b>ATP Concentration (μM)</b>	10*	10*	25*	100	N/A
<b>IC<sub>50</sub> (nM)</b>	NA	NA	>10000	5240	4850

Following the screen, JBJ-02-017-04 was confirmed to have activity against ALK both in the TR-FRET assay and by outside profiling through ThermoFisher Scientific's SelectScreen service (Figure 3.3, Table 3.1). Since the allosteric EGFR inhibitors were non-ATP-competitive, the activity of JBJ-02-017-04 against ALK at varying ATP concentrations was examined. In the TR-FRET assay JBJ-02-017-04 appears to be competitive with ATP (Figure 3.3B). However, SelectScreen profiling indicated that the compound activity may actually improve with increases in ATP concentration (Table 3.1). The activity of JBJ-02-017-04 against ALK with gatekeeper mutation L1196M was also examined. Both the TR-FRET assay and SelectScreen profiling confirmed that the hit compound maintains the same activity against the mutant as the wild-type, with SelectScreen indicating a slight increase in activity against the mutant (Figure 3.3C).

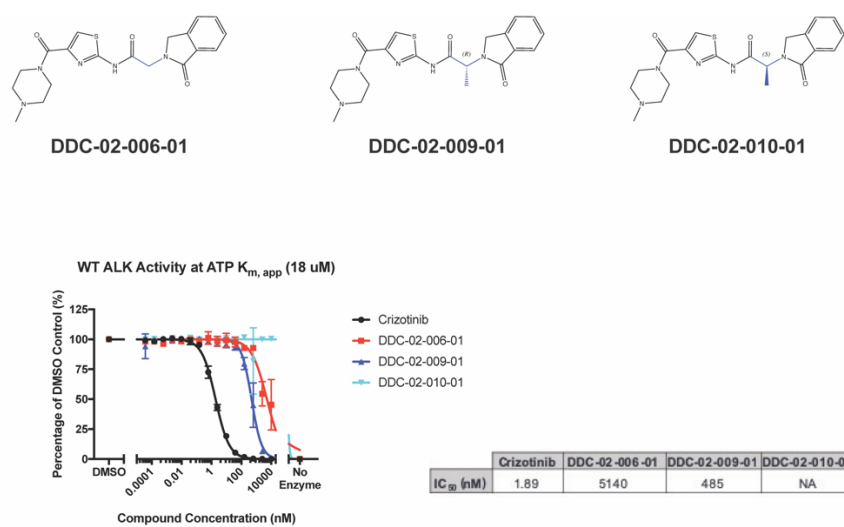


**Figure 3.4.** Initial medicinal chemistry efforts around potential stereoselectivity of JBJ-02-017-04. Activity in ALK TR-FRET assay is shown (3 biological replicates); NA = no activity.

Initial medicinal chemistry efforts with this lead potential ALK allosteric inhibitor have demonstrated that its activity may be stereoselective, indicating that it is binding to ALK in a specific manner (Figure 3.4). However, this data is presented with the caveat that this scaffold is easily epimerized.

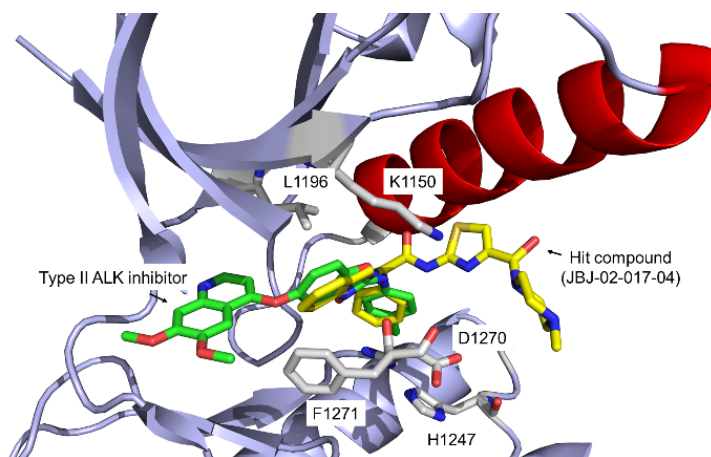


**Figure 3.5.** Molecular modeling of JBJ-02-017-04 with ALK kinase domain bound type II ALK inhibitor (PDB: 4FNY).

Molecular modeling of JBJ-02-017-04 in an inactive conformation of the ALK kinase domain (PDB: 4FNY) revealed that the compound (yellow) well occupies the allosteric site generated by the gatekeeper residue, DFG motif,  $\alpha$ C-helix and hydrophobic residues in a deep pocket (Figure 3.5). The phenyl moiety places in a deep hydrophobic pocket and the isoindolinone moiety occupies beside the gatekeeper residue. Both moieties are well aligned with the hydrophobic tail of the orthosteric type II ALK inhibitor (green). Moreover, 2-aminothiazole places along the  $\alpha$ C-helix and the 4-methylpiperazine extends to the solvent exposed exterior.

### 3.3 Conclusions

The mechanism of binding for this hit must be further explored and validated. Efforts to generate co-crystal structures of JBJ-02-017-04 with ALK in order to validate the binding site, clarify how ATP binding affects compound binding, and clarify how the compound can overcome the gatekeeper mutation have been unsuccessful so far. Further crystallography efforts are ongoing. We are also currently exploring the use of differential scanning fluorimetry (DSF) and isothermal titration calorimetry (ITC) to help validate JBJ-02-017-04 binding to ALK as well as to confirm whether or not the compound competes with ATP.

### 3.4 Experimental Methods

***in vitro* Kinase Assays.** ALK kinase activity was measured using ALK<sub>1058-1620</sub> (Carna Biosciences) and a biotinylated gastrin peptide (Carna Biosciences) in PerkinElmer's LANCE Classic assay format. In brief, 20 nL of compound in DMSO from stock plates was added by pin transfer using a Janus Workstation (PerkinElmer) to 0.4 nM of ALK protein with ATP in a buffer of 15 mM Tris-HCl (pH 7.5), 0.01% Tween-20, 5 mM MgCl<sub>2</sub>, and 2 mM DTT at a volume of 10  $\mu$ L in a 384-well plate (White OptiPlate-384, PerkinElmer). 10  $\mu$ L of 250 nM gastrin peptide in the same buffer was added to the wells before a 1 hr incubation at room temperature. 20  $\mu$ L of detection mixture containing 50 nM of allophycocyanin (APC)-streptavidin (PerkinElmer) and 0.8 nM of europium (Eu) labeled anti-phosphotyrosine antibody (Eu-W1024-anti-phosphotyrosine (PT66); PerkinElmer) in 15 mM Tris-HCl (pH 7.5) and 0.01% Tween-20 was then added to each well and incubated for 1.5 hr at room temperature. Plates were then read on an Envision 2104. IC<sub>50</sub>s were modeled from 3 biological replicates using GraphPad Prism 8 software. SelectScreen kinase assays were conducted at Life Technologies.

**ALK Protein Expression and Purification.** ALK<sub>1058-1411</sub> wild-type and C1097S constructs were generated based on the success of previous ALK crystallography efforts, where the C1097S mutation had been shown to improve ALK protein behavior for crystallography.<sup>22,25</sup> Constructs were prepared in a His-GST tag fusion format using the pFastBac system (ThermoFisher) for expression in Sf9 cells. ALK kinase protein was purified by nickel-affinity chromatography followed by glutathione-affinity chromatography. The His-GST tag was then cleaved overnight by tobacco etch virus (TEV) protease at 4 °C. Another nickel-affinity chromatography was performed to remove the protease and cleaved tag before a final size-exclusion chromatography. ALK protein was then concentrated and frozen in liquid nitrogen before being stored at -80 °C until use.

### **Author Contributions**

C.E.P conducted the experiments and analyzed the data. J.J. and D.J.H.D.C. designed and synthesized compounds. E.P. advised on protein expression and crystallography strategies. M.B., P.A.J., M.J.E., and N.S.G advised on project directions. C.E.P. wrote the chapter with editing from J.J., M.B., P.A.J., and N.S.G.

### **Funding Sources**

Funding for this work was received from the National Institutes of Health (NIH): Grant R01 CA136851-11 to P.A.J. and N.S.G. This work was also supported by NIH Grant Numbers 5 T32 GM095450-04, 2 T32 GM007306-40, and 5 F31 CA210619-02 (C.E.P.).

### **Notes**

The authors declare no competing financial interest.

## References

- (1) Arora, A.; Scholar, E. M. Role of Tyrosine Kinase Inhibitors in Cancer Therapy. *J Pharmacol Exp Ther* **2005**, *315* (3), 971 979. <https://doi.org/10.1124/jpet.105.084145> .
- (2) Jr, R. Anaplastic Lymphoma Kinase (ALK): Structure, Oncogenic Activation, and Pharmacological Inhibition. *Pharmacol Res* **2013**, *68* (1), 68 94. <https://doi.org/10.1016/j.phrs.2012.11.007> .
- (3) Chiarle, R.; Voena, C.; Ambrogio, C.; Piva, R.; Inghirami, G. The Anaplastic Lymphoma Kinase in the Pathogenesis of Cancer. *Nat Rev Cancer* **2008**, *8* (1), 11 23. <https://doi.org/10.1038/nrc2291> .
- (4) Collins, L. G.; Haines, C.; Perkel, R.; Enck, R. E. Lung Cancer: Diagnosis and Management. *American Family Physician* **2006**, *1* 8.
- (5) Shaw, A. T.; Kim, D.-W.; Mehra, R.; Tan, D. S.; Felip, E.; Chow, L. Q.; Camidge, R. D.; Vansteenkiste, J.; Sharma, S.; Pas, T.; et al. Ceritinib in ALK-Rearranged Non–Small-Cell Lung Cancer. *New Engl J Medicine* **2014**, *370* (13), 1189 1197. <https://doi.org/10.1056/nejmoa1311107> .
- (6) Peters, S.; Camidge, R. D.; Shaw, A. T.; Gadgeel, S.; Ahn, J. S.; Kim, D.-W.; Ou, S.-H. I.; Pérol, M.; Dziadziuszko, R.; Rosell, R.; et al. Alectinib Versus Crizotinib in Untreated ALK-Positive Non–Small-Cell Lung Cancer. *New Engl J Medicine* **2017**, *377* (9), 829 838. <https://doi.org/10.1056/nejmoa1704795> .
- (7) Soria, J.-C.; Tan, D. S.; Chiari, R.; Wu, Y.-L.; Paz-Ares, L.; Wolf, J.; Geater, S. L.; Orlov, S.; Cortinovis, D.; Yu, C.-J.; et al. First-Line Ceritinib Versus Platinum-Based Chemotherapy in Advanced ALK-Rearranged Non-Small-Cell Lung Cancer (ASCEND-4): A Randomised, Open-Label, Phase 3 Study. *Lancet* **2017**, *389* (10072), 917 929. [https://doi.org/10.1016/s0140-6736\(17\)30123-x](https://doi.org/10.1016/s0140-6736(17)30123-x) .
- (8) Katayama, R.; Shaw, A.; Khan, T.; Mino-Kenudson, M.; Solomon, B.; Halmos, B.; Jessop, N.; Wain, J.; Yeo, A.; Benes, C.; et al. Mechanisms of Acquired Crizotinib Resistance in ALK-Rearranged Lung Cancers. *Sci Transl Med* **2012**, *4* (120), 120ra17 120ra17. <https://doi.org/10.1126/scitranslmed.3003316> .
- (9) Cooper, M.; Chim, H.; Chan, H.; Durand, C. Ceritinib: A New Tyrosine Kinase Inhibitor for Non-Small-Cell Lung Cancer. *Ann Pharmacother* **2014**, *49* (1), 107 112. <https://doi.org/10.1177/1060028014553619> .
- (10) Sullivan, I.; Planchard, D. ALK Inhibitors in Non-Small Cell Lung Cancer: The Latest Evidence and Developments. *Ther Adv Med Oncol* **2015**, *8* (1), 32 47. <https://doi.org/10.1177/1758834015617355> .
- (11) Bayliss, R.; Choi, J.; Fennell, D. A.; Fry, A. M.; Richards, M. W. Molecular Mechanisms That Underpin EML4-ALK Driven Cancers and Their Response to Targeted Drugs. *Cell Mol Life Sci* **2016**, *73* (6), 1209 1224. <https://doi.org/10.1007/s00018-015-2117-6> .
- (12) Lin, J. J.; Riely, G. J.; Shaw, A. T. Targeting ALK: Precision Medicine Takes on Drug Resistance. *Cancer Discov* **2017**, *7* (2), 137 155. <https://doi.org/10.1158/2159-8290.cd-16-1123>

- (13) Akamine, T.; Toyokawa, G.; Tagawa, T.; Seto, T. Spotlight on Lorlatinib and Its Potential in the Treatment of NSCLC: The Evidence to Date. *Oncotargets Ther* **2018**, *11*, 5093–5101. <https://doi.org/10.2147/ott.s165511> .
- (14) Zhang, S.; Anjum, R.; Squillace, R.; Nadworny, S.; Zhou, T.; Keats, J.; Ning, Y.; Wardwell, S. D.; Miller, D.; Song, Y.; et al. The Potent ALK Inhibitor Brigatinib (AP26113) Overcomes Mechanisms of Resistance to First- and Second-Generation ALK Inhibitors in Preclinical Models. *Clin Cancer Res* **2016**, *22* (22), 5527–5538. <https://doi.org/10.1158/1078-0432.ccr-16-0569> .
- (15) Kirkland, L. O.; McInnes, C. Non-ATP Competitive Protein Kinase Inhibitors as Anti-Tumor Therapeutics. *Biochem Pharmacol* **2009**, *77* (10), 1–11. <https://doi.org/10.1016/j.bcp.2008.12.022> .
- (16) Jia, Y.; Yun, C.-H.; Park, E.; Ercan, D.; Manuia, M.; Juarez, J.; Xu, C.; Rhee, K.; Chen, T.; Zhang, H.; et al. Overcoming EGFR(T790M) and EGFR(C797S) Resistance with Mutant-Selective Allosteric Inhibitors. *Nature* **2016**, *534* (7605), 129–132. <https://doi.org/10.1038/nature17960> .
- (17) enath Sharma, V.; Bell, D. W.; Settleman, J.; Haber, D. A. Epidermal Growth Factor Receptor Mutations in Lung Cancer. *Clin Lung Cancer* **2007**, *7* (3), 169–181. [https://doi.org/10.1016/s1525-7304\(11\)70394-1](https://doi.org/10.1016/s1525-7304(11)70394-1) .
- (18) Palmer, R. H.; Vernersson, E.; Grabbe, C.; Hallberg, B. Anaplastic Lymphoma Kinase: Signalling in Development and Disease. *Biochem J* **2009**, *420* (3), 345–361. <https://doi.org/10.1042/bj20090387> .
- (19) Ladanyi, M.; Pao, W. Lung Adenocarcinoma: Guiding EGFR-Targeted Therapy and Beyond. *Nature* **2008**, *21* (7153), S16–S22. <https://doi.org/10.1038/nature05945> .
- (20) Pargellis, C.; Tong, L.; Churchill, L.; Cirillo, P. F.; Gilmore, T.; Graham, A. G.; Grob, P. M.; Hickey, E. R.; Moss, N.; Pav, S.; et al. Inhibition of P38 MAP Kinase by Utilizing a Novel Allosteric Binding Site. *Nat Struct Mol Biology* **2002**, *9* (4), 268–272. <https://doi.org/10.1038/nsb770> .
- (21) Cui, J. J.; Tran-Dubé, M.; Shen, H.; Nambu, M.; Kung, P.-P.; Pairish, M.; Jia, L.; Meng, J.; Funk, L.; Botrous, I.; et al. Structure Based Drug Design of Crizotinib (PF-02341066), a Potent and Selective Dual Inhibitor of Mesenchymal–Epithelial Transition Factor (c-MET) Kinase and Anaplastic Lymphoma Kinase (ALK). *J Med Chem* **2011**, *54* (18), 6342–6363. <https://doi.org/10.1021/jm2007613> .
- (22) Epstein, L. F.; Chen, H.; Emkey, R.; Whittington, D. A. The R1275Q Neuroblastoma Mutant and Certain ATP-Competitive Inhibitors Stabilize Alternative Activation Loop Conformations of Anaplastic Lymphoma Kinase. *J Biol Chem* **2012**, *287* (44), 37447–37457. <https://doi.org/10.1074/jbc.m112.391425> .
- (23) Tu, C.-H.; Lin, W.-H.; Peng, Y.-H.; Hsu, T.; Wu, J.-S.; Chang, C.-Y.; Lu, C.-T.; Lyu, P.-C.; Shih, C.; Jiaang, W.-T.; et al. Pyrazolylamine Derivatives Reveal the Conformational Switching between Type-I and Type-II Binding Modes of Anaplastic Lymphoma Kinase (ALK). *J Med*

*Chem* **2016**, *59* (8), acs.jmedchem.6b00106. <https://doi.org/10.1021/acs.jmedchem.6b00106> .

(24) Glickman, F. J.; Wu, X.; Mercuri, R.; Illy, C.; Bowen, B. R.; He, Y.; Sills, M. A Comparison of ALPHAScreen, TR-FRET, and TRF as Assay Methods for FXR Nuclear Receptors. *Journal of Biomolecular Screening* **2002**, *7* (1), 1-8.

(25) Lewis, R. T.; Bode, C. M.; Choquette, D. M.; Potashman, M.; Romero, K.; Stellwagen, J. C.; Teffera, Y.; Moore, E.; Whittington, D. A.; Chen, H.; et al. The Discovery and Optimization of a Novel Class of Potent, Selective, and Orally Bioavailable Anaplastic Lymphoma Kinase (ALK) Inhibitors with Potential Utility for the Treatment of Cancer. *J Med Chem* **2012**, *55* (14), 6523-6540. <https://doi.org/10.1021/jm3005866> .

**Chapter 4: Selective Degradation of GSPT1 by Novel  
Cereblon Modulators Generated from Kinase Inhibitor  
Scaffolds**

## **Attributions**

The work in this chapter is adapted from a manuscript that is being prepared for submission titled “Selective Degradation of GSPT1 by Novel Cereblon Modulators Generated from Kinase Inhibitor Scaffolds” by Powell *et al.* Author contributions, funding sources, and competing interests for this work can be found near the end of the chapter, before the references.

## **Chapter 4: Selective Degradation of GSPT1 by Novel Cereblon Modulators Generated from Kinase Inhibitor Scaffolds**

Chelsea E. Powell, Guangyan Du, Jianwei Che, Zhixiang He, Katherine A. Donovan, Radosław P. Nowak, Tinghu Zhang, Eric S. Fischer, Nathanael S. Gray\*

Department of Cancer Biology, Dana-Farber Cancer Institute, Boston, Massachusetts 02215, United States

Department of Biological Chemistry & Molecular Pharmacology, Harvard Medical School, Boston, Massachusetts 02115, United States

\* Correspondence: [Nathanael\\_Gray@dfci.harvard.edu](mailto:Nathanael_Gray@dfci.harvard.edu) (N.S.G.).

## **Abstract**

We generated a thalidomide analog library of 51 compounds by introducing kinase inhibitor scaffolds to lenalidomide. We screened the library in MM1.s cells for cereblon dependent antiproliferative activity and identified 5 hit compounds. We examined by western blot if these hit compounds induced the degradation of previously identified targets of cereblon modulators: IKZF1, IKZF3, CK1 $\alpha$ , and GSPT1. Expression proteomics was used to examine the activity of the compound that induced the least amount of degradation of known targets (ZXH-1-167); this demonstrated that ZXH-1-167 induced selective degradation of GSPT1. Docking studies of our hit compounds with CRBN and GSPT1 identified a possible hydrogen bond interaction with the central pyrimidine ring that may not be possible with zinc finger proteins, accounting for our hit compounds' selectivity. Generating an analog of hit compound ZXH-1-161 without the key nitrogen in the pyrimidine ring, demonstrated that this nitrogen is essential for the GSPT1 degradative activity seen.

## 4.1 Introduction

During the late 1950s and early 1960s thalidomide was sold as a sedative that was frequently prescribed to pregnant women. Infamously, thalidomide use during pregnancy had teratogenic activity, leading to birth defects such as limb, ear, cardiac, and gastrointestinal malformations.<sup>1</sup> Thalidomide was banned once the drug's use was linked to the observed birth defects. In the following decades thalidomide was demonstrated to have immunomodulatory, anti-inflammatory, and anti-angiogenic properties, which reignited interest in its therapeutic potential.<sup>2</sup> This led to thalidomide being given its first FDA approval in 1998 for the treatment of erythema nodosum leprosum (ENL), a life-threatening inflammatory complication of lepromatous leprosy.<sup>2</sup> Shortly afterwards thalidomide was shown to be an effective treatment for multiple myeloma, resulting in the development of more potent immunomodulatory drugs (IMiDs) with lower toxicities, lenalidomide and pomalidomide, as multiple myeloma therapies.<sup>2-4</sup>

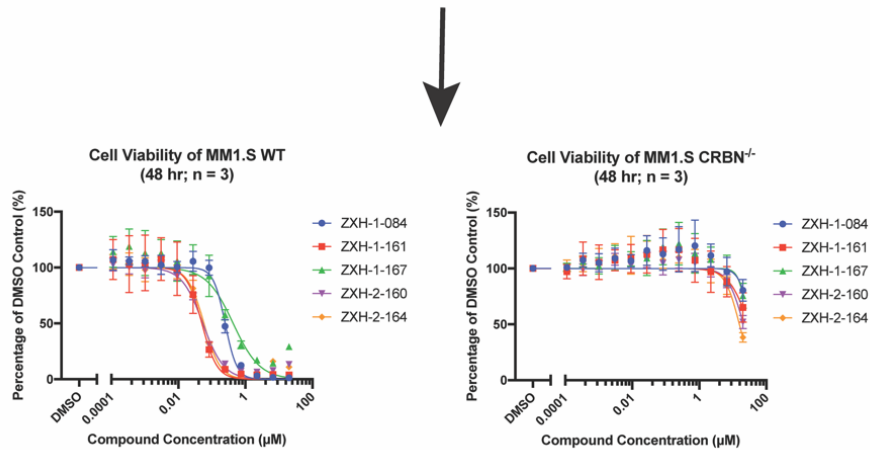
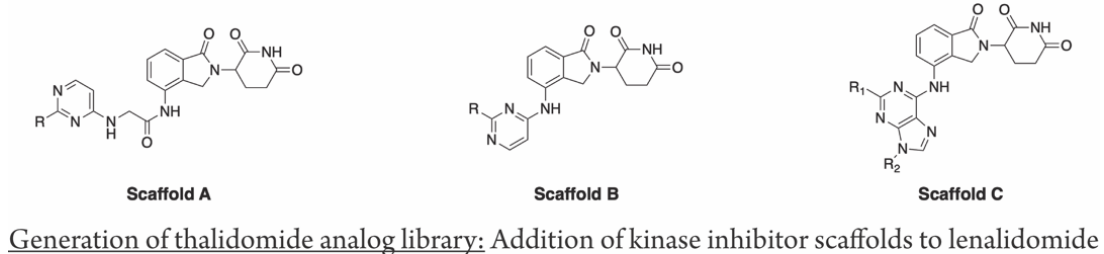
In 2010 the mechanism of action behind thalidomide's teratogenicity was identified; thalidomide was demonstrated to bind to cereblon (CRBN).<sup>1</sup> CRBN forms an E3 ubiquitin ligase complex with damaged DNA binding protein 1 (DDB1) and Cul4A. Ito et al. demonstrated that thalidomide may cause teratogenic effects in part by binding to CRBN and inhibiting the associated ubiquitin ligase activity, which was shown to be important for limb growth in zebrafish and chicks. Subsequently, the antiproliferative and immunomodulatory activity of thalidomide, lenalidomide, and pomalidomide in myeloma cells was shown to be CRBN mediated as well.<sup>5</sup> Through binding to CRBN, IMiDs are able to induce the ubiquitination and downstream degradation of the transcription factors Ikaros (IKZF1) and Aiolos (IKZF3), leading to the observed immunomodulatory effects and cytotoxicity in myeloma cells.<sup>6,7</sup>

These findings suggested that through the use of small molecules CRBN may be recruited to induce the degradation of therapeutic targets. Indeed, it has since been shown that the degradation of numerous other proteins may be induced through the use of heterobifunctional small molecule degraders (also known as PROTACs).<sup>8-10</sup> Unlike small molecule degraders,

CRBN modulators (also referred to as effectors), like IMiDs, have low molecular weights (~300 Da) and induce a much tighter protein-protein interaction by behaving as “molecular glues.”<sup>11</sup> Although novel cereblon modulators have been identified, there are only a few known degradable targets of these compounds. In addition to IKZF1 and IKZF3, cereblon modulators can induce the degradation of casein kinase 1A1 (CK1 $\alpha$ ) and translation termination factor G1 to S phase transition protein 1 (GSPT1).<sup>12,13</sup>

The discovery of these additional proteins that are amenable to degradation by CRBN modulators indicates that there are yet unidentified proteins that may also be targeted by this mechanism of action. Since the identified proteins do not need affinity for the CRBN modulators, this suggests that this mechanism of action provides a great opportunity to target proteins previously deemed to be “undruggable.”<sup>11</sup> Therefore, the development of libraries of novel CRBN modulators may help to identify new therapeutic targets that are amenable to degradation.

Here we describe the development of a thalidomide analog library through the introduction of kinase inhibitor scaffolds to lenalidomide. We screened this library for antiproliferative activity in the multiple myeloma cell line MM1.S (wild-type (WT) and CRBN knockout). Compounds with CRBN dependent antiproliferative activity were selected for expression proteomics in order to identify degraded proteins (Figure 4.1). Through this workflow we identified 5 hits from our library of 51 compounds. These 5 new CRBN modulators were all shown to induce degradation of GSPT1, a previously identified degradable target.



Phenotypic screen: Antiproliferative activity in MM1.s WT vs. CRBN<sup>-/-</sup>

↓

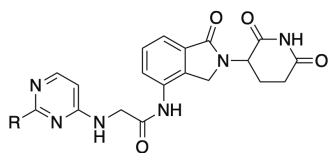
Target identification: Expression proteomics to identify degraded proteins

**Figure 4.1.** Workflow for identifying new CRBN modulators.

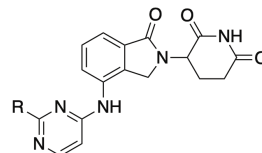
## 4.2 Results and Discussion

We generated a thalidomide analog library based around three scaffolds that introduced common moieties from kinase inhibitors to lenalidomide. Scaffolds A and B introduced an aminopyrimidine moiety, while Scaffold C introduced a benzimidazole moiety (Table 4.1).

**Table 4.1.** IC<sub>50</sub> (μM) values of thalidomide analogs. Cell viability in MM1.S WT and CRBN<sup>-/-</sup> cells after 48 hr treatment (3 biological replicates). NA = no activity. IC<sub>50</sub>s of **2**, **26**, and **29** shown as average of 2 separate runs (3 biological replicates each).



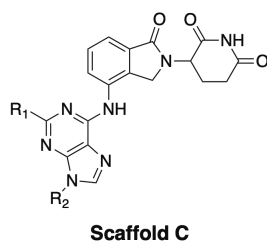
**Scaffold A**



**Scaffold B**

Compound	Scaffold	R	MM1.S WT	MM1.S CRBN <sup>-/-</sup>	Compound	Scaffold	R	MM1.S WT	MM1.S CRBN <sup>-/-</sup>	Compound	Scaffold	R	MM1.S WT	MM1.S CRBN <sup>-/-</sup>
1, ZXH-1-080	A		NA	NA	16, ZXH-1-143	A		NA	NA	31, ZXH-1-170	B		NA	NA
2, ZXH-1-084	A		0.180	57.4	17, ZXH-1-144	A		NA	50.0	32, ZXH-1-172	B		NA	NA
3, ZXH-1-086	A		NA	NA	18, ZXH-1-162	A		NA	NA	33, ZXH-1-173	B		NA	NA
4, ZXH-1-090	A		NA	NA	19, ZXH-1-179	A		NA	NA	34, ZXH-1-178	B		NA	NA
5, ZXH-1-101	A		NA	NA	20, ZXH-1-154	B		NA	NA	35, ZXH-1-181	B		NA	54.6
6, ZXH-1-102	A		NA	NA	21, ZXH-1-155	B		NA	NA	36, ZXH-1-182	B		2.98	2.72
7, ZXH-1-114	A		NA	NA	22, ZXH-1-156	B		NA	NA	37, ZXH-1-186	B		NA	NA
8, ZXH-1-120	A		41.1	54.3	23, ZXH-1-158	B		NA	NA	38, ZXH-2-005	B		NA	NA
9, ZXH-1-123	A		NA	NA	24, ZXH-1-159	B		NA	NA	39, ZXH-2-009	B		NA	36.7
10, ZXH-1-124	A		NA	NA	25, ZXH-1-160	B		21.1	19.6	40, ZXH-2-010	B		NA	NA
11, ZXH-1-125	A		NA	NA	26, ZXH-1-161	B		0.039	27.9	41, ZXH-2-050	B		NA	NA
12, ZXH-1-126	A		NA	NA	27, ZXH-1-163	B		NA	24.2	42, ZXH-2-058	B		8.86	10.6
13, ZXH-1-127	A		NA	NA	28, ZXH-1-166	B		NA	NA	43, ZXH-2-059	B		26.7	22.1
14, ZXH-1-137	A		33.8	NA	29, ZXH-1-167	B		0.784	20.9	44, ZXH-2-093	B		31.4	24.7
15, ZXH-1-138	A		NA	NA	30, ZXH-1-169	B		NA	NA	45, ZXH-2-160	B		0.054	20.8

**Table 4.1 (continued).**



Compound	R <sub>1</sub>	R <sub>2</sub>	MM1.S WT	MM1.S CRBN <sup>-/-</sup>	Compound	R <sub>1</sub>	R <sub>2</sub>	MM1.S WT	MM1.S CRBN <sup>-/-</sup>
46, ZXH-2-133		H	NA	NA	49, ZXH-2-156		H	NA	NA
47, ZXH-2-138		H	6.75	5.75	50, ZXH-2-159		H	NA	NA
48, ZXH-2-153		H	NA	24.3	51, ZXH-2-164			0.058	15.7

The majority of the 51 compounds in the library had no antiproliferative activity in either MM1.S WT or CRBN<sup>-/-</sup>. 7 compounds (**8**, **25**, **36**, **42**, **43**, **44**, and **47**) had notable to slight antiproliferative activity in both cell lines (Table 4.1). This indicated that these compounds have CRBN independent cytotoxicity. 5 compounds had strong antiproliferative activity in MM1.S WT cells with weak antiproliferative activity in MM1.S CRBN<sup>-/-</sup>: **2**, **26**, **29**, **45**, and **51**. These 5 compounds were considered hits for potential novel CRBN modulators since their cytotoxicity was CRBN dependent.

We then examined by western whether or not these hit compounds induced the degradation of previously identified targets of CRBN modulators. All 5 compounds induced some degradation of GSPT1 in MM1.S cells after 4 hr of treatment, with little to no detectable activity against IKZF1, IKZF3, and CK1 $\alpha$  (Figure 4.2B).

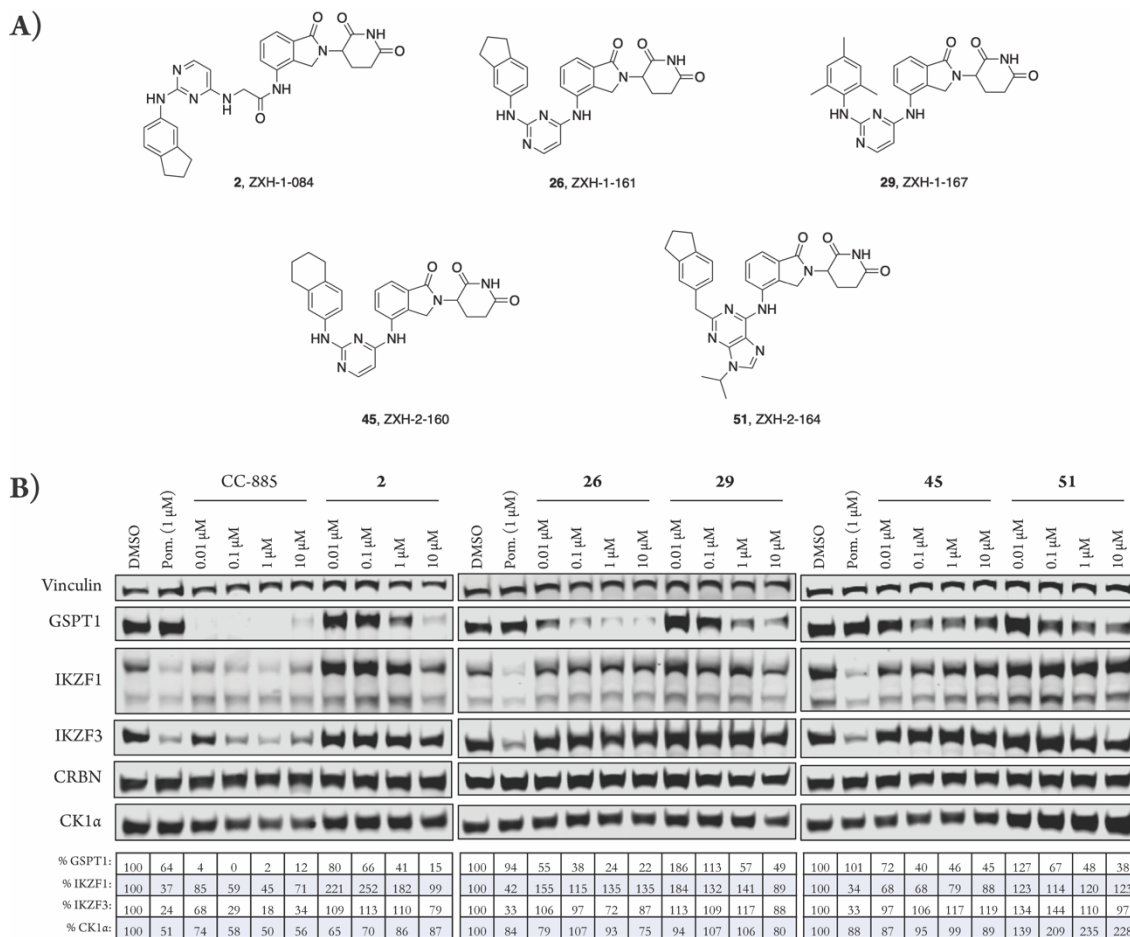


**Figure 4.2.** Hit compounds from cereblon dependent antiproliferative activity screening and their degradative activity of known cereblon modulator targets. (A) Structures of hit compounds. (B) Immunoblots after 4 hr treatments in MM1.s cells. Vinculin representative of 4 blots. Quantification shown as percentage of DMSO control normalized to vinculin.

In order to identify any potential new degradable targets of cereblon modulators, we selected the compound with the least amount of degradative activity against known targets as measure by western, **29**, for examination by expression proteomics. Expression proteomics was performed after 6 hr treatment in MM1.S cells with 1 μM of **29**. This demonstrated that **29** selectively induced the degradation of GSPT1, with no other statistically significant downregulated targets (Figure 4.3). Singlicate analysis of expression proteomics with **2** and **51** showed similarly selective degradation of GSPT1, with GSPT2, a close homolog of GSPT1, being the only other downregulated target observed after treatment with **51** (Figure 4.4).<sup>14</sup>

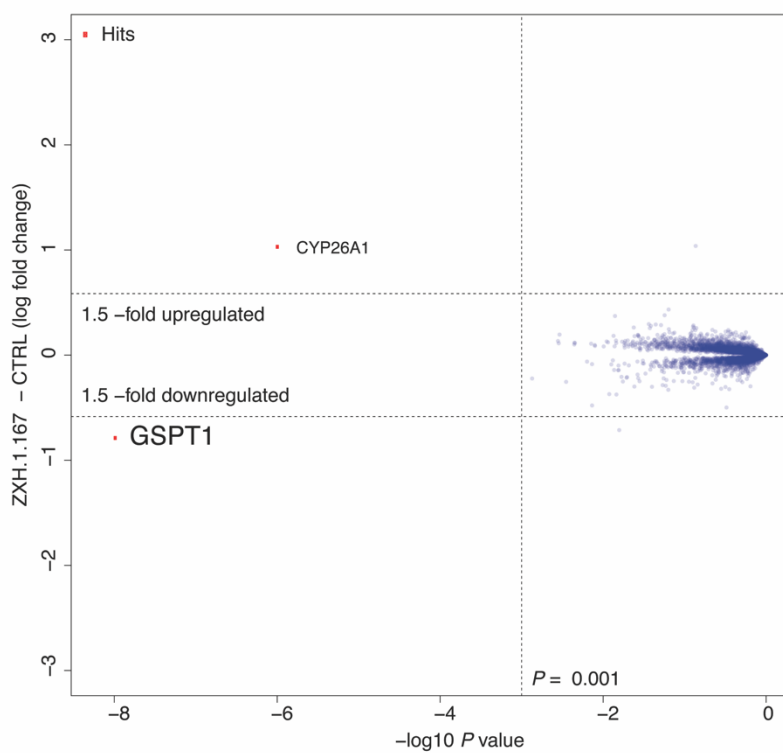


**Figure 4.3.** Expression proteomics in MM1.S cells after 6 hr treatment with 1  $\mu$ M of **29** or DMSO (triplicate analysis).

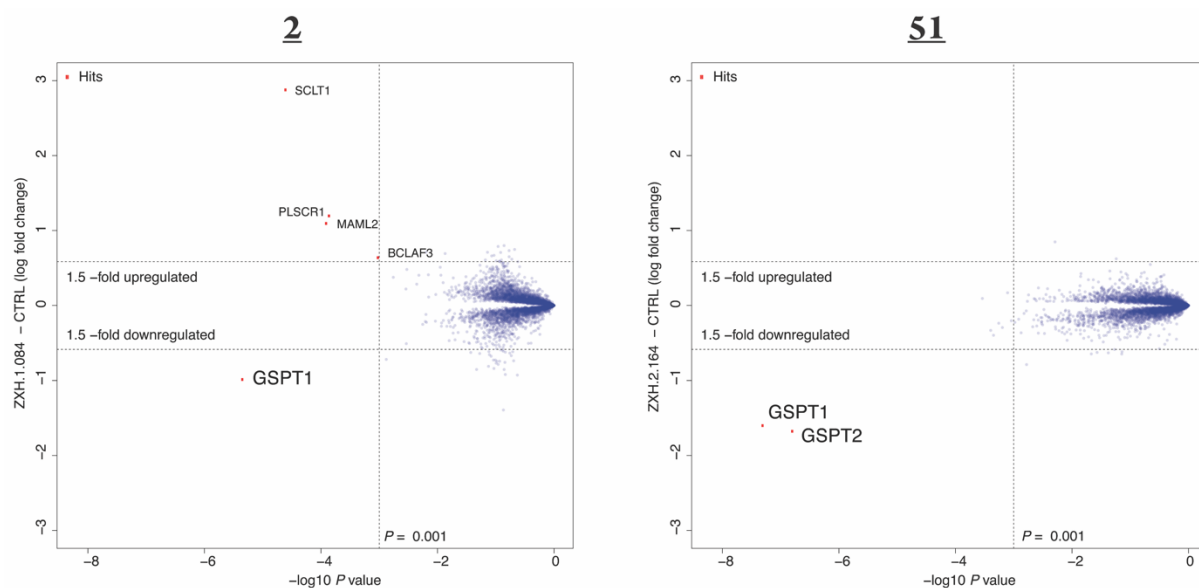


**Figure 4.4.** Expression proteomics in MM1.S cells after 6 hr treatment with 1  $\mu$ M of **2**, **51** or DMSO (singlicate analysis).

To understand how our hit compounds interact with CRBN and GSPT1, **26** was docked into the ternary complex model of CC-885 with CRBN and GSPT1 (PDB: 5HXB) using InducedFit protocol (Schrodinger suite release 2019-2). The binding mode of **26** is shown in green in Figure 4.5A and compared with CC-885 in gray. Overall, **26** occupies the same binding cavity formed at the interface between GSPT1 and CRBN, and has a very similar shape as CC-885. Besides forming the same interactions with the IMiD portion of the molecule, both CC-885 and **26** form a hydrogen bond with HIS353 of CRBN. Based on this putative binding mode, one key interaction of **26** is the hydrogen bond with LYS628 of GSPT1, which is not seen with CC-885. In addition, the central pyrimidine ring of **26** is able to keep the tail phenyl group with a minimal twist in comparison with CC-885 phenyl group. Therefore, the nitrogens of the pyrimidine ring play critical roles in GSPT1 binding. If we replace the 5 position of N with C, it should disrupt the hydrogen bond with LYS628 and force the terminal phenyl group to adopt twisted conformation. Both effects together should have detrimental consequences on the recruitment of GSPT1. To test the hypothesis, we made **52** (Figure 4.5B).

A comparison of **26** and **52** demonstrated that replacement of the 5 position of N with C results in a loss of CRBN dependent antiproliferative activity in MM1.s cells (Figure 4.5C). Additionally, examination by western showed that **52** does not induce degradation of GSPT1 to the same extent as **26** (Figure 4.5D). Together this indicates that the nitrogen in the pyrimidine rings of our hit compounds is essential for the GSPT1 degradation seen. Furthermore, it is possible that an equivalent hydrogen bond interaction with the pyrimidine ring cannot be made with zinc finger proteins, accounting for the selectivity seen by expression proteomics.

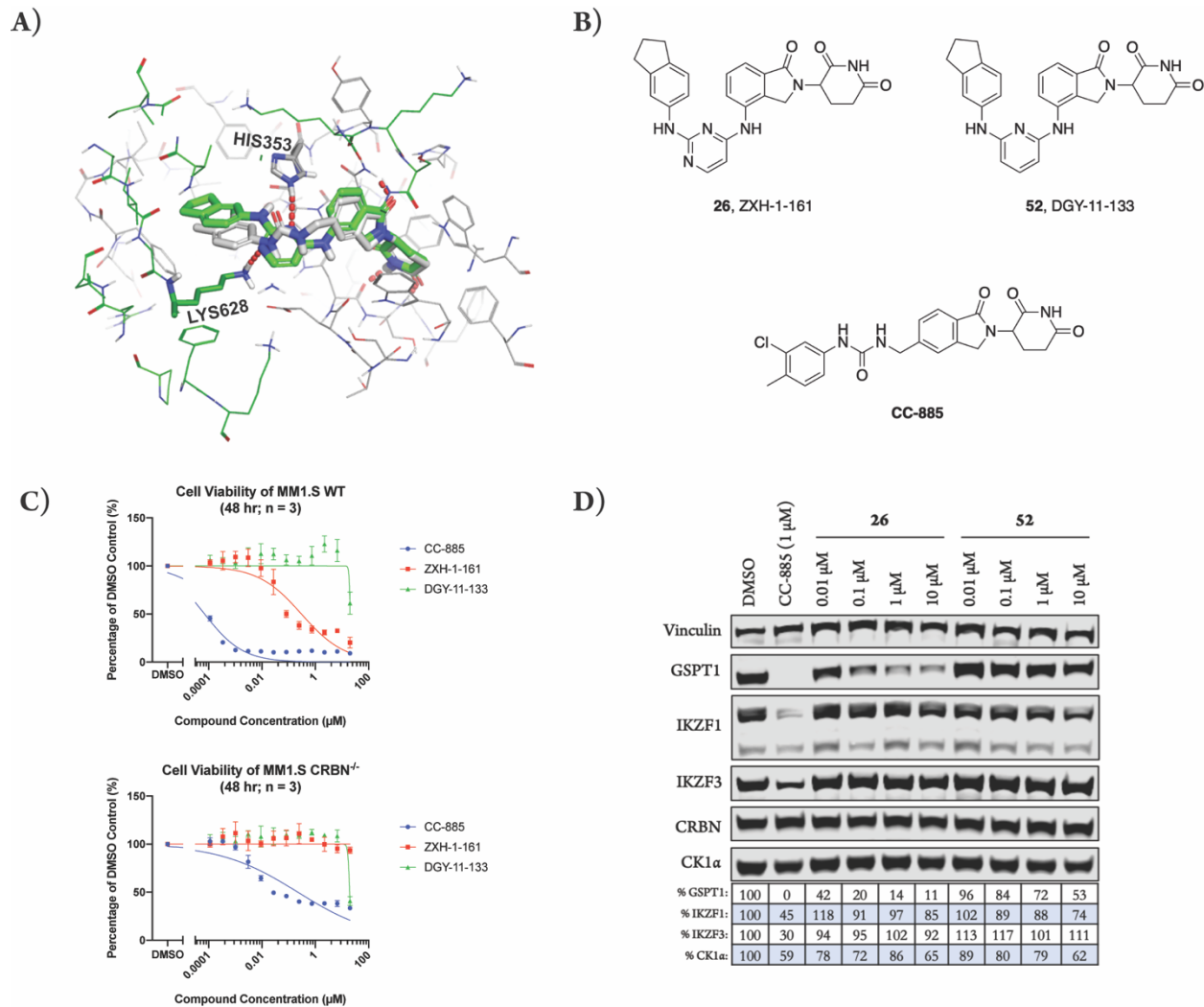


**Figure 4.5.** Molecular modeling of **26** identifies that the nitrogens in the pyrimidine ring are critical for GSPT1 degradation. (A) Docking of **26** (green) and CC-885 (gray) into the ternary complex model of CC-885 with CRBN (green) and GSPT1 (gray) (PDB: 5HXB). (B) Structures of **26** and its analog **52**, with the 5 position of N replaced with C. (C) Antiproliferative IC<sub>50</sub> curves ± SD after 48 hr treatments (three biological replicates; Graphpad Prism 8 software). (D) Immunoblot after 4 hr treatments in MM1.s cells. Vinculin representative of 4 blots. Quantification shown as percentage of DMSO control normalized to vinculin.

## Conclusion

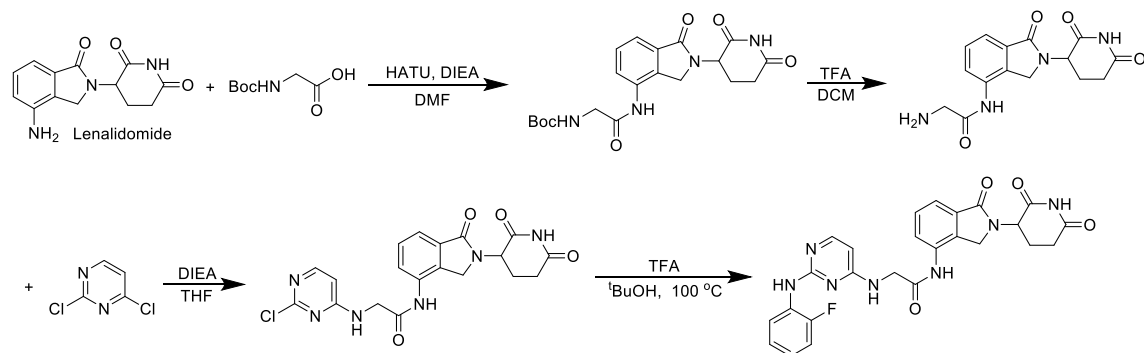
We have developed a thalidomide analog library by introducing kinase inhibitor scaffolds to lenalidomide. Screening for CRBN dependent antiproliferative effects led to the identification of CRBN modulators that can induce the selective degradation of GSPT1. This method of screening the library did not lead to the identification of new degradable targets of CRBN modulators. GSPT1 is a translation termination factor that binds eRF1 in order to mediate stop

codon recognition and nascent protein release from the ribosome.<sup>13</sup> It is possible that the degradation of this protein is so cytotoxic that our antiproliferative screening strategy was biased towards compounds affecting GSPT1. Additionally, our finding that the introduction of kinase inhibitor moieties to IMiDs results in GSPT1 degradation is supported by previous studies of the degradation of receptor tyrosine kinases by promiscuous small molecule degraders, which demonstrated that GSPT1 degradation is a converging off-target.<sup>15</sup> Future screening strategies with this library may benefit from focusing on potential kinase related activity of these compounds in order to identify novel CRBN modulator targets. However, this study has successfully identified novel CRBN modulators with selective activity against GSPT1, and has identified a structural reasoning for the activity seen. This may provide a method for therapeutically targeting GSPT1, which has been shown to be relevant in preclinical models of acute myeloid leukemia (AML).<sup>16</sup>

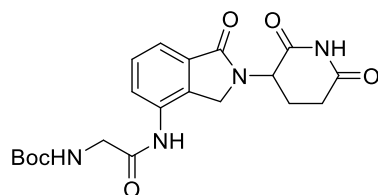
#### **4.4 Experimental Methods**

Unless otherwise noted, reagents and solvents were obtained from commercial suppliers and were used without further purification. <sup>1</sup>H NMR spectra were recorded on 500 MHz (Bruker A500), and chemical shifts are reported in parts per million (ppm,  $\delta$ ) downfield from tetramethylsilane (TMS). Coupling constants (*J*) are reported in Hz. Spin multiplicities are described as s (singlet), br (broad singlet), d (doublet), t (triplet), q (quartet), and m (multiplet). Mass spectra were obtained on a Waters Micromass ZQ instrument. Preparative HPLC was performed on a Waters Sunfire C18 column (19 x 50 mm, 5 $\mu$ M) using a gradient of 15-95% methanol in water containing 0.05% trifluoroacetic acid (TFA) over 22 min (28 min run time) at a flow rate of 20 mL/min. Purities of assayed compounds were in all cases greater than 95%, as determined by reverse-phase HPLC analysis.

#### Scheme 4.1. Synthesis of 1

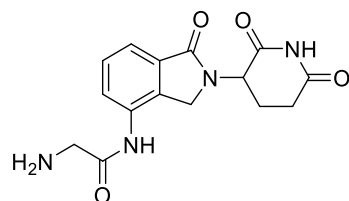


#### *tert*-Butyl (2-((2-(2,6-dioxopiperidin-3-yl)-1-oxoisindolin-4-yl)amino)-2-oxoethyl)-carbamate



To a solution of (*tert*-butoxycarbonyl)glycine (2.1 g, 12 mmol), DIEA (5 mL, 30 mmol) in DMF (30 mL) was added 1-[Bis(dimethylamino)methylene]-1H-1,2,3-triazolo[4,5-b]pyridinium 3-oxid hexafluorophosphate (HATU) (4.94 g, 13 mmol), stirred for 0.5h, and then Lenalidomide (2.59 g, 10 mmol) was added, the mixture was then stirred at room temperature for another 1h. The mixture was then purified by silica gel (MeOH/DCM = 0–10%) to obtain the title compound. LCMS (m/z): 417 [M+H]<sup>+</sup>.

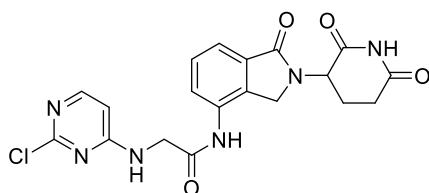
#### 2-Amino-N-(2-(2,6-dioxopiperidin-3-yl)-1-oxoisindolin-4-yl)acetamide



To a solution of tert-Butyl (2-((2-(2,6-dioxopiperidin-3-yl)-1-oxoisindolin-4-yl)amino)-2-oxoethyl)-carbamate in DCM (30 mL) was added TFA (10 mL), and stirred at room temperature for 3h. The mixture was then concentrated *in vacuo*, and purified by silica gel (MeOH/DCM = 0-30%) to obtain the title compound (972 mg, 23% for 2 steps).

LCMS (m/z): 317 [M+H]<sup>+</sup>.

**2-((2-chloropyrimidin-4-yl)amino)-N-(2-(2,6-dioxopiperidin-3-yl)-1-oxoisindolin-4-yl)acetamide**



To a solution of 2-amino-N-(2-(2,6-dioxopiperidin-3-yl)-1-oxoisindolin-4-yl)acetamide (972 mg, 2.26 mmol) and 2,4-dichloropyrimidine (332 mg, 2.26 mmol) in THF (20 mL) was added DIEA (1.1 mL, 6.78 mmol), and then stirred overnight. The mixture was then concentrated *in vacuo*, and purified by silica gel (MeOH/DCM = 0-10%) to obtain the title compound (693 mg, 72%).

LCMS (m/z): 429 [M+H]<sup>+</sup>.

**N-(2-(2,6-dioxopiperidin-3-yl)-1-oxoisindolin-4-yl)-2-((2-(2-fluorophenyl)amino)pyrimidin-4-yl)amino)acetamide (1)**

To a solution of 2-((2-chloropyrimidin-4-yl)amino)-N-(2-(2,6-dioxopiperidin-3-yl)-1-oxoisindolin-4-yl)acetamide (50 mg, 0.12 mmol) and 2-fluoroaniline (13 mg, 0.12 mmol) in <sup>t</sup>BuOH (1 mL) was added TFA (18 μL, 0.24 mmol), and then the mixture was heated to reflux overnight. The mixture was then concentrated *in vacuo*, and purified by prep-HPLC (MeOH/H<sub>2</sub>O, 0.05% TFA) to obtain compound **1** (4.6 mg, 6%).

<sup>1</sup>H NMR (500 MHz, DMSO-*d*<sub>6</sub>) δ 11.05 (s, 1H), 10.18 (s, 1H), 10.06 (s, 1H), 9.38 (t, *J* = 5.7 Hz, 1H), 7.90 (d, *J* = 7.2 Hz, 1H), 7.83 – 7.74 (m, 2H), 7.57 – 7.49 (m, 2H), 7.26 – 7.16 (m, 1H), 7.08 – 6.97 (m, 1H), 6.45 (d, *J* = 7.2 Hz, 1H), 5.16 (dd, *J* = 13.3, 5.2 Hz, 1H), 4.31 – 4.22 (m, 4H), 2.93

(ddd,  $J = 17.4, 13.6, 5.4$  Hz, 1H), 2.65 – 2.56 (m, 1H), 2.24 (qd,  $J = 13.2, 4.5$  Hz, 1H), 2.03 (ddd,  $J = 10.3, 5.4, 2.8$  Hz, 1H).

LCMS (m/z): 504 [M+H]<sup>+</sup>.

**2-((2-((2,3-dihydro-1H-inden-5-yl)amino)pyrimidin-4-yl)amino)-N-(2-(2,6-dioxopiperidin-3-yl)-1-oxoisoindolin-4-yl)acetamide (2)**

**2** (4.4 mg, 6%) was obtained according to the synthetic route of **1**, changing from 2-fluoroaniline to 2,3-dihydro-1H-inden-5-amine.

<sup>1</sup>H NMR (500 MHz, DMSO-*d*<sub>6</sub>)  $\delta$  11.01 (s, 1H), 10.32 (s, 1H), 10.11 (s, 1H), 9.30 (t,  $J = 5.9$  Hz, 1H), 7.82 (d,  $J = 7.2$  Hz, 1H), 7.58 – 7.48 (m, 2H), 7.34 (s, 1H), 7.26 – 7.18 (m, 2H), 7.08 (d,  $J = 8.0$  Hz, 1H), 6.39 (d,  $J = 7.2$  Hz, 1H), 5.12 (dd,  $J = 13.3, 5.1$  Hz, 1H), 4.33 – 4.25 (m, 4H), 2.85 (dt,  $J = 14.5, 7.7$  Hz, 2H), 2.73 (q,  $J = 7.5$  Hz, 4H), 2.07 – 1.96 (m, 2H), 1.91 (p,  $J = 7.0$  Hz, 2H).

LCMS (m/z): 526 [M+H]<sup>+</sup>.

**2-((2-((benzo[d][1,3]dioxol-5-ylmethyl)amino)pyrimidin-4-yl)amino)-N-(2-(2,6-dioxopiperidin-3-yl)-1-oxoisoindolin-4-yl)acetamide (3)**

**3** (6.5 mg, 4%) was obtained according to the synthetic route of **1**, changing from 2-fluoroaniline to benzo[d][1,3]dioxol-5-ylmethanamine.

<sup>1</sup>H NMR (500 MHz, DMSO-*d*<sub>6</sub>)  $\delta$  11.02 (s, 1H), 9.85 (d,  $J = 4.6$  Hz, 1H), 7.78 (dd,  $J = 7.6, 1.4$  Hz, 1H), 7.68 (d,  $J = 5.7$  Hz, 1H), 7.54 – 7.43 (m, 2H), 7.32 (s, 1H), 6.94 (s, 1H), 6.82 (s, 1H), 6.76 – 6.65 (m, 2H), 5.90 (s, 2H), 5.86 (d,  $J = 6.0$  Hz, 1H), 5.14 (dd,  $J = 13.3, 5.1$  Hz, 1H), 4.36 – 4.22 (m, 4H), 4.09 (d,  $J = 5.9$  Hz, 2H), 2.92 (ddd,  $J = 17.2, 13.6, 5.4$  Hz, 1H), 2.69 – 2.57 (m, 1H), 2.32 – 2.18 (m, 1H), 2.03 – 1.96 (m, 1H).

LCMS (m/z): 544 [M+H]<sup>+</sup>.

**N-(2-(2,6-dioxopiperidin-3-yl)-1-oxoisoindolin-4-yl)-2-((2-((R)-2-(hydroxymethyl)pyrrolidin-1-yl)pyrimidin-4-yl)amino)acetamide (4)**

**4** (1.9 mg, 3%) was obtained according to the synthetic route of **1**, changing from 2-fluoroaniline to (S)-pyrrolidin-2-ylmethanol.

<sup>1</sup>H NMR (500 MHz, DMSO-*d*<sub>6</sub>)  $\delta$  11.88 (s, 1H), 11.04 (s, 1H), 10.13 (s, 1H), 9.12 (s, 1H), 7.83 (dd,  $J = 7.6, 1.4$  Hz, 1H), 7.73 (d,  $J = 7.3$  Hz, 1H), 7.57 – 7.46 (m, 2H), 6.29 (d,  $J = 7.2$  Hz, 1H), 5.18 (dd,  $J = 13.3, 5.1$  Hz, 1H), 4.42 – 4.26 (m, 4H), 3.64 – 3.34 (m, 4H), 2.94 (ddd,  $J = 18.1, 13.5, 5.4$  Hz, 1H), 2.67 – 2.60 (m, 1H), 2.30 (dd,  $J = 13.1, 4.6$  Hz, 1H), 2.10 – 1.90 (m, 6H).

LCMS (m/z): 494 [M+H]<sup>+</sup>.

**2-((2-(benzo[d][1,3]dioxol-5-ylamino)pyrimidin-4-yl)amino)-N-(2-(2,6-dioxopiperidin-3-yl)-1-oxoisoindolin-4-yl)acetamide (5)**

**5** (5.2 mg, 6%) was obtained according to the synthetic route of **1**, changing from 2-fluoroaniline to 2,3-dihydrobenzo[b][1,4]dioxin-6-amine.

<sup>1</sup>H NMR (500 MHz, DMSO-*d*<sub>6</sub>) δ 11.02 (s, 1H), 10.25 (s, 1H), 10.12 (s, 1H), 9.28 (s, 1H), 7.83 – 7.74 (m, 2H), 7.56 – 7.47 (m, 2H), 7.01 (d, *J* = 2.5 Hz, 1H), 6.97 (d, *J* = 8.6 Hz, 1H), 6.74 (d, *J* = 8.7 Hz, 1H), 6.37 (d, *J* = 7.2 Hz, 1H), 5.14 (dd, *J* = 13.3, 5.1 Hz, 1H), 4.32 (s, 2H), 4.16 – 4.05 (m, 4H), 2.92 (ddd, *J* = 17.2, 13.5, 5.4 Hz, 1H), 2.64 – 2.56 (m, 1H), 2.32 – 2.20 (m, 1H), 2.06 – 1.95 (m, 1H).

LCMS (m/z): 530 [M+H]<sup>+</sup>.

**N-(2-(2,6-dioxopiperidin-3-yl)-1-oxoisoindolin-4-yl)-2-((2-((3-(2-oxopyrrolidin-1-yl)propyl)amino)pyrimidin-4-yl)amino)acetamide (6)**

**6** (4.1 mg, 5%) was obtained according to the synthetic route of **1**, changing from 2-fluoroaniline to 1-(3-aminopropyl)pyrrolidin-2-one.

<sup>1</sup>H NMR (500 MHz, DMSO-*d*<sub>6</sub>) δ 11.94 (s, 1H), 11.04 (d, *J* = 2.3 Hz, 1H), 10.20 – 10.08 (m, 1H), 8.04 – 7.93 (m, 1H), 7.85 (ddd, *J* = 17.0, 7.4, 1.6 Hz, 1H), 7.74 (d, *J* = 7.3 Hz, 1H), 7.58 – 7.46 (m, 2H), 6.30 – 6.23 (m, 1H), 5.17 (ddd, *J* = 13.3, 5.2, 2.9 Hz, 1H), 4.49 – 4.21 (m, 4H), 3.31 (d, *J* = 22.6 Hz, 2H), 3.19 – 3.08 (m, 2H), 2.98 – 2.90 (m, 1H), 2.67 – 2.59 (m, 1H), 2.34 – 2.25 (m, 1H), 2.14 (d, *J* = 7.8 Hz, 1H), 2.08 – 1.99 (m, 1H), 1.81 (s, 1H), 1.62 (s, 1H).

LCMS (m/z): 535 [M+H]<sup>+</sup>.

**N-(2-(2,6-dioxopiperidin-3-yl)-1-oxoisoindolin-4-yl)-2-((2-((4-methoxyphenyl)amino)pyrimidin-4-yl)amino)acetamide (7)**

**7** (10.9 mg, 7%) was obtained according to the synthetic route of **1**, changing from 2-fluoroaniline to 4-methoxyaniline.

<sup>1</sup>H NMR (500 MHz, DMSO-*d*<sub>6</sub>) δ 11.02 (s, 1H), 10.46 (s, 1H), 10.15 (s, 1H), 9.32 (d, *J* = 5.7 Hz, 1H), 7.81 (td, *J* = 9.1, 7.7, 4.1 Hz, 2H), 7.58 – 7.47 (m, 2H), 7.42 (d, *J* = 8.5 Hz, 2H), 6.78 (d, *J* = 8.5 Hz, 2H), 6.38 (d, *J* = 7.2 Hz, 1H), 5.14 (dd, *J* = 13.3, 5.1 Hz, 1H), 4.33 – 4.23 (m, 4H), 3.60 (s, 3H), 2.93 (ddd, *J* = 17.2, 13.5, 5.4 Hz, 1H), 2.65 – 2.56 (m, 1H), 2.23 (qd, *J* = 13.2, 4.4 Hz, 1H), 2.01 (dtd, *J* = 12.4, 7.4, 6.2, 3.7 Hz, 1H).

LCMS (m/z): 516 [M+H]<sup>+</sup>.

***N*-(2-(2,6-dioxopiperidin-3-yl)-1-oxoisoindolin-4-yl)-2-((2-((*S*)-2-(hydroxymethyl)pyrrolidin-1-yl)pyrimidin-4-yl)amino)acetamide (14)**

**14** (5.1 mg, 2%) was obtained according to the synthetic route of **1**, changing from 2-fluoroaniline to (*R*)-pyrrolidin-2-ylmethanol.

<sup>1</sup>H NMR (500 MHz, DMSO-*d*<sub>6</sub>) δ 11.04 (s, 1H), 10.15 (s, 1H), 9.13 (s, 1H), 7.83 (d, *J* = 7.6 Hz, 1H), 7.74 (d, *J* = 7.2 Hz, 1H), 7.60 – 7.47 (m, 2H), 6.29 (d, *J* = 7.2 Hz, 1H), 5.18 (dd, *J* = 13.3, 5.2 Hz, 1H), 4.44 – 4.27 (m, 4H), 3.60 – 3.36 (m, 5H), 2.94 (ddd, *J* = 18.1, 13.5, 5.5 Hz, 1H), 2.68 – 2.58 (m, 1H), 2.30 (tt, *J* = 13.1, 6.7 Hz, 1H), 2.06 – 2.00 (m, 1H), 1.91 (dq, *J* = 18.5, 12.4, 6.4 Hz, 4H).

LCMS (m/z): 494 [M+H]<sup>+</sup>.

***N*-(2-(2,6-dioxopiperidin-3-yl)-1-oxoisoindolin-4-yl)-2-((2-((2-methoxyphenyl)amino)pyrimidin-4-yl)amino)acetamide (15)**

**15** (9.5 mg, 5%) was obtained according to the synthetic route of **1**, changing from 2-fluoroaniline to 2-methoxyaniline.

<sup>1</sup>H NMR (500 MHz, DMSO-*d*<sub>6</sub>) δ 11.03 (s, 1H), 10.18 (s, 1H), 9.64 (s, 1H), 9.38 (t, *J* = 5.8 Hz, 1H), 7.94 – 7.77 (m, 3H), 7.56 – 7.49 (m, 2H), 7.12 (t, *J* = 7.7 Hz, 1H), 7.09 – 7.07 (m, 1H), 6.80 (t, *J* = 7.7 Hz, 1H), 5.14 (dd, *J* = 13.3, 5.2 Hz, 1H), 4.34 – 4.20 (m, 4H), 3.83 (s, 3H), 2.92 (ddd, *J* = 17.2, 13.5, 5.4 Hz, 1H), 2.66 – 2.54 (m, 1H), 2.19 (qd, *J* = 13.1, 4.4 Hz, 1H), 2.00 (dtd, *J* = 12.8, 5.4, 2.2 Hz, 1H).

LCMS (m/z): 516 [M+H]<sup>+</sup>.

***N*-(2-(2,6-dioxopiperidin-3-yl)-1-oxoisoindolin-4-yl)-2-((2-(4-(3-(trifluoromethyl)phenyl)piperazin-1-yl)pyrimidin-4-yl)amino)acetamide (16)**

**16** (12.1 mg, 5%) was obtained according to the synthetic route of **1**, changing from 2-fluoroaniline to 1-(3-(trifluoromethyl)phenyl)piperazine.

<sup>1</sup>H NMR (500 MHz, DMSO-*d*<sub>6</sub>) δ 11.04 (s, 1H), 10.27 (s, 1H), 9.27 (t, *J* = 5.6 Hz, 1H), 7.88 (dd, *J* = 7.4, 1.6 Hz, 1H), 7.80 (dd, *J* = 7.2, 2.1 Hz, 1H), 7.59 – 7.51 (m, 2H), 7.47 – 7.43 (m, 1H), 7.29 – 7.22 (m, 1H), 7.17 (t, *J* = 6.9 Hz, 1H), 7.11 (d, *J* = 7.5 Hz, 1H), 5.18 (dd, *J* = 13.3, 5.1 Hz, 1H), 4.36 (dd, *J* = 34.4, 7.4 Hz, 4H), 3.85 (t, *J* = 5.1 Hz, 4H), 3.37 (dt, *J* = 48.5, 5.2 Hz, 4H), 2.93 (ddd, *J* = 18.0, 13.5, 5.3 Hz, 1H), 2.64 – 2.57 (m, 1H), 2.31 (qd, *J* = 13.2, 4.4 Hz, 1H), 2.04 (ddd, *J* = 13.3, 5.8, 3.4 Hz, 1H).

LCMS (m/z): 623 [M+H]<sup>+</sup>.

***N*-(2-(2,6-dioxopiperidin-3-yl)-1-oxoisoindolin-4-yl)-2-((2-(methyl(phenyl)amino)pyrimidin-4-yl)amino)acetamide (17)**

**17** (16.5 mg, 6%) was obtained according to the synthetic route of **1**, changing from 2-fluoroaniline to *N*-methylaniline.

<sup>1</sup>H NMR (500 MHz, DMSO-*d*<sub>6</sub>) δ 11.04 (s, 1H), 10.20 (s, 1H), 9.35 (t, *J* = 5.7 Hz, 1H), 7.86 (dd, *J* = 7.4, 1.6 Hz, 1H), 7.60 (d, *J* = 7.2 Hz, 1H), 7.57 – 7.53 (m, 2H), 7.49 (d, *J* = 7.4 Hz, 2H), 7.45 (dt, *J* = 8.2, 2.6 Hz, 3H), 6.38 (d, *J* = 7.2 Hz, 1H), 5.18 (dd, *J* = 13.3, 5.1 Hz, 1H), 4.46 – 4.28 (m, 4H), 3.44 (s, 3H), 2.99 – 2.87 (m, 1H), 2.67 – 2.58 (m, 1H), 2.31 (qd, *J* = 13.2, 4.5 Hz, 1H), 2.13 – 1.96 (m, 1H).

LCMS (m/z): 500 [M+H]<sup>+</sup>.

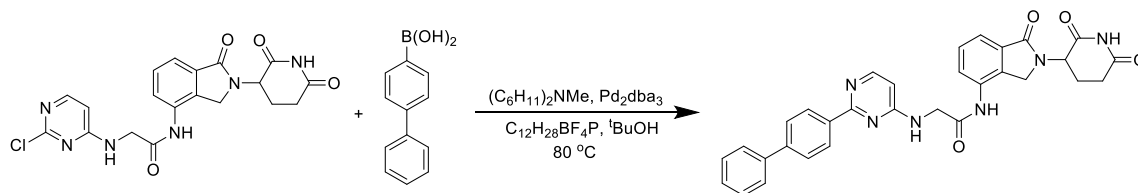
**2-((2-(benzyl(ethyl)amino)pyrimidin-4-yl)amino)-*N*-(2-(2,6-dioxopiperidin-3-yl)-1-oxoisoindolin-4-yl)acetamide (18)**

**18** (1.4 mg, 0.8%) was obtained according to the synthetic route of **1**, changing from 2-fluoroaniline to *N*-benzylethanamine.

<sup>1</sup>H NMR (500 MHz, DMSO-*d*<sub>6</sub>) δ 11.04 (s, 1H), 10.05 (s, 1H), 7.77 (dt, *J* = 13.2, 7.1 Hz, 2H), 7.54 – 7.46 (m, 2H), 7.40 – 7.18 (m, 6H), 6.33 (d, *J* = 6.6 Hz, 1H), 5.15 (dd, *J* = 13.2, 5.2 Hz, 1H), 4.78 (d, *J* = 16.6 Hz, 2H), 4.30 (d, *J* = 5.7 Hz, 4H), 3.52 (s, 2H), 2.93 (ddd, *J* = 17.4, 13.6, 5.4 Hz, 1H), 2.68 – 2.57 (m, 1H), 2.17 (d, *J* = 16.2 Hz, 1H), 2.01 (s, 1H), 1.03 (t, *J* = 7.0 Hz, 3H).

LCMS (m/z): 528 [M+H]<sup>+</sup>.

#### Scheme 4.2. Synthesis of **8**



#### **2-((2-([1,1'-biphenyl]-4-yl)pyrimidin-4-yl)amino)-N-(2-(2,6-dioxopiperidin-3-yl)-1-oxoisindolin-4-yl)acetamide (**8**)**

To a solution of 2-((2-chloropyrimidin-4-yl)amino)-N-(2-(2,6-dioxopiperidin-3-yl)-1-oxoisindolin-4-yl) acetamide (110 mg, 0.24 mmol) and [1,1'-biphenyl]-4-ylboronic acid (54 mg, 0.28 mmol) in <sup>t</sup>BuOH (2 mL) were added N,N-Dicyclohexylmethylamine (52 mg, 0.26 mmol), Pd<sub>2</sub>dba<sub>3</sub> (22 mg, 0.024 mmol) and Tri-*tert*-butylphosphonium tetrafluoroborate (20 mg, 0.048 mmol). The mixture was heated to 80 °C and stirred under N<sub>2</sub> atmosphere overnight. The mixture was then filtered, concentrated *in vacuo* and purified by prep-HPLC (MeOH/H<sub>2</sub>O, 0.05% TFA) to obtain **8** (4.4 mg, 3%).

<sup>1</sup>H NMR (500 MHz, DMSO-*d*<sub>6</sub>) δ 11.01 (s, 1H), 10.30 (s, 1H), 8.77 (dd, *J* = 4.4, 1.4 Hz, 1H), 8.36 (d, *J* = 8.2 Hz, 2H), 8.31 – 8.27 (m, 1H), 7.90 – 7.72 (m, 5H), 7.56 – 7.50 (m, 4H), 7.49 – 7.39 (m, 1H), 6.88 (d, *J* = 6.7 Hz, 1H), 5.11 (dd, *J* = 13.4, 5.0 Hz, 1H), 4.49 (d, *J* = 5.4 Hz, 2H), 4.37 (s, 2H), 2.87 (t, *J* = 13.9 Hz, 1H), 2.64 (d, *J* = 5.1 Hz, 1H), 2.17 (d, *J* = 13.4 Hz, 1H), 1.96 (s, 1H).  
LCMS (m/z): 547 [M+H]<sup>+</sup>.

#### **N-(2-(2,6-dioxopiperidin-3-yl)-1-oxoisindolin-4-yl)-2-((2-(3-methoxyphenyl)pyrimidin-4-yl)amino)acetamide (**9**)**

**9** (4.0 mg, 3%) was obtained according to the synthetic route of **8**, changing from [1,1'-biphenyl]-4-ylboronic acid to (3-methoxyphenyl)boronic acid.

<sup>1</sup>H NMR (500 MHz, DMSO-*d*<sub>6</sub>) δ 11.03 (s, 1H), 10.31 (s, 1H), 9.79 (s, 1H), 8.24 (d, *J* = 7.2 Hz, 1H), 8.19 – 8.17 (m, 1H), 7.81 (dd, *J* = 7.6, 1.5 Hz, 1H), 7.68 (ddd, *J* = 8.9, 7.3, 1.8 Hz, 1H), 7.56 – 7.52 (m, 2H), 7.32 (d, *J* = 8.4 Hz, 1H), 7.11 (t, *J* = 7.6 Hz, 1H), 6.98 (d, *J* = 7.2 Hz, 1H), 5.14 (dd, *J* = 13.3, 5.2 Hz, 1H), 4.50 (d, *J* = 5.5 Hz, 2H), 4.36 – 4.25 (m, 2H), 3.98 (s, 3H), 2.92 (ddd, *J* = 18.3, 13.4, 5.5 Hz, 1H), 2.62 – 2.56 (m, 1H), 2.15 – 2.07 (m, 1H), 2.00 – 1.96 (m, 1H).  
LCMS (m/z): 501 [M+H]<sup>+</sup>.

#### **2-((2-(2,4-dimethoxyphenyl)pyrimidin-4-yl)amino)-N-(2-(2,6-dioxopiperidin-3-yl)-1-oxoisindolin-4-yl)acetamide (**10**)**

**10** (2.8 mg, 1%) was obtained according to the synthetic route of **8**, changing from [1,1'-biphenyl]-4-ylboronic acid to (2,4-dimethoxyphenyl)boronic acid.

<sup>1</sup>H NMR (500 MHz, DMSO-*d*<sub>6</sub>) δ 11.01 (s, 1H), 10.30 (s, 1H), 9.60 (s, 1H), 8.23 (d, *J* = 9.3 Hz, 1H), 8.16 (d, *J* = 7.2 Hz, 1H), 7.84 – 7.78 (m, 1H), 7.59 – 7.49 (m, 2H), 6.88 (d, *J* = 7.1 Hz, 1H), 6.80 (d, *J* = 2.4 Hz, 1H), 6.66 (dt, *J* = 8.9, 2.0 Hz, 1H), 5.13 (dd, *J* = 13.3, 5.1 Hz, 1H), 4.47 (d, *J* = 5.5 Hz, 2H), 4.32 (s, 2H), 4.01 (s, 3H), 3.89 (s, 3H), 2.92 (ddd, *J* = 18.3, 13.5, 5.4 Hz, 1H), 2.58 (d, *J* = 17.5 Hz, 1H), 2.20 – 2.08 (m, 1H), 2.01 – 1.90 (m, 1H).

LCMS (m/z): 531 [M+H]<sup>+</sup>.

***N*-(2-(2,6-dioxopiperidin-3-yl)-1-oxoisoindolin-4-yl)-2-((2-(4-fluorophenyl)pyrimidin-4-yl)amino)acetamide (11)**

**11** (10.0 mg, 3%) was obtained according to the synthetic route of **8**, changing from [1,1'-biphenyl]-4-ylboronic acid to (4-fluorophenyl)boronic acid.

<sup>1</sup>H NMR (500 MHz, DMSO-*d*<sub>6</sub>) δ 11.02 (s, 1H), 10.30 (s, 1H), 9.30 (s, 1H), 8.36 – 8.23 (m, 2H), 7.81 (d, *J* = 7.2 Hz, 1H), 7.57 – 7.49 (m, 3H), 7.42 (t, *J* = 8.6 Hz, 2H), 6.88 (d, *J* = 6.8 Hz, 1H), 5.13 (dd, *J* = 13.3, 5.1 Hz, 1H), 4.47 (d, *J* = 5.3 Hz, 2H), 4.34 (s, 2H), 2.92 (ddt, *J* = 18.1, 13.6, 4.7 Hz, 1H), 2.65 – 2.57 (m, 1H), 2.19 – 2.12 (m, 1H), 1.98 (d, *J* = 10.2 Hz, 1H).

LCMS (m/z): 489 [M+H]<sup>+</sup>.

***2-((2-(4-acetylphenyl)pyrimidin-4-yl)amino)-N-(2-(2,6-dioxopiperidin-3-yl)-1-oxoisoindolin-4-yl)acetamide (12)***

**12** (3.6 mg, 3%) was obtained according to the synthetic route of **8**, changing from [1,1'-biphenyl]-4-ylboronic acid to (4-acetylphenyl)boronic acid.

<sup>1</sup>H NMR (500 MHz, DMSO-*d*<sub>6</sub>) δ 10.99 (s, 1H), 10.22 (s, 1H), 8.75 (s, 1H), 8.40 (d, *J* = 8.4 Hz, 2H), 8.29 (d, *J* = 6.4 Hz, 1H), 8.06 (d, *J* = 8.1 Hz, 2H), 7.81 (d, *J* = 7.4 Hz, 1H), 7.57 – 7.47 (m, 2H), 6.82 (d, *J* = 6.4 Hz, 1H), 5.11 (dd, *J* = 13.1, 5.1 Hz, 1H), 4.43 – 4.38 (m, 2H), 4.33 (s, 2H), 2.90 (ddd, *J* = 18.2, 13.5, 5.4 Hz, 1H), 2.63 (s, 3H), 2.57 (d, *J* = 19.1 Hz, 1H), 2.14 (d, *J* = 13.6 Hz, 1H), 2.00 – 1.91 (m, 1H).

LCMS (m/z): 513 [M+H]<sup>+</sup>.

***2-((2-(benzofuran-2-yl)pyrimidin-4-yl)amino)-N-(2-(2,6-dioxopiperidin-3-yl)-1-oxoisoindolin-4-yl)acetamide (13)***

**13** (12.3 mg, 6%) was obtained according to the synthetic route of **8**, changing from [1,1'-biphenyl]-4-ylboronic acid to benzofuran-2-ylboronic acid.

<sup>1</sup>H NMR (500 MHz, DMSO-*d*<sub>6</sub>) δ 10.99 (s, 1H), 10.20 (s, 1H), 8.22 (d, *J* = 5.8 Hz, 1H), 8.14 (s, 1H), 7.83 (dd, *J* = 7.4, 1.6 Hz, 1H), 7.72 (d, *J* = 7.8 Hz, 1H), 7.66 (s, 1H), 7.63 (d, *J* = 8.3 Hz, 1H), 7.56 – 7.49 (m, 2H), 7.43 – 7.38 (m, 1H), 7.29 (s, 1H), 6.67 (s, 1H), 5.07 (dd, *J* = 13.4, 4.9 Hz, 1H), 4.36 (d, *J* = 22.3 Hz, 4H), 2.92 – 2.79 (m, 1H), 2.46 (s, 1H), 2.13 (d, *J* = 13.9 Hz, 1H), 1.89 (s, 1H).

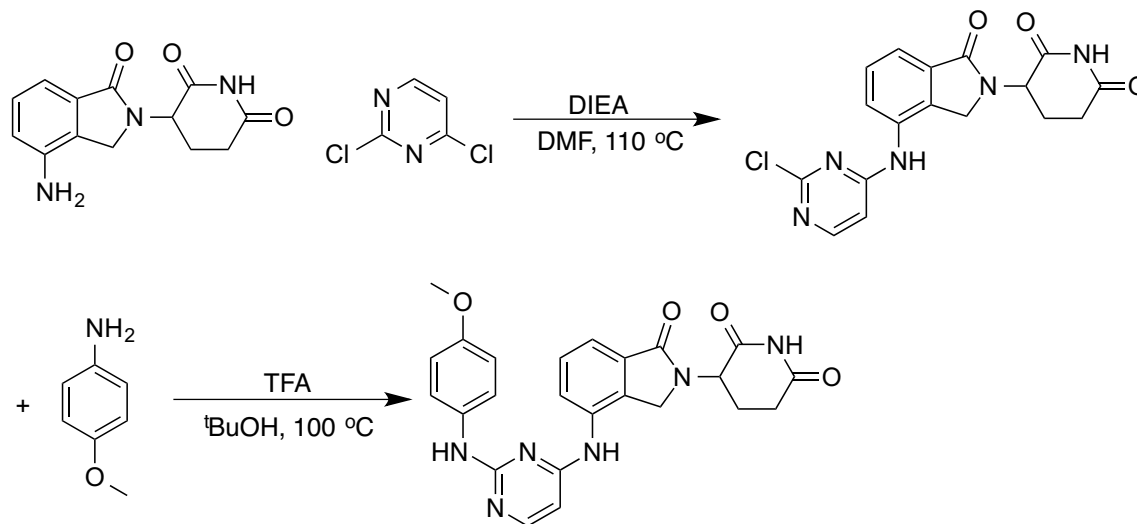
LCMS (*m/z*): 511 [M+H]<sup>+</sup>.

***N*-((2-(2,6-dioxopiperidin-3-yl)-1-oxoisindolin-4-yl)-2-((2-(4-fluoro-2-methoxyphenyl)pyrimidin-4-yl)amino)acetamide (19)**

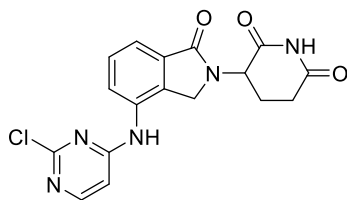
**19** (1.6 mg, 1%) was obtained according to the synthetic route of **8**, changing from [1,1'-biphenyl]-4-ylboronic acid to (4-fluoro-2-methoxyphenyl)boronic acid.

LCMS (*m/z*): 519 [M+H]<sup>+</sup>.

**Scheme 4.3. Synthesis of 20**



**3-(4-((2-Chloropyrimidin-4-yl)amino)-1-oxoisindolin-2-yl)piperidine-2,6-dione**



To a solution of Lenalidomide (777 mg, 3 mmol) and 2,4-dichloropyrimidine (882 mg, 6 mmol) in DMF (6 mL) was added DIEA (1.5 mL, 9 mmol), and then the mixture was heated to 110 °C

overnight. The mixture was concentrated *in vacuo* and then purified by silica gel (MeOH/DCM = 0-6%) to obtain the title compound (321 mg, 29%) as pale white solid.

LCMS (m/z): 372 [M+H]<sup>+</sup>.

**3-(4-((2-((4-methoxyphenyl)amino)pyrimidin-4-yl)amino)-1-oxoisoindolin-2-yl)piperidine-2,6-dione (20)**

To a solution of 3-(4-((2-chloropyrimidin-4-yl)amino)-1-oxoisoindolin-2-yl)piperidine-2,6-dione (112 mg, 0.3 mmol) and 4-methoxyaniline (37 mg, 0.3 mmol) in <sup>t</sup>BuOH (2 mL) was added TFA (45 μL, 0.6 mmol), and then the mixture was heated to reflux overnight. The mixture was then concentrated *in vacuo* and purified by prep-HPLC (MeOH/H<sub>2</sub>O, 0.05% TFA) to obtain compound **20** (64.3 mg, 38%).

<sup>1</sup>H NMR (500 MHz, DMSO-*d*<sub>6</sub>) δ 11.01 (s, 1H), 10.36 (d, *J* = 51.4 Hz, 2H), 7.94 (dd, *J* = 41.2, 7.4 Hz, 2H), 7.65 (d, *J* = 7.5 Hz, 1H), 7.56 (t, *J* = 7.7 Hz, 1H), 7.32 (d, *J* = 8.4 Hz, 2H), 6.85 (d, *J* = 8.4 Hz, 2H), 6.43 (d, *J* = 6.9 Hz, 1H), 5.14 (dd, *J* = 13.2, 5.2 Hz, 1H), 4.46 (d, *J* = 17.5 Hz, 1H), 4.33 (d, *J* = 17.4 Hz, 1H), 3.74 (s, 3H), 2.90 (ddd, *J* = 18.1, 13.6, 5.4 Hz, 1H), 2.62 – 2.53 (m, 1H), 2.35 – 2.24 (m, 1H), 1.87 (d, *J* = 11.2 Hz, 1H).

LCMS (m/z): 459 [M+H]<sup>+</sup>.

**3-(4-((2-((2,3-dihydrobenzo[*b*][1,4]dioxin-6-yl)amino)pyrimidin-4-yl)amino)-1-oxoisoindolin-2-yl)piperidine-2,6-dione (21)**

**21** (15.9 mg, 10.1%) was obtained according to the synthetic route of **20**, changing from 4-methoxyaniline to 2,3-dihydrobenzo[*b*][1,4]dioxin-6-amine.

<sup>1</sup>H NMR (500 MHz, DMSO-*d*<sub>6</sub>) δ 11.01 (s, 1H), 10.41 (d, *J* = 52.9 Hz, 2H), 7.94 (dd, *J* = 57.8, 7.2 Hz, 2H), 7.69 – 7.49 (m, 2H), 6.99 (s, 1H), 6.85 – 6.71 (m, 2H), 6.43 (d, *J* = 6.9 Hz, 1H), 5.14 (dd, *J* = 13.3, 5.3 Hz, 1H), 4.46 (d, *J* = 17.5 Hz, 1H), 4.30 (d, *J* = 17.4 Hz, 1H), 4.20 (s, 4H), 2.97 – 2.85 (m, 1H), 2.57 (s, 1H), 2.25 (s, 1H), 1.82 (s, 1H).

LCMS (m/z): 487 [M+H]<sup>+</sup>.

**3-(4-((2-((2-fluorophenyl)amino)pyrimidin-4-yl)amino)-1-oxoisoindolin-2-yl)piperidine-2,6-dione (23)**

**23** (11.0 mg, 9%) was obtained according to the synthetic route of **20**, changing from 4-methoxyaniline to 2-fluoroaniline.

<sup>1</sup>H NMR (500 MHz, DMSO-*d*<sub>6</sub>) δ 11.02 (s, 1H), 10.31 (s, 1H), 10.01 (s, 1H), 8.07 (d, *J* = 6.8 Hz, 1H), 7.89 (d, *J* = 7.9 Hz, 1H), 7.59 (dd, *J* = 9.9, 7.0 Hz, 2H), 7.46 (t, *J* = 7.7 Hz, 1H), 7.30 (ddd, *J*

= 10.5, 8.3, 1.4 Hz, 1H), 7.24 (tdd,  $J = 7.9, 5.2, 1.6$  Hz, 1H), 7.11 (t,  $J = 7.7$  Hz, 1H), 6.49 (d,  $J = 6.7$  Hz, 1H), 5.14 (dd,  $J = 13.3, 5.1$  Hz, 1H), 4.45 (d,  $J = 17.5$  Hz, 1H), 4.33 (d,  $J = 17.4$  Hz, 1H), 2.96 – 2.84 (m, 1H), 2.59 (dt,  $J = 17.0, 3.3$  Hz, 1H), 2.31 (qd,  $J = 13.2, 4.4$  Hz, 1H), 1.97 – 1.84 (m, 1H). LCMS (m/z): 447 [M+H]<sup>+</sup>.

**3-(1-oxo-4-((2-((3-(2-oxopyrrolidin-1-yl)propyl)amino)pyrimidin-4-yl)amino)isoindolin-2-yl)piperidine-2,6-dione (24)**

**24** (8.6 mg, 6%) was obtained according to the synthetic route of **20**, changing from 4-methoxyaniline to 1-(3-aminopropyl)pyrrolidin-2-one.

<sup>1</sup>H NMR (500 MHz, DMSO-*d*<sub>6</sub>)  $\delta$  11.03 (s, 1H), 10.58 (s, 1H), 8.32 (s, 1H), 7.93 (d,  $J = 6.9$  Hz, 2H), 7.65 (dd,  $J = 18.8, 7.5$  Hz, 2H), 6.38 (s, 1H), 5.19 (dd,  $J = 13.3, 5.1$  Hz, 1H), 4.48 (d,  $J = 17.7$  Hz, 1H), 4.38 (d,  $J = 17.8$  Hz, 1H), 3.17 (d,  $J = 21.2$  Hz, 6H), 2.94 (ddd,  $J = 18.0, 13.7, 5.4$  Hz, 1H), 2.60 (d,  $J = 17.2$  Hz, 1H), 2.39 (qd,  $J = 13.2, 4.5$  Hz, 1H), 2.14 (s, 2H), 2.02 (d,  $J = 12.2$  Hz, 1H), 1.73 (d,  $J = 83.3$  Hz, 4H).

LCMS (m/z): 478 [M+H]<sup>+</sup>.

**3-(1-oxo-4-((2-(4-(3-(trifluoromethyl)phenyl)piperazin-1-yl)pyrimidin-4-yl)amino)isoindolin-2-yl)piperidine-2,6-dione (25)**

**25** (10.9 mg, 7%) was obtained according to the synthetic route of **20**, changing from 4-methoxyaniline to 1-(3-(trifluoromethyl)phenyl)piperazine.

<sup>1</sup>H NMR (500 MHz, DMSO-*d*<sub>6</sub>)  $\delta$  11.03 (s, 1H), 10.53 (s, 1H), 8.00 (d,  $J = 6.9$  Hz, 1H), 7.84 (d,  $J = 7.8$  Hz, 1H), 7.68 (d,  $J = 7.4$  Hz, 1H), 7.62 (t,  $J = 7.7$  Hz, 1H), 7.44 (t,  $J = 8.0$  Hz, 1H), 7.28 – 7.23 (m, 1H), 7.22 (t,  $J = 1.9$  Hz, 1H), 7.10 (d,  $J = 7.6$  Hz, 1H), 6.41 (d,  $J = 6.9$  Hz, 1H), 5.19 (dd,  $J = 13.3, 5.2$  Hz, 1H), 4.47 (d,  $J = 17.6$  Hz, 1H), 4.37 (d,  $J = 17.5$  Hz, 1H), 3.76 (q,  $J = 4.0$  Hz, 4H), 3.39 (t,  $J = 4.3$  Hz, 4H), 2.93 (ddd,  $J = 17.4, 13.7, 5.4$  Hz, 1H), 2.58 (dt,  $J = 17.2, 3.1$  Hz, 1H), 2.38 (qd,  $J = 13.2, 4.4$  Hz, 1H), 2.02 (ddq,  $J = 10.5, 5.6, 3.3, 2.7$  Hz, 1H).

LCMS (m/z): 566 [M+H]<sup>+</sup>.

**3-(4-((2-((2,3-dihydro-1H-inden-5-yl)amino)pyrimidin-4-yl)amino)-1-oxoisoindolin-2-yl)piperidine-2,6-dione (26)**

**26** (15.6 mg, 11%) was obtained according to the synthetic route of **20**, changing from 4-methoxyaniline to 2,3-dihydro-1H-inden-5-amine.

<sup>1</sup>H NMR (500 MHz, DMSO-*d*<sub>6</sub>)  $\delta$  10.99 (s, 1H), 10.47 (d,  $J = 32.6$  Hz, 2H), 8.03 (d,  $J = 6.9$  Hz, 1H), 7.87 (d,  $J = 7.9$  Hz, 1H), 7.68 (d,  $J = 7.4$  Hz, 1H), 7.58 (t,  $J = 7.7$  Hz, 1H), 7.32 (s, 1H), 7.09

(q,  $J = 8.2$  Hz, 2H), 6.45 (d,  $J = 6.9$  Hz, 1H), 5.12 (dd,  $J = 13.3, 5.1$  Hz, 1H), 4.46 (d,  $J = 17.5$  Hz, 1H), 4.31 (d,  $J = 17.5$  Hz, 1H), 2.88 (ddd,  $J = 18.0, 13.6, 5.4$  Hz, 1H), 2.79 (t,  $J = 7.4$  Hz, 2H), 2.68 (t,  $J = 6.8$  Hz, 2H), 2.57 – 2.55 (m, 1H), 2.22 (qd,  $J = 13.3, 4.4$  Hz, 1H), 1.98 (p,  $J = 7.4$  Hz, 2H), 1.75 (d,  $J = 12.2$  Hz, 1H).

LCMS (m/z): 469 [M+H]<sup>+</sup>.

**3-(4-((2-(benzyl(ethyl)amino)pyrimidin-4-yl)amino)-1-oxoisoindolin-2-yl)piperidine-2,6-dione (27)**

**27** (7.6 mg, 5%) was obtained according to the synthetic route of **20**, changing from 4-methoxyaniline to *N*-benzylethanamine.

<sup>1</sup>H NMR (500 MHz, DMSO-*d*<sub>6</sub>)  $\delta$  11.04 (s, 1H), 10.38 (s, 1H), 7.96 (d,  $J = 7.0$  Hz, 1H), 7.64 – 7.55 (m, 1H), 7.38 – 7.24 (m, 4H), 7.18 (s, 2H), 6.43 (s, 1H), 5.17 (dd,  $J = 13.3, 5.1$  Hz, 1H), 4.74 (s, 2H), 4.50 – 4.28 (m, 2H), 3.55 (s, 2H), 2.93 (ddd,  $J = 17.3, 13.6, 5.4$  Hz, 1H), 2.61 (dt,  $J = 17.2, 3.3$  Hz, 1H), 2.36 (qd,  $J = 12.9, 4.4$  Hz, 1H), 2.07 – 1.93 (m, 1H), 1.10 (s, 3H).

LCMS (m/z): 471 [M+H]<sup>+</sup>.

**3-(4-((2-(methyl(phenyl)amino)pyrimidin-4-yl)amino)-1-oxoisoindolin-2-yl)piperidine-2,6-dione (28)**

**28** (17.4 mg, 14%) was obtained according to the synthetic route of **20**, changing from 4-methoxyaniline to *N*-methylaniline.

<sup>1</sup>H NMR (500 MHz, DMSO-*d*<sub>6</sub>)  $\delta$  11.05 (s, 1H), 10.50 (s, 1H), 7.86 (dd,  $J = 22.4, 7.5$  Hz, 2H), 7.58 (d,  $J = 7.5$  Hz, 1H), 7.53 (t,  $J = 7.6$  Hz, 2H), 7.47 – 7.39 (m, 4H), 6.50 (d,  $J = 7.0$  Hz, 1H), 5.18 (dd,  $J = 13.3, 5.1$  Hz, 1H), 4.47 (d,  $J = 17.5$  Hz, 1H), 4.37 (d,  $J = 17.5$  Hz, 1H), 3.39 (s, 3H), 2.94 (ddd,  $J = 17.3, 13.6, 5.4$  Hz, 1H), 2.62 (dt,  $J = 17.2, 3.4$  Hz, 1H), 2.37 (qd,  $J = 13.2, 4.4$  Hz, 1H), 2.02 (dtd,  $J = 12.8, 5.3, 2.3$  Hz, 1H).

LCMS (m/z): 443 [M+H]<sup>+</sup>.

**3-(4-((2-(mesitylamino)pyrimidin-4-yl)amino)-1-oxoisoindolin-2-yl)piperidine-2,6-dione (29)**

**29** (4.7 mg, 4%) was obtained according to the synthetic route of ZXH-1-154, changing from 4-methoxyaniline to 2,4,6-trimethylaniline.

LCMS (m/z): 471 [M+H]<sup>+</sup>.

**3-(4-((2-((S)-2-(hydroxymethyl)pyrrolidin-1-yl)pyrimidin-4-yl)amino)-1-oxoisoindolin-2-yl)piperidine-2,6-dione (30)**

**30** (6.3 mg, 5%) was obtained according to the synthetic route of **20**, changing from 4-methoxyaniline to (*S*)-pyrrolidin-2-ylmethanol.

<sup>1</sup>H NMR (500 MHz, DMSO-*d*<sub>6</sub>) δ 11.03 (s, 1H), 10.46 (s, 2H), 8.12 – 7.87 (m, 2H), 7.63 (dd, *J* = 20.9, 7.6 Hz, 2H), 6.44 (s, 1H), 5.19 (dt, *J* = 13.3, 5.2 Hz, 1H), 4.57 – 4.31 (m, 2H), 4.11 (s, 1H), 3.47 (d, *J* = 38.9 Hz, 4H), 2.94 (ddd, *J* = 18.2, 13.9, 5.0 Hz, 1H), 2.66 – 2.56 (m, 1H), 2.40 – 2.31 (m, 1H), 2.09 (s, 1H), 2.05 – 1.84 (m, 4H).

LCMS (m/z): 437 [M+H]<sup>+</sup>.

**3-(4-((2-((*R*)-2-(hydroxymethyl)pyrrolidin-1-yl)pyrimidin-4-yl)amino)-1-oxoisoindolin-2-yl)piperidine-2,6-dione (31)**

**31** (12.0 mg, 10%) was obtained according to the synthetic route of **20**, changing from 4-methoxyaniline to (*R*)-pyrrolidin-2-ylmethanol.

<sup>1</sup>H NMR (500 MHz, DMSO-*d*<sub>6</sub>) δ 11.03 (s, 1H), 10.49 (s, 1H), 8.22 – 7.88 (m, 2H), 7.74 – 7.37 (m, 2H), 6.44 (s, 1H), 5.18 (dt, *J* = 13.3, 5.2 Hz, 1H), 4.56 – 4.28 (m, 2H), 4.11 (s, 1H), 3.63 – 3.37 (m, 4H), 2.99 – 2.85 (m, 1H), 2.67 – 2.56 (m, 1H), 2.43 – 2.32 (m, 1H), 2.11 (d, *J* = 15.7 Hz, 1H), 2.06 – 1.83 (m, 5H).

LCMS (m/z): 437 [M+H]<sup>+</sup>.

**3-(4-((2-(((*R*)-1-hydroxy-3-methylbutan-2-yl)amino)pyrimidin-4-yl)amino)-1-oxoisoindolin-2-yl)piperidine-2,6-dione (37)**

**37** (4.5 mg, 3%) was obtained according to the synthetic route of **20**, changing from 4-methoxyaniline to (*R*)-2-amino-3-methylbutan-1-ol.

<sup>1</sup>H NMR (500 MHz, DMSO-*d*<sub>6</sub>) δ 11.02 (s, 1H), 10.50 (s, 1H), 8.21 (s, 1H), 7.94 (d, *J* = 7.3 Hz, 2H), 7.66 (d, *J* = 7.1 Hz, 1H), 7.60 (t, *J* = 7.7 Hz, 1H), 6.37 (s, 1H), 5.17 (dd, *J* = 13.1, 5.1 Hz, 1H), 4.59 – 4.34 (m, 2H), 3.48 (d, *J* = 9.0 Hz, 2H), 2.99 – 2.87 (m, 1H), 2.62 (dd, *J* = 15.3, 11.7 Hz, 1H), 2.44 – 2.31 (m, 1H), 2.01 (d, *J* = 16.2 Hz, 1H), 1.84 (s, 1H), 0.86 (d, *J* = 42.6 Hz, 6H).

LCMS (m/z): 439 [M+H]<sup>+</sup>.

**3-(4-((2-((2-methoxyphenyl)amino)pyrimidin-4-yl)amino)-1-oxoisoindolin-2-yl)piperidine-2,6-dione (38)**

**38** (20.6 mg, 13%) was obtained according to the synthetic route of **20**, changing from 4-methoxyaniline to 2-methoxyaniline.

<sup>1</sup>H NMR (500 MHz, DMSO-*d*<sub>6</sub>) δ 11.02 (s, 1H), 10.64 (s, 1H), 9.86 – 9.75 (m, 1H), 8.04 (d, *J* = 7.0 Hz, 1H), 7.88 (d, *J* = 7.9 Hz, 1H), 7.65 (dd, *J* = 7.5, 0.9 Hz, 1H), 7.53 (t, *J* = 7.6 Hz, 2H), 7.20 (t,

$J = 7.6$  Hz, 1H), 7.11 (dd,  $J = 8.4, 1.4$  Hz, 1H), 6.82 (t,  $J = 7.8$  Hz, 1H), 6.51 (d,  $J = 7.1$  Hz, 1H), 5.14 (dd,  $J = 13.2, 5.2$  Hz, 1H), 4.47 (d,  $J = 17.5$  Hz, 1H), 4.34 (d,  $J = 17.5$  Hz, 1H), 3.82 (s, 3H), 2.90 (ddd,  $J = 17.3, 13.7, 5.4$  Hz, 1H), 2.57 (dt,  $J = 17.2, 3.4$  Hz, 1H), 2.28 (qd,  $J = 13.2, 4.4$  Hz, 1H), 1.87 (d,  $J = 12.6$  Hz, 1H).

LCMS (m/z): 459 [M+H]<sup>+</sup>.

**4-((4-((2-(2,6-dioxopiperidin-3-yl)-1-oxoisoindolin-4-yl)amino)pyrimidin-2-yl)amino)benzenesulfonamide (40)**

**40** (9.0 mg, 9%) was obtained according to the synthetic route of **20**, changing from 4-methoxyaniline to 4-aminobenzenesulfonamide.

<sup>1</sup>H NMR (500 MHz, DMSO-*d*<sub>6</sub>)  $\delta$  11.01 (s, 1H), 10.39 (s, 1H), 10.17 (s, 1H), 8.12 (d,  $J = 6.5$  Hz, 1H), 7.97 (d,  $J = 7.7$  Hz, 1H), 7.72 – 7.55 (m, 6H), 7.24 (s, 2H), 6.48 (d,  $J = 6.6$  Hz, 1H), 5.15 (dd,  $J = 13.3, 5.2$  Hz, 1H), 4.48 (d,  $J = 17.5$  Hz, 1H), 4.37 (d,  $J = 17.5$  Hz, 1H), 2.90 (ddd,  $J = 17.3, 13.6, 5.4$  Hz, 1H), 2.56 (dt,  $J = 16.9, 3.4$  Hz, 1H), 2.30 (qd,  $J = 13.2, 4.5$  Hz, 1H), 1.90 (dtd,  $J = 12.9, 5.4, 2.3$  Hz, 1H).

LCMS (m/z): 508 [M+H]<sup>+</sup>.

**3-(4-((2-(indolin-5-ylamino)pyrimidin-4-yl)amino)-1-oxoisoindolin-2-yl)piperidine-2,6-dione (41)**

**41** (10.4 mg, 13%) was obtained according to the synthetic route of **20**, changing from 4-methoxyaniline to *tert*-butyl 5-aminoindoline-1-carboxylate.

<sup>1</sup>H NMR (500 MHz, DMSO-*d*<sub>6</sub>)  $\delta$  11.01 (s, 1H), 10.48 (d,  $J = 30.2$  Hz, 2H), 8.02 (d,  $J = 6.9$  Hz, 1H), 7.95 (d,  $J = 7.8$  Hz, 1H), 7.66 (dd,  $J = 7.5, 1.1$  Hz, 1H), 7.61 (t,  $J = 7.6$  Hz, 1H), 7.07 (s, 1H), 7.01 (s, 2H), 6.46 (d,  $J = 6.9$  Hz, 1H), 5.15 (dd,  $J = 13.2, 5.1$  Hz, 1H), 4.49 (d,  $J = 17.5$  Hz, 1H), 4.34 (d,  $J = 17.5$  Hz, 1H), 3.56 (t,  $J = 8.2$  Hz, 2H), 2.99 (t,  $J = 8.1$  Hz, 2H), 2.94 – 2.85 (m, 1H), 2.64 – 2.55 (m, 1H), 2.33 (ddd,  $J = 26.6, 13.2, 3.2$  Hz, 1H), 2.25 (s, 1H), 1.90 (dd,  $J = 11.1, 5.2$  Hz, 1H).

LCMS (m/z): 470 [M+H]<sup>+</sup>.

**3-(4-((2-(((3s,5s,7s)-adamantan-1-yl)amino)pyrimidin-4-yl)amino)-1-oxoisoindolin-2-yl)piperidine-2,6-dione (42)**

**42** (4.1 mg, 3%) was obtained according to the synthetic route of **20**, changing from 4-methoxyaniline to (3s,5s,7s)-adamantan-1-amine.

$^1\text{H}$  NMR (500 MHz,  $\text{DMSO-}d_6$ )  $\delta$  11.01 (s, 1H), 10.61 (s, 1H), 7.99 (s, 1H), 7.93 (d,  $J = 7.2$  Hz, 1H), 7.72 (dd,  $J = 10.6, 7.6$  Hz, 2H), 7.62 (t,  $J = 7.6$  Hz, 1H), 6.33 (d,  $J = 7.2$  Hz, 1H), 5.16 (dd,  $J = 13.3, 5.2$  Hz, 1H), 4.40 (d,  $J = 17.6$  Hz, 1H), 4.30 (d,  $J = 17.6$  Hz, 1H), 2.92 (ddd,  $J = 17.3, 13.6, 5.4$  Hz, 1H), 2.64 – 2.53 (m, 1H), 2.44 – 2.36 (m, 1H), 2.09 (s, 1H), 1.96 – 1.91 (m, 1H), 1.86 (s, 3H), 1.76 (s, 6H), 1.50 (d,  $J = 12.2$  Hz, 3H), 1.33 (d,  $J = 11.9$  Hz, 3H).

LCMS (m/z): 487  $[\text{M}+\text{H}]^+$ .

**3-(4-((2-(naphthalen-2-ylamino)pyrimidin-4-yl)amino)-1-oxoisoindolin-2-yl)piperidine-2,6-dione (43)**

**43** (16.8 mg, 21%) was obtained according to the synthetic route of **20**, changing from 4-methoxyaniline to naphthalen-2-amine.

$^1\text{H}$  NMR (500 MHz,  $\text{DMSO-}d_6$ )  $\delta$  10.98 (s, 1H), 10.79 (s, 1H), 10.61 (s, 1H), 8.11 (d,  $J = 7.0$  Hz, 1H), 8.03 – 8.00 (m, 1H), 7.95 (d,  $J = 7.9$  Hz, 1H), 7.84 (t,  $J = 8.3$  Hz, 2H), 7.71 (d,  $J = 7.5$  Hz, 1H), 7.58 (d,  $J = 7.7$  Hz, 1H), 7.55 – 7.39 (m, 4H), 6.52 (d,  $J = 6.9$  Hz, 1H), 5.08 (dd,  $J = 13.2, 5.2$  Hz, 1H), 4.49 (d,  $J = 17.6$  Hz, 1H), 4.35 (d,  $J = 17.6$  Hz, 1H), 2.81 (ddd,  $J = 17.2, 13.7, 5.4$  Hz, 1H), 2.45 (s, 1H), 2.16 (dt,  $J = 11.5, 5.3$  Hz, 1H), 1.62 (s, 1H).

LCMS (m/z): 479  $[\text{M}+\text{H}]^+$ .

**3-(4-((2-((9H-fluoren-3-yl)amino)pyrimidin-4-yl)amino)-1-oxoisoindolin-2-yl)piperidine-2,6-dione (44)**

**44** (30.0 mg, 37%) was obtained according to the synthetic route of **20**, changing from 4-methoxyaniline to 9H-fluoren-3-amine.

$^1\text{H}$  NMR (500 MHz,  $\text{DMSO-}d_6$ )  $\delta$  10.99 (s, 1H), 10.79 (s, 1H), 10.64 (s, 1H), 8.10 (d,  $J = 6.9$  Hz, 1H), 7.92 (d,  $J = 7.9$  Hz, 1H), 7.82 (d,  $J = 7.5$  Hz, 1H), 7.79 – 7.74 (m, 1H), 7.74 – 7.70 (m, 2H), 7.63 (t,  $J = 7.7$  Hz, 1H), 7.55 (d,  $J = 7.4$  Hz, 1H), 7.39 – 7.33 (m, 2H), 7.28 (td,  $J = 7.4, 1.2$  Hz, 1H), 6.50 (d,  $J = 7.0$  Hz, 1H), 5.12 (dd,  $J = 13.2, 5.2$  Hz, 1H), 4.51 (d,  $J = 17.6$  Hz, 1H), 4.36 (d,  $J = 17.5$  Hz, 1H), 2.85 (ddd,  $J = 17.3, 13.6, 5.4$  Hz, 1H), 2.54 (d,  $J = 11.7$  Hz, 1H), 2.30 – 2.15 (m, 1H), 1.80 – 1.67 (m, 1H).

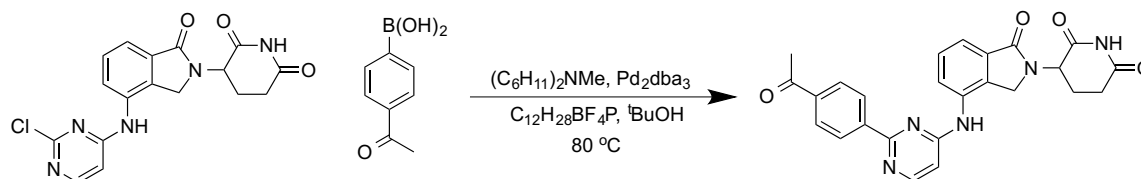
LCMS (m/z): 517  $[\text{M}+\text{H}]^+$ .

**3-(1-oxo-4-((2-((5,6,7,8-tetrahydronaphthalen-2-yl)amino)pyrimidin-4-yl)amino)isoindolin-2-yl)piperidine-2,6-dione (45)**

**45** (70.4 mg, 44%) was obtained according to the synthetic route of **20**, changing from 4-methoxyaniline to 5,6,7,8-tetrahydronaphthalen-2-amine.

$^1\text{H}$  NMR (500 MHz,  $\text{DMSO-}d_6$ )  $\delta$  10.99 (s, 1H), 10.62 (s, 1H), 10.54 (s, 1H), 8.03 (d,  $J = 7.0$  Hz, 1H), 7.85 (d,  $J = 7.9$  Hz, 1H), 7.68 (d,  $J = 7.5$  Hz, 1H), 7.58 (t,  $J = 7.7$  Hz, 1H), 7.09 (d,  $J = 2.2$  Hz, 1H), 7.04 (dd,  $J = 8.3, 2.2$  Hz, 1H), 6.93 (d,  $J = 8.3$  Hz, 1H), 6.46 (d,  $J = 7.0$  Hz, 1H), 5.12 (dd,  $J = 13.2, 5.2$  Hz, 1H), 4.45 (d,  $J = 17.6$  Hz, 1H), 4.29 (d,  $J = 17.5$  Hz, 1H), 2.89 (ddd,  $J = 17.3, 13.7, 5.4$  Hz, 1H), 2.64 (d,  $J = 6.2$  Hz, 2H), 2.55 (d,  $J = 2.6$  Hz, 1H), 2.45 (s, 2H), 2.20 (qd,  $J = 13.4, 4.3$  Hz, 1H), 1.68 (dd,  $J = 7.6, 4.3$  Hz, 4H). LCMS (m/z): 483  $[\text{M}+\text{H}]^+$ .

**Scheme 4.4.** Synthesis of **22**



**3-(4-((2-(4-acetylphenyl)pyrimidin-4-yl)amino)-1-oxoisoindolin-2-yl)piperidine-2,6-dione (22)**

To a solution of 3-(4-((2-chloropyrimidin-4-yl)amino)-1-oxoisoindolin-2-yl)piperidine-2,6-dione (115 mg, 0.3 mmol) and (4-acetylphenyl)boronic acid (61 mg, 0.36 mmol) in  $^t\text{BuOH}$  (2 mL) were added  $N,N$ -dicyclohexylmethylamine (64 mg, 0.33 mmol),  $\text{Pd}_2\text{dba}_3$  (27 mg, 0.03 mmol) and Tri-*tert*-butylphosphonium tetrafluoroborate (18 mg, 0.06 mmol). The mixture was heated to 80  $^\circ\text{C}$  and stirred under  $\text{N}_2$  atmosphere overnight. The mixture was then filtered, concentrated *in vacuo* and purified by prep-HPLC (MeOH/ $\text{H}_2\text{O}$ , 0.05% TFA) to obtain compound **22** (10.0 mg, 6%).

$^1\text{H}$  NMR (500 MHz,  $\text{DMSO-}d_6$ )  $\delta$  11.00 (s, 1H), 9.65 (s, 1H), 8.49 (d,  $J = 5.8$  Hz, 1H), 8.37 (d,  $J = 8.3$  Hz, 2H), 8.13 (d,  $J = 7.8$  Hz, 1H), 8.07 (d,  $J = 8.3$  Hz, 2H), 7.67 – 7.53 (m, 2H), 6.87 (d,  $J = 5.9$  Hz, 1H), 5.17 (dd,  $J = 13.3, 5.1$  Hz, 1H), 4.52 (d,  $J = 17.3$  Hz, 1H), 4.43 (d,  $J = 17.3$  Hz, 1H), 2.92 (ddd,  $J = 17.2, 13.6, 5.4$  Hz, 1H), 2.63 (s, 3H), 2.61 – 2.55 (m, 1H), 2.35 (qd,  $J = 13.2, 4.4$  Hz, 1H), 2.01 (dtd,  $J = 12.7, 5.3, 2.2$  Hz, 1H).

LCMS (m/z): 456  $[\text{M}+\text{H}]^+$ .

**3-(4-((2-([1,1'-biphenyl]-4-yl)pyrimidin-4-yl)amino)-1-oxoisoindolin-2-yl)piperidine-2,6-dione (32)**

**32** (4.0 mg, 2%) was obtained according to the synthetic route of **22**, changing from (4-acetylphenyl)boronic acid to [1,1'-biphenyl]-4-ylboronic acid.

<sup>1</sup>H NMR (500 MHz, DMSO-*d*<sub>6</sub>) δ 11.01 (s, 1H), 9.99 (s, 1H), 8.47 (d, *J* = 6.1 Hz, 1H), 8.30 (d, *J* = 8.5 Hz, 2H), 8.10 (dd, *J* = 7.3, 1.6 Hz, 1H), 7.85 (d, *J* = 8.5 Hz, 2H), 7.79 – 7.75 (m, 2H), 7.67 – 7.61 (m, 2H), 7.51 (dd, *J* = 8.4, 7.0 Hz, 2H), 7.44 – 7.39 (m, 1H), 6.88 (d, *J* = 6.2 Hz, 1H), 5.18 (dd, *J* = 13.4, 5.1 Hz, 1H), 4.54 (d, *J* = 17.4 Hz, 1H), 4.44 (d, *J* = 17.4 Hz, 1H), 2.92 (ddd, *J* = 18.0, 13.6, 5.4 Hz, 1H), 2.64 – 2.54 (m, 1H), 2.35 (qd, *J* = 13.2, 4.5 Hz, 1H), 2.07 – 1.96 (m, 1H).  
LCMS (m/z): 490 [M+H]<sup>+</sup>.

**3-(4-((2-(3-methoxyphenyl)pyrimidin-4-yl)amino)-1-oxoisoindolin-2-yl)piperidine-2,6-dione (33)**

**33** (13.7 mg, 12%) was obtained according to the synthetic route of **22**, changing from (4-acetylphenyl)boronic acid to (3-methoxyphenyl)boronic acid.

<sup>1</sup>H NMR (500 MHz, DMSO-*d*<sub>6</sub>) δ 11.19 (s, 1H), 11.02 (s, 1H), 8.44 (d, *J* = 7.1 Hz, 1H), 7.96 (d, *J* = 7.8 Hz, 1H), 7.86 (d, *J* = 7.8 Hz, 1H), 7.73 (dd, *J* = 7.5, 1.1 Hz, 1H), 7.67 (td, *J* = 7.8, 7.3, 1.3 Hz, 2H), 7.32 (dd, *J* = 8.5, 0.9 Hz, 1H), 7.17 (td, *J* = 7.5, 1.0 Hz, 1H), 7.06 (d, *J* = 6.9 Hz, 1H), 5.18 (dd, *J* = 13.3, 5.1 Hz, 1H), 4.52 (d, *J* = 17.6 Hz, 1H), 4.42 (d, *J* = 17.6 Hz, 1H), 3.98 (s, 3H), 2.93 (ddd, *J* = 17.3, 13.7, 5.4 Hz, 1H), 2.64 – 2.55 (m, 1H), 2.38 – 2.29 (m, 1H), 2.00 (ddq, *J* = 10.3, 5.4, 3.1, 2.6 Hz, 1H).  
LCMS (m/z): 444 [M+H]<sup>+</sup>.

**3-(4-((2-(4-fluoro-2-methoxyphenyl)pyrimidin-4-yl)amino)-1-oxoisoindolin-2-yl)piperidine-2,6-dione (34)**

**34** (17.1 mg, 11%) was obtained according to the synthetic route of **22**, changing from (4-acetylphenyl)boronic acid to (4-fluoro-2-methoxyphenyl)boronic acid.

<sup>1</sup>H NMR (500 MHz, DMSO-*d*<sub>6</sub>) δ 11.14 (s, 1H), 11.03 (s, 1H), 8.43 (d, *J* = 7.0 Hz, 1H), 7.94 (d, *J* = 7.8 Hz, 1H), 7.89 (dd, *J* = 8.8, 6.7 Hz, 1H), 7.72 (dd, *J* = 7.6, 1.0 Hz, 1H), 7.66 (t, *J* = 7.7 Hz, 1H), 7.26 (dd, *J* = 11.3, 2.4 Hz, 1H), 7.03 (td, *J* = 8.5, 4.1 Hz, 2H), 5.18 (dd, *J* = 13.3, 5.1 Hz, 1H), 4.50 (d, *J* = 17.6 Hz, 1H), 4.41 (d, *J* = 17.6 Hz, 1H), 3.98 (s, 3H), 2.93 (ddd, *J* = 17.3, 13.6, 5.4 Hz, 1H), 2.64 – 2.56 (m, 1H), 2.33 (qd, *J* = 13.2, 4.4 Hz, 1H), 2.00 (dtd, *J* = 12.6, 5.1, 2.1 Hz, 1H).  
LCMS (m/z): 462 [M+H]<sup>+</sup>.

**3-(4-((2-(2,4-dimethoxyphenyl)pyrimidin-4-yl)amino)-1-oxoisoindolin-2-yl)piperidine-2,6-dione (35)**

**35** (9.3 mg, 6%) was obtained according to the synthetic route of **22**, changing from (4-acetylphenyl)boronic acid to (2,4-dimethoxyphenyl)boronic acid.

<sup>1</sup>H NMR (500 MHz, DMSO-*d*<sub>6</sub>) δ 11.11 (s, 1H), 11.02 (s, 1H), 8.35 (d, *J* = 7.1 Hz, 1H), 7.93 (d, *J* = 8.5 Hz, 2H), 7.74 (d, *J* = 7.5 Hz, 1H), 7.68 (t, *J* = 7.7 Hz, 1H), 6.99 (s, 1H), 6.82 (d, *J* = 2.3 Hz, 1H), 6.80 – 6.76 (m, 1H), 5.18 (dd, *J* = 13.3, 5.1 Hz, 1H), 4.51 (d, *J* = 17.6 Hz, 1H), 4.40 (d, *J* = 17.6 Hz, 1H), 4.03 (s, 3H), 3.89 (s, 3H), 2.92 (ddd, *J* = 17.3, 13.6, 5.4 Hz, 1H), 2.63 – 2.55 (m, 1H), 2.33 (qd, *J* = 12.9, 4.2 Hz, 1H), 2.00 (td, *J* = 6.0, 2.3 Hz, 1H).

LCMS (m/z): 474 [M+H]<sup>+</sup>.

**3-(4-((2-(benzofuran-2-yl)pyrimidin-4-yl)amino)-1-oxoisoindolin-2-yl)piperidine-2,6-dione (36)**

**36** (5.0 mg, 3%) was obtained according to the synthetic route of **22**, changing from (4-acetylphenyl)boronic acid to benzofuran-2-ylboronic acid.

<sup>1</sup>H NMR (500 MHz, DMSO-*d*<sub>6</sub>) δ 10.99 (s, 1H), 9.75 (s, 1H), 8.44 (d, *J* = 5.9 Hz, 1H), 8.08 (d, *J* = 7.7 Hz, 1H), 7.78 (dt, *J* = 7.8, 1.0 Hz, 1H), 7.68 (dq, *J* = 8.3, 0.9 Hz, 1H), 7.63 (t, *J* = 7.6 Hz, 1H), 7.61 – 7.57 (m, 2H), 7.43 (ddd, *J* = 8.4, 7.2, 1.4 Hz, 1H), 7.34 – 7.30 (m, 1H), 6.83 (d, *J* = 6.0 Hz, 1H), 5.16 (dd, *J* = 13.2, 5.1 Hz, 1H), 4.60 (d, *J* = 17.4 Hz, 1H), 4.44 (d, *J* = 17.4 Hz, 1H), 2.90 (ddd, *J* = 17.3, 13.6, 5.4 Hz, 1H), 2.59 – 2.53 (m, 1H), 2.37 (ddd, *J* = 15.6, 12.4, 4.5 Hz, 1H), 2.03 (ddq, *J* = 10.6, 5.6, 3.3, 2.7 Hz, 1H).

LCMS (m/z): 454 [M+H]<sup>+</sup>.

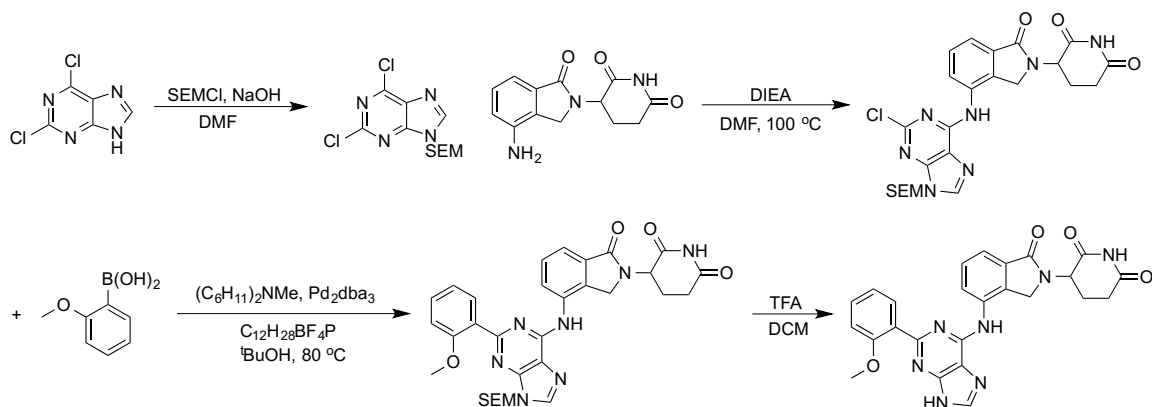
**3-(4-((2-(4-fluorophenyl)pyrimidin-4-yl)amino)-1-oxoisoindolin-2-yl)piperidine-2,6-dione (39)**

**39** (1.5 mg, 2%) was obtained according to the synthetic route of **22**, changing from (4-acetylphenyl)boronic acid to (4-fluorophenyl)boronic acid.

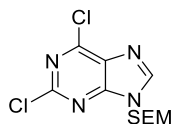
<sup>1</sup>H NMR (500 MHz, DMSO-*d*<sub>6</sub>) δ 11.01 (s, 1H), 9.96 (s, 1H), 8.44 (d, *J* = 6.1 Hz, 1H), 8.25 (dd, *J* = 8.6, 5.7 Hz, 1H), 8.04 (dd, *J* = 7.0, 1.9 Hz, 1H), 7.84 (dd, *J* = 8.3, 6.3 Hz, 1H), 7.62 (d, *J* = 7.0 Hz, 2H), 7.36 (t, *J* = 8.7 Hz, 1H), 7.15 (t, *J* = 8.9 Hz, 1H), 6.86 (d, *J* = 6.1 Hz, 1H), 5.17 (dd, *J* = 13.3, 5.1 Hz, 1H), 4.50 (d, *J* = 17.4 Hz, 1H), 4.42 (d, *J* = 17.4 Hz, 1H), 2.92 (ddd, *J* = 18.2, 13.5, 5.4 Hz, 1H), 2.66 – 2.55 (m, 1H), 2.34 (qd, *J* = 13.3, 4.6 Hz, 1H), 2.03 – 1.97 (m, 1H).

LCMS (m/z): 432 [M+H]<sup>+</sup>.

### Scheme 4.5. Synthesis of 46



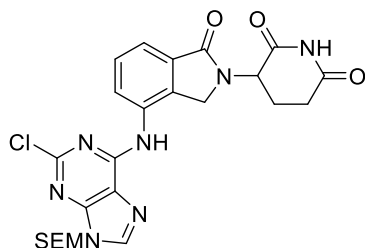
### 2,6-Dichloro-9-((2-(trimethylsilyl)ethoxy)methyl)-9H-purine



To a solution of 2,6-dichloro-9H-purine (1.89 g, 10 mmol) and NaOH (1.2 g, 30 mmol) in DMF (30 mL) was added 2-(Trimethylsilyl)ethoxymethyl chloride (3.5 mL, 20 mmol), and then the mixture was stirred for 4h. The mixture was then extracted with EtOAc, washed with brine, dried over Na<sub>2</sub>SO<sub>4</sub>, and concentrated *in vacuo* to next step without any purification.

LCMS (m/z): 319 [M+H]<sup>+</sup>.

### 3-(4-((2-Chloro-9-((2-(trimethylsilyl)ethoxy)methyl)-9H-purin-6-yl)amino)-1-oxoisoindolin-2-yl)piperidine-2,6-dione



To a solution of 2,6-dichloro-9-((2-(trimethylsilyl)ethoxy)methyl)-9H-purine (10 mmol) and lenalidomide (2.6 g, 10 mmol) in DMF (30 mL) was added DIEA (3.3 mL, 20 mmol), and then heated up to 110 °C, stirred overnight. The mixture was purified by silica gel (MeOH/DCM = 0-4%) directly to provide the title compound (1.0 g, 19% for 2 steps) as yellow solid.

LCMS (m/z): 542 [M+H]<sup>+</sup>.

**3-(4-((2-(2-methoxyphenyl)-9H-purin-6-yl)amino)-1-oxoisindolin-2-yl)piperidine-2,6-dione (46)**

To a solution of 3-(4-((2-chloro-9-((2-(trimethylsilyl)ethoxy)methyl)-9H-purin-6-yl)amino)-1-oxoisindolin-2-yl)piperidine-2,6-dione (83 mg, 0.15 mmol) and (2-methoxyphenyl)boronic acid (27 mg, 0.18 mmol) in <sup>t</sup>BuOH (2 mL) were added N,N-Dicyclohexylmethylamine (32 mg, 0.17 mmol), Pd<sub>2</sub>dba<sub>3</sub> (14 mg, 0.015 mmol) and Tri-*tert*-butylphosphonium tetrafluoroborate (9 mg, 0.03 mmol). The mixture was heated to 80 °C and stirred under N<sub>2</sub> atmosphere overnight. The mixture was then filtered, concentrated *in vacuo* and purified by silica gel (MeOH/DCM = 0-4%) to provide the intermediate. The intermediate was then concentrated *in vacuo*, dissolved in TFA/DCM = 1/1, stirred for 2h, and then concentrated again *in vacuo*, purified by prep-HPLC (MeOH/H<sub>2</sub>O, 0.05% TFA) to provide compound **46** (26.0 mg, 29%).

<sup>1</sup>H NMR (500 MHz, DMSO-*d*<sub>6</sub>) δ 10.99 (s, 1H), 8.50 (s, 1H), 8.05 (dd, *J* = 6.9, 2.1 Hz, 1H), 7.62 – 7.50 (m, 4H), 7.45 (ddd, *J* = 8.9, 7.5, 1.8 Hz, 1H), 7.17 – 7.12 (m, 1H), 7.04 (td, *J* = 7.5, 0.9 Hz, 1H), 5.15 (dd, *J* = 13.3, 5.1 Hz, 1H), 4.60 (d, *J* = 17.5 Hz, 1H), 4.45 (d, *J* = 17.4 Hz, 1H), 2.92 (ddd, *J* = 17.2, 13.6, 5.4 Hz, 1H), 2.60 (d, *J* = 3.3 Hz, 1H), 2.55 (s, 3H), 2.32 (qd, *J* = 13.3, 4.6 Hz, 1H), 1.95 (dt, *J* = 10.0, 4.0 Hz, 1H).

LCMS (m/z): 484 [M+H]<sup>+</sup>.

**3-(4-((2-([1,1'-biphenyl]-4-yl)-9H-purin-6-yl)amino)-1-oxoisindolin-2-yl)piperidine-2,6-dione (47)**

**47** (1.7 mg, 2%) was obtained according to the synthetic route of **46**, changing from (2-methoxyphenyl)boronic acid to [1,1'-biphenyl]-4-ylboronic acid.

<sup>1</sup>H NMR (500 MHz, DMSO-*d*<sub>6</sub>) δ 10.94 (s, 1H), 9.91 (s, 1H), 8.36 – 8.24 (m, 3H), 8.01 – 7.96 (m, 1H), 7.75 (dd, *J* = 9.9, 7.9 Hz, 4H), 7.64 – 7.59 (m, 2H), 7.49 (dd, *J* = 8.3, 7.1 Hz, 2H), 7.42 – 7.35 (m, 1H), 5.13 (dd, *J* = 13.1, 5.1 Hz, 1H), 4.64 (d, *J* = 17.4 Hz, 1H), 4.51 (d, *J* = 17.4 Hz, 1H), 2.93 – 2.78 (m, 1H), 2.51 (d, *J* = 1.9 Hz, 1H), 2.34 (qd, *J* = 13.2, 4.8 Hz, 1H), 1.96 (dd, *J* = 14.9, 8.4 Hz, 1H).

LCMS (m/z): 530 [M+H]<sup>+</sup>.

**3-(4-((2-(4-fluoro-2-methoxyphenyl)-9H-purin-6-yl)amino)-1-oxoisindolin-2-yl)piperidine-2,6-dione (48)**

**48** (16.4 mg, 18%) was obtained according to the synthetic route of **46**, changing from (2-methoxyphenyl)boronic acid to (4-fluoro-2-methoxyphenyl)boronic acid.

<sup>1</sup>H NMR (500 MHz, DMSO-*d*<sub>6</sub>) δ 10.98 (s, 1H), 9.74 (s, 1H), 8.30 (s, 1H), 8.11 – 7.99 (m, 1H), 7.58 – 7.48 (m, 3H), 6.98 (dd, *J* = 11.6, 2.4 Hz, 1H), 6.82 (td, *J* = 8.4, 2.4 Hz, 1H), 5.13 (dd, *J* = 13.3, 5.1 Hz, 1H), 4.59 (d, *J* = 17.4 Hz, 1H), 4.45 (d, *J* = 17.3 Hz, 1H), 3.77 (s, 3H), 2.91 (ddd, *J* = 17.9, 13.5, 5.4 Hz, 1H), 2.63 – 2.55 (m, 1H), 2.36 (qd, *J* = 13.2, 4.5 Hz, 1H), 1.94 (d, *J* = 12.8 Hz, 1H).

LCMS (m/z): 502 [M+H]<sup>+</sup>.

**3-(4-((2-(4-fluorophenyl)-9H-purin-6-yl)amino)-1-oxoisoindolin-2-yl)piperidine-2,6-dione (49)**

**49** (6.3 mg, 7%) was obtained according to the synthetic route of **46**, changing from (2-methoxyphenyl)boronic acid to (4-fluorophenyl)boronic acid.

<sup>1</sup>H NMR (500 MHz, DMSO-*d*<sub>6</sub>) δ 10.94 (s, 1H), 9.89 (s, 1H), 8.34 (s, 1H), 8.27 – 8.20 (m, 2H), 7.95 (dd, *J* = 6.0, 2.9 Hz, 1H), 7.61 (q, *J* = 3.9, 3.1 Hz, 2H), 7.31 – 7.19 (m, 2H), 5.13 (dd, *J* = 13.2, 5.1 Hz, 1H), 4.58 (d, *J* = 17.4 Hz, 1H), 4.48 (d, *J* = 17.3 Hz, 1H), 2.88 (ddd, *J* = 18.0, 11.5, 5.4 Hz, 1H), 2.55 (s, 1H), 2.33 (qd, *J* = 13.1, 4.4 Hz, 1H), 2.01 – 1.91 (m, 1H).

LCMS (m/z): 472 [M+H]<sup>+</sup>.

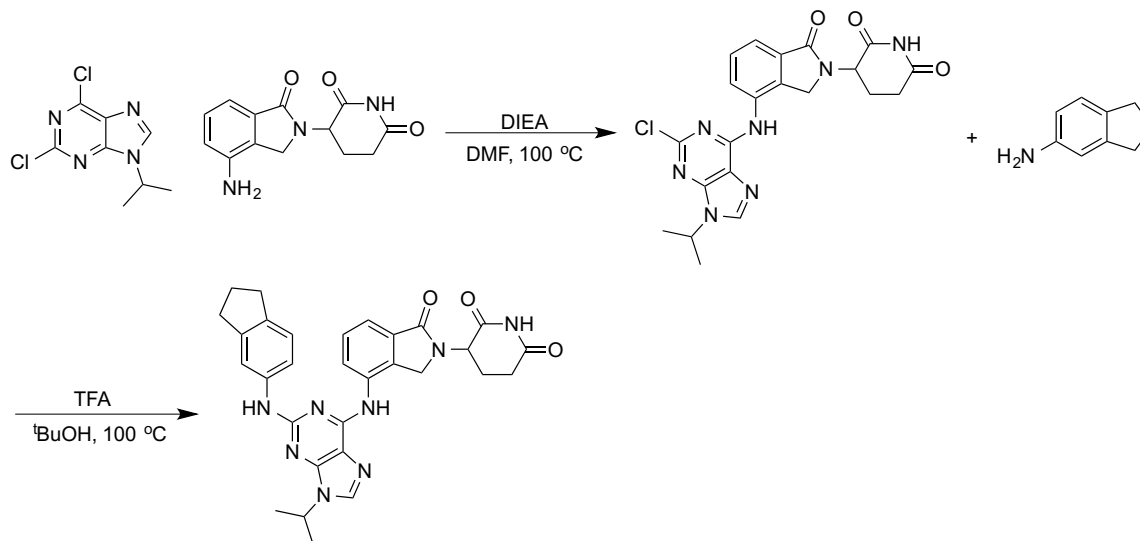
**3-(4-((2-(3,5-dimethoxyphenyl)-9H-purin-6-yl)amino)-1-oxoisoindolin-2-yl)piperidine-2,6-dione (50)**

**50** (4.5 mg, 4%) was obtained according to the synthetic route of **46**, changing from (2-methoxyphenyl)boronic acid to (3,5-dimethoxyphenyl)boronic acid.

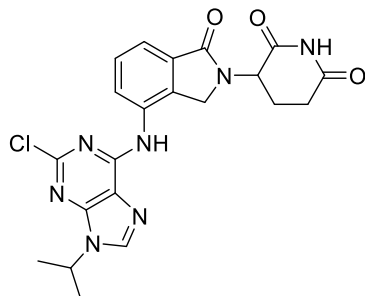
<sup>1</sup>H NMR (500 MHz, DMSO-*d*<sub>6</sub>) δ 11.00 (s, 1H), 8.46 (s, 1H), 8.07 (d, *J* = 7.3 Hz, 1H), 7.73 – 7.40 (m, 3H), 6.69 (d, *J* = 2.3 Hz, 1H), 6.65 (dd, *J* = 8.6, 2.3 Hz, 1H), 5.16 (dd, *J* = 13.2, 5.1 Hz, 1H), 4.59 (d, *J* = 17.5 Hz, 1H), 4.47 (s, 1H), 3.83 (s, 3H), 3.81 (s, 3H), 2.92 (ddd, *J* = 17.2, 13.5, 5.3 Hz, 1H), 2.68 – 2.54 (m, 1H), 2.33 (qd, *J* = 13.2, 4.4 Hz, 1H), 1.96 (ddd, *J* = 9.6, 5.4, 2.6 Hz, 1H).

LCMS (m/z): 514 [M+H]<sup>+</sup>.

### Scheme 4.6. Synthesis of **51**



### 3-(4-((2-chloro-9-isopropyl-9H-purin-6-yl)amino)-1-oxoisoindolin-2-yl)piperidine-2,6-dione



To a solution of Lenalidomide (78 mg, 0.34 mmol) and 2,6-dichloro-9-isopropyl-9H-purine (88 mg, 0.34 mmol) in DMF (2 mL) was added DIEA (169  $\mu$ L, 1.02 mmol), and then the mixture was heated to 100 °C overnight. The mixture was then concentrated *in vacuo* and purified by prep-HPLC (MeOH/H<sub>2</sub>O, 0.05% TFA) to obtain the title compound.

LCMS (m/z): 454 [M+H]<sup>+</sup>.

### 3-(4-((2,3-dihydro-1H-inden-5-yl)amino)-9-isopropyl-9H-purin-6-yl)amino)-1-oxoisoindolin-2-yl)piperidine-2,6-dione (**51**)

To a solution of 3-(4-((2-chloro-9-isopropyl-9H-purin-6-yl)amino)-1-oxoisoindolin-2-yl)piperidine-2,6-dione (60 mg, 0.13 mmol) and 2,3-dihydro-1H-inden-5-amine (18 mg, 0.13 mmol) in *t*BuOH (1 mL) was added TFA (20  $\mu$ L, 0.26 mmol), and then the mixture was heated to reflux overnight. The mixture was then concentrated *in vacuo* and purified by prep-HPLC (MeOH/H<sub>2</sub>O, 0.05% TFA) to obtain compound **51** (19.8 mg, 23%).

$^1\text{H}$  NMR (500 MHz,  $\text{DMSO-}d_6$ )  $\delta$  10.93 (s, 1H), 9.74 (s, 1H), 9.03 (s, 1H), 8.31 (s, 1H), 7.85 (d,  $J$  = 7.7 Hz, 1H), 7.69 – 7.50 (m, 3H), 7.28 (d,  $J$  = 8.3 Hz, 1H), 6.96 (d,  $J$  = 8.2 Hz, 1H), 5.08 (dd,  $J$  = 13.2, 5.2 Hz, 1H), 4.78 – 4.68 (m, 1H), 4.57 (d,  $J$  = 17.3 Hz, 1H), 4.34 (d,  $J$  = 17.3 Hz, 1H), 2.85 (ddd,  $J$  = 18.3, 13.6, 5.4 Hz, 1H), 2.74 (t,  $J$  = 7.3 Hz, 2H), 2.64 (t,  $J$  = 7.5 Hz, 2H), 2.48 (s, 1H), 2.20 (dd,  $J$  = 13.3, 4.5 Hz, 1H), 1.98 – 1.88 (m, 2H), 1.74 – 1.67 (m, 1H), 1.57 (d,  $J$  = 6.7 Hz, 6H).  
LCMS (m/z): 551 [M+H]<sup>+</sup>.

**Cell Culture.** MM1.S WT and MM1.S CRBN<sup>-/-</sup> cells were generously provided by James Bradner (DFCI, Boston, MA). MM1.S cell lines were cultured in RPMI-1640 media containing L-glutamine, supplemented with 10% fetal bovine serum (FBS) and 1% penicillin/streptomycin. Mycoplasma testing was performed on a monthly basis and all lines were negative.

**Cell Viability Assays.** Cell viability was evaluated using the CellTiter-Glo Luminescent Cell Viability Assay (Promega) following the manufacturer's standards.

**Immunoblotting.** Cells were washed with PBS before being lysed with Cell Lysis Buffer (Cell Signaling) supplemented with protease and phosphatase inhibitor cocktails (Roche) at 4°C for 15 minutes. The cell lysate vortexed before being centrifuged at 14,000 x g for 20 min at 4°C. Protein in cell lysate was quantified by BCA assay (Pierce). Primary antibodies used in this study include CK1 $\alpha$  (Abcam, ab206652), CRBN (Novus Biologicals, NBP1-91810), eRF3/GSPT1 (Abcam, ab49878), IKZF1 (Cell Signaling Technology, 5443S), IKZF3 (Cell Signaling Technology, 15103S), and vinculin (Abcam, ab130007). Blot quantification was performed using Image Studio 4.0 software, normalizing to loading controls.

**Sample preparation TMT LC-MS3 mass spectrometry.** MM1.s cells were treated with DMSO or 1  $\mu\text{M}$  of compound 29 in biological triplicates and **2** and **51** in biological singlicate for 6 hours. Cells were harvested by centrifugation. Lysis buffer (8 M Urea, 50 mM NaCl, 50 mM 4-(2hydroxyethyl)-1-piperazineethanesulfonic acid (EPPS) pH 8.5, Protease and Phosphatase inhibitors from Roche) was added to the cell pellets and homogenized by 20 passes through a 21 gauge (1.25 in. long) needle to achieve a cell lysate with a protein concentration between 1 – 4

mg mL<sup>-1</sup>. A micro-BCA assay (Pierce) was used to determine the final protein concentration of protein in the cell lysate. 200 µg of protein for each sample were reduced and alkylated as previously described<sup>17</sup>

Proteins were precipitated using methanol/chloroform. In brief, four volumes of methanol were added to the cell lysate, followed by one volume of chloroform, and finally three volumes of water. The mixture was vortexed and centrifuged to separate the chloroform phase from the aqueous phase. The precipitated protein was washed with one volume of methanol, centrifuged and the resulting washed precipitated protein was allowed to air dry. Precipitated protein was resuspended in 4 M Urea, 50 mM HEPES pH 7.4, followed by dilution to 1 M urea with the addition of 200 mM EPPS, pH 8. Proteins were first digested with LysC (1:50; enzyme:protein) for 12 hours at room temperature. The LysC digestion was diluted down to 0.5 M Urea with 200 mM EPPS pH 8 and then digested with trypsin (1:50; enzyme:protein) for 6 hours at 37 °C. Tandem mass tag (TMT) reagents (Thermo Fisher Scientific) were dissolved in anhydrous acetonitrile (ACN) according to manufacturer's instructions. Anhydrous ACN was added to each peptide sample to a final concentration of 30% v/v, and labeling was induced with the addition of TMT reagent to each sample at a ratio of 1:4 peptide:TMT label. The 10-plex labeling reactions were performed for 1.5 hours at RT and the reaction quenched by the addition of hydroxylamine to a final concentration of 0.3% for 15 minutes at RT. The sample channels were combined at a 1:1:1:1:1:1:1:1:1:1 ratio, desalted using C18 solid phase extraction cartridges (Waters) and analyzed by LC-MS for channel ratio comparison. Samples were then combined using the adjusted volumes determined in the channel ratio analysis and dried down in a speed vacuum. The combined sample was then resuspended in 1% formic acid, and acidified (pH 2–3) before being subjected to desalting with C18 SPE (Sep-Pak, Waters). Samples were then offline fractionated into 96 fractions by high pH reverse-phase HPLC (Agilent LC1260) through an aeris peptide xb-c18 column (phenomenex) with mobile phase A containing 5% acetonitrile and 10 mM NH<sub>4</sub>HCO<sub>3</sub> in LC-MS grade H<sub>2</sub>O, and mobile phase B containing 90% acetonitrile and 10 mM

NH<sub>4</sub>HCO<sub>3</sub> in LC-MS grade H<sub>2</sub>O (both pH 8.0). The 96 resulting fractions were then pooled in a non-continuous manner into 24 fractions and these fractions were used for subsequent mass spectrometry analysis.

Data were collected using an Orbitrap Fusion Lumos mass spectrometer (Thermo Fisher Scientific, San Jose, CA, USA) coupled with a Proxeon EASY-nLC 1200 LC pump (Thermo Fisher Scientific). Peptides were separated on a 75  $\mu$ M inner diameter microcapillary column packed with ~50 cm of Accucore C18 resin (1.8  $\mu$ M, 100 Å, Thermo Fisher Scientific). Peptides were separated using a 180 min gradient of 6–27% acetonitrile in 1.0% formic acid with a flow rate of 350 nL/min.

Each analysis used an MS<sub>3</sub>-based TMT method as described previously.<sup>18</sup> The data were acquired using a mass range of m/z 250-1400, resolution 120,000, AGC target 5 x 10<sup>6</sup>., maximum injection time 100 ms, dynamic exclusion of 90 seconds for the peptide measurements in the Orbitrap. Data dependent MS<sub>2</sub> spectra were acquired in the ion trap with a normalized collision energy (NCE) set at 35%, AGC target set to 2 x 10<sup>4</sup> and a maximum injection time of 150ms. MS<sub>3</sub> scans were acquired in the Orbitrap with a HCD collision energy set to 65%, AGC target set to 1.0 x 10<sup>5</sup>, maximum injection time of 200ms, resolution at 50,000 and with a maximum synchronous precursor selection (SPS) precursors set to 10.

**LC-MS data analysis.** Proteome Discoverer 2.2 (Thermo Fisher Scientific) was used for .RAW file processing and controlling peptide and protein level false discovery rates, assembling proteins from peptides, and protein quantification from peptides. MS/MS spectra were searched against a Uniprot human database (September 2016) with both the forward and reverse sequences. Database search criteria are as follows: tryptic with two missed cleavages, a precursor mass tolerance of 20 ppm, fragment ion mass tolerance of 0.6 Da, static alkylation of cysteine (57.02146 Da), static TMT labelling of lysine residues and N-termini of peptides (229.16293 Da), and variable oxidation of methionine (15.99491 Da). TMT reporter ion intensities were measured using a 0.003 Da window around the theoretical m/z for each reporter ion in the

MS3 scan. Peptide spectral matches with poor quality MS3 spectra were excluded from quantitation (summed signal-to-noise across 10 channels < 200 and precursor isolation specificity < 0.5), and resulting data was filtered to only include proteins that had a minimum of 3 unique peptides identified. Reporter ion intensities were normalised and scaled using in-house scripts in the R framework.<sup>19</sup> Statistical analysis was carried out using the limma package within the R framework.<sup>20</sup>

### **Author Contributions**

C.E.P conducted the experiments and analyzed the data. G.D. designed the compound library. G.D. and Z.H. synthesized compounds. J.C. performed and analyzed docking studies. K.A.D. ran and analyzed expression proteomics. R.P.N ran CRBN binding assay. T.Z., E.S.F., and N.S.G advised on project directions. C.E.P. wrote the paper with additional editing and writing from G.D. and J.C.

### **Funding Sources**

Funding for this work was received from the National Institutes of Health (NIH): Grant R01 CA214608 (E.S.F.) and 5 F31 CA210619-02 (C.E.P.).

### **Notes**

The authors declare no competing financial interest.

## References

- (1) Ito, T.; Ando, H.; Suzuki, T.; Ogura, T.; Hotta, K.; Imamura, Y.; Yamaguchi, Y.; Handa, H. Identification of a Primary Target of Thalidomide Teratogenicity. *Science* **2010**, *327* (5971), 1345–1350. <https://doi.org/10.1126/science.1177319> .
- (2) Bartlett, B. J.; Dredge, K.; Dalgleish, A. G. The Evolution of Thalidomide and Its IMiD Derivatives as Anticancer Agents. *Nat Rev Cancer* **2004**, *4* (4), nrc1323. <https://doi.org/10.1038/nrc1323> .
- (3) Rajkumar, V. S.; Hayman, S. R.; Lacy, M. Q.; Dispenzieri, A.; Geyer, S. M.; Kabat, B.; Zeldenrust, S. R.; Kumar, S.; Greipp, P. R.; Fonseca, R.; et al. Combination Therapy with Lenalidomide plus Dexamethasone (Rev/Dex) for Newly Diagnosed Myeloma. *Blood* **2005**, *106* (13), 4050. <https://doi.org/10.1182/blood-2005-07-2817> .
- (4) Lacy, M. Q.; Hayman, S. R.; Gertz, M. A.; Dispenzieri, A.; Buadi, F.; Kumar, S.; Greipp, P. R.; Lust, J. A.; Russell, S. J.; Dingli, D.; et al. Pomalidomide (CC4047) Plus Low-Dose Dexamethasone As Therapy for Relapsed Multiple Myeloma. *J Clin Oncol* **2009**, *27* (30), 5008–5014. <https://doi.org/10.1200/jco.2009.23.6802> .
- (5) Lopez-Girona, A.; Mendy, D.; Ito, T.; Miller, K.; Gandhi, A.; Kang, J.; Karasawa, S.; Carmel, G.; Jackson, P.; Abbasian, M.; et al. Cereblon Is a Direct Protein Target for Immunomodulatory and Antiproliferative Activities of Lenalidomide and Pomalidomide. *Leukemia* **2012**, *26* (11), 2326–2335. <https://doi.org/10.1038/leu.2012.119> .
- (6) Kronke, J.; Udeshi, N.; Narla, A.; Grauman, P.; Hurst, S.; McConkey, M.; Svinkina, T.; Heckl, D.; Comer, E.; Li, X.; et al. Lenalidomide Causes Selective Degradation of IKZF1 and IKZF3 in Multiple Myeloma Cells. *Science* **2014**, *343* (6168), 301–305. <https://doi.org/10.1126/science.1244851> .
- (7) Lu, G.; Middleton, R. E.; Sun, H.; Naniong, M.; Ott, C. J.; Mitsiades, C. S.; Wong, K.-K.; Bradner, J. E.; Comer, E.; Li, X.; et al. The Myeloma Drug Lenalidomide Promotes the Cereblon-Dependent Destruction of Ikaros Proteins. *Science* **2014**, *343* (6168), 305–309. <https://doi.org/10.1126/science.1244917> .
- (8) Winter, G.; Buckley, D.; Paulk, J.; Roberts, J.; Souza, A.; Dhe-Paganon, S.; Bradner, J. Phthalimide Conjugation as a Strategy for in Vivo Target Protein Degradation. *Science* **2015**, *348* (6241), 1376–1381. <https://doi.org/10.1126/science.aab1433> .
- (9) Huang, H.-T.; Dobrovolsky, D.; Paulk, J.; Yang, G.; Weisberg, E. L.; Citor, Z.; Buckley, D. L.; Cho, J.-H.; Ko, E.; Jang, J.; et al. A Chemoproteomic Approach to Query the Degradable Kinome Using a Multi-Kinase Degradator. *Cell Chem Biol* **2017**, *25* (1), 1–19. <https://doi.org/10.1016/j.chembiol.2017.10.005> .
- (10) Bondeson, D. P.; Smith, B. E.; Burslem, G. M.; Buhimschi, A. D.; Hines, J.; Jaime-Figueroa, S.; Wang, J.; Hamman, B. D.; Ishchenko, A.; Crews, C. M. Lessons in PROTAC Design from Selective Degradation with a Promiscuous Warhead. *Cell Chem Biol* **2017**, *25* (1), 1–34. <https://doi.org/10.1016/j.chembiol.2017.09.010> .
- (11) Chamberlain, P. P.; Cathers, B. E. Cereblon Modulators: Low Molecular Weight Inducers of Protein Degradation. *Drug Discov Today Technologies* **2019**, *31* (Curr Med Chem 25 31 2018).

<https://doi.org/10.1016/j.ddtec.2019.02.004> .

(12) Krönke, J.; Fink, E. C.; Hollenbach, P. W.; MacBeth, K. J.; Hurst, S. N.; Udeshi, N. D.; Chamberlain, P. P.; Mani, D.; Man, H.-W.; Gandhi, A. K.; et al. Lenalidomide Induces Ubiquitination and Degradation of CK1 $\alpha$  in Del(5q) MDS. *Cell* **2015**, 523 (7559), 183–188. <https://doi.org/10.1016/j.cell.2014.04.028> .

(13) Matyskiela, M. E.; Ito, T.; Pagarigan, B.; Lu, C.-C.; Miller, K.; Fang, W.; Wang, N.-Y.; Nguyen, D.; Houston, J.; Carmel, G.; et al. A Novel Cereblon Modulator Recruits GSPT1 to the CRL4CRBN Ubiquitin Ligase. *Nature* **2016**, 535 (7611), 252–257. <https://doi.org/10.1038/nature18611> .

(14) Goff, C.; Zemlyanko, O.; Moskalenko, S.; Berkova, N.; Inge-Vechtomov, S.; Philippe, M.; Zhouravleva, G. Mouse GSPT2, but Not GSPT1, Can Substitute for Yeast ERF3 in Vivo. *Genes Cells* **2002**, 7 (10), 1043–1057. <https://doi.org/10.1046/j.1365-2443.2002.00585.x> .

(15) Ishoey, M.; Chorn, S.; Singh, N.; Jaeger, M. G.; Brand, M.; Paulk, J.; Bauer, S.; Erb, M. A.; Parapatics, K.; Müller, A. C.; et al. Translation Termination Factor GSPT1 Is a Phenotypically Relevant Off-Target of Heterobifunctional Phthalimide Degraders. *ACS Chem Biol* **2018**, 13 (3), 553–560. <https://doi.org/10.1021/acscchembio.7b00969> .

(16) Jin, L.; Mbong, N.; Ng, S.; Wang, J.; Minden, M. D.; Fan, J.; Pierce, D. W.; Pourdehnad, M.; Dick, J. E. A Novel Cereblon E3 Ligase Modulator Eradicates Acute Myeloid Leukemia Stem Cells through Degradation of Translation Termination Factor GSPT1. *Blood* **2019**, 134 (Supplement\_1), 3940–3940. <https://doi.org/10.1182/blood-2019-128450> .

(17) Donovan, K. A.; An, J.; Nowak, R. P.; Yuan, J. C.; Fink, E. C.; Berry, B. C.; Ebert, B. L.; Fischer, E. S. Thalidomide Promotes Degradation of SALL4, a Transcription Factor Implicated in Duane Radial Ray Syndrome. *Elife* **2018**, 7, e38430. <https://doi.org/10.7554/elife.38430> .

(18) McAlister, G. C.; Nusinow, D. P.; Jedrychowski, M. P.; Wühr, M.; Huttlin, E. L.; Erickson, B. K.; Rad, R.; Haas, W.; Gygi, S. P. MultiNotch MS3 Enables Accurate, Sensitive, and Multiplexed Detection of Differential Expression across Cancer Cell Line Proteomes. *Anal Chem* **2014**, 86 (14), 7150–7158. <https://doi.org/10.1021/ac502040v> .

(19) Team, C. R. R. A Language and Environment for Statistical Computing. *R Foundation for Statistical Computing* **2014**.

(20) Ritchie, M. E.; Phipson, B.; Wu, D.; Hu, Y.; Law, C. W.; Shi, W.; Smyth, G. K. Limma Powers Differential Expression Analyses for RNA-Sequencing and Microarray Studies. *Nucleic Acids Res* **2015**, 43 (7), e47–e47. <https://doi.org/10.1093/nar/gkv007> .

**Chapter 5: Chemically Induced Cereblon (CRBN)  
Degradation: Efficacy of Recruiting CRBN in Comparison  
to VHL**

## **Attributions**

The work in this chapter is adapted from a manuscript that is being prepared for submission titled “Chemically Induced Cereblon (CRBN) Degradation: Efficacy of Recruiting CRBN in Comparison to VHL” by Powell *et al.* Author contributions, funding sources, and competing interests for this work can be found near the end of the chapter, before the references.

## **Chapter 5: Chemically Induced Cereblon (CRBN) Degradation: Efficacy of Recruiting CRBN in Comparison to VHL**

Chelsea E. Powell, Jonathan Bushman, Guangyan Du, Zhixiang He, Tinghu Zhang, Eric S. Fischer, Nathanael S. Gray\*

Department of Cancer Biology, Dana-Farber Cancer Institute, Boston, Massachusetts 02215, United States

Department of Biological Chemistry & Molecular Pharmacology, Harvard Medical School, Boston, Massachusetts 02115, United States

\* Correspondence: [Nathanael\\_Gray@dfci.harvard.edu](mailto:Nathanael_Gray@dfci.harvard.edu) (N.S.G.).

## **Abstract**

As small molecule degrader technology has developed, it has raised the question of whether or not E3 ligases could be induced to ubiquitinate themselves, leading to proteasomal degradation. Here we report the generation of 6 CRBN-CRBN degraders (also referred to as homo-PROTACs) and 6 CRBN-VHL degraders in order to identify selective CRBN degraders that may be used as probes to study CRBN biology. We identify two potent and selective CRBN degraders from the CRBN-VHL compounds that both use a 10-carbon linker, ZXH-4-130 and ZXH-4-137. Comparison of our compounds to the previously reported most potent degraders of CRBN, further validates our observation that CRBN-VHL degraders are more potent degraders of CRBN than CRBN-CRBN degraders, with our lead compounds displaying comparable activity to the previously reported lead CRBN degrader, CRBN-6-5-5-VHL.

## 5.1 Introduction

Cereblon (CRBN) is a substrate receptor that forms an E3 ubiquitin ligase complex with damaged DNA binding protein 1 (DDB1), cullin-4A (CUL4A), and RING-box protein 1 (RBX1 or ROC1). In 2010 the immunomodulatory drug (IMiD) thalidomide was shown to bind to cereblon.<sup>1</sup> Shortly afterwards thalidomide along with other IMiDs, lenalidomide and pomalidomide, were demonstrated to induce the degradation of the transcription factors Ikaros (IKZF1) and Aiolos (IKZF3) through binding to CRBN, providing a mechanism of action for the antiproliferative and immunomodulatory effects of IMiDs in multiple myeloma cells.<sup>2,3</sup>

This discovery that small molecule drugs acted as CRBN ligands led in part to the development of small molecule degraders (also called PROTACs or degronimides), which are heterobifunctional small molecules that can induce the degradation of a protein by bringing it into proximity of an E3 ligase.<sup>4-6</sup> When the ternary complex is formed, the E3 ligase ubiquitinates the target protein, leading to its proteasomal degradation. Small molecule degraders are an exciting new technology because they provide the advantages of genetic knockdown while remaining in a small molecule drug framework. Additionally, small molecule degraders act in a catalytic manner with one degrader molecule being able to induce the degradation of multiple protein molecules, which allows them to be effective at much lower intracellular concentrations than inhibitors. This is due to the fact that once a target protein is ubiquitinated it is marked for proteasomal degradation, allowing the degrader to only need a transient interaction with a protein before being free to form a new ternary complex. Both the CRBN E3 ligase and the von-Hippel Lindau (VHL) E3 ligase have been successfully recruited by small molecule degraders to induce the degradation of numerous target proteins, including BRD4, BCR-ABL, CDK9, Aurora A, PTK2, FER, BTK, ALK, and other kinases.<sup>4,7-11</sup>

Although CRBN is a well-established target for therapeutic small molecules, little is known about its endogenous biological function. Individual studies have suggested that CRBN may play a role in metabolic regulation or a protective role against DNA damage-induced apoptosis, but

these hypotheses have not yet been demonstrated more widely.<sup>12,13</sup> In this work, we aimed to develop selective small molecule degraders of CRBN that could be used as tool compounds to probe CRBN biology.

Other CRBN targeting degraders have been reported recently with 15a (referred to in this work as **St-15a**) being the most potent CRBN-CRBN recruiting degrader (called a homo-PROTAC) and **CRBN-6-5-5-VHL** being the most potent CRBN-VHL recruiting degrader (called a hetero-PROTAC).<sup>14–16</sup>

Here we report the development of 6 CRBN-CRBN degraders and 6 CRBN-VHL degraders.

## 5.2 Results and Discussion

For CRBN-CRBN degraders we first designed 3 compounds that linked two pomalidomide groups together with all carbon linkers of varying lengths (Figure 5.1A). All 3 compounds were potent CRBN degraders at a dose range of 10 – 100 nM after 4 hr treatments in MM1.s cells (Figure 5.1B). At a higher dose range of 1 – 10  $\mu$ M the degraders displayed the “hook effect” that has been previously reported as a trait of small molecule degraders, where at higher doses degrader potency is lost.<sup>17,18</sup> In Figure 5.1B the cause of the hook effect is well illustrated, with CRBN degradation decreasing as Ikaros degradation decreases, indicating that the degraders are out-competing themselves for binding and behaving similar to single agent pomalidomide. These pomalidomide derived CRBN-CRBN degraders were able to induce degradation as early as 1 hr and as late as 24 hr after treatment, with the most potent degradation being seen roughly between 4 – 8 hr (Figure 5.1C).

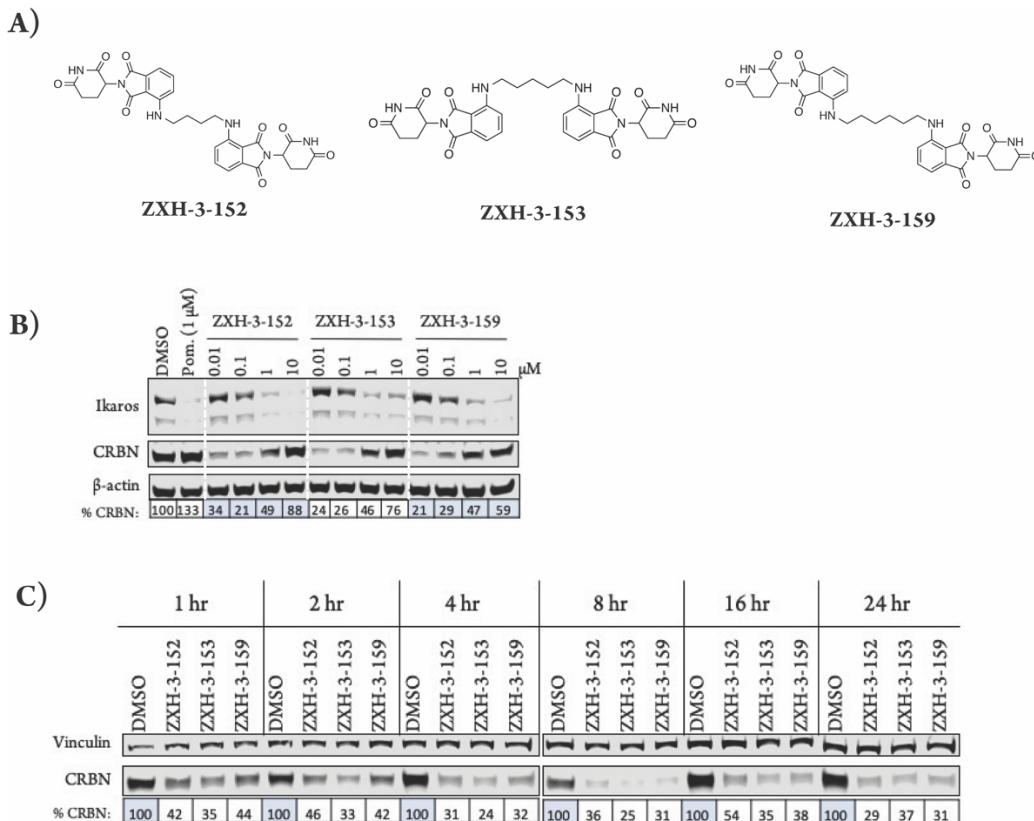


**Figure 5.1.** Pomalidomide CRBN-CRBN degrader behavior in MM1.s cells. (A) Structures of pomalidomide derived CRBN-CRBN degraders. (B) Immunoblot after 4 hours of treatment with dose titrations of degraders. (C) Immunoblot after treatment with 50 nM of compound for the indicated amount of time. Quantification shown as percentage of DMSO control normalized to  $\beta$ -actin or vinculin.

When the selectivity profile of **ZXH-3-159** was examined by expression proteomics, it was shown to be highly promiscuous, with several proteins with zinc finger domains being downregulated in addition to CRBN (Figure 5.2). This is similar to the zinc finger protein activity that has been reported with IMiDs previously.<sup>19</sup> In an effort to increase the selectivity profile of the CRBN-CRBN degraders, we generated 3 CRBN-CRBN, homo-PROTAC compounds that used a tricyclic analog of thalidomide (Figure 5.3A). Although these compounds did demonstrate decreased potency against the zinc finger transcription factor Ikaros, they also had much lower degradative activity against CRBN than the pomalidomide-pomalidomide compounds (Figure 5.3B).

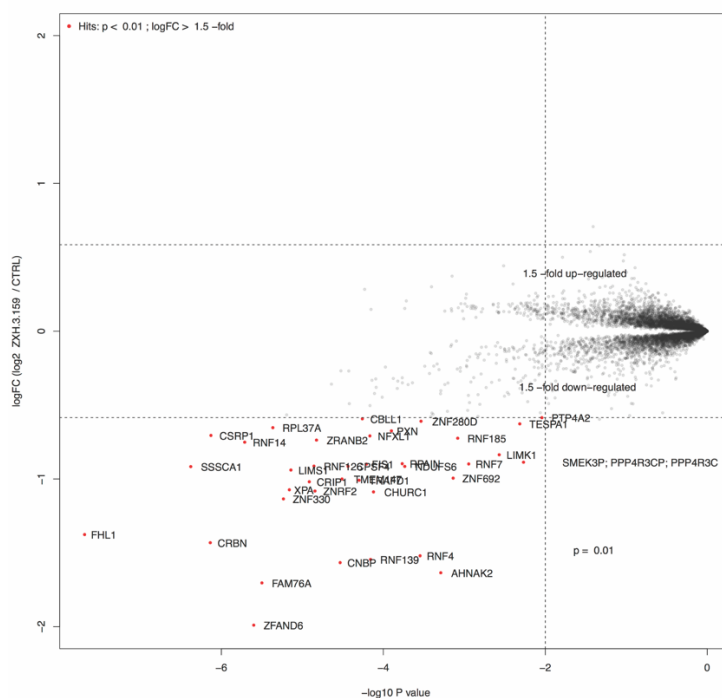


**Figure 5.2.** Expression proteomics in MM1.S cells after 6 hr treatment with 10 nM of **ZXH-3-159** or DMSO (singlicate analysis).

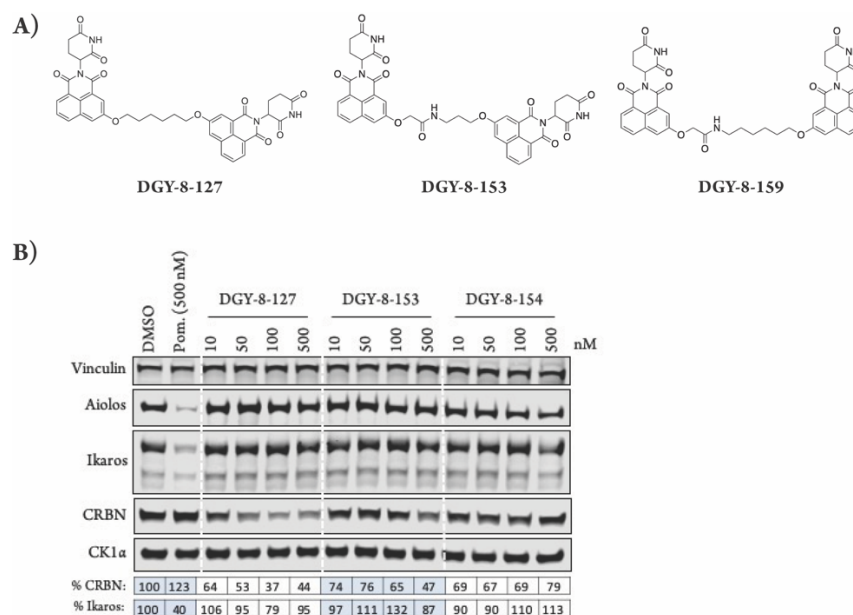


**Figure 5.3.** Tricyclic thalidomide analog CRBN-CRBN degrader behavior in MM1.S cells. (A) Structures of tricyclic thalidomide analog derived CRBN-CRBN degraders. (B) Immunoblot after 4 hours of treatment with dose titrations of degraders. Vinculin representative of 3 blots. Quantification shown as percentage of DMSO control normalized to vinculin.

Our next effort towards developing a selective CRBN degrader focused on recruiting both the CRBN and VHL E3 ligases. We generated 6 pomalidomide-VHL ligand based CRBN-VHL degraders using varying linkers (Figure 5.4A). 4 hr dose titration treatments in MM1.s cells indicated that **ZXH-4-130** and **ZXH-4-137** were highly potent and selective degraders of CRBN (Figure 5.4B). These two compounds use the same 11-carbon linker, with the VHL ligand used in **ZXH-4-137** being a methylated analog of the VHL ligand in **ZXH-4-130**. Interestingly, **ZXH-4-133** and **ZXH-4-136** also share a linker (4-carbon) with **ZXH-4-136** containing a methylated VHL ligand. For the **ZXH-4-133**, **ZXH-4-136** pair the methylated VHL ligand improves potency, with **ZXH-4-136** being the most potent after that **ZXH-4-130** and **ZXH-4-137**. However, for the **ZXH-4-130**, **ZXH-4-137** pair the potencies are equivalent. A time course in MM1.s cells at a 50 nM dose demonstrated that **ZXH-4-130** was the most potent between 2 – 8 hrs, while **ZXH-4-137** was the most potent between 2 – 16 hrs (Figure 5.4C).

Expression proteomics in MM1.s cells with 50 nM of **ZXH-4-130** and **ZXH-4-137** further validated that these degraders are highly selective for CRBN, with CRBN being the only significantly downregulated target (Figure 5.5). Neither VHL nor degradable targets of IMiDs, such as Ikaros and Aiolos, were downregulated. This indicated that both of these compounds were promising lead probes for chemically inducing CRBN degradation.

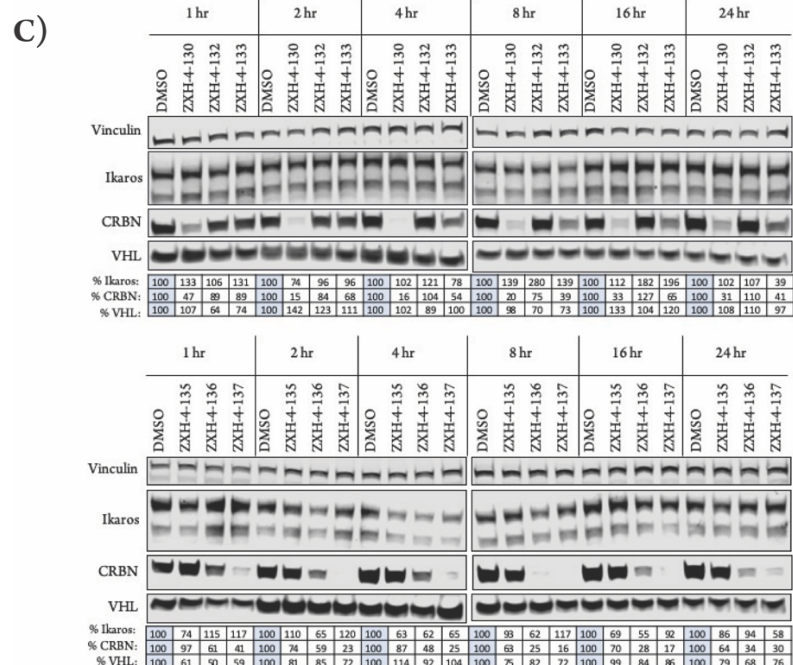
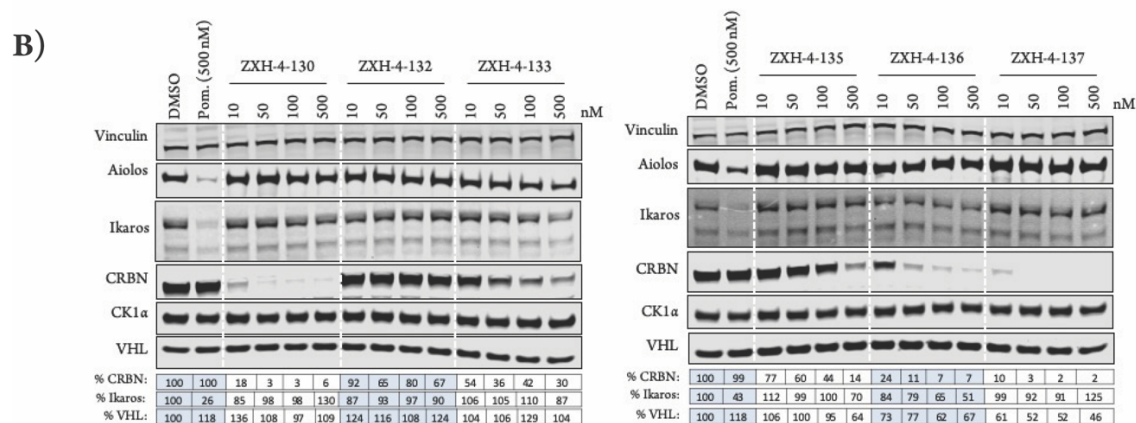
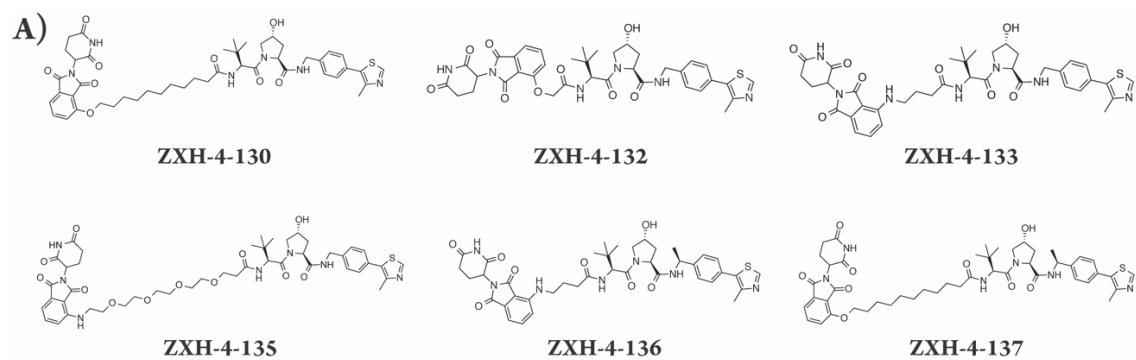


**Figure 5.4.** Thalidomide-VHL ligand based CRBN-VHL degrader behavior in MM1.s cells. (A) Structures of thalidomide and VHL ligand derived CRBN-VHL degraders. (B) Immunoblots after 4 hours of treatment with dose titrations of degraders. Vinculin representative of 3 blots. (C) Immunoblots after treatment with 50 nM of compound for the indicated amount of time. Vinculin representative of 2 blots. Quantification shown as percentage of DMSO control normalized to vinculin.

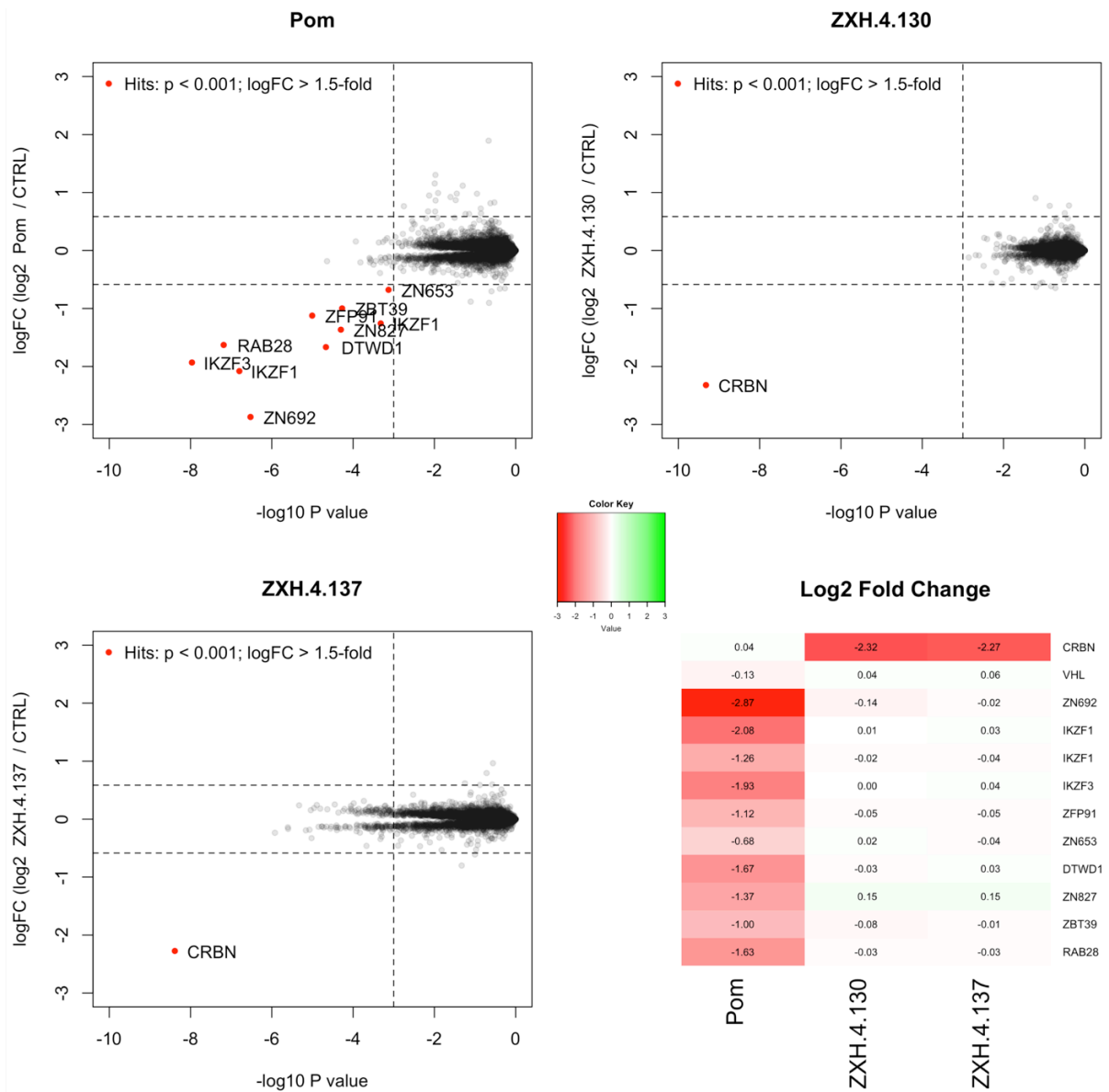


**Figure 5.5.** Expression proteomics in MM1.S cells after 6 hr treatment with 1  $\mu$ M of pomalidomide (pom), 50 nM of **ZXH-4-130**, 50 nM of **ZXH-4-137**, or DMSO (triplicate analysis for **ZXH-4-130** and **ZXH-4-137**; singlicate analysis for pomalidomide).

We next compared **ZXH-4-130** to the lead pomalidomide based CRBN-CRBN degrader reported by Steinebach et al., 15a (**St-15a**).<sup>16</sup> While **St-15a** appeared similarly selective to **ZXH-4-130** for CRBN over Ikaros by western, **ZXH-4-130** was a much for potent degrader of CRBN (Figure 5.6). We also examined whether or not **ZXH-4-130**, **ZXH-4-137**, one of our pomalidomide based CRBN-CRBN degraders (**ZXH-3-159**), or **St-15a** affected the expression of other members of the CRBN E3 ligase complex: DDB1, CUL4A, and ROC1 (Figure 5.6C). All of the degraders only degraded CRBN, with the other members of the complex maintaining expression levels similar to those seen in the DMSO control. This further validates what was observed by proteomics, as neither DDB1, CUL4A, or ROC1 were significantly up or downregulated after treatment with **ZXH-3-159**, **ZXH-4-130**, or **ZXH-4-137**. Additionally, this western demonstrated that **ZXH-3-159** had similar activity against CRBN as **St-15a**.

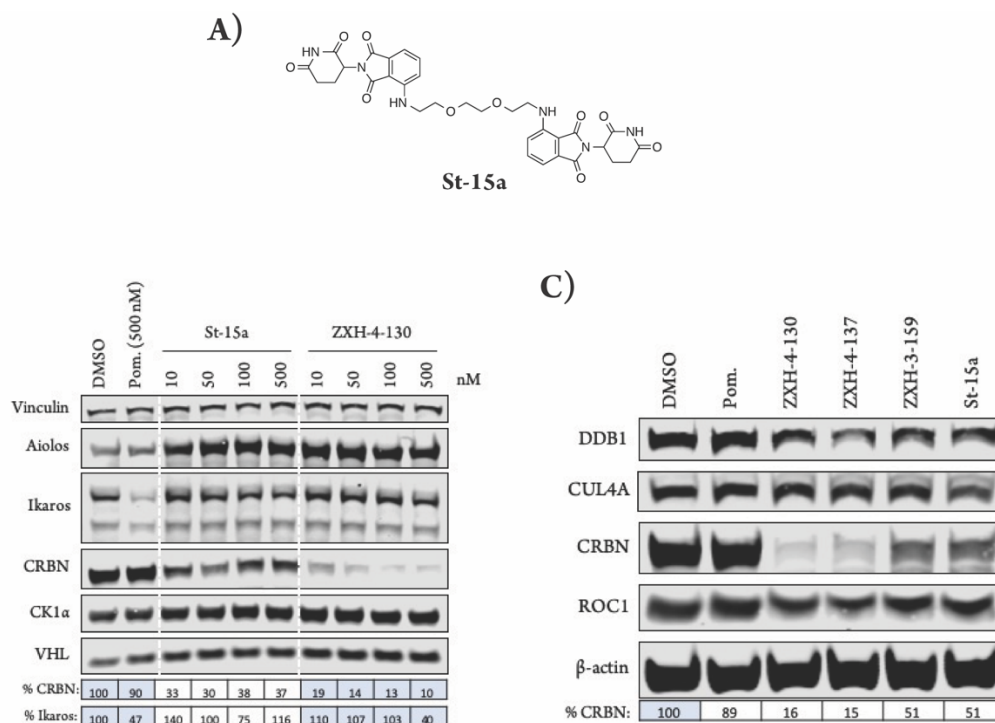


**Figure 5.6.** Comparison of lead CRBN degraders to **St-15a**. (A) Structure of pomalidomide based CRBN-CRBN degrader **St-15a**. (B) Immunoblot after 4 hours of treatment with dose titrations of degraders. Vinculin representative of 4 blots. (C) Immunoblot after treatment with 50 nM of compound for 4 hours.  $\beta$ -actin representative of 2 blots. Quantification shown as percentage of DMSO control normalized to  $\beta$ -actin or vinculin.

We next examined the potential of using **ZXH-4-130** and **ZXH-4-137** as probes for studying CRBN biology by determining if chemically induced CRBN knockdown could prevent induced GSPT1 degradation. GSPT1 degradation is induced via CRBN upon treatment with the compound CC-885 in a manner that is equivalent to Ikaros and Aiolos induced degradation upon treatment with an IMiD.<sup>20</sup> A 2 hr pre-treatment with 50 nM of **ZXH-4-130** or **ZXH-4-137** did indeed prevent induced GSPT1 degradation after 4 hr treatment with CC-885 (Figure 5.7A). This prevention of induced degradation was comparable to that observed after pre-treatment with the proteasome inhibitor carfilzomib. Pre-treatment with 50 nM or 10  $\mu$ M of pomalidomide did not prevent GSPT1 degradation to a similar level as pre-treatment with **ZXH-4-130** or **ZXH-4-137**, indicating that the ability to prevent induced GSPT1 degradation was due to the CRBN degradative abilities of **ZXH-4-130** and **ZXH-4-137**, not just competition for CRBN binding.

We then determined if pomalidomide's CRBN-mediated cytotoxicity in MM1.s cells could be prevented by induced CRBN degradation. We compared out lead CRBN degraders to **St-15a** as well as **CRBN-6-5-5-VHL**, a potent CRBN targeting thalidomide-VHL ligand based degrader that had been previously reported by Steinebach et al (Figure 5.7B).<sup>15</sup> All four CRBN degraders prevented pomalidomide cytotoxicity to a significant extent, with **St-15a** having the least statistically significant amount of prevention and **ZXH-4-130**, **ZXH-4-137**, and **CRBN-6-5-5-VHL** having equally statistically significant amounts of prevention (Figure 5.7C). **CRBN-6-5-5-VHL** showed the most complete prevention of cytotoxicity.

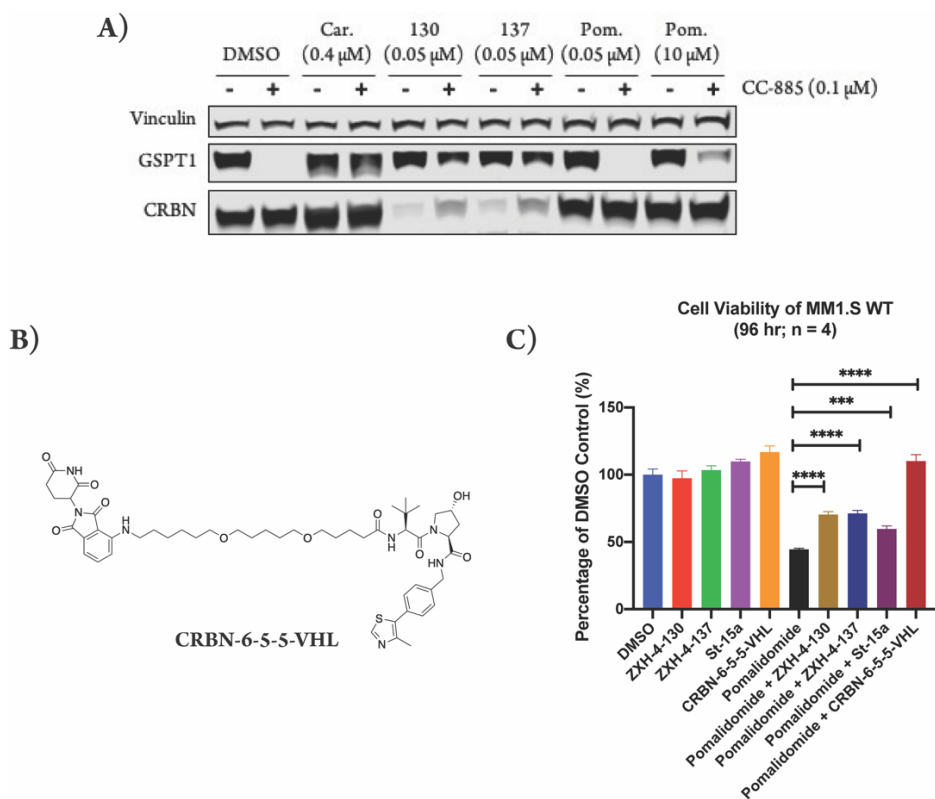


**Figure 5.7.** CRBN degraders as probes. (A) Immunoblots after 2-hour pre-treatments with DMSO, carfilzomib (Car), **ZXH-4-130** (130), **ZXH-4-137** (137), or pomalidomide (Pom) followed by 4-hour treatment with CC-885. (B) Structure of CRBN-VHL degrader **CRBN-6-5-5-VHL**. (C) Cell viability after 2-hour pre-treatments with 100 nM of **ZXH-4-130**, **ZXH-4-137**, **St-15a**, or **CRBN-6-5-5-VHL** followed by 96-hour treatment with 1  $\mu$ M of pomalidomide (four biological replicates; Graphpad Prism 8 software).

### 5.3 Conclusion

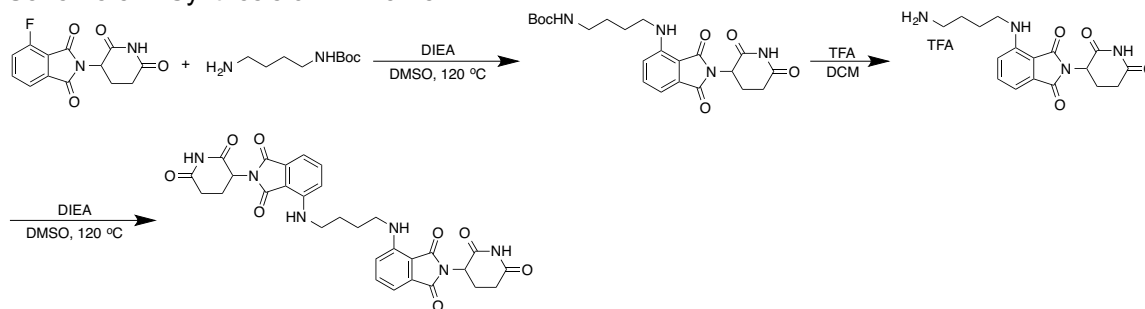
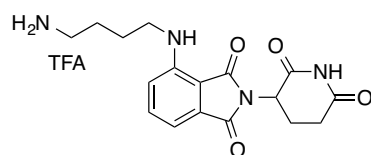
Here we have presented potent and highly selective degraders of CRBN, **ZXH-4-130** and **ZXH-4-137**. These compounds recruited both the CRBN and VHL E3 ligase, which was a more effective strategy for degrading CRBN than recruiting CRBN to degrade itself. This observation was consistent with the literature where **CRBN-6-5-5-VHL** was shown to be a more potent degrader of CRBN than **St-15a**.<sup>15</sup> This is likely because as CRBN is degraded by a CRBN-CRBN degrader (homo-PROTAC), it reaches a point where the amount of CRBN is lowered to a level where all of the remaining CRBN can be occupied by one end of a degrader compound. In a sense this is a reverse hook effect that prevents CRBN from being completely degraded by

CRBN-CRBN degraders. By recruiting two different E3 ligases we may reach a more complete level of CRBN degradation.

Interestingly, the CRBN-VHL degraders only induced degradation of CRBN and not VHL, which is also consistent with the literature on **CRBN-6-5-5-VHL**.<sup>15</sup> This may be because the VHL E3 ligase is more abundant in the cell than the CRBN E3 ligase, making CRBN more susceptible to degradation than VHL. Another possible explanation is that the ternary complex formed by the small molecule degraders positions the E3 ligases in a manner where CRBN is more amenable to degradation than VHL. Additionally, it has been suggested by the use of VHL-VHL degraders that VHL in the CRL2-VHL ubiquitin ligase complex may be protected from ubiquitination as selective degradation of pVHL30, a form of VHL that is thought to have ligase independent functions, was seen over degradation of pVHL19, a form of VHL that may preferentially act in the E3 ligase complex.<sup>21</sup>

## 5.4 Experimental Methods

Unless otherwise noted, reagents and solvents were obtained from commercial suppliers and were used without further purification. <sup>1</sup>H NMR spectra were recorded on 500 MHz (Bruker A500), and chemical shifts are reported in parts per million (ppm,  $\delta$ ) downfield from tetramethylsilane (TMS). Coupling constants (*J*) are reported in Hz. Spin multiplicities are described as s (singlet), br (broad singlet), d (doublet), t (triplet), q (quartet), and m (multiplet). Mass spectra were obtained on a Waters Micromass ZQ instrument. Preparative HPLC was performed on a Waters Sunfire C18 column (19 x 50 mm, 5 $\mu$ M) using a gradient of 15-95% methanol in water containing 0.05% trifluoroacetic acid (TFA) over 22 min (28 min run time) at a flow rate of 20 mL/min. Purities of assayed compounds were in all cases greater than 95%, as determined by reverse-phase HPLC analysis.

**Scheme 5.1. Synthesis of ZXH-3-152.****4-((4-aminobutyl)amino)-2-(2,6-dioxopiperidin-3-yl)isoindoline-1,3-dione.**

To a solution of 2-(2,6-dioxopiperidin-3-yl)-4-fluoroisoindoline-1,3-dione (180 mg, 0.65 mmol) and *tert*-butyl (4-aminobutyl)carbamate (122 mg, 0.65 mmol) in DMSO (2 mL) was added DIEA (215  $\mu$ L, 1.3 mmol), and then the mixture was stirred at 120 °C for 30 mins. After completed, the mixture was purified by pre-HPLC to obtain intermediate. The intermediate was then dissolved in TFA/DCM (*v/v* = 1/1), stirred at room temperature for 1 h, and then concentrated in vacuo to obtain desired product (190 mg, 64%) as TFA salt, which was used in next step without any purification.

LCMS: 345 [M + H]<sup>+</sup>.

**4,4'-(butane-1,4-diylbis(azanediyl))bis(2-(2,6-dioxopiperidin-3-yl)isoindoline-1,3-dione) (ZXH-3-152).**

To a solution of 4-((4-aminobutyl)amino)-2-(2,6-dioxopiperidin-3-yl)isoindoline-1,3-dione (46 mg, 0.1 mmol) and 2-(2,6-dioxopiperidin-3-yl)-4-fluoroisoindoline-1,3-dione (27 mg, 0.1 mmol) in DMSO (1 mL) was added DIEA (82  $\mu$ L, 0.5 mmol), and then the mixture was stirred at 120 °C for 30 mins. After completed, the mixture was purified by pre-HPLC to obtain product (1.8 mg, 3%) as TFA salt.

LCMS: 601 [M + H]<sup>+</sup>.

**4,4'-(pentane-1,5-diylbis(azanediy))bis(2-(2,6-dioxopiperidin-3-yl)isoindoline-1,3-dione)  
(ZXH-3-153.)**

**ZXH-3-153** was obtained according to the synthetic route of **ZXH-3-152**, changing from *tert-butyl* (4-aminobutyl)carbamate to *tert-butyl* (5-aminobutyl)carbamate.

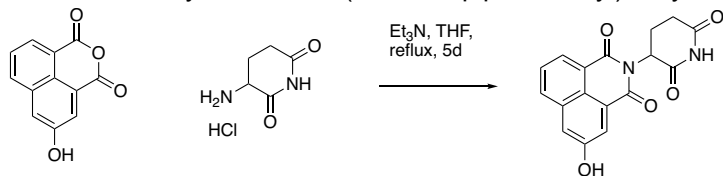
LCMS: 615 [M + H]<sup>+</sup>.

**4,4'-(hexane-1,6-diylbis(azanediy))bis(2-(2,6-dioxopiperidin-3-yl)isoindoline-1,3-dione)  
(ZXH-3-159).**

**ZXH-3-159** was obtained according to the synthetic route of **ZXH-3-152**, changing from *tert-butyl* (4-aminobutyl)carbamate to *tert-butyl* (6-aminobutyl)carbamate.

LCMS: 629 [M + H]<sup>+</sup>.

**Scheme 5.2.** Synthesis of 2-(2,6-dioxopiperidin-3-yl)-5-hydroxy-1H-benzo[de]isoquinoline-1,3(2H)-dione.

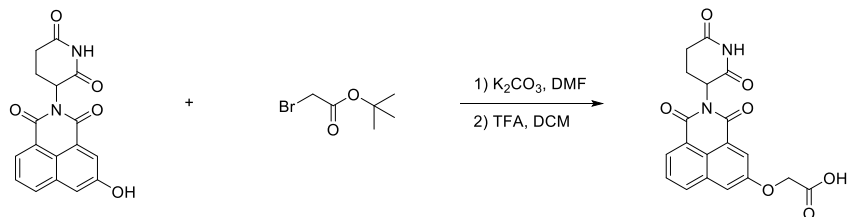


**2-(2,6-dioxopiperidin-3-yl)-5-hydroxy-1H-benzo[de]isoquinoline-1,3(2H)-dione.**

3-hydroxy-1,8-naphthalic anhydride (2.14 g, 10.0 mmol) and 3-aminopiperidine-2,6-dione (1.65 g, 10.0 mmol) were dissolved in THF (40 mL) at room temperature, and triethylamine (2.78 mL, 20.0 mmol) was added. The suspension was then refluxed for 5 days, with a green precipitate forming in the first 24 hours and eventually turning black. The solvent was evaporated, water was added, and the mixture was acidified, and stirred for 1 hour. The suspension was then filtered to provide the title compound (3.44g, 9.53 mmol, 95%) as a green solid.

LC/MS *m/z* calculated for [M+H]<sup>+</sup> 325.1, found 325.1.

**Scheme 5.3.** Synthesis of 2-((2-(2,6-dioxopiperidin-3-yl)-1,3-dioxo-2,3-dihydro-1H-benzo[de]isoquinolin-5-yl)oxy)acetic acid.

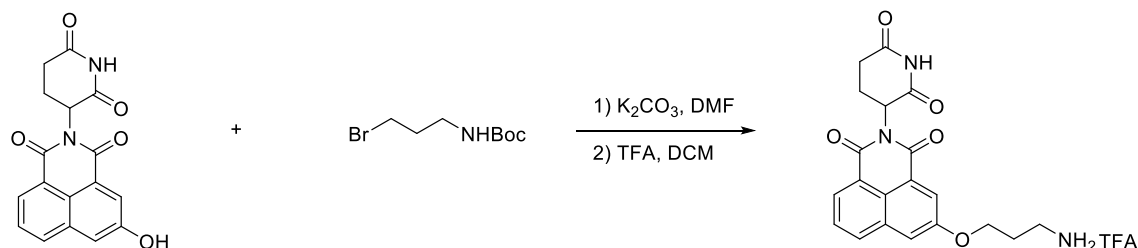


**2-((2-(2,6-dioxopiperidin-3-yl)-1,3-dioxo-2,3-dihydro-1H-benzo[de]isoquinolin-5-yl)oxy)acetic acid.**

2-(2,6-dioxopiperidin-3-yl)-5-hydroxy-1H-benzo[de]isoquinoline-1,3(2H)-dione (361 mg, 1.1 mmol) was suspended in 3 mL DMF, followed by addition of  $K_2CO_3$  (276 mg, 2.0 mmol) and t-butyl bromoacetate (234 mg, 1.2 mmol). The blue suspension was stirred at 35 °C for 4 hours, at which point an additional 1.0 mmol of t-butyl bromoacetate was added. After continuing to stir at 35 °C overnight, water was added, and the suspension was filtered to provide the title compound (464 mg, 1.06 mmol, 95%) as a light gray solid. Then the solid was dissolved in DCM, TFA was added to the suspension at room temperature. After 2 hours, the solvent was removed to get crude product. (quant. yield for the second step.)

LC/MS  $m/z$  calculated for  $[M+H]^+$  383.1, found 383.2.

**Scheme 5.4.** Synthesis of 5-(3-aminopropoxy)-2-(2,6-dioxopiperidin-3-yl)-1H-benzo[de]isoquinoline-1,3(2H)-dione TFA salt.



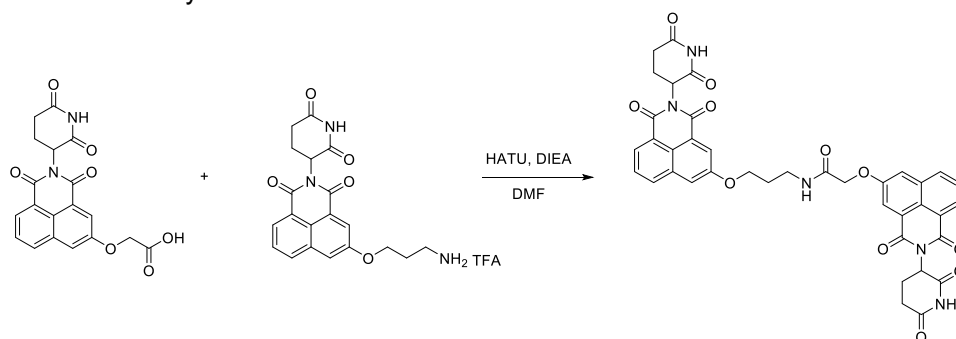
**5-(3-aminopropoxy)-2-(2,6-dioxopiperidin-3-yl)-1H-benzo[de]isoquinoline-1,3(2H)-dione**

**TFA salt.**

2-(2,6-dioxopiperidin-3-yl)-5-hydroxy-1H-benzo[de]isoquinoline-1,3(2H)-dione (100 mg, 0.31 mmol) was suspended in 2 mL DMF, followed by addition of  $K_2CO_3$  (128 mg, 0.93 mmol) and tert-butyl (3-bromopropyl)carbamate (74 mg, 0.31 mmol). The suspension was stirred at room temperature overnight. After the reaction was finished, the solvent was removed under vacuum. The residue was purified with flash chromatography to yield the product. The product was dissolved in DCM, TFA was then added to the mixture. After 2 hours, the solvent was removed under vacuum to get the crude product TFA salt without any further purification (143.7 mg, 0.30 mmol, 97%).

LC/MS  $m/z$  calculated for  $[M+H]^+$  382.1, found 382.2.

**Scheme 5.5. Synthesis of DGY-8-153.**



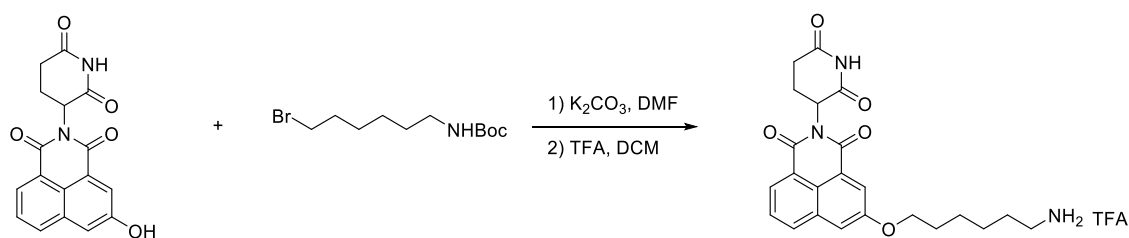
**2-((2-(2,6-dioxopiperidin-3-yl)-1,3-dioxo-2,3-dihydro-1H-benzo[de]isoquinolin-5-yl)oxy)-N-(3-((2-(2,6-dioxopiperidin-3-yl)-1,3-dioxo-2,3-dihydro-1H-benzo[de]isoquinolin-5-yl)oxy)propyl)acetamide (DGY-8-153).**

To the solution of 5-(3-aminopropoxy)-2-(2,6-dioxopiperidin-3-yl)-1H-benzo[de]isoquinoline-1,3(2H)-dione TFA salt (10 mg, 0.02 mmol) and 2-((2-(2,6-dioxopiperidin-3-yl)-1,3-dioxo-2,3-dihydro-1H-benzo[de]isoquinolin-5-yl)oxy)acetic acid (7.7 mg, 0.02 mmol) in DMF (1 mL), HATU (20 mg, 0.052 mmol) and DIEA (17 mg, 0.13 mmol) was added at room temperature. After 10 mins, the reaction mixture was purified with reverse phase HPLC to yield the product (9.3 mg,

0.012 mmol, 60%).  $^1\text{H NMR}$  (500 MHz,  $\text{DMSO-}d_6$ )  $\delta$  10.94 (s, 2H), 8.37 (d,  $J = 25.2$  Hz, 1H), 8.32 – 8.16 (m, 4H), 8.10 (d,  $J = 35.5$  Hz, 1H), 8.01 – 7.81 (m, 2H), 7.80 – 7.63 (m, 3H), 5.74 (dd,  $J = 11.8, 5.9$  Hz, 2H), 4.69 (d,  $J = 2.5$  Hz, 2H), 4.17 – 4.02 (m, 2H), 3.40 – 3.30 (m, 2H), 2.87 (t,  $J = 15.9$  Hz, 2H), 2.59 – 2.46 (m, 4H), 1.96 (s, 4H).

LC/MS  $m/z$  calculated for  $[\text{M}+\text{H}]^+$  746.2, found 746.2.

**Scheme 5.6.** Synthesis of 5-((6-aminohexyl)oxy)-2-(2,6-dioxopiperidin-3-yl)-1H-benzo[de]isoquinoline-1,3(2H)-dione TFA salt.

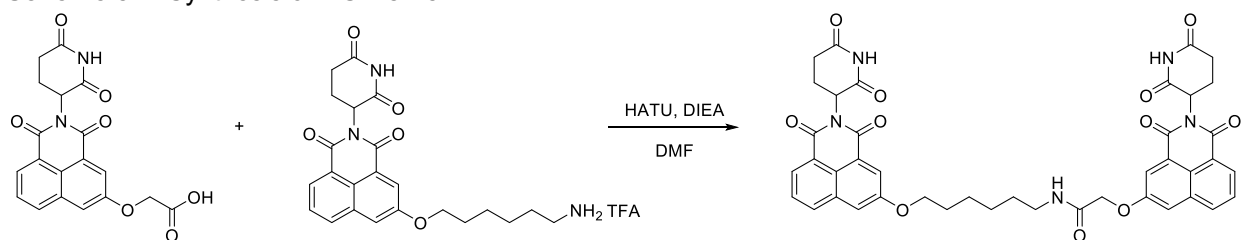


**5-((6-aminohexyl)oxy)-2-(2,6-dioxopiperidin-3-yl)-1H-benzo[de]isoquinoline-1,3(2H)-dione TFA salt.**

This compound was synthesized via the same route with 5-(3-aminopropoxy)-2-(2,6-dioxopiperidin-3-yl)-1H-benzo[de]isoquinoline-1,3(2H)-dione.

LC/MS  $m/z$  calculated for  $[\text{M}+\text{H}]^+$  424.2, found 424.2.

**Scheme 5.7.** Synthesis of **DGY-8-154**.

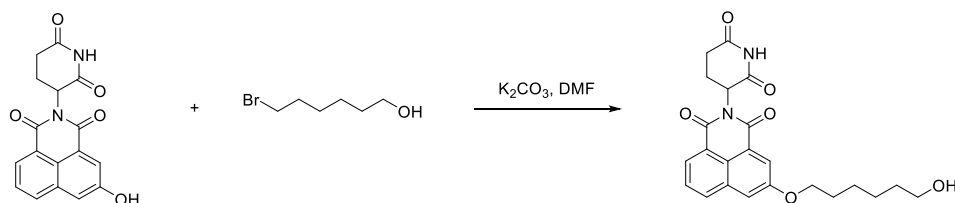


**2-((2-(2,6-dioxopiperidin-3-yl)-1,3-dioxo-2,3-dihydro-1H-benzo[de]isoquinolin-5-yl)oxy)-N-(6-((2-(2,6-dioxopiperidin-3-yl)-1,3-dioxo-2,3-dihydro-1H-benzo[de]isoquinolin-5-yl)oxy)hexyl)acetamide (DGY-8-154).**

This compound was synthesized via the same route with **DGY-8-153**.  $^1\text{H}$  NMR (500 MHz, DMSO- $d_6$ )  $\delta$  10.95 (s, 2H), 8.32 – 8.03 (m, 6H), 8.01 – 7.68 (m, 5H), 5.75 (dd,  $J$  = 11.9, 5.8 Hz, 2H), 4.65 (d,  $J$  = 8.1 Hz, 2H), 4.08 (s, 2H), 3.12 (s, 2H), 2.93 – 2.82 (m, 2H), 2.53 (d,  $J$  = 16.1 Hz, 4H), 1.99 (d,  $J$  = 13.0 Hz, 2H), 1.68 (s, 2H), 1.49 – 1.34 (m, 4H), 1.27 (d,  $J$  = 7.4 Hz, 2H).

LC/MS  $m/z$  calculated for  $[\text{M}+\text{H}]^+$  788.2, found 788.2.

**Scheme 5.8.** Synthesis of 2-(2,6-dioxopiperidin-3-yl)-5-((6-hydroxyhexyl)oxy)-1H-benzo[de]isoquinoline-1,3(2H)-dione.

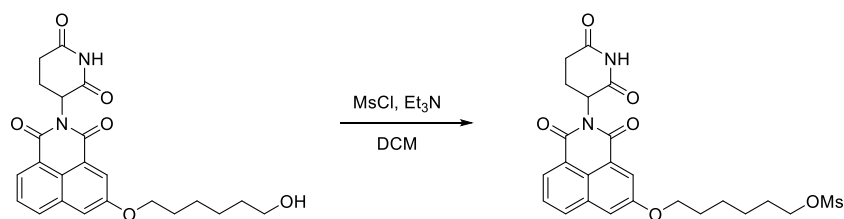


**2-(2,6-dioxopiperidin-3-yl)-5-((6-hydroxyhexyl)oxy)-1H-benzo[de]isoquinoline-1,3(2H)-dione.**

This compound was synthesized via the same route with 5-(3-aminopropoxy)-2-(2,6-dioxopiperidin-3-yl)-1H-benzo[de]isoquinoline-1,3(2H)-dione.

LC/MS  $m/z$  calculated for  $[\text{M}+\text{H}]^+$  425.2, found 425.2.

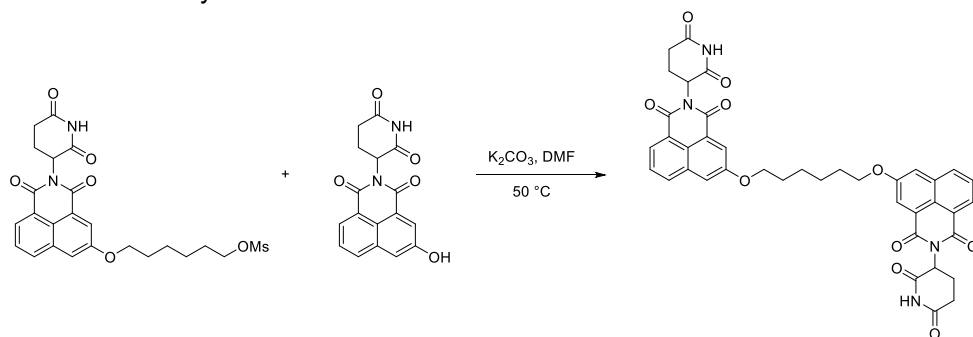
**Scheme 5.9.** Synthesis of 6-((2-(2,6-dioxopiperidin-3-yl)-1,3-dioxo-2,3-dihydro-1H-benzo[de]isoquinolin-5-yl)oxy)hexyl methanesulfonate.



**6-((2-(2,6-dioxopiperidin-3-yl)-1,3-dioxo-2,3-dihydro-1H-benzo[de]isoquinolin-5-yl)oxy)hexyl methanesulfonate.**

To the solution of 2-(2,6-dioxopiperidin-3-yl)-5-((6-hydroxyhexyl)oxy)-1H-benzo[de]isoquinoline-1,3(2H)-dione (17 mg, 0.04 mmol) and Et<sub>3</sub>N (16 mg, 0.16 mmol) in DCM (1 mL), MsCl (4.6  $\mu$ L, 0.06 mmol) was added at 0 °C. After 2 hours, the solvent was removed under vacuum. The residue was purified with flash chromatography to obtain the product (7 mg, 0.014 mmol, 35%).

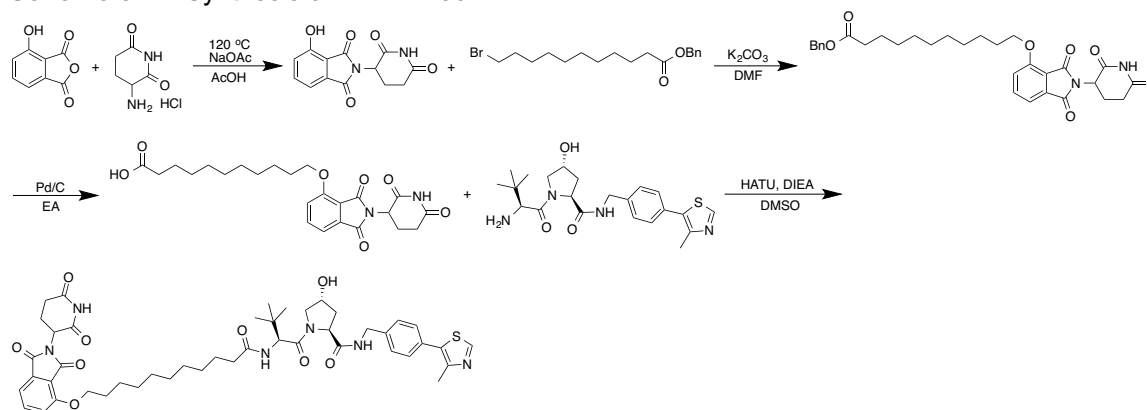
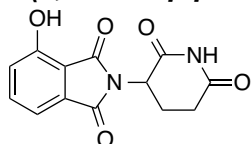
**Scheme 5.10. Synthesis of DGY-8-127.**



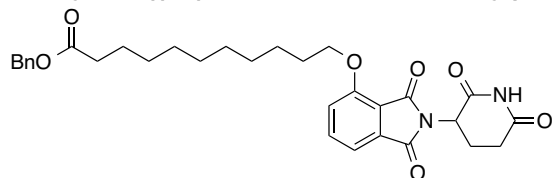
**5,5'-(hexane-1,6-diylbis(oxy))bis(2-(2,6-dioxopiperidin-3-yl)-1H-benzo[de]isoquinoline-1,3(2H)-dione) (DGY-8-127).**

To the solution of 6-((2-(2,6-dioxopiperidin-3-yl)-1,3-dioxo-2,3-dihydro-1H-benzo[de]isoquinolin-5-yl)oxy)hexyl methanesulfonate (7 mg, 0.014 mmol) and 2-(2,6-dioxopiperidin-3-yl)-5-hydroxy-1H-benzo[de]isoquinoline-1,3(2H)-dione (4.5 mg, 0.014 mmol) in DMF (1 mL), K<sub>2</sub>CO<sub>3</sub> (5.8 mg, 0.042 mmol) was added at room temperature. Then the reaction was heated to 50 °C overnight. The reaction mixture was purified with reverse phase HPLC to obtain the titled product (1.3 mg, 0.0018 mmol, 13%). <sup>1</sup>H NMR (500 MHz, DMSO-*d*<sub>6</sub>)  $\delta$  10.94 (s, 2H), 8.37 – 8.17 (m, 4H), 8.03 (d, *J* = 6.2 Hz, 1H), 7.96 – 7.84 (m, 3H), 7.75 (d, *J* = 6.4 Hz, 2H), 5.75 (dt, *J* = 11.7, 5.9 Hz, 2H), 4.23 – 4.10 (m, 4H), 2.95 – 2.81 (m, 2H), 2.52 (dd, *J* = 31.9, 15.8 Hz, 4H), 2.15 – 2.04 (m, 2H), 1.99 (d, *J* = 16.5 Hz, 2H), 1.82 (s, 2H), 1.54 (s, 2H), 1.40 (t, *J* = 7.2 Hz, 2H).

LC/MS *m/z* calculated for [M+H]<sup>+</sup> 731.2, found 731.2.

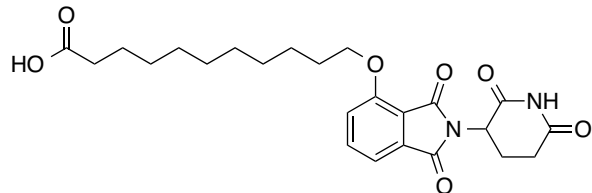
**Scheme 5.11. Synthesis of ZXH-4-130.****2-(2,6-dioxopiperidin-3-yl)-4-hydroxyisobenzofuran-1,3-dione.**

To a solution of 4-hydroxyisobenzofuran-1,3-dione (1.64 g, 10 mmol) and 3-aminopiperidine-2,6-dione hydrochloride (1.65 g, 10 mmol) in acetic acid (30 mL) was added NaOAc (984 mg, 12 mmol), then the mixture solution was stirred at 120 °C for 12 hrs. After completed, the mixture was cooled down to room temperature, filtered, and the solid was washed with some water and hexane, and then air dried for overnight to obtain crude product (2.23 g, 82%) as gray powder. LCMS: 275 [M + H]<sup>+</sup>.

**benzyl 11-((2-(2,6-dioxopiperidin-3-yl)-1,3-dioxoisindolin-4-yl)oxy)undecanoate.**

To a solution of 2-(2,6-dioxopiperidin-3-yl)-4-hydroxyisobenzofuran-1,3-dione (200 mg, 0.73 mmol) and benzyl 11-bromoundecanoate (310 mg, 0.87 mmol) in DMF (4 mL) was added K<sub>2</sub>CO<sub>3</sub> (152 mg, 1.1 mmol), and then the mixture was stirred at room temperature until reaction completed. The mixture was then filtered, and the filtrate was collected, purified by HPLC (MeOH/water, 0.035% TFA) to obtain product (180 mg, 37%) as TFA salt. LCMS: 549 [M + H]<sup>+</sup>.

**11-((2-(2,6-dioxopiperidin-3-yl)-1,3-dioxoisindolin-4-yl)oxy)undecanoic acid.**



To a solution of benzyl 11-((2-(2,6-dioxopiperidin-3-yl)-1,3-dioxoisindolin-4-yl)oxy)undecanoate (180 mg, 0.27 mmol) in EA (20 mL) was added Pd/C (20 mg, 60% w.t. in mineral oil), and then the mixture was stirred at N<sub>2</sub> atmosphere until reaction completed. The mixture was then filtered, and the filtrate was collected, concentrated in vacuo to obtain product (105 mg, 82%) which was used in the next step without any purification.

LCMS: 459 [M + H]<sup>+</sup>.

**(2S,4R)-1-((2S)-2-(11-((2-(2,6-dioxopiperidin-3-yl)-1,3-dioxoisindolin-4-yl)oxy)undecanamido)-3,3-dimethylbutanoyl)-4-hydroxy-N-(4-(4-methylthiazol-5-yl)benzyl)pyrrolidine-2-carboxamide (ZXH-4-130).**

To a solution of 11-((2-(2,6-dioxopiperidin-3-yl)-1,3-dioxoisindolin-4-yl)oxy)undecanoic acid (7 mg, 0.016 mmol) and (4R)-3-methyl-L-valyl-4-hydroxy-N-[[4-(4-methyl-5-thiazolyl)phenyl]methyl]-L-prolinamide (7 mg, 0.016 mmol) in DMSO (1 mL) were added HATU (7 mg, 0.019 mmol) and DIEA (8 uL, 0.048 mmol). The mixture was stirred at room temperature for 1 h, and then purified by HPLC (MeOH/water, 0.035% TFA) to obtain product (1 mg, 6%) as TFA salt.

LCMS: 871 [M + H]<sup>+</sup>.

**(2S,4R)-1-((2S)-2-(2-((2-(2,6-dioxopiperidin-3-yl)-1,3-dioxoisindolin-4-yl)oxy)acetamido)-3,3-dimethylbutanoyl)-4-hydroxy-N-(4-(4-methylthiazol-5-yl)benzyl)pyrrolidine-2-carboxamide (ZXH-4-132).**

**ZXH-4-132** (2.7 mg, 19%) was obtained according the synthetic route of **ZXH-4-130**, changing from benzyl 11-bromoundecanoate to benzyl 2-bromoacetate.

LCMS: 745 [M + H]<sup>+</sup>.

$^1\text{H}$  NMR (500 MHz,  $\text{DMSO-}d_6$ )  $\delta$  11.10 (s, 1H), 8.99 (s, 1H), 8.59 (d,  $J = 5.1$  Hz, 1H), 8.01 (dd,  $J = 9.3, 3.6$  Hz, 1H), 7.82 (t,  $J = 7.9$  Hz, 1H), 7.49 (d,  $J = 7.2$  Hz, 1H), 7.45 (d,  $J = 8.6$  Hz, 1H), 7.41 (d,  $J = 2.9$  Hz, 3H), 5.11 (dd,  $J = 13.4, 5.3$  Hz, 2H), 4.95 (dd,  $J = 14.9, 2.8$  Hz, 1H), 4.87 (dd,  $J = 14.8, 2.2$  Hz, 1H), 4.60 (dd,  $J = 9.5, 3.5$  Hz, 1H), 4.45 (dt,  $J = 8.2, 4.2$  Hz, 1H), 4.36 (d,  $J = 5.5$  Hz, 2H), 4.29 (ddd,  $J = 15.7, 5.9, 2.9$  Hz, 1H), 3.74 – 3.58 (m, 2H), 2.97 – 2.79 (m, 1H), 2.45 (s, 3H), 2.05 (dd,  $J = 12.1, 5.6$  Hz, 2H), 1.91 (ddd,  $J = 12.9, 9.3, 4.5$  Hz, 1H), 1.00 (s, 7H).

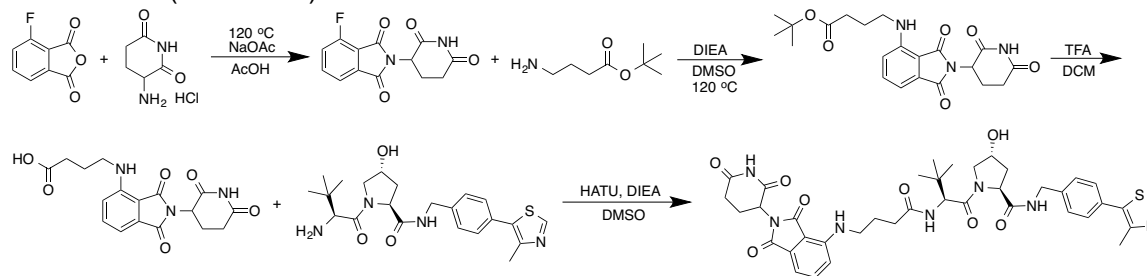
***(2S,4R)-1-((2S)-2-(11-((2-(2,6-dioxopiperidin-3-yl)-1,3-dioxoisindolin-4-yl)oxy)undecanamido)-3,3-dimethylbutanoyl)-4-hydroxy-N-((S)-1-(4-(4-methylthiazol-5-yl)phenyl)ethyl)pyrrolidine-2-carboxamide (ZXH-4-137).***

**ZXH-4-137** (14.2 mg, 65%) was obtained according to the synthetic route of **ZXH-4-130**, changing from (4R)-3-methyl-L-valyl-4-hydroxy-N-[[4-(4-methyl-5-thiazolyl)phenyl]methyl]-L-prolinamide to (2S,4R)-1-((S)-2-amino-3,3-dimethylbutanoyl)-4-hydroxy-N-((S)-1-(4-(4-methylthiazol-5-yl)phenyl)ethyl)pyrrolidine-2-carboxamide dihydrochloride (E3 ligase ligand 1).

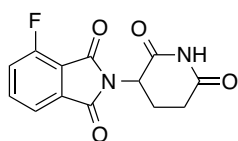
LCMS: 885  $[\text{M} + \text{H}]^+$ .

$^1\text{H}$  NMR (500 MHz,  $\text{DMSO-}d_6$ )  $\delta$  11.10 (s, 1H), 9.00 (s, 1H), 8.37 (d,  $J = 7.8$  Hz, 1H), 7.86 – 7.76 (m, 2H), 7.52 (d,  $J = 8.6$  Hz, 1H), 7.46 – 7.41 (m, 3H), 7.39 (d,  $J = 8.1$  Hz, 2H), 5.09 (dd,  $J = 12.8, 5.4$  Hz, 1H), 4.92 (p,  $J = 7.2$  Hz, 1H), 4.52 (d,  $J = 9.3$  Hz, 1H), 4.43 (t,  $J = 8.0$  Hz, 1H), 4.28 (t,  $J = 3.6$  Hz, 1H), 4.21 (t,  $J = 6.4$  Hz, 2H), 3.67 – 3.55 (m, 2H), 2.89 (ddd,  $J = 16.9, 13.8, 5.4$  Hz, 1H), 2.61 (d,  $J = 3.4$  Hz, 2H), 2.46 (s, 3H), 2.26 (dd,  $J = 14.4, 7.5$  Hz, 1H), 2.17 – 2.09 (m, 1H), 2.08 – 1.98 (m, 2H), 1.76 (p,  $J = 6.8, 6.1$  Hz, 2H), 1.47 – 1.23 (m, 15H), 0.94 (s, 9H).

**Scheme 5.12.** Synthesis of (2S,4R)-1-((2S)-2-(4-((2-(2,6-dioxopiperidin-3-yl)-1,3-dioxoisindolin-4-yl)amino)butanamido)-3,3-dimethylbutanoyl)-4-hydroxy-N-(4-(4-methylthiazol-5-yl)benzyl)pyrrolidine-2-carboxamide (**ZXH-4-133**)

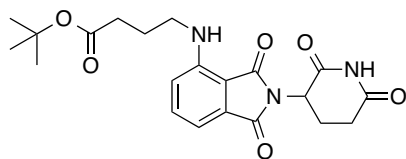


### 2-(2,6-dioxopiperidin-3-yl)-4-fluoroisindoline-1,3-dione



To a solution of 4-fluoroisobenzofuran-1,3-dione (1660 mg, 10 mmol) and 3-aminopiperidine-2,6-dione hydrochloride (1650 mg, 10 mmol) in acetic acid (30 mL) was added NaOAc (984 mg, 12 mmol), then the mixture solution was stirred at 120 °C for 12 hrs. After completed, the mixture was cooled down to room temperature, filtered, and the solid was washed with some water and hexane, and then air dried for overnight to obtain crude product (1.68 g, 50%) as gray powder. LCMS: 277 [M + H]<sup>+</sup>.

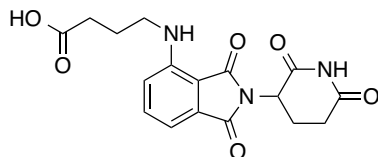
### tert-butyl 4-((2-(2,6-dioxopiperidin-3-yl)-1,3-dioxoisindolin-4-yl)amino)butanoate



To a solution of 2-(2,6-dioxopiperidin-3-yl)-4-fluoroisindoline-1,3-dione (55 mg, 0.2 mmol) and tert-butyl 4-aminobutanoate (32 mg, 0.2 mmol) in DMSO (2 mL) was added DIEA (66  $\mu$ L, 0.4 mmol). The mixture was stirred at 120 °C for 1 h, and then purified by HPLC (MeOH/water, 0.035% TFA) to obtain product as TFA salt, which was used in the next step directly.

LCMS: 416 [M + H]<sup>+</sup>.

**4-((2-(2,6-dioxopiperidin-3-yl)-1,3-dioxoisindolin-4-yl)amino)butanoic acid**



To a solution of *tert*-butyl 4-((2-(2,6-dioxopiperidin-3-yl)-1,3-dioxoisindolin-4-yl)amino)butanoate (0.2 mmol) in DCM (3 mL) was added TFA (1 mL), and then stirred at room temperature for 1 h, then concentrated in *vacuo* to obtain product (34 mg, 36%) as TFA salt, which was used in the next step without any purification.

LCMS: 360 [M + H]<sup>+</sup>.

**(2S,4R)-1-((2S)-2-(4-((2-(2,6-dioxopiperidin-3-yl)-1,3-dioxoisindolin-4-yl)amino)butanamido)-3,3-dimethylbutanoyl)-4-hydroxy-N-(4-(4-methylthiazol-5-yl)benzyl)pyrrolidine-2-carboxamide (ZXH-4-133)**

To a solution of 4-((2-(2,6-dioxopiperidin-3-yl)-1,3-dioxoisindolin-4-yl)amino)butanoic acid (8 mg, 0.016 mmol) and (4R)-3-methyl-L-valyl-4-hydroxy-N-[[4-(4-methyl-5-thiazolyl)phenyl]methyl]-L-prolinamide (7 mg, 0.016 mmol) in DMSO (1 mL) were added HATU (7 mg, 0.019 mmol) and DIEA (8  $\mu$ L, 0.048 mmol). The mixture was stirred at room temperature for 1 h, and then purified by HPLC (MeOH/water, 0.035% TFA) to obtain product (3 mg, 21%) as TFA salt.

LCMS: 772 [M + H]<sup>+</sup>.

<sup>1</sup>H NMR (500 MHz, DMSO-*d*<sub>6</sub>)  $\delta$  11.09 (s, 1H), 9.00 (s, 1H), 8.56 (t, *J* = 6.1 Hz, 1H), 7.99 (d, *J* = 9.3 Hz, 1H), 7.59 (dd, *J* = 8.6, 7.1 Hz, 1H), 7.43 (d, *J* = 8.1 Hz, 2H), 7.39 (d, *J* = 8.3 Hz, 2H), 7.11 (d, *J* = 8.6 Hz, 1H), 7.02 (d, *J* = 7.0 Hz, 1H), 6.64 (s, 1H), 5.06 (dd, *J* = 12.7, 5.5 Hz, 1H), 4.57 (d, *J* = 9.4 Hz, 1H), 4.47 – 4.34 (m, 4H), 4.22 (dd, *J* = 15.9, 5.5 Hz, 1H), 3.68 (d, *J* = 3.5 Hz, 2H), 2.89 (ddd, *J* = 16.9, 13.7, 5.4 Hz, 1H), 2.66 – 2.57 (m, 1H), 2.45 (s, 3H), 2.36 (dd, *J* = 14.6, 7.2 Hz,

1H), 2.26 (dt,  $J = 14.4, 7.1$  Hz, 1H), 2.08 – 1.99 (m, 2H), 1.91 (ddd,  $J = 12.9, 8.6, 4.6$  Hz, 1H), 1.79 (dq,  $J = 17.9, 6.8$  Hz, 2H), 0.95 (s, 9H).

**(2S,4R)-1-((17S)-17-(tert-butyl)-1-((2-(2,6-dioxopiperidin-3-yl)-1,3-dioxoisindolin-4-yl)amino)-15-oxo-3,6,9,12-tetraoxa-16-azaoctadecan-18-oyl)-4-hydroxy-N-(4-(4-methylthiazol-5-yl)benzyl)pyrrolidine-2-carboxamide (ZXH-4-135)**

**ZXH-4-135** (1 mg, 6%) was obtained according to the synthetic route of **ZXH-4-133**, changing from *tert*-butyl 4-aminobutanoate to 3,6,9,12-Tetraoxapentadecan-15-oic acid.

LCMS: 934 [M + H]<sup>+</sup>.

**(2S,4R)-1-((2S)-2-(4-((2-(2,6-dioxopiperidin-3-yl)-1,3-dioxoisindolin-4-yl)amino)butanamido)-3,3-dimethylbutanoyl)-4-hydroxy-N-((S)-1-(4-(4-methylthiazol-5-yl)phenyl)ethyl)pyrrolidine-2-carboxamide (ZXH-4-136)**

**ZXH-4-136** (20.2 mg, 61%) was obtained according to the synthetic route of **ZXH-4-133**, changing from (4R)-3-methyl-L-valyl-4-hydroxy-N-[[4-(4-methyl-5-thiazolyl)phenyl]methyl]-L-prolinamide to (2S,4R)-1-((S)-2-amino-3,3-dimethylbutanoyl)-4-hydroxy-N-((S)-1-(4-(4-methylthiazol-5-yl)phenyl)ethyl)pyrrolidine-2-carboxamide dihydrochloride (E3 ligase ligand 1).

LCMS: 786 [M + H]<sup>+</sup>.

<sup>1</sup>H NMR (500 MHz, DMSO-*d*<sub>6</sub>)  $\delta$  11.10 (s, 1H), 9.00 (s, 1H), 8.37 (d,  $J = 7.8$  Hz, 1H), 7.94 (d,  $J = 9.2$  Hz, 1H), 7.59 (dd,  $J = 8.6, 7.1$  Hz, 1H), 7.44 (d,  $J = 8.1$  Hz, 2H), 7.39 (d,  $J = 8.0$  Hz, 2H), 7.11 (d,  $J = 8.7$  Hz, 1H), 7.03 (d,  $J = 7.0$  Hz, 1H), 6.65 (s, 1H), 5.06 (dd,  $J = 12.7, 5.4$  Hz, 1H), 4.92 (p,  $J = 7.1$  Hz, 1H), 4.55 (d,  $J = 9.3$  Hz, 1H), 4.43 (t,  $J = 8.0$  Hz, 1H), 4.29 (t,  $J = 3.8$  Hz, 1H), 3.63 (d,  $J = 3.2$  Hz, 2H), 2.89 (ddd,  $J = 16.7, 13.7, 5.4$  Hz, 1H), 2.65 – 2.57 (m, 2H), 2.46 (s, 3H), 2.34 (dt,  $J = 14.7, 7.4$  Hz, 1H), 2.25 (dt,  $J = 14.6, 7.2$  Hz, 1H), 2.03 (dtd,  $J = 12.9, 7.9, 7.1, 3.5$  Hz, 2H), 1.85 – 1.72 (m, 3H), 0.95 (s, 9H).

**Cell Culture.** MM1.S cells were generously provided by James Bradner (DFCI, Boston, MA). MM1.S cells were cultured in RPMI-1640 media containing L-glutamine, supplemented with 10% fetal bovine serum (FBS) and 1% penicillin/streptomycin. Mycoplasma testing was performed on a monthly basis and all lines were negative.

**Cell Viability Assays.** Cell viability was evaluated using the CellTiter-Glo Luminescent Cell Viability Assay (Promega) following the manufacturer's standards.

**Immunoblotting.** Cells were washed with PBS before being lysed with Cell Lysis Buffer (Cell Signaling) supplemented with protease and phosphatase inhibitor cocktails (Roche) at 4°C for 15 minutes. The cell lysate vortexed before being centrifuged at 14,000 x g for 20 min at 4°C. Protein in cell lysate was quantified by BCA assay (Pierce). Primary antibodies used in this study include  $\beta$ -actin (Cell Signaling Technology, 3700S), CK1 $\alpha$  (Abcam, ab206652), CRBN (Novus Biologicals, NBP1-91810), CUL4A (Cell Signaling Technology, 2699S), DDB1 (Cell Signaling Technology, 5428S), eRF3/GSPT1 (Abcam, ab49878), IKZF1 (Ikaros) (Cell Signaling Technology, 5443S), IKZF3 (Aiolos) (Cell Signaling Technology, 15103S), RBX1 (ROC1) (Cell Signaling Technology, 11922S), and vinculin (Abcam, ab130007). Blot quantification was performed using Image Studio 4.0 software, normalizing to loading controls.

**Sample preparation TMT LC-MS3 mass spectrometry.** MM1.s cells were treated with DMSO, 10 nM **ZXH-3-159**, or 1  $\mu$ M of pomalidomide in biological singlicate, or DMSO, 50 nM of **ZXH-4-130** or 50 nM of **ZXH-4-137** in biological triplicate for 6 hours. Cells were harvested by centrifugation. Lysis buffer (8 M Urea, 50 mM NaCl, 50 mM 4-(2-hydroxyethyl)-1-piperazineethanesulfonic acid (EPPS) pH 8.5, Protease and Phosphatase inhibitors from Roche) was added to the cell pellets and homogenized by 20 passes through a 21 gauge (1.25 in. long) needle to achieve a cell lysate with a protein concentration between 1 – 4 mg mL<sup>-1</sup>. A micro-BCA assay (Pierce) was used to determine the final protein concentration of protein in the cell lysate. 200  $\mu$ g of protein for each sample were reduced and alkylated as previously described.<sup>19</sup>

Proteins were precipitated using methanol/chloroform. In brief, four volumes of methanol were added to the cell lysate, followed by one volume of chloroform, and finally three volumes of water. The mixture was vortexed and centrifuged to separate the chloroform phase from the aqueous phase. The precipitated protein was washed with one volume of methanol, centrifuged and the resulting washed precipitated protein was allowed to air dry. Precipitated protein was resuspended in 4 M Urea, 50 mM HEPES pH 7.4, followed by dilution to 1 M urea with the addition of 200 mM EPPS, pH 8. Proteins were first digested with LysC (1:50; enzyme:protein) for 12 hours at room temperature. The LysC digestion was diluted down to 0.5 M Urea with 200 mM EPPS pH 8 and then digested with trypsin (1:50; enzyme:protein) for 6 hours at 37 °C. Tandem mass tag (TMT) reagents (Thermo Fisher Scientific) were dissolved in anhydrous acetonitrile (ACN) according to manufacturer's instructions. Anhydrous ACN was added to each peptide sample to a final concentration of 30% v/v, and labeling was induced with the addition of TMT reagent to each sample at a ratio of 1:4 peptide:TMT label. The 10-plex labeling reactions were performed for 1.5 hours at RT and the reaction quenched by the addition of hydroxylamine to a final concentration of 0.3% for 15 minutes at RT. The sample channels were combined at a 1:1:1:1:1:1:1:1:1:1 ratio, desalted using C18 solid phase extraction cartridges (Waters) and analyzed by LC-MS for channel ratio comparison. Samples were then combined using the adjusted volumes determined in the channel ratio analysis and dried down in a speed vacuum. The combined sample was then resuspended in 1% formic acid, and acidified (pH 2–3) before being subjected to desalting with C18 SPE (Sep-Pak, Waters). Samples were then offline fractionated into 96 fractions by high pH reverse-phase HPLC (Agilent LC1260) through an aeris peptide xb-c18 column (phenomenex) with mobile phase A containing 5% acetonitrile and 10 mM NH<sub>4</sub>HCO<sub>3</sub> in LC-MS grade H<sub>2</sub>O, and mobile phase B containing 90% acetonitrile and 10 mM NH<sub>4</sub>HCO<sub>3</sub> in LC-MS grade H<sub>2</sub>O (both pH 8.0). The 96 resulting fractions were then pooled in a non-continuous manner into 24 fractions and these fractions were used for subsequent mass spectrometry analysis.

Data were collected using an Orbitrap Fusion Lumos mass spectrometer (Thermo Fisher Scientific, San Jose, CA, USA) coupled with a Proxeon EASY-nLC 1200 LC pump (Thermo Fisher Scientific). Peptides were separated on a 75  $\mu$ M inner diameter microcapillary column packed with ~50 cm of Accucore C18 resin (1.8  $\mu$ M, 100 Å, Thermo Fisher Scientific). Peptides were separated using a 180 min gradient of 6–27% acetonitrile in 1.0% formic acid with a flow rate of 350 nL/min.

Each analysis used an MS3-based TMT method as described previously<sup>22</sup>. The data were acquired using a mass range of  $m/z$  250-1400, resolution 120,000, AGC target  $5 \times 10^6$ , maximum injection time 100 ms, dynamic exclusion of 90 seconds for the peptide measurements in the Orbitrap. Data dependent MS2 spectra were acquired in the ion trap with a normalized collision energy (NCE) set at 35%, AGC target set to  $2 \times 10^4$  and a maximum injection time of 150ms. MS3 scans were acquired in the Orbitrap with a HCD collision energy set to 65%, AGC target set to  $1.0 \times 10^5$ , maximum injection time of 200ms, resolution at 50,000 and with a maximum synchronous precursor selection (SPS) precursors set to 10.

**LC-MS data analysis.** Proteome Discoverer 2.2 (Thermo Fisher Scientific) was used for .RAW file processing and controlling peptide and protein level false discovery rates, assembling proteins from peptides, and protein quantification from peptides. MS/MS spectra were searched against a Uniprot human database (September 2016) with both the forward and reverse sequences. Database search criteria are as follows: tryptic with two missed cleavages, a precursor mass tolerance of 20 ppm, fragment ion mass tolerance of 0.6 Da, static alkylation of cysteine (57.02146 Da), static TMT labelling of lysine residues and N-termini of peptides (229.16293 Da), and variable oxidation of methionine (15.99491 Da). TMT reporter ion intensities were measured using a 0.003 Da window around the theoretical  $m/z$  for each reporter ion in the MS3 scan. Peptide spectral matches with poor quality MS3 spectra were excluded from quantitation (summed signal-to-noise across 10 channels  $< 200$  and precursor isolation specificity  $< 0.5$ ), and resulting data was filtered to only include proteins that had a minimum of 3 unique

peptides identified. Reporter ion intensities were normalised and scaled using in-house scripts in the R framework.<sup>23</sup> Statistical analysis was carried out using the limma package within the R framework.<sup>24</sup>

### **Author Contributions**

C.E.P conducted the experiments and analyzed the data. J.B. ran and analyzed expression proteomics. G.D. and Z.H. designed and synthesized compounds. T.Z., E.S.F., and N.S.G advised on project directions. C.E.P. wrote the paper.

### **Funding Sources**

Funding for this work was received from the National Institutes of Health (NIH): Grant R01 CA214608 (E.S.F.) and 5 F31 CA210619-02 (C.E.P.).

### **Notes**

The authors declare no competing financial interest.

## References

- (1) Ito, T.; Ando, H.; Suzuki, T.; Ogura, T.; Hotta, K.; Imamura, Y.; Yamaguchi, Y.; Handa, H. Identification of a Primary Target of Thalidomide Teratogenicity. *Science* **2010**, *327* (5971), 1345–1350. <https://doi.org/10.1126/science.1177319> .
- (2) Kronke, J.; Udeshi, N.; Narla, A.; Grauman, P.; Hurst, S.; McConkey, M.; Svinkina, T.; Heckl, D.; Comer, E.; Li, X.; et al. Lenalidomide Causes Selective Degradation of IKZF1 and IKZF3 in Multiple Myeloma Cells. *Science* **2014**, *343* (6168), 301–305. <https://doi.org/10.1126/science.1244851> .
- (3) Lu, G.; Middleton, R. E.; Sun, H.; Naniong, M.; Ott, C. J.; Mtsiades, C. S.; Wong, K.-K.; Bradner, J. E.; Jr., W. G. The Myeloma Drug Lenalidomide Promotes the Cereblon-Dependent Destruction of Ikaros Proteins. *Science* **2014**, *343* (6168), 305–309. <https://doi.org/10.1126/science.1244917> .
- (4) Winter, G.; Buckley, D.; Paulk, J.; Roberts, J.; Souza, A.; Dhe-Paganon, S.; Bradner, J. Phthalimide Conjugation as a Strategy for in Vivo Target Protein Degradation. *Science* **2015**, *348* (6241), 1376–1381. <https://doi.org/10.1126/science.aab1433> .
- (5) Zengerle, M.; Chan, K.-H.; Ciulli, A. Selective Small Molecule Induced Degradation of the BET Bromodomain Protein BRD4. *Acs Chem Biol* **2015**, *10* (8), 1770–1777. <https://doi.org/10.1021/acscchembio.5b00216> .
- (6) Bondeson, D. P.; Mares, A.; Smith, I. E.; Ko, E.; Campos, S.; Miah, A. H.; Mulholland, K. E.; Routly, N.; Buckley, D. L.; Gustafson, J. L.; et al. Catalytic in Vivo Protein Knockdown by Small-Molecule PROTACs. *Nat Chem Biol* **2015**, *11* (8), 611–617. <https://doi.org/10.1038/nchembio.1858> .
- (7) Lai, A. C.; Toure, M.; Hellerschmied, D.; Salami, J.; Jaime-Figueroa, S.; Ko, E.; Hines, J.; Crews, C. M. Modular PROTAC Design for the Degradation of Oncogenic BCR-ABL. *Angew Chem-ger Edit* **2015**, *128* (2), 818–821. <https://doi.org/10.1002/ange.201507634> .
- (8) Olson, C. M.; Jiang, B.; Erb, M. A.; Liang, Y.; Ctor, Z.; Zhang, Z.; Zhang, T.; Kwiatkowski, N.; Boukhali, M.; Green, J. L.; et al. Pharmacological Perturbation of CDK9 Using Selective CDK9 Inhibition or Degradation. *Nat Chem Biol* **2018**, *14* (2), 163–170. <https://doi.org/10.1038/nchembio.2538> .
- (9) Huang, H.-T.; Dobrovolsky, D.; Paulk, J.; Yang, G.; Weisberg, E. L.; Ctor, Z.; Buckley, D. L.; Cho, J.-H.; Ko, E.; Jang, J.; et al. A Chemoproteomic Approach to Query the Degradable Kinome Using a Multi-Kinase Degradator. *Cell Chem Biol* **2017**, *25* (1), 1–19. <https://doi.org/10.1016/j.chembiol.2017.10.005> .
- (10) Powell, C. E.; Gao, Y.; Tan, L.; Donovan, K. A.; Nowak, R. P.; Loehr, A.; Bahcall, M.; Fischer, E. S.; Jänne, P. A.; George, R. E.; et al. Chemically Induced Degradation of Anaplastic Lymphoma Kinase (ALK). *J Med Chem* **2018**, *61* (9), 4249–4255. <https://doi.org/10.1021/acscjmedchem.7b01655> .
- (11) Kang, C.; Lee, D.; Lee, C.; Ha, J.; Park, C.; Hwang, J. Induced Protein Degradation of Anaplastic Lymphoma Kinase (ALK) by Proteolysis Targeting Chimera (PROTAC). *Biochem Bioph Res Co* **2018**, *505* (2), 1–6. <https://doi.org/10.1016/j.bbrc.2018.09.169> .

- (12) Nguyen, T.; Lee, E. J.; Sweredoski, M. J.; Yang, S.-J.; Jeon, S.-J.; Harrison, J. S.; Yim, J.-H.; Lee, S.; Handa, H.; Kuhlman, B.; et al. Glutamine Triggers Acetylation-Dependent Degradation of Glutamine Synthetase via the Thalidomide Receptor Cereblon. *Mol Cell* **2016**, *61* (6), 809–820. <https://doi.org/10.1016/j.molcel.2016.02.032> .
- (13) Zhou, L.; Xu, G. Cereblon Attenuates DNA Damage-Induced Apoptosis by Regulating the Transcription-Independent Function of P53. *Cell Death Dis* **2019**, *10* (2), 1–13. <https://doi.org/10.1038/s41419-019-1317-7> .
- (14) Girardini, M.; Maniaci, C.; Hughes, S. J.; Testa, A.; Ciulli, A. Cereblon versus VHL: Hijacking E3 Ligases Against Each Other Using PROTACs. *Bioorganic & Medicinal Chemistry* **2019**, *27*, 2466–2479. <https://doi.org/10.26434/chemrxiv.7698185.v2> .
- (15) Steinebach, C.; Kehm, H.; Lindner, S.; Vu, L.; Köpff, S.; Mármol, Á.; Weiler, C.; Wagner, K. G.; Reichenzeller, M.; Krönke, J.; et al. PROTAC-Mediated Crosstalk between E3 Ligases. *Chem Commun* **2019**, *55* (12), 1821–1824. <https://doi.org/10.1039/c8cc09541h> .
- (16) Steinebach, C.; Lindner, S.; Udeshi, N. D.; Mani, D. C.; Kehm, H.; Köpff, S.; Carr, S. A.; Gütschow, M.; Krönke, J. Homo-PROTACs for the Chemical Knockdown of Cereblon. *ACS Chem Biol* **2018**, *13* (9), 2771–2782. <https://doi.org/10.1021/acscchembio.8b00693> .
- (17) Churcher, I. Protac-Induced Protein Degradation in Drug Discovery: Breaking the Rules or Just Making New Ones? *J Med Chem* **2017**, *61* (2), 444–452. <https://doi.org/10.1021/acs.jmedchem.7b01272> .
- (18) An, S.; Fu, L. Small-Molecule PROTACs: An Emerging and Promising Approach for the Development of Targeted Therapy Drugs. *Ebiomedicine* **2018**, *36* (Integr Cancer Sci Ther 1 2014), 553–562. <https://doi.org/10.1016/j.ebiom.2018.09.005> .
- (19) Donovan, K. A.; An, J.; Nowak, R. P.; Yuan, J. C.; Fink, E. C.; Berry, B. C.; Ebert, B. L.; Fischer, E. S. Thalidomide Promotes Degradation of SALL4, a Transcription Factor Implicated in Duane Radial Ray Syndrome. *Elife* **2018**, *7*, e38430. <https://doi.org/10.7554/elife.38430> .
- (20) Matyskiela, M. E.; Ito, T.; Pagarigan, B.; Lu, C.-C.; Miller, K.; Fang, W.; Wang, N.-Y.; Nguyen, D.; Houston, J.; Carmel, G.; et al. A Novel Cereblon Modulator Recruits GSPT1 to the CRL4CRBN Ubiquitin Ligase. *Nature* **2016**, *535* (7611), 252–257. <https://doi.org/10.1038/nature18611> .
- (21) Maniaci, C.; Hughes, S. J.; Testa, A.; Chen, W.; Lamont, D. J.; Rocha, S.; Alessi, D. R.; Romeo, R.; Ciulli, A. Homo-PROTACs: Bivalent Small-Molecule Dimerizers of the VHL E3 Ubiquitin Ligase to Induce Self-Degradation. *Nat Commun* **2017**, *8* (1), 830. <https://doi.org/10.1038/s41467-017-00954-1> .
- (22) McAlister, G. C.; Nusinow, D. P.; Jedrychowski, M. P.; Wühr, M.; Huttlin, E. L.; Erickson, B. K.; Rad, R.; Haas, W.; Gygi, S. P. MultiNotch MS3 Enables Accurate, Sensitive, and Multiplexed Detection of Differential Expression across Cancer Cell Line Proteomes. *Anal Chem* **2014**, *86* (14), 7150–7158. <https://doi.org/10.1021/ac502040v> .
- (23) Team, C. R. R. A Language and Environment for Statistical Computing. *R Foundation for Statistical Computing* **2014**.

(24) Ritchie, M. E.; Phipson, B.; Wu, D.; Hu, Y.; Law, C. W.; Shi, W.; Smyth, G. K. Limma Powers Differential Expression Analyses for RNA-Sequencing and Microarray Studies. *Nucleic Acids Res* **2015**, *43* (7), e47 e47. <https://doi.org/10.1093/nar/gkv007> .

## **Chapter 6: Novel Macrocyclic Inhibitors of DYRK1A**

## **Attributions**

The work in this chapter is adapted from a manuscript that is being prepared for submission titled “Novel Macrocyclic Inhibitors of DYRK1A” by Powell *et al.* Author contributions and competing interests for this work can be found near the end of the chapter, before the references.

## **Chapter 6: Novel Macrocyclic Inhibitors of DYRK1A.**

Chelsea E. Powell,<sup>#</sup> John M. Hatcher,<sup>#</sup> and Nathanael S. Gray<sup>\*</sup>

Department of Cancer Biology, Dana-Farber Cancer Institute, Boston, Massachusetts 02215, United States

Department of Biological Chemistry & Molecular Pharmacology, Harvard Medical School, Boston, Massachusetts 02115, United States

<sup>#</sup> These authors contributed equally.

<sup>\*</sup> Correspondence: [Nathanael.Gray@dfci.harvard.edu](mailto:Nathanael.Gray@dfci.harvard.edu) (N.S.G.).

## Abstract

Dual-specificity tyrosine-(Y)-phosphorylation regulated kinase 1A (DYRK1A) is a therapeutic target of great interest due to the roles it plays in both neurological diseases and cancer. We present the discovery of the first macrocyclic inhibitors of DYRK1A. The most potent inhibitor from this set, JH-XIV-68-3, displays strong selectivity *in vitro* and *in vivo*. Examination of the potential application of this DYRK1A inhibitor in head and neck squamous cell carcinoma (HNSCC) cell lines demonstrated antitumor efficacy. Overall, JH-XIV-68-3 presents a new scaffold for DYRK1A inhibitors, which may lead to a new avenue for therapeutic development.

## 6.1 Introduction

Dual-specificity tyrosine-(Y)-phosphorylation regulated kinase 1A (DYRK1A) is a member of the dual-specificity tyrosine-(Y)-phosphorylation regulated kinase (DYRK) family. These kinases are defined as having dual specificity due to the fact that they are activated via autophosphorylation of tyrosine residues in the activation loop, but they phosphorylate their substrates on serine and threonine residues.<sup>1</sup> DYRK1A has been a target of therapeutic interest due to its location on chromosome 21 because an extra copy of chromosome 21 is the cause of Down syndrome.<sup>2</sup> DYRK1A has since been shown to play a role in some of the cognitive disabilities associated with Down syndrome. In addition, DYRK1A has been demonstrated to be present at increased levels in neurodegenerative diseases, including Alzheimer's disease, Parkinson's disease, Huntington's disease, and Pick syndrome.<sup>3</sup> It is also overexpressed in tumor cells as well as in diabetes.<sup>4</sup> These many disease links clearly illustrate that overexpression of DYRK1A has adverse effects on human health. This may potentially be addressed through the development of potent and selective DYRK1A inhibitors.

DYRK1A has been shown to be involved in cell proliferation, cell cycle regulation, splicing, signaling pathways, brain growth, neuronal development, neurodegeneration, cancer, and cognitive disabilities.<sup>4</sup> This very broad association of DYRK1A's functions is due in part to the lack of selective DYRK1A inhibitors that may serve as probes for better understanding its physiological roles.

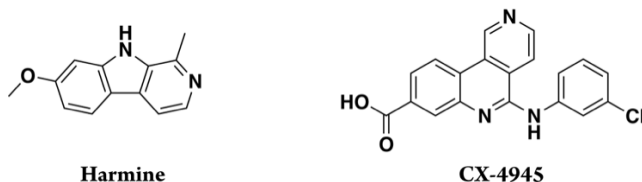


**Figure 6.1.** Structures of harmine and CX-4945.

Two major DYRK1A inhibitors are Harmine and CX-4945 (Figure 6.1). Although Harmine is a potent inhibitor of DYRK1A, it is also a potent inhibitor of monoamine oxidase (MAO)-A. MAO-

A inhibition leads to hallucinogenic and toxic side effects, which significantly limit the therapeutic potential of Harmine.<sup>4</sup> CX-4945 was first developed as a potent and selective inhibitor of protein kinase CK2, and is currently in clinical trials as a CK2 targeting cancer therapeutic.<sup>5</sup> CX-4945 has since been shown to rescue Down syndrome phenotypes through DYRK1A inhibition.<sup>6</sup> Although CX-4945 has potential as a DYRK1A targeting therapeutic, its activity against CK2 makes its use as a probe less clear since CK2 inhibition has such strong antiproliferative effects in cancer cells.

We generated a series of macrocyclic compounds through an exploration of kinase inhibitor scaffolds similar to the approved ALK inhibitor lorlatinib.<sup>7</sup> We are interested in these macrocyclic scaffolds because macrocycles can provide diverse functionality and stereochemical complexity while maintaining a specific conformation, which can lead to high affinity and selectivity for targets.<sup>8</sup> Macrocyclic structures are also associated with improved metabolic stability and blood-brain barrier penetration, a feature that may be of particular use for neurologically relevant targets like DYRK1A.<sup>9</sup>

From these macrocyclic compounds we identified compounds with DYRK1A activity: **JH-XIV-68-3**, **JH-XIV-71**, **JH-XIV-73-1**, and **JH-XIV-73-2**.

## 6.2 Results and Discussion

Based on biochemical kinase profiling (KINOMEscan) of **JH-XIV-68-3** (1  $\mu$ M) we identified DYRK1A as a primary target of this macrocyclic compound (Figure 6.2A). Z'-LYTE kinase activity assays confirmed that **JH-XIV-68-3** and the related compounds **JH-XIV-71**, **JH-XIV-73-1**, and **JH-XIV-73-2** were inhibitors of DYRK1A and DYRK1B, with **JH-XIV-68-3** being the most potent, followed by **JH-XIV-73-2** (Figure 6.2B). CAL27, a head and neck squamous cell carcinoma (HNSCC) cell line, was selected for cellular kinase profiling based on its previously identified DYRK1A-dependence for tumor growth.<sup>10</sup> Cellular kinase profiling (KiNativ) of harmine, CX-4945, and **JH-XIV-68-3** at 1  $\mu$ M showed that **JH-XIV-68-3** to be the most selective of the three compounds, with DYRK1A as the only observed target (Figure 6.3). CX-4945 was also active

against CK2, as expected, and ATR. Harmine was also active against CDK8 and CDK11, which are members of the CMGC group of kinases along with DYRKs.

We further examined the macrocyclic compounds' potentials as antitumor agents in HNSCC cell lines by measuring antiproliferative activity in CAL27 and FaDu cells, another HNSCC cell line shown to be sensitive to DYRK1A inhibition. CX-4945 was the most potent agent in both these cell lines, which may be due to CK2 inhibition as well as DYRK1A (Figure 6.4, Table 6.1). HEK293FT cells were used as a control cell line because they do not endogenously express DYRK1A and both harmine and CX-4945 still showed antiproliferative effects in this cell line, while the macrocyclic compounds did not. **JH-XIV-71** was the second most potent in CAL27 cells followed by **JH-XIV-68-3**, with **JH-XIV-68-3** as the second most potent in FaDu cells followed by **JH-XIV-71** (Table 6.1). **JH-XIV-73-1** and **JH-XIV-73-2** had no antiproliferative effects in any of the cell lines.

Markers of apoptosis were examined by western after 24 hr treatments in CAL27 cells. **JH-XIV-68-3** induced the strongest increase in pro-apoptotic marker cleaved-PARP, while **JH-XIV-73-2** induced the largest decrease in anti-apoptotic protein BCL-xL (Figure 6.5A). Examination of CAL27 colony formation after 10 days of treatment showed that **JH-XIV-68-3** inhibited colony formation to a similar extent as harmine, with **JH-XIV-71** showing slightly less inhibition than harmine and **JH-XIV-68-3** (Figure 6.5B).

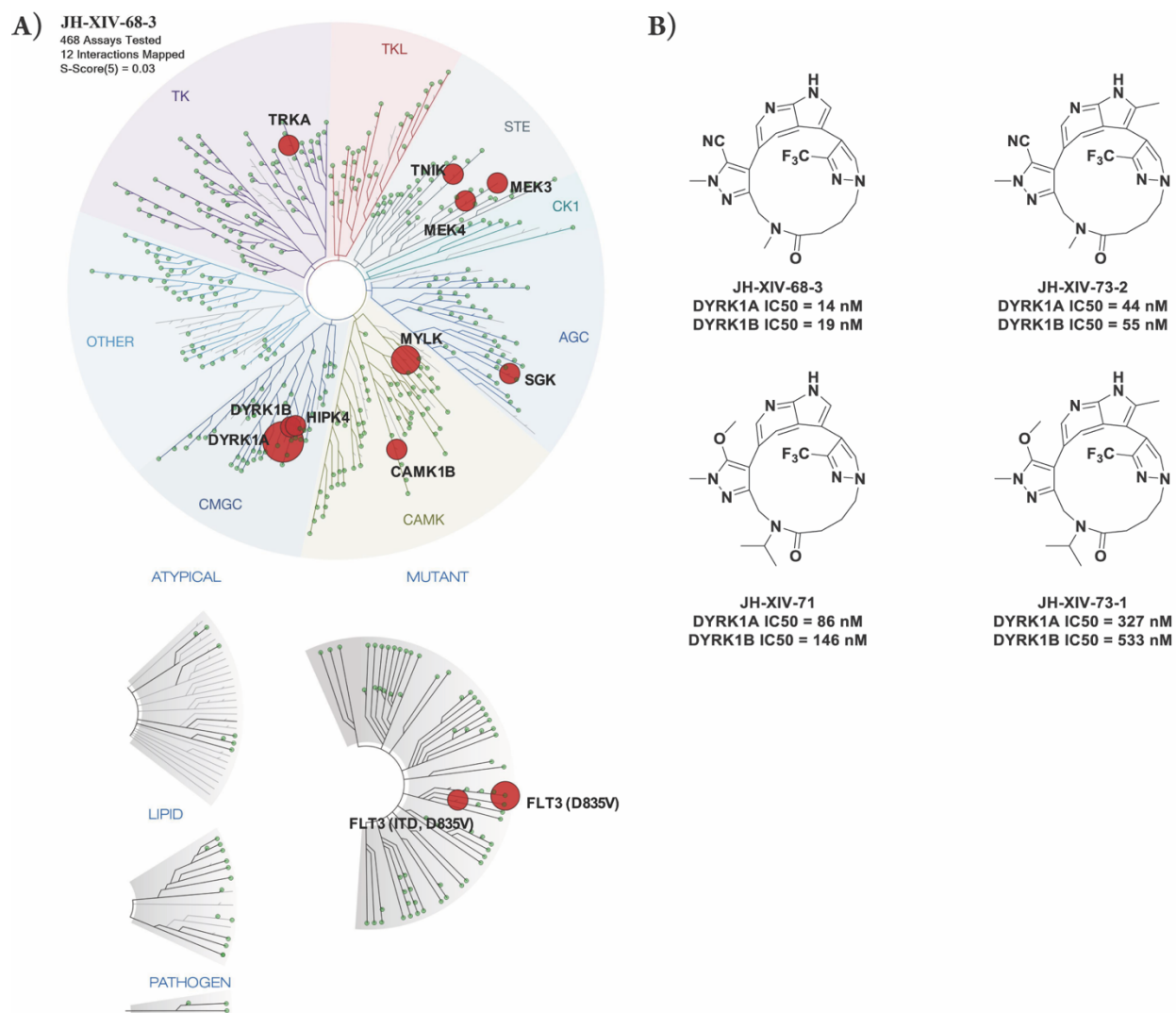


**Figure 6.2.** Biochemical kinase profiling. (A) Biochemical kinase profile of **JH-XIV-68-3** at 1  $\mu$ M (KINOMEscan, 468 kinases). Bound kinases are in red. (B) Biochemical IC<sub>50</sub>s from Z'LYTE activity assay.

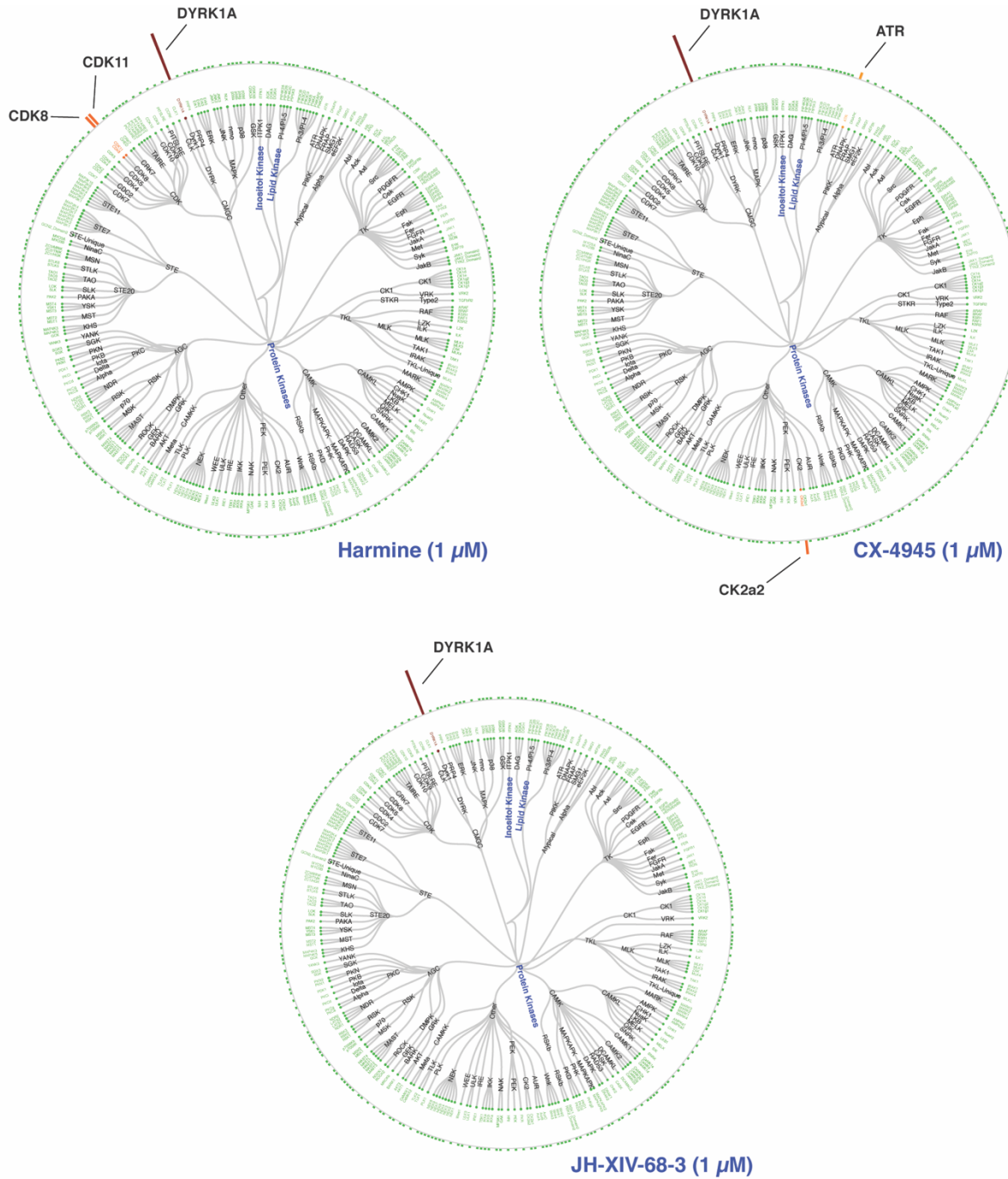


**Figure 6.3.** Cellular kinase profiling. KiNativ profiles of harmine, CX-4945, and **JH-XIV-68-3** at 1 μM after 6-hour treatment in CAL27 cells.

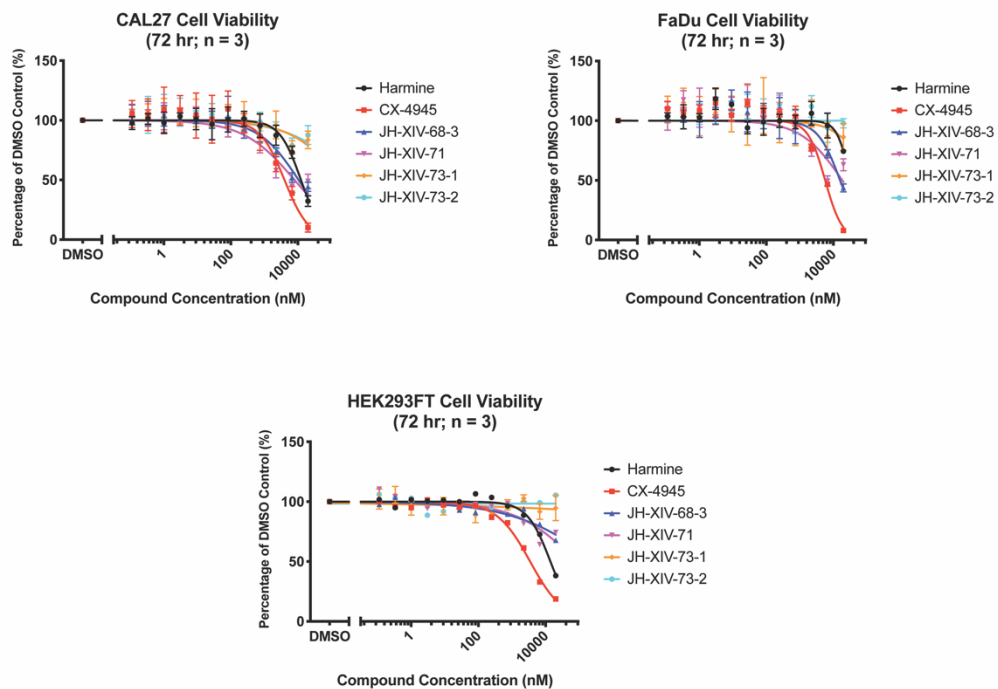
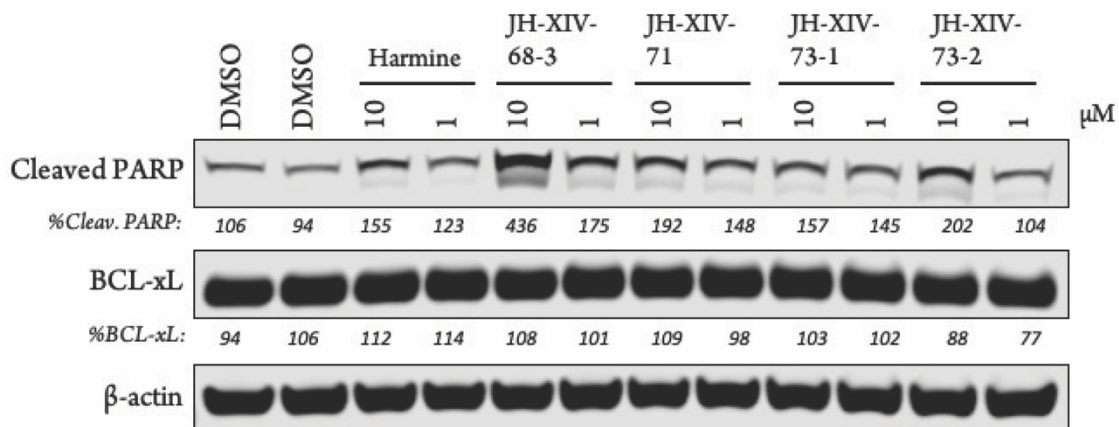


**Figure 6.4.** Antiproliferative activity in HNSCC cell lines after 72 hr treatments (three biological replicates; Graphpad Prism 7 software).

**Table 6.1.** Antiproliferative IC<sub>50</sub> values (μM) after 72 hr treatments (three biological replicates; Graphpad Prism 7 software).

	Harmine	CX-4945	JH-XIV-68-3	JH-XIV-71	JH-XIV-73-1	JH-XIV-73-2
<b>CAL27</b>	12.3	4.0	10.4	7.9	NA	NA
<b>FaDu</b>	32.2	5.7	15.9	18.5	NA	NA
<b>HEK293FT</b>	13.8	3.5	NA	NA	NA	NA

A)



B)

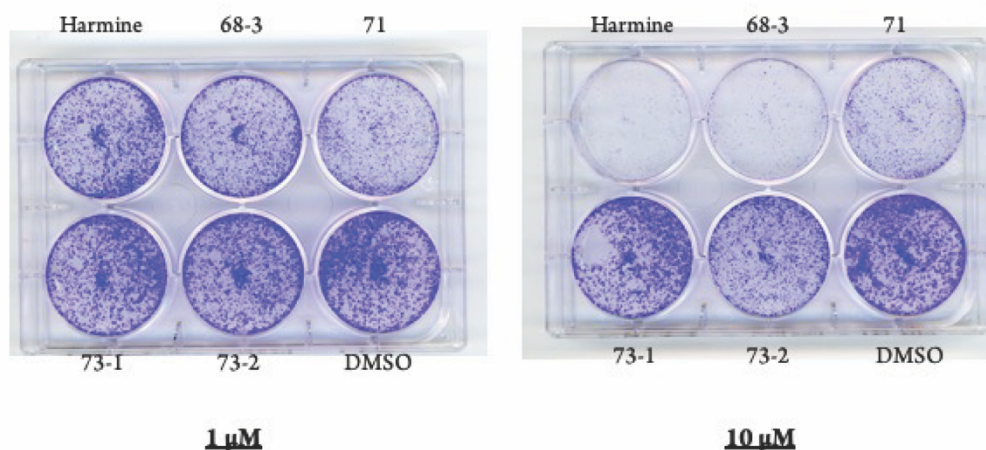


**Figure 6.5.** Apoptosis and colony formation in CAL27 cells. (A) Immunoblot after 24-hour treatment. Quantification normalized to  $\beta$ -actin and displayed as percentage of average DMSO. (B) Crystal violet staining after 10-day treatment. **JH-XIV-68-3** (68-3), **JH-XIV-71** (71), **JH-XIV-73-1** (73-1), and **JH-XIV-73-2** (73-2).

### 6.3 Conclusion

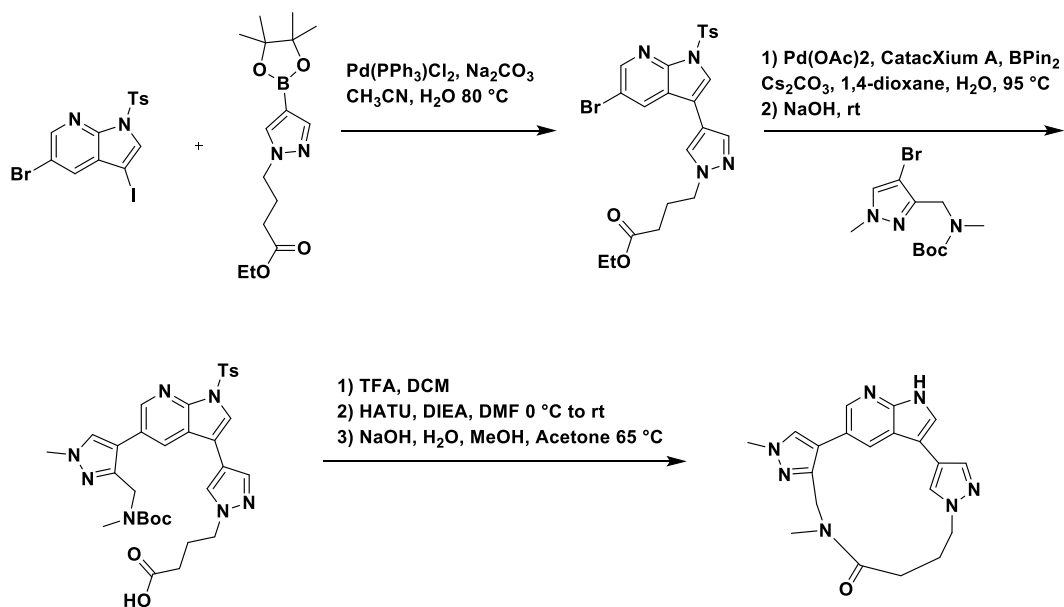
Biochemical and cellular kinase profiling of **JH-XIV-68-3** shows that it is a potent and selective inhibitor of DYRK1A, with a selectivity profile that is higher than two of the lead DYRK1A probe compounds in the literature. Examining if the macrocyclic compounds could induce DYRK1A inhibitor mediated antitumor effects in HNSCC cells similar to those seen in the literature demonstrated that **JH-XIV-68-3** behaves similar or better than harmine in terms of antiproliferative effects, increases in apoptosis, and decreases in colony formation. Together this indicates that

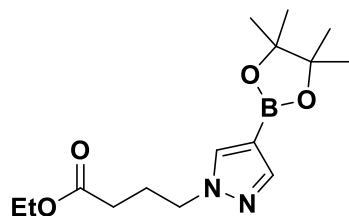
**JH-XIV-68-3** is a promising probe compound for better understanding DYRK1A physiological functions and a new scaffold for potential therapeutic development targeting DYRK1A.

## 6.4 Experimental Methods

Unless otherwise noted, reagents and solvents were obtained from commercial suppliers and were used without further purification.  $^1\text{H}$  NMR spectra were recorded on 500 MHz (Bruker A500), and chemical shifts are reported in parts per million (ppm,  $\delta$ ) downfield from tetramethylsilane (TMS). Coupling constants ( $J$ ) are reported in Hz. Spin multiplicities are described as s (singlet), br (broad singlet), d (doublet), t (triplet), q (quartet), and m (multiplet). Mass spectra were obtained on a Waters Micromass ZQ instrument. Preparative HPLC was performed on a Waters Sunfire C18 column (19 x 50 mm, 5 $\mu\text{M}$ ) using a gradient of 15-95% methanol in water containing 0.05% trifluoroacetic acid (TFA) over 22 min (28 min run time) at a flow rate of 20 mL/min. Purities of assayed compounds were in all cases greater than 95%, as determined by reverse-phase HPLC analysis.

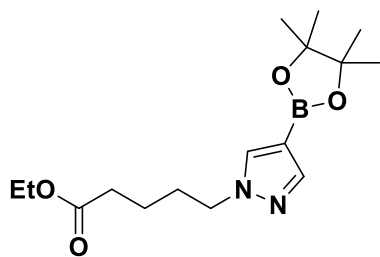
### Scheme 6.1. Synthesis of **42**.





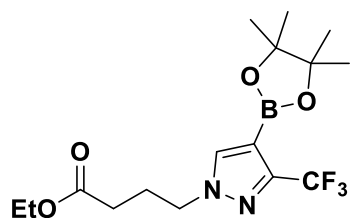
**ethyl 4-(4-(4,4,5,5-tetramethyl-1,3,2-dioxaborolan-2-yl)-1H-pyrazol-1-yl)butanoate (1)**

To a solution of 4-(4,4,5,5-tetramethyl-1,3,2-dioxaborolan-2-yl)-1H-pyrazole (1 g, 5.15 mmol) in DMF (30 mL) was added ethyl 4-bromobutanoate (0.98 mL, 6.18 mmol) followed by  $K_2CO_3$  (1.8 g, 12.9 mmol). The reaction mixture was heated to 80 °C for 16 hours. The mixture was quenched with  $H_2O$  and extracted with EtOAc. The combined organic extracts were washed with brine, dried over  $MgSO_4$  and condensed to give a light-brown oil that was used without further purification (1.42g, 90% yield). MS (ESI) m/z: 309.42 (M+H)<sup>+</sup>.



**ethyl 5-(4-(4,4,5,5-tetramethyl-1,3,2-dioxaborolan-2-yl)-1H-pyrazol-1-yl)pentanoate (2)**

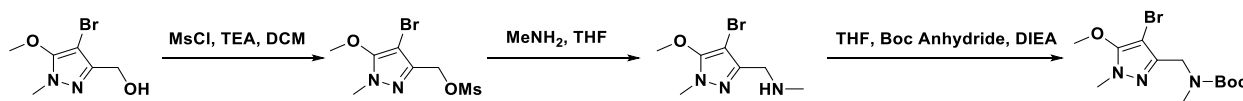
Prepared according to the procedure used for **1** using ethyl 5-bromopentanoate. Light-brown oil (1.57g, 95% yield). MS (ESI) m/z: 323.61 (M+H)<sup>+</sup>.



**ethyl 4-(4-(4,4,5,5-tetramethyl-1,3,2-dioxaborolan-2-yl)-3-(trifluoromethyl)-1H-pyrazol-1-yl)butanoate(3)**

Prepared according to the procedure used for **1** using 4-(4,4,5,5-tetramethyl-1,3,2-dioxaborolan-2-yl)-3-(trifluoromethyl)-1H-pyrazole. Light-brown oil (1.21g, 84% yield). MS (ESI)  $m/z$ : 377.34 (M+H)<sup>+</sup>.

**Scheme 6.2.** Representative synthesis of pyrazoles.



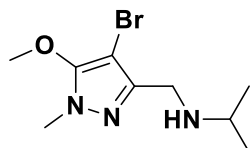
**(4-bromo-5-methoxy-1-methyl-1H-pyrazol-3-yl)methyl methanesulfonate (5)**

To a 0 °C solution of (4-bromo-5-methoxy-1-methyl-1H-pyrazol-3-yl)methanol (1 g, 4.52 mmol) was added TEA (0.95 mL, 6.79 mmol) followed by methanesulfonyl chloride (0.53 mL, 6.79 mmol). The mixture was stirred for 2 hours at room temperature then quenched with NaHCO<sub>3</sub> sat. aq. and extracted with DCM. The combined organic layer was dried over MgSO<sub>4</sub> and condensed to give a yellow solid (1.2g, 89% yield) that was used without further purification.



#### 1-(4-bromo-5-methoxy-1-methyl-1H-pyrazol-3-yl)-N-methylmethanamine (6)

To a solution of (4-bromo-5-methoxy-1-methyl-1H-pyrazol-3-yl)methyl methanesulfonate (1.2 g, 4.01 mmol) in THF (10 mL) was added a solution of methylamine 2M in THF (4.01 mL, 8.02 mmol) along with DIEA (1.4 mL, 8.02 mmol). The mixture was heated to 60 °C for 1 hour. The reaction was quenched with H<sub>2</sub>O and extracted with EtOAc. The combined organic layer was dried over MgSO<sub>4</sub> and condensed to give a brown oil that was used without further purification. MS (ESI) m/z 235.62 (M+H)<sup>+</sup>.



#### N-((4-bromo-5-methoxy-1-methyl-1H-pyrazol-3-yl)methyl)propan-2-amine (7)

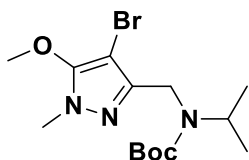
Light-brown oil (0.95g, 90% yield). MS (ESI) m/z: 263.28 (M+H)<sup>+</sup>.



#### tert-butyl ((4-bromo-5-methoxy-1-methyl-1H-pyrazol-3-yl)methyl)(methyl)carbamate (8)

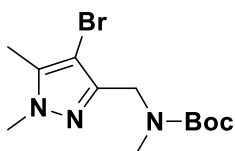
To a solution of 1-(4-bromo-5-methoxy-1-methyl-1H-pyrazol-3-yl)-N-methylmethanamine (250 mg, 1.07 mmol) in THF (5 mL) was added Boc anhydride (344 μL, 1.5 mmol), TEA (208 μL, 1.5 mmol) along with a catalytic amount of DMAP. The mixture was stirred for 1 hour, quenched with H<sub>2</sub>O and extracted with EtOAc. The combined organic layer was dried over MgSO<sub>4</sub> and condensed to give a brown oil that was purified by F.C. using a gradient of 20% to 70% EtOAc in

hexanes to give the desired product as a clear oil (324 mg, 91% yield).  $^1\text{H}$  NMR (500 MHz, DMSO)  $\delta$  4.25 (s, 2H), 3.98 (s, 3H), 3.62 (s, 3H), 2.71 (s, 3H) 1.40 (s, 9H). MS (ESI)  $m/z$  335.27 (M+H) $^+$ .



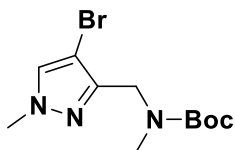
**tert-butyl ((4-bromo-5-methoxy-1-methyl-1H-pyrazol-3-yl)methyl)(isopropyl)carbamate (9)**

91% yield as a clear oil. MS (ESI)  $m/z$ : 363.78 (M+H) $^+$ .



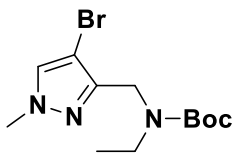
**tert-butyl ((4-bromo-1,5-dimethyl-1H-pyrazol-3-yl)methyl)(methyl)carbamate (10)**

94% yield as a clear oil.  $^1\text{H}$  NMR (500 MHz, DMSO)  $\delta$  4.25 (s, 2H), 3.73 (s, 3H), 2.70 (s, 3H), 2.21 (s, 3H) 1.40 (s, 9H). MS (ESI)  $m/z$  319.56 (M+H) $^+$ .



**tert-butyl ((4-bromo-1-methyl-1H-pyrazol-3-yl)methyl)(methyl)carbamate (12)**

90% yield as a clear oil.  $^1\text{H}$  NMR (500 MHz, DMSO)  $\delta$  7.97 (s, 1H), 4.26 (s, 2H), 3.86 (s, 3H), 2.72 (s, 3H), 1.40 (s, 9H). MS (ESI)  $m/z$  305.63 (M+H) $^+$ .



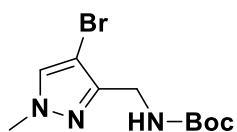
**tert-butyl ((4-bromo-1-methyl-1H-pyrazol-3-yl)methyl)(ethyl)carbamate (12)**

88% yield as a yellow solid. MS (ESI)  $m/z$  319.26 (M+H)+.



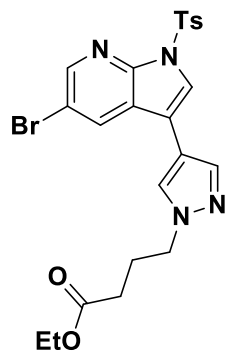
**tert-butyl ((4-bromo-1-methyl-1H-pyrazol-3-yl)methyl)(isopropyl)carbamate (14)**

90% yield as a clear oil. MS (ESI)  $m/z$  333.41 (M+H)+.



**tert-butyl ((4-bromo-1-methyl-1H-pyrazol-3-yl)methyl)carbamate (15)**

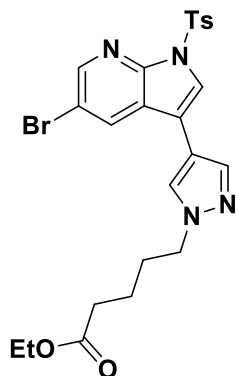
88% yield as a clear oil. MS (ESI)  $m/z$  291.36 (M+H)+.



**Ethyl 4-(4-(5-bromo-1-tosyl-1H-pyrrolo[2,3-b]pyridine-3-yl)-1H-pyrazol-1-yl)butanoate (16)**

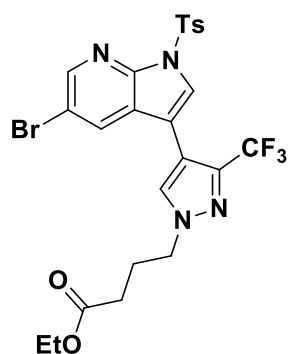
To a solution of 5-bromo-3-iodo-1-tosyl-1H-pyrrolo[2,3-b]pyridine (1 g, 2.1 mmol), ethyl 4-(4-(4,4,5,5-tetramethyl-1,3,2-dioxaborolan-2-yl)-1H-pyrazol-1-yl)butanoate (976 mg, 3.14 mmol) in  $\text{CH}_3\text{CN}$  (15 mL) was added 2M  $\text{Na}_2\text{CO}_3$  (3.15 mL, 6.3 mmol). This solution was degassed using a sonicator for 2 minutes, then  $\text{Pd}(\text{PPh}_3)\text{Cl}_2$  (74 mg, 0.105 mmol) was added and the mixture

stirred at 80 °C for 1 hour. The mixture was quenched with H<sub>2</sub>O and extracted with EtOAc. The combined extracts were washed with brine, dried over MgSO<sub>4</sub> and condensed. The residue was purified by F.C using a gradient of 10% to 40% EtOAc in Hexanes to give the desired product as a yellow solid (780mg, 70% yield). MS (ESI) m/z 532.71 (M+H)<sup>+</sup>.



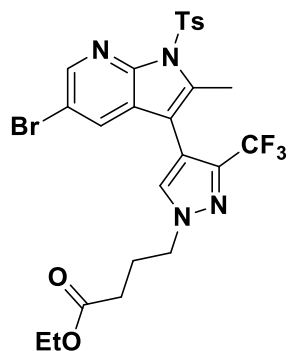
**ethyl 5-(4-(5-bromo-1-tosyl-1H-pyrrolo[2,3-b]pyridin-3-yl)-1H-pyrazol-1-yl)pentanoate (17)**

Prepared according to the procedure used for **14** using ethyl 5-(4-(4,4,5,5-tetramethyl-1,3,2-dioxaborolan-2-yl)-1H-pyrazol-1-yl)pentanoate. Clear oil (810mg, 71% yield). MS (ESI) m/z: 545.52 (M+H)<sup>+</sup>.



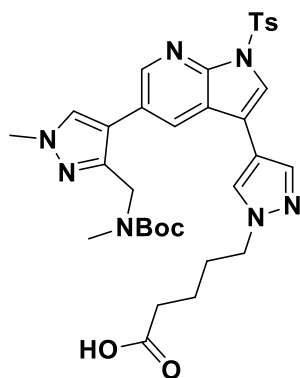
**ethyl 4-(4-(5-bromo-1-tosyl-1H-pyrrolo[2,3-b]pyridin-3-yl)-3-(trifluoromethyl)-1H-pyrazol-1-yl)butanoate (18)**

Prepared according to the procedure used for **14** using ethyl 4-(4-(4,4,5,5-tetramethyl-1,3,2-dioxaborolan-2-yl)-3-(trifluoromethyl)-1H-pyrazol-1-yl)butanoate. Clear oil (980mg, 78% yield). MS (ESI) m/z: 600.82 (M+H)<sup>+</sup>.



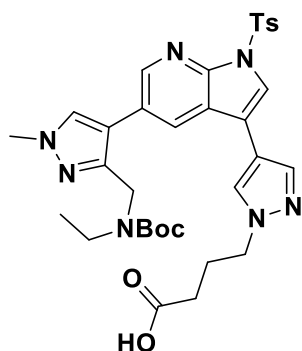
**ethyl 4-(4-(5-bromo-2-methyl-1-tosyl-1H-pyrrolo[2,3-b]pyridin-3-yl)-3-(trifluoromethyl)-1H-pyrazol-1-yl)butanoate (20)**

Prepared according to the procedure used for **14** using ethyl 4-(4-(4,4,5,5-tetramethyl-1,3,2-dioxaborolan-2-yl)-3-(trifluoromethyl)-1H-pyrazol-1-yl)butanoate and 5-bromo-3-iodo-2-methyl-1-tosyl-1H-pyrrolo[2,3-b]pyridine. Clear oil (860mg, 70% yield). MS (ESI) m/z: 614.47 (M+H)<sup>+</sup>.



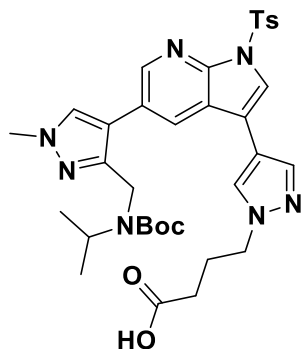
**5-(4-(5-(3-(((tert-butoxycarbonyl)(methyl)amino)methyl)-1-methyl-1H-pyrazol-4-yl)-1-tosyl-1H-pyrrolo[2,3-b]pyridin-3-yl)-1H-pyrazol-1-yl)pentanoic acid (21)**

To a degassed solution of ethyl 4-(4-(5-bromo-1-tosyl-1H-pyrrolo[2,3-b]pyridin-3-yl)-1H-pyrazol-1-yl)butanoate (300 mg, 0.55 mmol), tert-butyl ((4-bromo-1-methyl-1H-pyrazol-3-yl)methyl)(methyl)carbamate (220 mg, 0.71 mmol), Bis(pinacolato)diboron (210 mg, 0.82 mmol) and Cs<sub>2</sub>CO<sub>3</sub> (896 mg, 2.75 mmol) in 1,4-dioxane (9 mL) and H<sub>2</sub>O (1 mL) was added Pd(OAc)<sub>2</sub> (19 mg, 0.08 mmol) and CataCXium A (60 mg, 0.16 mmol). The reaction was stirred at 95 °C for 1 hour. The mixture was cooled to rt and NaOH (44 mg, 1.1 mmol) in H<sub>2</sub>O (1 mL) was added and the reaction stirred for an additional 2 hours. The mixture was filtered and purified by HPLC using a gradient of 0 to 70% ACN in H<sub>2</sub>O to give the desired compound as a beige solid (124 mg, 35% yield). MS (ESI) m/z: 648.46 (M+H)<sup>+</sup>.



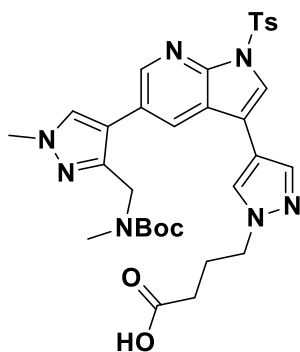
**4-(4-(5-(3-(((tert-butoxycarbonyl)(ethyl)amino)methyl)-1-methyl-1H-pyrazol-4-yl)-1-tosyl-1H-pyrrolo[2,3-b]pyridin-3-yl)-1H-pyrazol-1-yl)butanoic acid (22)**

Beige solid (132 mg, 36% yield). MS (ESI) m/z: 662.74 (M+H)<sup>+</sup>.



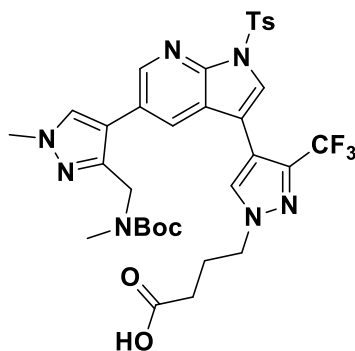
**4-(4-(5-(3-(((tert-butoxycarbonyl)(isopropyl)amino)methyl)-1-methyl-1H-pyrazol-4-yl)-1-tosyl-1H-pyrrolo[2,3-b]pyridin-3-yl)-1H-pyrazol-1-yl)butanoic acid (23)**

Beige solid (117 mg, 32% yield). MS (ESI) m/z: 676.36 (M+H)<sup>+</sup>.



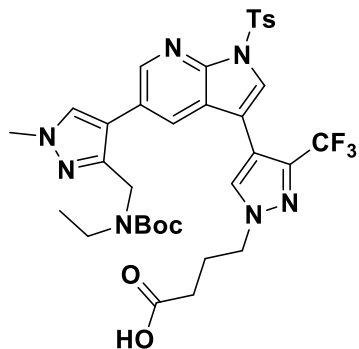
**4-(4-(5-(3-(((tert-butoxycarbonyl)(methyl)amino)methyl)-1-methyl-1H-pyrazol-4-yl)-1-tosyl-1H-pyrrolo[2,3-b]pyridin-3-yl)-1H-pyrazol-1-yl)butanoic acid (25)**

Brown solid (128 mg, 36% yield). MS (ESI) m/z: 648.62 (M+H)<sup>+</sup>.



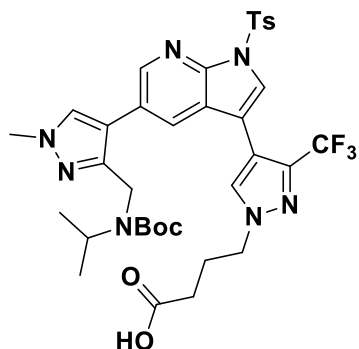
**4-(4-(5-(3-(((tert-butoxycarbonyl)(methyl)amino)methyl)-1-methyl-1H-pyrazol-4-yl)-1-tosyl-1H-pyrrolo[2,3-b]pyridin-3-yl)-3-(trifluoromethyl)-1H-pyrazol-1-yl)butanoic acid (26)**

White solid (138 mg, 34% yield). MS (ESI) m/z: 716.32 (M+H)<sup>+</sup>.



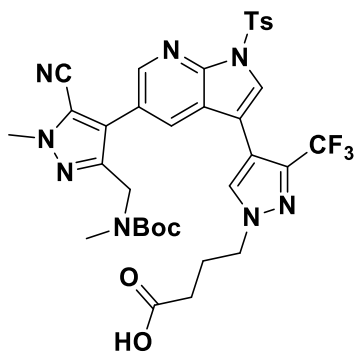
**4-(4-(5-(3-(((tert-butoxycarbonyl)(ethyl)amino)methyl)-1-methyl-1H-pyrazol-4-yl)-1-tosyl-1H-pyrrolo[2,3-b]pyridin-3-yl)-3-(trifluoromethyl)-1H-pyrazol-1-yl)butanoic acid (27)**

White solid (146 mg, 35% yield). MS (ESI)  $m/z$ : 730.73 (M+H)<sup>+</sup>.



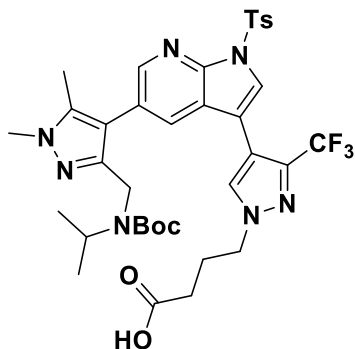
**4-(4-(5-(3-(((tert-butoxycarbonyl)(isopropyl)amino)methyl)-1-methyl-1H-pyrazol-4-yl)-1-tosyl-1H-pyrrolo[2,3-b]pyridin-3-yl)-3-(trifluoromethyl)-1H-pyrazol-1-yl)butanoic acid (28)**

White solid (156 mg, 37% yield). MS (ESI)  $m/z$ : 744.65 (M+H)<sup>+</sup>.



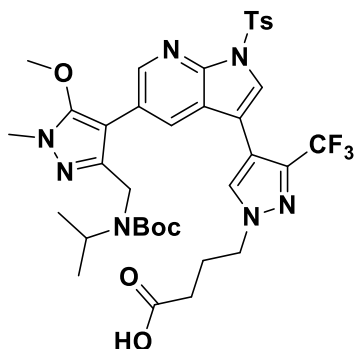
**4-(4-(5-(3-(((tert-butoxycarbonyl)(methyl)amino)methyl)-5-cyano-1-methyl-1H-pyrazol-4-yl)-1-tosyl-1H-pyrrolo[2,3-b]pyridin-3-yl)-3-(trifluoromethyl)-1H-pyrazol-1-yl)butanoic acid (30)**

White solid (123 mg, 29% yield). MS (ESI) m/z: 741.84 (M+H)<sup>+</sup>.



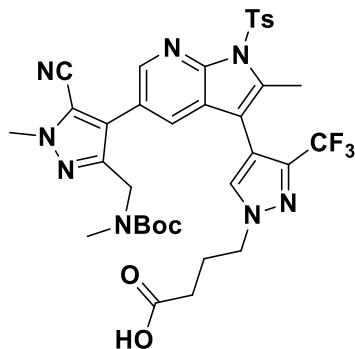
**4-(4-(5-(3-(((tert-butoxycarbonyl)(isopropyl)amino)methyl)-1,5-dimethyl-1H-pyrazol-4-yl)-1-tosyl-1H-pyrrolo[2,3-b]pyridin-3-yl)-3-(trifluoromethyl)-1H-pyrazol-1-yl)butanoic acid (31)**

White solid (120 mg, 28% yield). MS (ESI) m/z: 758.32 (M+H)<sup>+</sup>.



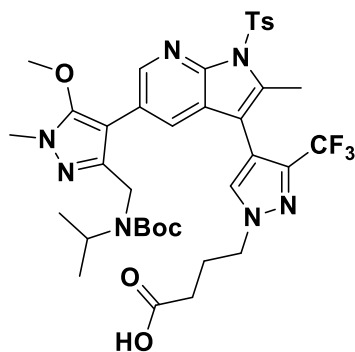
**4-(4-(5-(3-(((tert-butoxycarbonyl)(isopropyl)amino)methyl)-5-methoxy-1-methyl-1H-pyrazol-4-yl)-1-tosyl-1H-pyrrolo[2,3-b]pyridin-3-yl)-3-(trifluoromethyl)-1H-pyrazol-1-yl)butanoic acid (32)**

White solid (136 mg, 31% yield). MS (ESI) m/z: 774.41 (M+H)<sup>+</sup>.



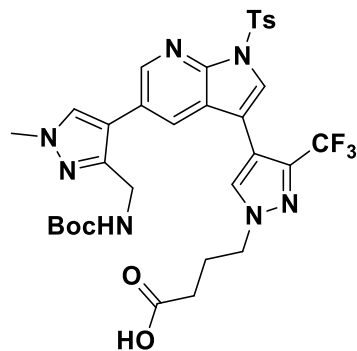
**4-(4-(5-(3-(((tert-butoxycarbonyl)(methyl)amino)methyl)-5-cyano-1-methyl-1H-pyrazol-4-yl)-2-methyl-1-tosyl-1H-pyrrolo[2,3-b]pyridin-3-yl)-3-(trifluoromethyl)-1H-pyrazol-1-yl)butanoic acid (33)**

White solid (132 mg, 29% yield). MS (ESI)  $m/z$ : 755.61 (M+H)<sup>+</sup>.



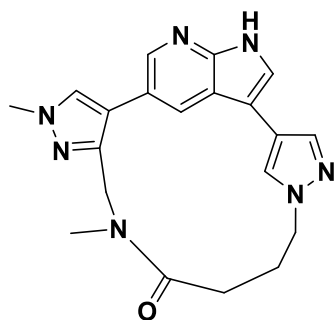
**4-(4-(5-(3-(((tert-butoxycarbonyl)(isopropyl)amino)methyl)-5-methoxy-1-methyl-1H-pyrazol-4-yl)-2-methyl-1-tosyl-1H-pyrrolo[2,3-b]pyridin-3-yl)-3-(trifluoromethyl)-1H-pyrazol-1-yl)butanoic acid (34)**

White solid (130 mg, 28% yield). MS (ESI)  $m/z$ : 788.43 (M+H)<sup>+</sup>.



**4-(4-(5-(3-(((tert-butoxycarbonyl)amino)methyl)-1-methyl-1H-pyrazol-4-yl)-1-tosyl-1H-pyrrolo[2,3-b]pyridin-3-yl)-3-(trifluoromethyl)-1H-pyrazol-1-yl)butanoic acid(40)**

White solid (110 mg, 21% yield). MS (ESI) m/z: 702.27 (M+H)<sup>+</sup>.



**(Z)-31,5-dimethyl-11H,21H,31H-5-aza-2(3,5)-pyrrolo[2,3-b]pyridina-1(4,1),3(4,3)-dipyrazolacyclonaphan-6-one (42)**

To a solution of 4-(4-(5-(3-(((tert-butoxycarbonyl)(methyl)amino)methyl)-1-methyl-1H-pyrazol-4-yl)-1-tosyl-1H-pyrrolo[2,3-b]pyridin-3-yl)-1H-pyrazol-1-yl)butanoic acid (100 mg, 0.154 mmol) in DCM (10 mL) was added TFA (1 mL). The mixture was stirred for 1 hour and then the solvent was removed in vacuo to give a brown residue that was dissolved in DMF (4 mL). DIEA (135 $\mu$ L, 0.772 mmol) was added and the mixture was added dropwise over 30 minutes via syringe pump to a 0 °C solution of HATU (117 mg, 0.308 mmol) in DMF (20 mL). The mixture was warmed to rt and stirred for an additional 15 minutes, then quenched with H<sub>2</sub>O and extracted with EtOAc. The combined organic extracts were washed with water, brine, dried over MgSO<sub>4</sub> and condensed to give a brown oil that was dissolved in MeOH (3 mL), Acetone (3 mL) and NaOH 3M (3 mL). The

mixture was heated to 65 °C for 30 minutes then cooled to rt and extracted with EtOAc. The combined organic layer was washed with H<sub>2</sub>O, brine, dried over MgSO<sub>4</sub> and condensed to give a brown oil that was purified by reverse phase HPLC using a gradient of 0 to 60% ACN in H<sub>2</sub>O to give the desired product as a white solid (28 mg, 48% yield over 3 steps). <sup>1</sup>H NMR (500 MHz, DMSO) δ 11.67 (s, 1H), 8.49 (s, 1H), (7.79 (s, 1H), 7.75 (s, 1H), 7.51 (m, 2H), 4.49 (t, *J* = 6 Hz, 2H), 4.34 (m, 2H), 3.89 (s, 3H), 2.74, (s, 3H), 2.61 (m, 2H), 2.16 (m, 2H). MS (ESI) *m/z* 376.47 (M+H)<sup>+</sup>.

**(Z)-31,5-dimethyl-6-oxo-13-(trifluoromethyl)-11H,21H,31H-5-aza-2(3,5)-pyrrolo[2,3-b]pyridina-1(4,1),3(4,3)-dipyrazolacyclonaphane-35-carbonitrile (JH-XIV-68-3)**

White solid (36 mg, 57% yield over 3 steps). <sup>1</sup>H NMR (500 MHz, DMSO) δ 12.01 (s, 1H), 8.61 (s, 1H), 8.14 (s, 1H) 7.71 (s, 1H), 7.53 (s, 1H), 4.55 (m, 2H), 4.34 (t, *J* = 6 Hz, 2H), 4.13 (s, 3H), 2.83 (s, 3H), 2.71, (m, 2H), 2.22 (m, 2H). MS (ESI) *m/z* 469.26 (M+H)<sup>+</sup>.

**(Z)-5-isopropyl-35-methoxy-31-methyl-13-(trifluoromethyl)-11H,21H,31H-5-aza-2(3,5)-pyrrolo[2,3-b]pyridina-1(4,1),3(4,3)-dipyrazolacyclonaphan-6-one (JH-XIV-71)**

White solid (30 mg, 46% yield over 3 steps). <sup>1</sup>H NMR (500 MHz, DMSO) δ 11.90 (s, 1H), 8.58 (s, 1H), 8.05 (s, 1H) 7.61 (s, 1H), 7.42 (s, 1H), 4.64 (m, 2H), 4.38 (t, *J* = 6 Hz, 2H), 3.75 (s, 3H), 3.73 (s, 3H), 2.70 (m, 2H), 2.31, (m, 2H), 2.0 (m, 1H), 1.10 (s, 6H). MS (ESI) *m/z* 502.37 (M+H)<sup>+</sup>.

**(Z)-5-isopropyl-35-methoxy-22,31-dimethyl-13-(trifluoromethyl)-11H,21H,31H-5-aza-2(3,5)-pyrrolo[2,3-b]pyridina-1(4,1),3(4,3)-dipyrazolacyclonaphan-6-one (JH-XIV-73-1)**

White solid (34 mg, 52% yield over 3 steps). <sup>1</sup>H NMR (500 MHz, DMSO) δ 11.71 (s, 1H), 8.43 (s, 1H), 7.90 (s, 1H) 7.31 (s, 1H), 4.58 (m, 2H), 4.38 (t, *J* = 6 Hz, 2H), 3.74 (s, 3H), 3.72 (s, 3H),

2.70 (m, 2H), 2.33 (s, 3H), 2.30, (m, 2H), 1.81 (m, 1H), 1.05 (s, 6H). MS (ESI) m/z 516.74 (M+H)<sup>+</sup>.

**(Z)-22,31,5-trimethyl-6-oxo-13-(trifluoromethyl)-11H,21H,31H-5-aza-2(3,5)-pyrrolo[2,3-b]pyridina-1(4,1),3(4,3)-dipyrazolacyclononaphane-35-carbonitrile (JH-XIV-73-2)**

White solid (31 mg, 48% yield over 3 steps). <sup>1</sup>H NMR (500 MHz, DMSO) δ 11.94 (s, 1H), 8.47 (s, 1H), 7.93 (s, 1H) 7.32 (s, 1H), 4.52 (m, 2H), 4.37 (t, *J* = 6 Hz, 2H), 4.08 (s, 3H), 2.75 (s, 3H), 2.60 (m, 2H), 2.36 (s, 3H), 2.26, (m, 2H). MS (ESI) m/z 483.28 (M+H)<sup>+</sup>.

**Biochemical Kinase Profiling.** A KINOMEscan was conducted with 1 μM compound by DiscoverX.

***in vitro* Kinase Assays.** Z'LYTE kinase assays were conducted for DYRK1A and DYRK1B at Life Technologies using Km ATP concentrations.

**Cell Culture.** CAL27 and FaDu cells were generously provided by Ravindra Uppaluri (DFCI, Boston, MA). CAL27 and HEK293FT cell lines were cultured in DMEM media containing L-glutamine and 4.5 g/L D-glucose, supplemented with 10% fetal bovine serum (FBS) and 1% penicillin/streptomycin and FaDu cells were cultured in RPMI-1640 media containing L-glutamine, supplemented with 10% FBS and 1% penicillin/streptomycin. Mycoplasma testing was performed on a monthly basis and all lines were negative.

**Sample Preparation for KiNativ Live-cell Target Engagement Assay.** ATP and ADP acyl-nucleotide probes were synthesized as described previously.<sup>11</sup> CAL27 cells were treated in duplicate with DMSO and in singlicate with 1 μM of harmine, CX-4945, or **JH-XIV-68-3** for 6 hours. Cells were washed with ice-cold PBS once, pelleted, and snap-frozen with liquid nitrogen. The cell pellets were lysed by sonication in lysis buffer (50 mM HEPES, pH 7.5, 150 mM NaCl, 0.1% Triton-X-100, phosphatase inhibitors (Cocktail II AG Scientific #P-1518)). After lysis, the samples

were cleared by centrifugation, and the supernatant collected for probe labeling. For live cell treatment, 50mL of a 10X aqueous solution of the desthiobiotin-ATP probe was added to each sample for a final probe concentration of 20mM, and samples were incubated with probe for 10 minutes. Samples were prepared for MS analysis as described previously.<sup>12</sup> Briefly, probe-labeled lysates were denatured and reduced (6 M urea, 10 mM DTT, 65 °C, 15 min), alkylated (40 mM iodoacetamide, 37 °C, 30 min), and gel filtered (BioradEcono-Pac<sup>®</sup>10G) into 10 mM ammonium bicarbonate, 2 M urea, 5 mM methionine. The desalted protein mixture was digested with trypsin (0.015 mg/ml) for 1 hour at 37 °C, and desthiobiotinylated peptides captured using 12.5ml high-capacity streptavidin resin (Thermo Scientific). Captured peptides were then washed extensively, and probe-labeled peptides eluted from the streptavidinbeads using two 35-ml washes of a 50% CH<sub>3</sub>CN/water mixture containing 0.1% TFA at room temperature.

**Cell Viability Assays.** Cell viability was evaluated using the CellTiter-Glo Luminescent Cell Viability Assay (Promega) following the manufacturer's standards.

**Immunoblotting.** Cells were washed with PBS before being lysed with Cell Lysis Buffer (Cell Signaling) supplemented with protease and phosphatase inhibitor cocktails (Roche) at 4°C for 15 minutes. The cell lysate vortexed before being centrifuged at 14,000 x g for 20 min at 4°C. Protein in cell lysate was quantified by BCA assay (Pierce). Primary antibodies used in this study include  $\beta$ -actin (Cell Signaling Technology, 3700S), BCL-xL (Cell Signaling Technology, 2762S) and cleaved PARP (Cell Signaling Technology, 9541S). Blot quantification was performed using Image Studio 4.0 software, normalizing to loading controls.

### **Author Contributions**

C.E.P conducted the experiments and analyzed the data. J.M.H. designed and synthesized compounds. N.S.G advised on project directions. C.E.P. wrote the paper. The authors declare no competing financial interest.

## References

- (1) Walte, A.; Rüben, K.; Birner-Gruenberger, R.; Preisinger, C.; Bamberg-Lemper, S.; Hilz, N.; Bracher, F.; Becker, W. Mechanism of Dual Specificity Kinase Activity of DYRK1A. *Febs J* **2013**, *280* (18), 4495–4511. <https://doi.org/10.1111/febs.12411> .
- (2) Neumann, F.; Gourdain, S.; Albac, C.; Dekker, A. D.; Bui, L.; Dairou, J.; Schmitz-Afonso, I.; Hue, N.; Rodrigues-Lima, F.; Delabar, J. M.; et al. DYRK1A Inhibition and Cognitive Rescue in a Down Syndrome Mouse Model Are Induced by New Fluoro-DANDY Derivatives. *Sci Rep-uk* **2018**, *8* (1), 2859. <https://doi.org/10.1038/s41598-018-20984-z> .
- (3) Czarna, A.; Wang, J.; Zelencova, D.; Liu, Y.; Deng, X.; Choi, H.; Zhang, T.; Zhou, W.; Chang, J.; Kildalsen, H.; et al. Novel Scaffolds for Dual Specificity Tyrosine-Phosphorylation-Regulated Kinase (DYRK1A) Inhibitors. *J Med Chem* **2018**, *61* (17), 7560–7572. <https://doi.org/10.1021/acs.jmedchem.7b01847> .
- (4) Jarhad, D. B.; Mashelkar, K. K.; Kim, H.-R.; Noh, M.; Jeong, L. Dual-Specificity Tyrosine Phosphorylation-Regulated Kinase 1A (DYRK1A) Inhibitors as Potential Therapeutics. *J Med Chem* **2018**, *61* (22), 9791–9810. <https://doi.org/10.1021/acs.jmedchem.8b00185> .
- (5) Siddiqui-Jain, A.; Drygin, D.; Streiner, N.; Chua, P.; Pierre, F.; O'Brien, S. E.; Bliesath, J.; Omori, M.; Huser, N.; Ho, C.; et al. CX-4945, an Orally Bioavailable Selective Inhibitor of Protein Kinase CK2, Inhibits Prosurvival and Angiogenic Signaling and Exhibits Antitumor Efficacy. *Cancer Res* **2010**, *70* (24), 10288–10298. <https://doi.org/10.1158/0008-5472.can-10-1893> .
- (6) Kim, H.; Lee, K.-S.; Kim, A.-K.; Choi, M.; Choi, K.; Kang, M.; Chi, S.-W.; Lee, M.-S.; Lee, J.-S.; Lee, S.-Y.; et al. A Chemical with Proven Clinical Safety Rescues Down-Syndrome-Related Phenotypes in through DYRK1A Inhibition. *Dis Model Mech* **2016**, *9* (8), 839–848. <https://doi.org/10.1242/dmm.025668> .
- (7) Johnson, T. W.; Richardson, P. F.; Bailey, S.; Brooun, A.; Burke, B. J.; Collins, M. R.; Cui, J. J.; Deal, J. G.; Deng, Y.-L.; Dinh, D.; et al. Discovery of (10R)-7-Amino-12-Fluoro-2,10,16-Trimethyl-15-Oxo-10,15,16,17-Tetrahydro-2H-8,4-(Metheno)Pyrazolo[4,3-h][2,5,11]-Benzoxadiazacyclotetradecine-3-Carbonitrile (PF-06463922), a Macrocyclic Inhibitor of Anaplastic Lymphoma Kinase (ALK) and c-Ros Oncogene 1 (ROS1) with Preclinical Brain Exposure and Broad-Spectrum Potency against ALK-Resistant Mutations. *J Med Chem* **2014**, *57* (11), 4720–4744. <https://doi.org/10.1021/jm500261q> .
- (8) Driggers, E. M.; Hale, S. P.; Lee, J.; Terrett, N. K. The Exploration of Macrocycles for Drug Discovery — an Underexploited Structural Class. *Nat Rev Drug Discov* **2008**, *7* (7), 608. <https://doi.org/10.1038/nrd2590> .
- (9) Akamine, T.; Toyokawa, G.; Tagawa, T.; Seto, T. Spotlight on Lorlatinib and Its Potential in the Treatment of NSCLC: The Evidence to Date. *Oncotargets Ther* **2018**, *11*, 5093–5101. <https://doi.org/10.2147/ott.s165511> .
- (10) Radhakrishnan, A.; Nanjappa, V.; Raja, R.; Sathe, G.; Puttamalles, V. N.; Jain, A. P.; Pinto, S. M.; Balaji, S. A.; Chavan, S.; Sahasrabuddhe, N. A.; et al. A Dual Specificity Kinase, DYRK1A, as a Potential Therapeutic Target for Head and Neck Squamous Cell Carcinoma. *Sci Rep-uk* **2016**, *6* (1), srep36132. <https://doi.org/10.1038/srep36132> .

(11) Patricelli, M. P.; Szardenings, K. A.; Liyanage, M.; Nomanbhoy, T. K.; Wu, M.; Weissig, H.; Aban, A.; Chun, D.; Tanner, S.; Kozarich, J. W. Functional Interrogation of the Kinome Using Nucleotide Acyl Phosphates. *Biochemistry-us* **2007**, *46* (2), 350–358.  
<https://doi.org/10.1021/bi062142x> .

(12) Patricelli, M. P.; Nomanbhoy, T. K.; Wu, J.; Brown, H.; Zhou, D.; Zhang, J.; Jagannathan, S.; Aban, A.; Okerberg, E.; Herring, C.; et al. In Situ Kinase Profiling Reveals Functionally Relevant Properties of Native Kinases. *Chem Biol* **2011**, *18* (6), 699 710.  
<https://doi.org/10.1016/j.chembiol.2011.04.011> .

## **Chapter 7: Benzopyrimidodiazepinone Inhibitors of TNK2**

## Attributions

The work in this chapter is adapted from a manuscript accepted for publication in *Bioorganic and Medicinal Chemistry Letters*, titled “Benzopyrimidodiazepinone Inhibitors of TNK2” by Groendyke *et al.*<sup>1</sup> We thank Vivid BioSciences for funding support. Author contributions and competing interests for this work are listed at the end of the chapter, before the references.

## Chapter 7: Benzopyrimidodiazepinone Inhibitors of TNK2.

Brian J. Groendyke,<sup>a,b</sup> Chelsea E. Powell,<sup>a,b</sup> Frederic Feru,<sup>a,b</sup> Thomas W. Gero,<sup>a,b</sup> Zhengnian Li,<sup>a,b</sup> Hilary Szabo,<sup>c</sup> Kevin Pang,<sup>d</sup> John Feutrill,<sup>e</sup> Bailing Chen,<sup>e</sup> Bin Li,<sup>e</sup> Nathanael S. Gray,<sup>a,b</sup> David A. Scott<sup>a,b,\*</sup>

<sup>a</sup> Department of Cancer Biology, Dana-Farber Cancer Institute, Boston, Massachusetts 02215, United States

<sup>b</sup> Department of Biological Chemistry & Molecular Pharmacology, Harvard Medical School, Boston, Massachusetts 02115, United States

<sup>c</sup> Vivid BioSciences, Boston, Massachusetts 02110, United States

<sup>d</sup> Northeastern University, Boston, Massachusetts 02115, United States

<sup>e</sup> SYNthesis Med Chem, Suzhou Industry Park, Suzhou, Jiangsu, China

\* Correspondence: [DavidA.Scott@dfci.harvard.edu](mailto:DavidA.Scott@dfci.harvard.edu) (D.A.S.).

**Abstract**

Tyrosine Kinase Nonreceptor 2 (TNK2, also known as ACK1) has recently been shown to be a potential therapeutic target in acute myelogenous leukemia (AML). In this study we present the use of a cell viability assay based on Ba/F3 cells expressing TNK2 in order to develop and optimize lead TNK2 inhibitors from the benzopyrimidodiazepinone scaffold, starting from the potent and selective compound XMD8-87.

## 7.1 Introduction

The tricyclic benzopyrimidodiazepinone series and related scaffolds have delivered both highly selective tool compounds,<sup>2-5</sup> and advanced lead molecules for ERK5, (XMD8-92)<sup>6,7</sup> and LRRK2, (LRRK2-IN-1)<sup>8</sup> (Figure 7.1). Most compounds derived from this scaffold have an aniline group installed on the pyrimidine ring, and for these inhibitors the overall kinase selectivity profile is typically enhanced by a methoxy substituent at the aniline 2-position. The 2-MeO aniline group is present in other pyrimidine-based kinase inhibitor scaffolds,<sup>9-12</sup> but is not sufficient by itself to confer good selectivity. In the benzopyrimidodiazepinone series, the combination of the 2-MeO aniline and the tricyclic core likely drives the high level of overall kinase selectivity, with further optimization for specific targets achieved through fine-tuning of substituents on both the tricyclic core and the aniline.

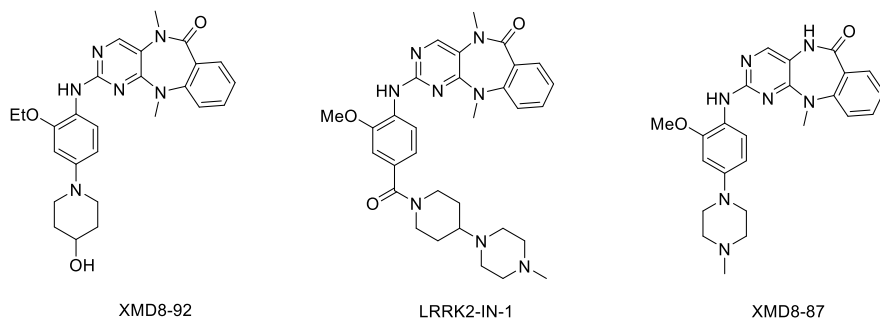


**Figure 7.1.** Benzopyrimidodiazepinone kinase inhibitors.

Tyrosine Kinase Nonreceptor 2 (TNK2, also known as ACK1) is a cytoplasmic kinase that was first identified based on its binding to the cell-cycle regulator, CDC42.<sup>13</sup> TNK2 acts as an effector of CDC42, which in turn regulates cell migration.<sup>14</sup> Overexpression of TNK2 in cancer cell lines can increase cellular motility, invasiveness, and the cells' ability to metastasize.<sup>15</sup> TNK2 mutations and/or overexpression are associated with numerous cancers, including renal, lung, ovarian, gastric, prostate, and breast cancers.<sup>5</sup> Small molecule inhibitors from several structural

classes have been explored as potential treatments for a range of indications, though none have yet reached the clinic.<sup>16–19</sup>

Recently, Maxson et al. identified two point mutations, D163E and R806Q, in TNK2 that act as driver mutations of acute myelogenous leukemia (AML).<sup>5</sup> This work indicated that targeting TNK2 D163E or TNK2 R806Q with kinase inhibitors may lead to a new therapy for AML. In this study we used a cell viability assay based on Ba/F3 cells expressing TNK2 D163E, with IL-3 dependent parental Ba/F3 cells as a control, in order to develop and optimize lead TNK2 inhibitors from the benzopyrimidodiazepinone scaffold.

## 7.2 Results and Discussion

Kinase selectivity profiling of compounds from the benzopyrimidodiazepinone scaffold led to the identification of XMD8-87 as a potent and highly selective TNK2 inhibitor.<sup>5,20</sup> XMD8-87 showed very little activity against other kinases in both cellular (KiNativ) and biochemical (KINOMEscan) kinase panels (Figure 7.2) and is therefore a useful pharmacological tool to explore the effects of TNK2 inhibition.

Based on our kinase profiling data, the benzopyrimidodiazepinones with the greatest activity against TNK2 were unsubstituted on the central ring amide. For compounds from this scaffold targeting other kinases, a methyl substituent on the amide was typically preferred. Modeling studies suggested that the amide NH interacts with the Thr205 gatekeeper residue of TNK2, in a manner similar to that proposed for a series of pyrazolopyrimidines.<sup>17</sup>

Disappointingly, XMD8-87 was very highly cleared *in vivo* in rodent PK studies (Table 7.4). This was in contrast to several *N*-methyl amide examples designed to target other kinases,<sup>6,8</sup> and also XMD8-85, the exact *N*-methyl matched pair of XMD8-87, all of which demonstrated good *in vivo* mouse PK profiles.

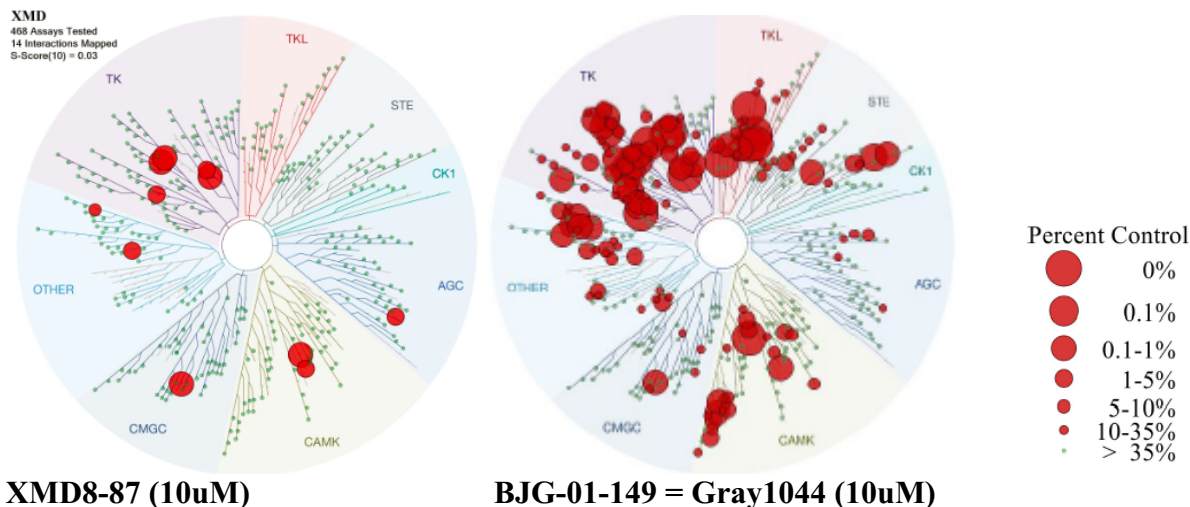
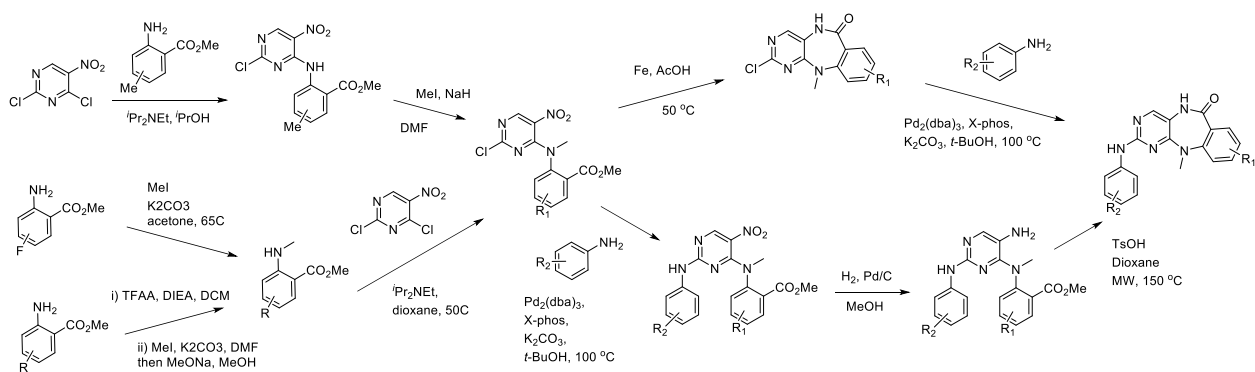


**Figure 7.2.** DiscoverX KinomeScan Treespot interaction maps of XMD8-87 and BJJ-01-149.

With the goal of developing a TNK2 inhibitor from the benzopyrimidodiazepinone series, we sought to further explore the SAR and to improve the *in vivo* PK profile. We were keen to retain the exquisite kinase selectivity of XMD8-87 to confirm the relevance of TNK2 as a therapeutic target. We first explored substituents on the phenyl ring of the tricyclic core, as well as a broader range of anilines and aniline replacements at the C2 position of the pyrimidine ring.

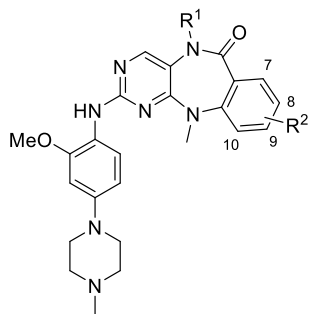
**Scheme 7.1.** Synthesis of pyrimidobenzodiazepinones.



Compounds were prepared using chemistry similar to that previously described, with modifications to the reaction sequence in some cases.<sup>6</sup> Scheme 7.1. Anthranilic esters were installed at the 4-position of 2,4-dichloronitropyrimidine, with moderate heating required for

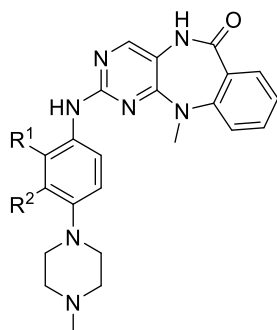
anilines substituted with electron-withdrawing groups. In some cases, the methylanilines were commercially available or readily prepared, but in others the unsubstituted anilines were installed followed by an additional methylation step. A one-pot reduction/cyclization was achieved with iron in acetic acid and moderate heating for most examples, with a final step to install the aniline substituent at the pyrimidine C2 position via Pd coupling chemistry. In some cases, the aniline was incorporated prior to the formation of the tricyclic core, and a two step nitro reduction/cyclization sequence was employed to generate the final compounds.

TNK2 enzyme IC<sub>50</sub>s and TNK2 D163E antiproliferative data for compounds with modifications to the phenyl ring are shown in Table 7.1. None of the substituents we introduced to the phenyl ring led to significantly improved potency in either the TNK2 enzyme assay, or our TNK2 D163E cell proliferation assay. The majority of compounds showed reduced TNK2 activity relative to XMD8-87 in both the enzyme and cell, but a methyl group was tolerated adjacent to the central ring amine (SYN-DFCI-00001) and fluorine could also be introduced at two positions. We also profiled XMD8-85, the *N*-methyl amide analog of XMD8-87, and confirmed that the loss of the amide NH led to reduced TNK2 potency in the enzyme and cell assays. We felt that small modifications on the right hand side of the molecule were unlikely to address the key PK liability of XMD8-87, and therefore conducted all our efforts on the aniline substituent on the original unsubstituted scaffold.

**Table 7.1.** Enzyme and cell data for examples with phenyl substituents.

Compound ID	R <sup>1</sup>	R <sup>2</sup>	TNK2 IC <sub>50</sub> (nM)	Cell TNK2 D163E (uM)
XMD8-87	-	-	44	0.19
XMD8-85	Me	-	959	0.57
SYN-DFCI-00019	-	7-Me	1610	1.63
SYN-DFCI-00013	-	8-Me	363	1.92
SYN-DFCI-00007	-	9-Me	223	0.26
SYN-DFCI-00001	-	10-Me	73 (IV)	0.13
KP-01-046	-	7-F	217	0.38
KP-01-041	-	8-F	26 (IV)	0.09
KP-01-061	-	9-F	308	1.01
FRF-04-063	-	10-F	101	0.23
FRF-04-176	-	8-CN	723	3.59
FRF-04-152	-	9-CN	2480	1.39

We prepared a set of compounds combining small substituents at the aniline 2- and 3-positions with a 4-*N*-methyl piperazine group (Table 7.2). Compared to XMD8-87, the compound which lacked the 2-MeO group, XMD16-47, was more potent, but our archive of kinase selectivity profiling data suggested that compounds of this type would be less selective. Similarly, a 3-MeO group (R<sup>2</sup>) led to enhanced TNK2 potency in both enzyme and cells (BJG-01-149), but reduced selectivity, and we concluded that 2-MeO gave the best balance of potency and kinase selectivity.

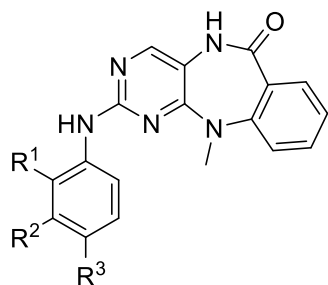
**Table 7.2.** Enzyme and cell data for aniline SAR.

Compound ID	R <sup>1</sup>	R <sup>2</sup>	TNK2 IC50 (nM)	Cell TNK2 D163E (uM)
XMD8-87	OMe	H	44	0.19
XMD16-47	H	H	16 (IV)	0.04
XMD10-32	OEt	H		0.40
BJG-01-194	Me	H	97	0.37
BJG-01-204	Cl	H	63	0.38
BJG-01-149	H	OMe	4	0.012
FRF-04-112	H	OEt	4	0.016
BJG-01-200	H	Me	6	0.05
BJG-01-205	H	Cl	11	0.11

We also prepared a set of structurally diverse cyclic amines at the 4-position, designed to deliver acceptable physical properties (Table 7.3). The 1,4-diamino substitution pattern on a phenyl ring is a perceived risk in terms of formation of a reactive quinone diimine. This concern has been successfully addressed in a number of kinase inhibitors, in which a piperazine substituent at the aniline 4-position has been replaced by a piperidine,<sup>21-23</sup> and in addition to compounds such as XMD16-10, BJG-01-109, SYN-DFCI-00076 and SYN-DFCI-00077, we therefore prepared the piperidines SYN-DFCI-00078 and SYN-DFCI-00079, attached through carbon. Compounds with the 2-MeO substituent and a piperazine or N-linked piperidine at the aniline 4-position typically showed good potency in our cell assay, while the C-linked piperidines were less potent. 3-MeO anilines (SYN-DFCI-238, -239, -240) delivered consistently improved potency in both the enzyme and cell assays, although we assumed that their overall kinase selectivity profiles would resemble that of BJG-01-149. Moving the piperazine substituent to the 3-position (SYN-DFCI-00081) led to a 10-fold reduction in enzyme and cell potency. We also installed a set of bicyclic anilines as an alternative strategy to mitigate potential quinone diimine

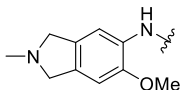
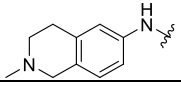
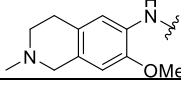
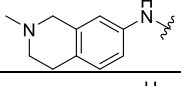
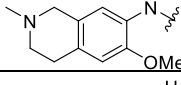
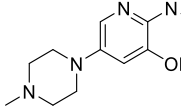
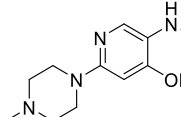
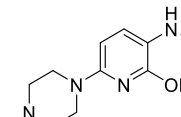
formation, following a similar approach adopted in the development of tetrahydroisoquinoline pyrimidine ALK inhibitors.<sup>24</sup> As with the aniline examples, compounds lacking the 2-MeO group (126, 128, 130) were more potent in the enzyme and cell.

**Table 7.3.** Enzyme and cell data for aniline SAR and aniline replacements.



Compound ID	R <sup>1</sup>	R <sup>2</sup>	R <sup>3</sup> or aniline replacement	TNK2 IC <sub>50</sub> (nM)	Cell TNK2 D163E (μM)
XMD8-87	OMe	H	N-Me piperazine	44	0.19
XMD16-10	OMe	H	4-OH piperidine	37 (IV)	0.14
XMD16-5	H	H	4-OH piperidine	7 (IV)	0.08
BJG-01-109	OMe	H	morpholine	41	0.19
SYN00076	OMe	H		37	0.08
SYN00077	OMe	H		29	0.06
SYN00078	OMe	H		62	0.25
SYN00079	OMe	H		66	0.26
SYN00238	H	OMe		7	0.013
SYN00239	H	OMe		4	0.013
SYN00240	H	OMe		13	0.12
SYN00081	OMe	H		254	1.10
SYN00126	-	-		26	0.26

**Table 7.3 (continued).**

SYN00127	-	-		91	0.94
SYN00128	-	-		18	0.11
SYN00129	-	-		50	0.26
SYN00130	-	-		28	0.12
SYN00131	-	-		140	0.11
SYN00132	-	-		>10uM	>10uM
SYN00180	-	-		152	0.57
SYN00134	-	-		63	0.35

We did not see a good correlation between *in vitro* and *in vivo* PK for this series, with compounds typically showing relatively good stability in mouse microsomes and hepatocytes, and similar *in vitro* data for XMD8-87 and XMD8-85 (Table 7.4). The contrasting PK profiles of XMD8-87 and *N*-methyl analog XMD8-85 suggested that the metabolic liability might derive from the tricyclic core rather than the aniline. However, *in vitro* metabolic identification (met ID) data did not suggest a metabolic pathway directly involving the unsubstituted amide. Instead, an oxidation pathway appeared to be the major metabolic pathway for XMD8-87, with the only significant metabolite having a MW one less than the parent (Figure 7.3). This was also the major metabolite in rat urine in an *in vivo* met ID study, and we speculated that it corresponded to the quinone diimine. Interestingly, despite having low *in vivo* clearance in mice, the *in vitro* met ID data for

XMD8-85 showed a corresponding MW-1 metabolite, but with a reduced rate of conversion (Figure 7.3).

**Table 7.4.** Mouse microsome and hepatocyte stability, and *in vivo* mouse PK data (3 mg/kg IV, 10 mg/kg PO).

Compound ID	Mouse microsomes ( $T_{1/2}$ )	Mouse hepatocytes ( $T_{1/2}$ )	IV Cl (ml/min/kg)	IV $T_{1/2}$ (hr)	F %	Auc inf (ng*hr/ml)
XMD8-87	28	347 mins	150	0.7	5	56
XMD8-85	22	>500	25	4.4	46	2000
SYN00076	139	75	140	2.0	-	-
SYN00077	-	-	130	0.9	11	141
SYN00078	94	64	100	1.7	-	-
SYN00079	-	-	130	1.8	-	-
SYN00129	-	-	120	10	7	125
SYN00131	-	-	86	1.4	22	525

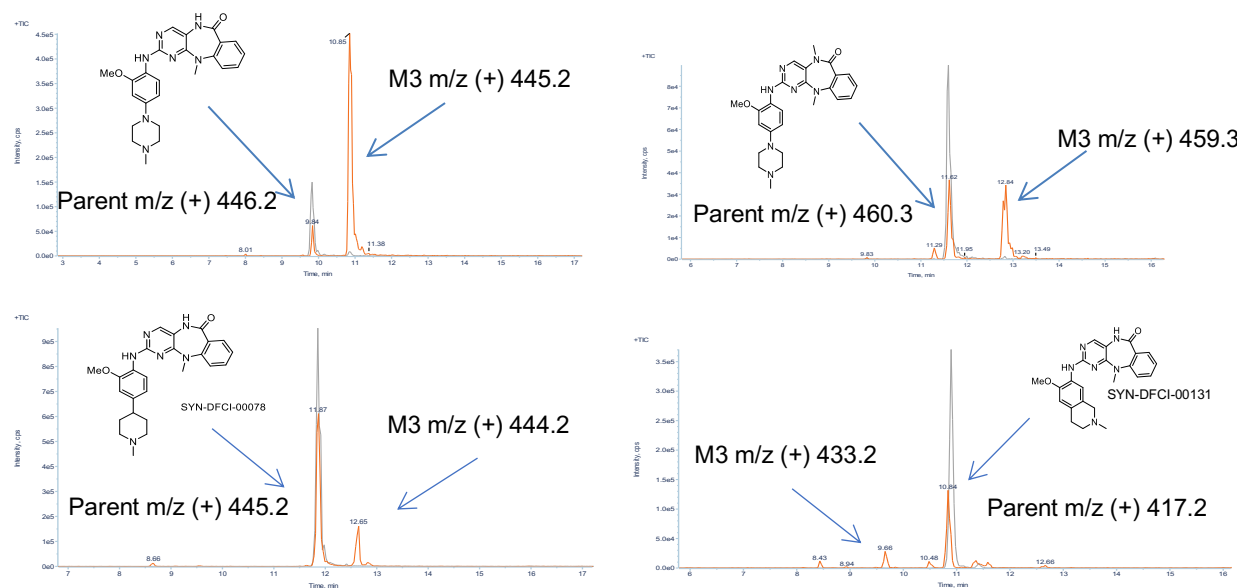


**Figure 7.3.** Metabolite identification after incubation in mouse liver microsomes. (A) XMD8-87 at 0 min (Grey Line) and 60 min (Red Line). (B) XMD8-85 at 0 min (Grey Line) and 60 min (Red Line). (C) SYN-DFCI-00078 at 0 min (Grey Line) and 120 min (Red Line). (D) SYN-DFCI-00131 at 0 min (Grey Line) and 120 min (Red Line).

Examples SYN-DFCI-00076 through -00079 were profiled for IV PK in mice, and we observed similarly high levels of clearance compared to those previously seen for XMD8-87 (Table 7.4). This was particularly disappointing for the piperidine examples, for which an *in vitro* met ID study with SYN-DFCI-00078 showed a greatly reduced rate of conversion to an MW-1 oxidation product (Figure 7.3).

An elegant study evaluating the level of reactive quinone diimine formation in a series of pyrrolotriazine kinase inhibitors used a GSH trapping assay to show that examples containing a 1,4-diamino substituted aniline gave unprecedented levels of GSH adducts.<sup>25</sup> This was mitigated through the replacement of the piperazine substituent with a piperidine.<sup>22</sup> The data suggested that the pyrrolotriazine scaffold greatly increased susceptibility to reactive metabolite formation through interactions with the P450 active site, and it is possible that benzopyrimidodiazepinones with an unsubstituted central ring amide do likewise.

*In vitro* met ID data for one of the bicyclic anilines SYN-DFCI-00131 showed a completely distinct metabolite profile relative to the other compounds, with no evidence of the MW-1 metabolite, mostly parent remaining, and the major metabolite a +16 oxidation product (Figure 7.3). Disappointingly, however, this did not translate into a significantly better *in vivo* result (Table 7.4).

### 7.3 Conclusion

This project was part of a very productive effort to assess SAR around the benzopyrimidodiazepinone kinase inhibitor scaffold where we generated over 350 new compounds and measured their cellular activity against the clinically relevant AML target TNK2 D163E. Although more work must be done in order to optimize this series for *in vivo* efficacy, this study highlights the power of chemical biology for generating large data sets that may allow us to identify lead potential probes and therapeutics.

## 7.4 Experimental Methods

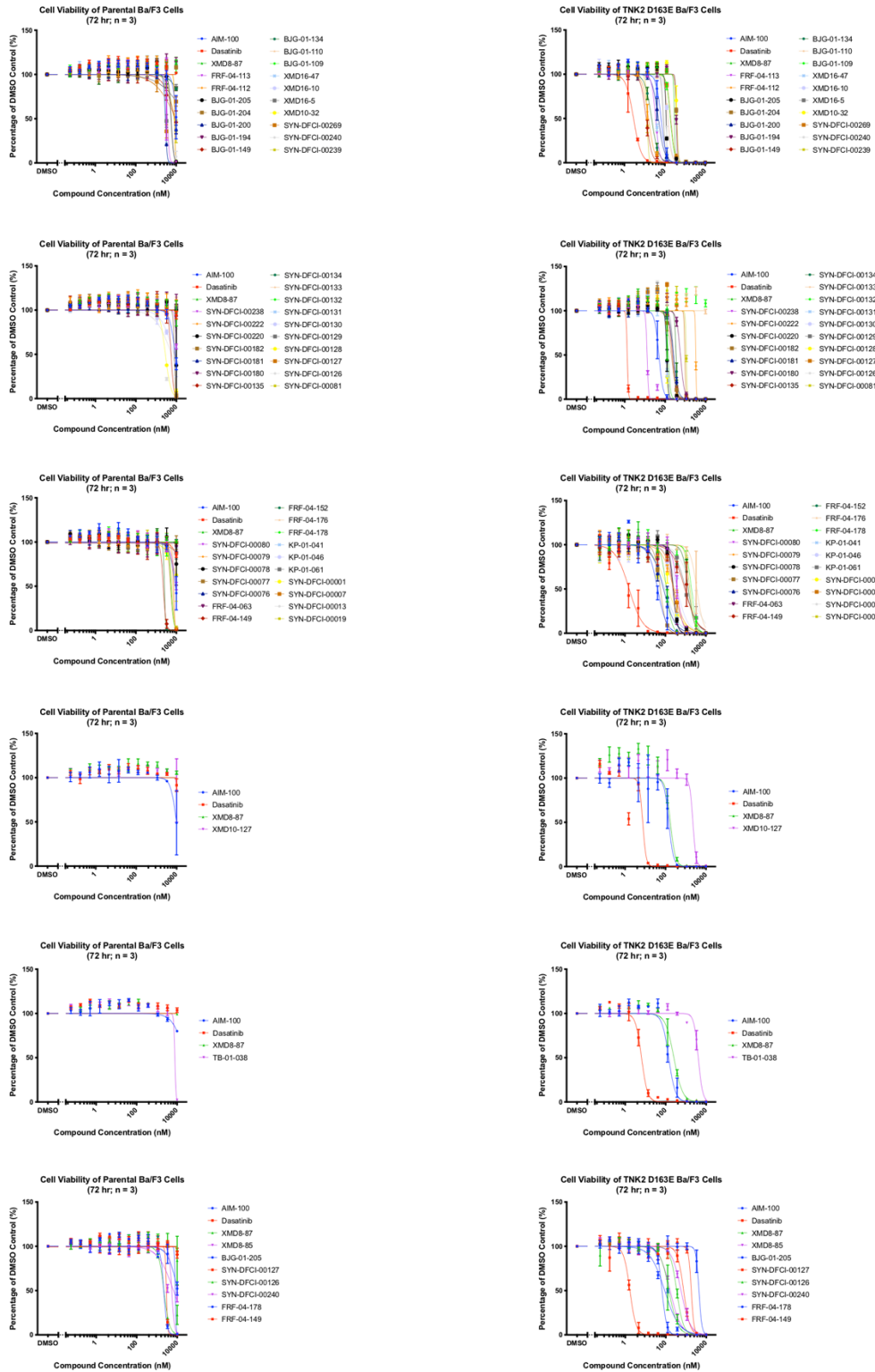


**Figure 7.4.** Antiproliferation  $IC_{50}$  curves  $\pm$  SD after 72 hr treatments (three biological replicates; Graphpad Prism 8 software).

**Table 7.5.** Compound characterization.

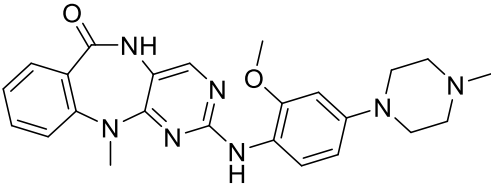
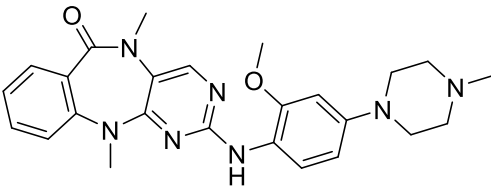
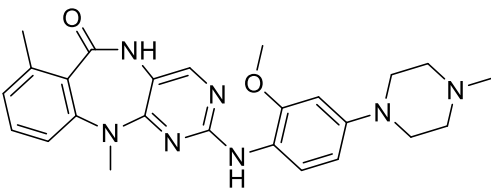
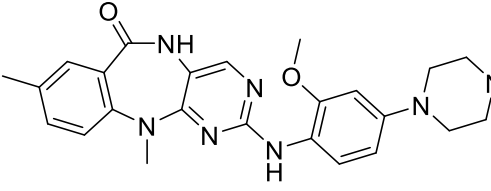
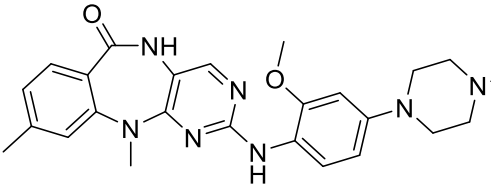
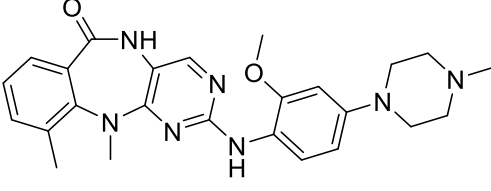
Compound ID	Structure	LCMS (M+H)	<sup>1</sup> H NMR (DMSO unless stated)
XMD8-87		446.3	10.05 (s, 1H) 9.82 (br s, 1H) 7.94 (br s, 1H) 7.93 (s, 1H) 7.84 (d, 1H) 7.71 (dd, 1H) 7.54 (m, 1H) 7.24 (d, 1H) 7.18 (m, 1H) 6.72 (d, 1H) 6.56 (dd, 1H) 3.83 (s, 3H) 3.82 (d, 2H) 3.54 (d, 2H) 3.31 (s, 3H) 3.18 (m, 2H) 2.94 (m, 2H) 2.88 (s, 3H)
XMD8-85		460.4	9.68 (1H, br s) 8.31 (s, 1H) 8.04 (s, 1H) 7.80 (d, 1H) 7.67 (dd, 1H) 7.50 (m, 1H) 7.23 (d, 1H) 7.17 (m, 1H) 6.71 (d, 1H) 6.57 (dd, 1H) 3.84 (d, 2H) 3.82 (s, 3H) 3.53 (d, 2H) 3.38 (s, 3H) 3.28 (s, 3H) 3.17 (m, 2H) 2.94 (m, 2H) 2.88 (d, 3H)
SYN-DFCI-00019		460.2	9.94 (1H, s) 7.91 (s, 1H) 7.78 (d, 1H) 7.74 (s, 1H) 7.31 (m, 1H) 7.08 (d, 1H) 7.02 (d, 1H) 6.61 (s, 1H) 6.47 (d, 1H) 3.80 (s, 3H) 3.24 (s, 3H) 3.10 (m, 4H) 2.45 (m, 4H) 2.35 (s, 3H) 2.22 (s, 3H)
SYN-DFCI-00013		460.2	10.02 (s, 1H) 9.97 (1H, br s) 8.06 (br s, 1H) 7.90 (s, 1H) 7.81 (d, 1H) 7.50 (d, 1H) 7.34 (m, 1H) 7.12 (d, 1H) 6.71 (d, 1H) 6.56 (m, 1H) 3.82 (s, 3H) 3.28 (s, 5H) 3.53 (m, 2H) 3.28 (s, 3H) 3.17 (m, 2H) 2.96 (m, 2H) 2.87 (s, 3H) 2.27 (s, 3H)
SYN-DFCI-00007		460.2	9.91 (1H, s) 7.91 (s, 1H) 7.79 (d, 1H) 7.72 (s, 1H) 7.58 (d, 1H) 7.04 (s, 1H) 6.97 (d, 1H) 6.63 (d, 1H) 6.48 (m, 1H) 3.81 (s, 3H) 3.28 (s, 3H) 3.11 (m, 4H) 2.47 (m, 4H) 2.32 (s, 3H) 2.23 (s, 3H)
SYN-DFCI-00001		460.2	9.99 (1H, s) 7.90 (s, 1H) 7.82 (d, 1H) 7.72 (s, 1H) 7.47 (d, 1H) 7.39 (d, 1H) 7.16 (m, 1H) 6.63 (d, 1H) 6.48 (m, 1H) 3.81 (s, 3H) 3.37 (s, 3H) 3.10 (m, 4H) 2.45 (m, 4H) 2.33 (s, 3H) 2.22 (s, 3H)

Table 7.5 (continued).

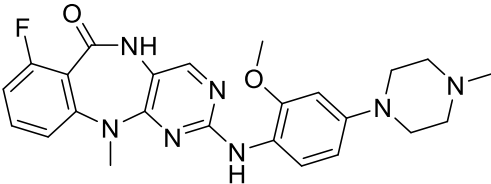
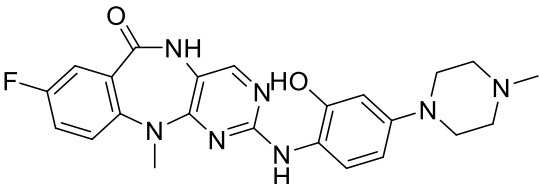
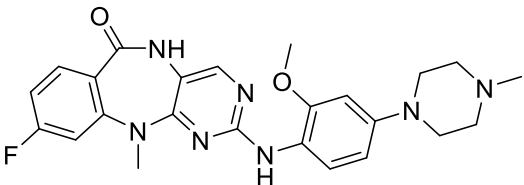
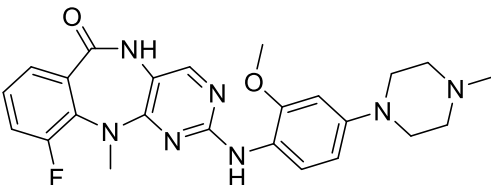
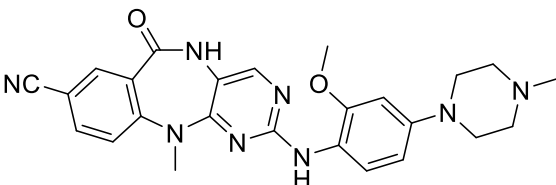
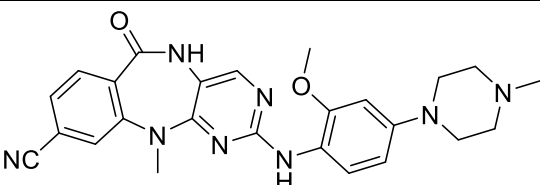
KP-01-046		464.3	10.11 (1H, s) 9.57 (br s, 1H) 7.97 (s, 1H) 7.93 (s, 1H) 7.79 (d, 1H) 7.50 (m, 1H) 7.10 (d, 1H) 7.03 (m, 1H) 6.70 (s, 1H) 6.55 (d, 1H) 3.83 (d, 2H) 3.82 (s, 3H) 3.52 (d, 2H) 3.27 (s, 3H) 3.17 (m, 2H) 2.93 (m, 2H) 2.88 (s, 3H)
KP-01-041		464.3	10.18 (s, 1H) 9.65 (1H, br s) 7.94 (s, 1H) 7.88 (s, 1H) 7.84 (d, 1H) 7.43 (m, 2H) 7.28 (dd, 1H) 6.71 (d, 1H) 6.56 (dd, 1H) 3.83 (s, 3H) 3.82 (d, 2H) 3.53 (d, 2H) 3.29 (s, 3H) 3.18 (m, 2H) 2.93 (m, 2H) 2.88 (d, 3H)
KP-01-061		464.3	10.05 (1H, s) 9.80 (br s, 1H) 7.95 (s, 1H) 7.81 (d, 1H) 7.77 (m, 1H) 7.11 (dd, 1H) 7.02 (m, 1H) 6.71 (d, 1H) 6.55 (dd, 1H) 3.83 (s, 3H) 3.82 (d, 2H) 3.53 (d, 2H) 3.29 (s, 3H) 3.17 (m, 2H) 2.94 (m, 2H) 2.88 (d, 3H)
FRF-04-063		464.2	10.15 (1H, s) 9.75 (br s, 1H) 8.00 (s, 1H) 7.93 (s, 1H) 7.80 (d, 1H) 7.50 (d, 1H) 7.46 (dd, 1H) 7.27 (m, 1H) 6.71 (d, 1H) 6.58 (dd, 1H) 3.85 (d, 2H) 3.83 (d, 3H) 3.52 (d, 2H) 3.42 (s, 3H) 3.18 (m, 2H) 2.95 (m, 2H) 2.88 (s, 3H)
FRF-04-176		471.3	10.27 (1H, s) 9.79 (br s, 1H) 8.06 (d, 1H) 8.01 (s, 1H) 7.99 (s, 1H) 7.97 (dd, 1H) 7.77 (d, 1H) 7.40 (d, 1H) 6.71 (d, 1H) 6.56 (dd, 1H) 3.84 (d, 2H) 3.82 (s, 3H) 3.54 (d, 2H) 3.34 (s, 3H) 3.17 (m, 2H) 2.94 (m, 2H) 2.88 (s, 3H)
FRF-04-152		471.3	10.28 (1H, s) 9.68 (br s, 1H) 7.97 (s, 1H) 7.95 (s, 1H) 7.83 (d, 1H) 7.80 (d, 1H) 7.72 (d, 1H) 7.61 (dd, 1H) 6.71 (d, 1H) 6.56 (dd, 1H) 3.84 (d, 2H) 3.82 (s, 3H) 3.53 (d, 2H) 3.32 (s, 3H) 3.17 (m, 2H) 2.93 (m, 2H) 2.88 (s, 3H)

Table 7.5 (continued).

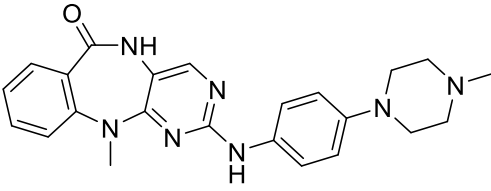
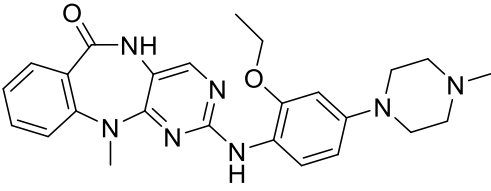
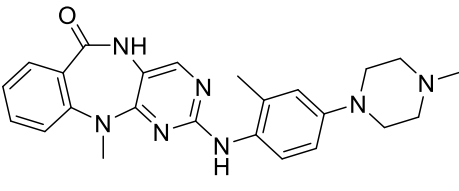
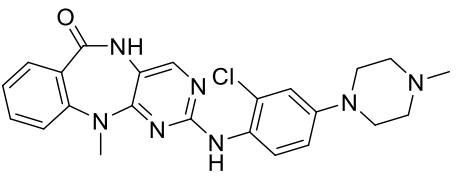
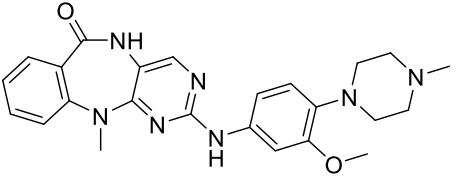
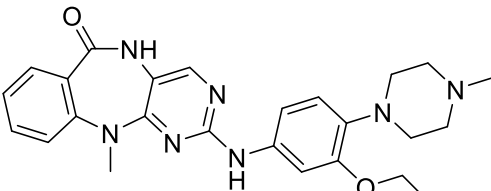
XMD16-47		416.6	10.04 (s, 1H) 9.67 (br s, 1H) 9.33 (s, 1H) 7.97 (s, 1H) 7.71 (d, 1H) 7.62 (d, 2H) 7.54 (m, 1H) 7.25 (d, 1H) 7.18 (m, 1H) 6.96 (d, 2H) 3.74 (d, 2H) 3.52 (d, 2H) 3.35 (s, 3H) 3.18 (dd, 2H) 2.90 (m, 5H) 2.88 (d, 3H)
XMD10-32		460.7	10.06 (s, 1H) 9.74 (br s, 1H) 7.95 (s, 1H) 7.90 (d, 1H) 7.71 (dd, 1H) 7.55 (m, 1H) 7.25 (d, 1H) 7.18 (m, 1H) 6.71 (d, 1H) 6.56 (dd, 1H) 4.10 (q, 2H) 3.81 (d, 2H) 3.53 (d, 2H) 3.31 (s, 3H) 3.17 (m, 2H) 2.93 (m, 2H) 2.88 (d, 3H) 1.33 (t, 3H)
BJG-01-194		430.3	9.98 (s, 1H), 9.75 (br s, 1H), 8.54 (s, 1H), 7.85 (s, 1H), 7.69 (dd, 1H), 7.52 (t, 1H), 7.29 (d, 1H), 7.20 (d, 1H), 7.16 (t, 1H), 6.86 (d, 1H), 6.81 (dd, 1H), 3.79 (d, 2H), 3.52 (d, 2H), 3.23 (s, 3H), 3.16 (q, 2H), 2.92 (t, 2H), 2.87 (d, 3H), 2.16 (s, 3H)
BJG-01-204		450.3	10.01 (s, 1H), 9.76 (br s, 1H), 8.54 (s, 1H), 7.90 (s, 1H), 7.69 (d, 1H), 7.61 – 7.49 (m, 2H), 7.21 (d, 1H), 7.16 (t, 1H), 7.12 (d, 1H), 6.98 (dd, 1H), 3.86 (d, 2H), 3.52 (d, 2H), 3.16 (q, 2H), 2.97 (t, 2H), 2.87 (d, 3H)
BJG-01-149		446.0	10.05 (s, 1H), 9.63 (br s, 1H), 9.39 (s, 1H), 7.99 (s, 1H), 7.71 (dd, 1H), 7.60 – 7.47 (m, 2H), 7.26 (d, 1H), 7.22 (dd, 1H), 7.18 (t, 1H), 6.87 (d, 1H), 3.81 (s, 3H), 3.49 (d, 2H), 3.42 (d, 2H), 3.38 (s, 3H), 3.20 (q, 2H), 2.94 – 2.80 (m, 5H).
FRF-04-112		460.3	10.06 (1H, s) 9.67 (br s, 1H) 9.37 (s, 1H) 7.99 (s, 1H) 7.71 (m, 1H) 7.56 (m, 1H) 7.48 (d, 1H) 7.26 (d, 1H) 7.24 (m, 1H) 7.18 (m, 1H) 6.87 (d, 1H) 4.06 (q, 2H) 3.52 (m, 2H) 3.45 (m, 2H) 3.38 (s, 3H) 3.19 (m, 2H) 2.90 (m, 2H) 2.87 (s, 3H)

Table 7.5 (continued).

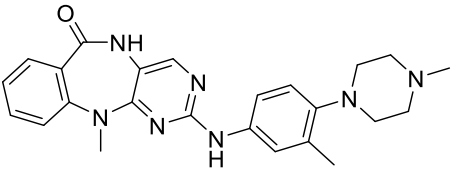
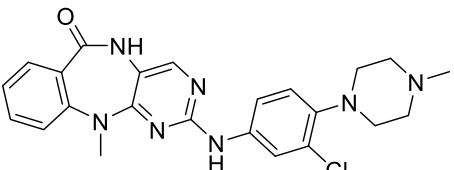
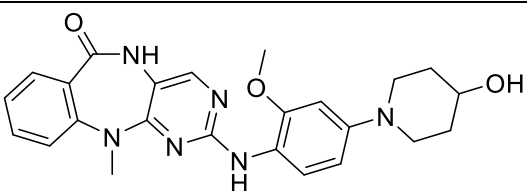
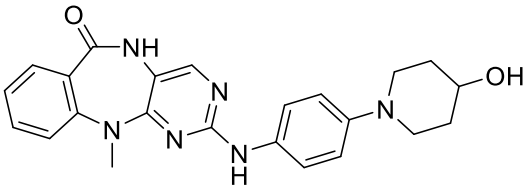
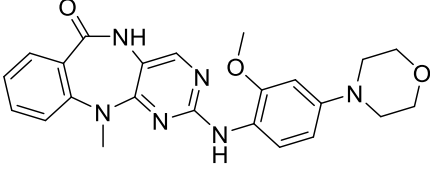
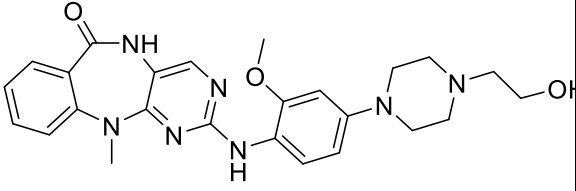
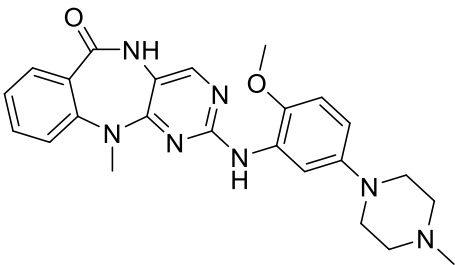
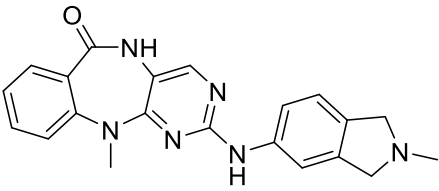
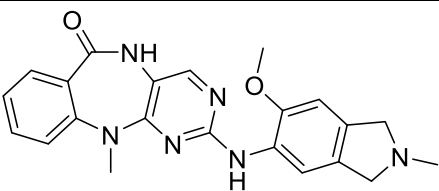
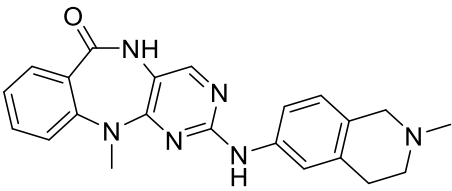
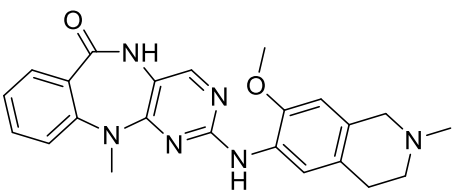
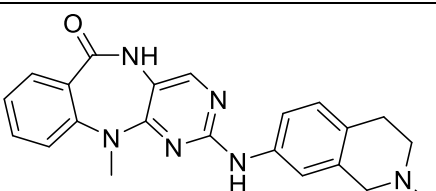
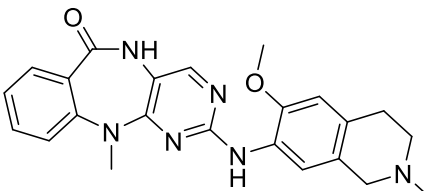
BJG-01-200		430.3	10.05 (s, 1H), 9.65 (br s, 1H), 9.36 (s, 1H), 7.98 (s, 1H), 7.71 (dd, 1H), 7.59 (d, 1H), 7.54 (t, 2H), 7.26 (d, 1H), 7.17 (t, 1H), 7.00 (d, 1H), 3.50 (d, 2H), 3.37 (s, 3H), 3.26 – 3.09 (m, 4H), 2.96 – 2.82 (m, 5H), 2.26 (s, 3H)
BJG-01-205		450.0	10.09 (s, 1H), 9.61 (br s, 2H), 8.02 (s, 1H), 7.99 (d, 1H), 7.71 (dd, 1H), 7.62 (dd, 1H), 7.55 (t, 1H), 7.26 (d, 1H), 7.18 (t, 2H), 3.53 (d, 2H), 3.41 – 3.31 (m, 5H), 3.26 – 3.15 (m, 2H), 2.96 (t, 2H), 2.89 (d, 3H)
XMD16-10		447.3	10.10 (s, 1H) 8.07 (br s, 2H) 7.97 (s, 1H) 7.71 (d, 1H) 7.55 (m, 1H) 7.25 (d, 1H) 7.19 (m, 1H) 7.05 (br s, 1H) 3.88 (s, 3H) 3.84 (m, 2H) 3.60 (br s, 3H) 3.31 (s, 3H) 1.99 (br s, 2H) 1.71 (br s, 2H)
XMD16-5		417.6	10.11 (s, 1H) 9.71 (s, 1H) 8.03 (s, 1H) 7.82 (br s, 2H) 7.72 (dd, 1H) 7.56 (m, 1H) 7.47 (br s, 2H) 7.27 (d, 1H) 7.20 (dd, 1H) 3.88 (m, 2H) 3.58 (m, 3H) 3.38 (s, 3H) 2.01 (br s, 2H) 1.76 (br s, 2H)
BJG-01-109		433.0	10.03 (s, 1H), 8.00 (br s, 1H), 7.91 (s, 1H), 7.77 (d, 1H), 7.70 (dd, 1H), 7.53 (t, 1H), 7.25 (d, 1H), 7.17 (t, 1H), 6.66 (d, 1H), 6.52 (dd, 1H), 3.81 (s, 3H), 3.75 (t, 4H), 3.31 (s, 3H), 3.11 (t, 4H).
SYN-DFCI-00076		476.3	10.01 (1H, s) 7.92 (s, 1H) 7.77 (d, 1H) 7.76 (s, 1H) 7.69 (d, 1H) 7.52 (m, 1H) 7.22 (d, 1H) 7.16 (m, 1H) 6.61 (s, 1H) 6.47 (d, 1H) 4.44 (t, 1H) 3.80 (s, 3H) 3.54 (m, 2H) 3.29 (s, 3H) 3.10 (m, 4H) 2.56 (m, 4H) 2.43 (t, 2H)

Table 7.5 (continued).

SYN-DFCI-00077		460.2	10.00 (1H, s) 7.92 (s, 1H) 7.77 (d, 1H) 7.74 (s, 1H) 7.69 (m, 1H) 7.52 (m, 1H) 7.22 (d, 1H) 7.16 (m, 1H) 6.60 (d, 1H) 6.46 (m, 1H) 3.81 (s, 3H) 3.49 (d, 2H) 3.29 (s, 3H) 2.86 (m, 2H) 2.10 (m, 2H) 1.03 (d, 6H)
SYN-DFCI-00078		445.4	10.07 (1H, s) 8.03 (d, 1H) 7.97 (s, 1H) 7.81 (s, 1H) 7.70 (d, 1H) 7.53 (m, 1H) 7.24 (d, 1H) 7.16 (m, 1H) 6.89 (s, 1H) 6.80 (d, 1H) 3.84 (s, 3H) 3.32 (s, 3H) 2.87 (d, 2H) 2.42 (m, 1H) 2.20 (s, 3H) 1.97 (m, 2H) 1.72 (m, 4H)
SYN-DFCI-00079		475.3	10.07 (1H, s) 8.02 (d, 1H) 7.97 (s, 1H) 7.80 (s, 1H) 7.70 (m, 1H) 7.54 (m, 1H) 7.24 (d, 1H) 7.16 (m, 1H) 6.89 (d, 1H) 6.79 (d, 1H) 4.40 (t, 1H) 3.84 (s, 3H) 3.51 (m, 2H) 3.32 (s, 3H) 2.96 (d, 2H) 2.40 (t, 2H) 2.02 (m, 2H) 1.72 (m, 4H)
SYN-DFCI-00238		476.2	10.02 (1H, s) 9.29 (s, 1H) 7.98 (s, 1H) 7.70 (d, 1H) 7.53 (m, 1H) 7.46 (s, 1H) 7.26 (d, 1H) 7.17 (m, 2H) 6.80 (d, 1H) 4.40 (t, 1H) 3.79 (s, 3H) 3.53 (m, 2H) 3.37 (s, 3H) 2.90 (m, 4H) 2.54 (m, 4H) 2.45 (m, 2H)
SYN-DFCI-00239		460.3	10.03 (1H, s) 9.28 (s, 1H) 7.98 (s, 1H) 7.70 (m, 1H) 7.54 (m, 1H) 7.44 (d, 1H) 7.26 (d, 1H) 7.18 (m, 2H) 6.77 (d, 1H) 3.79 (s, 3H) 3.37 (s, 3H) 3.12 (d, 2H) 2.89 (m, 2H) 2.04 (m, 2H) 0.96 (d, 6H)
SYN-DFCI-00240		445.3	10.07 (1H, s) 9.45 (s, 1H) 8.01 (s, 1H) 7.71 (m, 1H) 7.53 (m, 2H) 7.26 (m, 2H) 7.17 (m, 1H) 7.02 (d, 1H) 3.81 (s, 3H) 3.39 (s, 3H) 3.31 (m, 2H) 2.97 (m, 1H) 2.81 (m, 2H) 2.62 (s, 3H) 1.85 (m, 4H)

Table 7.5 (continued).

SYN-DFCI-00081		446.2	10.11 (1H, s) 8.03 (s, 1H) 7.98 (d, 1H) 7.80 (s, 1H) 7.73 (d, 1H) 7.56 (m, 1H) 7.28 (d, 1H) 7.20 (m, 1H) 6.91 (d, 1H) 6.55 (d, 1H) 3.81 (s, 3H) 3.39 (s, 3H) 3.08 (m, 4H) 2.49 (m, 4H) 2.25 (s, 3H)
SYN-DFCI-00126		373.2	10.05 (1H, s) 9.42 (s, 1H) 7.99 (s, 1H) 7.70 (d, 1H) 7.66 (s, 1H) 7.53 (m, 1H) 7.47 (d, 1H) 7.25 (d, 1H) 7.17 (m, 1H) 7.10 (d, 1H) 3.79 (s, 2H) 3.75 (s, 2H) 3.35 (s, 3H) 2.47 (s, 3H)
SYN-DFCI-00127		403.1	CDCl <sub>3</sub> 8.62 (br s, 1H) 8.26 (s, 1H) 7.93 (s, 1H) 7.90 (d, 1H) 7.59 (s, 1H) 7.47 (m, 1H) 7.11 (m, 2H) 6.74 (s, 1H) 3.92 (d, 4H) 3.88 (s, 3H) 3.41 (s, 3H) 2.62 (s, 3H)
SYN-DFCI-00128		387.3	10.09 (1H, s) 9.48 (s, 1H) 8.01 (s, 1H) 7.70 (m, 1H) 7.66 (s, 1H) 7.54 (m, 1H) 7.49 (m, 1H) 7.26 (d, 1H) 7.17 (m, 1H) 7.02 (d, 1H) 3.95 (br s, 2H) 3.34 (s, 3H) 3.12 (m, 2H) 2.99 (m, 2H) 2.67 (s, 3H)
SYN-DFCI-00129		417.2	10.12 (1H, s) 8.07 (s, 1H) 8.01 (s, 1H) 7.88 (s, 1H) 7.71 (d, 1H) 7.54 (m, 1H) 7.26 (d, 1H) 7.18 (m, 1H) 6.82 (s, 1H) 4.11 (br s, 2H) 3.83 (s, 3H) 3.33 (s, 3H) 3.29 (m, 2H) 3.01 (m, 2H) 2.78 (s, 3H)
SYN-DFCI-00130		387.1	10.04 (1H, s) 9.35 (s, 1H) 7.99 (s, 1H) 7.71 (m, 1H) 7.55 (m, 2H) 7.39 (m, 1H) 7.25 (d, 1H) 7.17 (m, 1H) 6.99 (d, 1H) 3.47 (s, 2H) 3.36 (s, 3H) 2.75 (m, 2H) 2.58 (m, 2H) 2.34 (s, 3H)
SYN-DFCI-00131		417.3	10.06 (1H, s) 7.98 (s, 1H) 7.87 (s, 1H) 7.78 (s, 1H) 7.70 (m, 1H) 7.53 (m, 1H) 7.26 (d, 1H) 7.17 (d, 1H) 6.74 (s, 1H) 3.80 (s, 3H) 3.43 (s, 2H) 3.34 (s, 3H) 2.78 (m, 2H) 2.57 (m, 2H) 2.33 (s, 3H)

**Table 7.5 (continued).**

SYN-DFCI-00132		447.2	9.95 (1H, s) 8.65 (s, 1H) 7.85 (s, 1H) 7.68 (m, 1H) 7.60 (d, 1H) 7.50 (m, 1H) 7.16 (m, 2H) 7.03 (d, 1H) 3.73 (s, 3H) 3.35 (s, 3H) 3.16 (s, 3H) 2.67 (m, 4H) 2.39 (m, 4H)
SYN-DFCI-00180		447.3	9.96 (1H, s) 8.17 (s, 1H) 8.00 (s, 1H) 7.87 (s, 1H) 7.68 (d, 1H) 7.51 (m, 1H) 7.21 (d, 1H) 7.15 (m, 1H) 6.42 (s, 1H) 3.80 (s, 3H) 3.47 (m, 4H) 3.23 (s, 3H) 2.44 (m, 4H) 2.25 (s, 3H)
SYN-DFCI-00134		447.3	9.98 (1H, s) 7.91 (d, 1H) 7.89 (s, 1H) 7.83 (d, 1H) 7.68 (d, 1H) 7.51 (m, 1H) 7.20 (d, 1H) 7.15 (m, 1H) 6.33 (d, 1H) 3.81 (s, 3H) 3.44 (m, 4H) 3.24 (s, 3H) 2.50 (m, 4H) 2.29 (s, 3H)

**Cell Culture.** Ba/F3 cells expressing TNK2 D163E were generously provided by Jeffrey W. Tyner (Oregon Health and Science University, Portland, OR). Ba/F3 cell lines were cultured in RPMI-1640 media containing L-glutamine, supplemented with 10% fetal bovine serum (FBS) and 1% penicillin/streptomycin. Parental Ba/F3 cells were cultured with an additional 1 ng/mL recombinant mouse IL-3 (Prospec). Mycoplasma testing was performed on a monthly basis and all lines were negative.

**Cell Viability Assays.** Cells were plated at a volume of 50  $\mu$ L with a density of  $10^5$  cells/mL in white 384-well plates (Corning 3570). 100 nL of compound in DMSO from stock plates was added by pin transfer using a Janus Workstation (PerkinElmer). After 72 hr, cell viability was evaluated using the CellTiter-Glo Luminescent Cell Viability Assay (Promega) following the manufacturer's standards. IC<sub>50</sub>s were modeled from 3 biological replicates using GraphPad Prism 8 software.

## **Acknowledgements**

In vitro and in vivo PK studies were conducted at BioDuro, Shanghai, under the supervision of Cindy Liang and Ying Zhou.

## **Author Contributions**

B.J.G. led design of compounds. C.E.P designed and ran the proliferation assay, and analyzed the data. F.F., T.W.G., Z.L., and K.P further designed and synthesized compounds. D.A.S. and N.S.G advised on project directions. B.J.G., C.E.P.. and D.A.S. wrote the paper.

## **Notes**

The authors declare no competing financial interest.

## References

- (1) Groendyke, B. J.; Powell, C. E.; Feru, F.; Gero, T. W.; Li, Z.; Szabo, H.; Pang, K.; Feutrell, J.; Chen, B.; Li, B.; et al. Benzopyrimidodiazepinone Inhibitors of TNK2. *Bioorg Med Chem Lett* **2020**, 126948. <https://doi.org/10.1016/j.bmcl.2020.126948> .
- (2) Fan, F.; He, Z.; Kong, L.-L.; Chen, Q.; Yuan, Q.; Zhang, S.; Ye, J.; Liu, H.; Sun, X.; Geng, J.; et al. Pharmacological Targeting of Kinases MST1 and MST2 Augments Tissue Repair and Regeneration. *Sci Transl Med* **2016**, 8 (352), 352ra108-352ra108. <https://doi.org/10.1126/scitranslmed.aaf2304> .
- (3) Ferguson, F. M.; Ni, J.; Zhang, T.; Tesar, B.; Sim, T.; Kim, N.; Deng, X.; Brown, J. R.; Zhao, J. J.; Gray, N. S. Discovery of a Series of 5,11-Dihydro-6 H -Benzo[ e ]Pyrimido[5,4- b ][1,4]Diazepin-6-Ones as Selective PI3K- $\delta/\gamma$  Inhibitors. *Acs Med Chem Lett* **2016**, 7 (10), 908–912. <https://doi.org/10.1021/acsmchemlett.6b00209> .
- (4) Banerjee, S.; Buhrlage, S. J.; Huang, H.-T.; Deng, X.; Zhou, W.; Wang, J.; Traynor, R.; Prescott, A. R.; Alessi, D. R.; Gray, N. S. Characterization of WZ4003 and HTH-01-015 as Selective Inhibitors of the LKB1-Tumour-Suppressor-Activated NIAK Kinases. *Biochem J* **2014**, 457 (1), 215–225. <https://doi.org/10.1042/bj20131152> .
- (5) Maxson, J.; Abel, M.; Wang, J.; Deng, X.; Reckel, S.; Luty, S.; Sun, H.; Gorenstein, J.; Hughes, S.; Bottomly, D.; et al. Identification and Characterization of Tyrosine Kinase Nonreceptor 2 Mutations in Leukemia through Integration of Kinase Inhibitor Screening and Genomic Analysis. *Cancer Res* **1AD**, 76 (1), 127–138. <https://doi.org/10.1158/0008-5472.can-15-0817> .
- (6) Deng, X.; Yang, Q.; Kwiatkowski, N.; Sim, T.; rmott, U.; Settleman, J. E.; Lee, J.-D.; Gray, N. S. Discovery of a Benzo[e]Pyrimido-[5,4-b][1,4]Diazepin-6(11H)-One as a Potent and Selective Inhibitor of Big MAP Kinase 1. *Acs Med Chem Lett* **2011**, 2 (3), 195–200. <https://doi.org/10.1021/ml100304b> .
- (7) Deng, X.; Elkins, J. M.; Zhang, J.; Yang, Q.; Erazo, T.; Gomez, N.; Choi, H.; Wang, J.; Dzamko, N.; Lee, J.-D.; et al. Structural Determinants for ERK5 (MAPK7) and Leucine Rich Repeat Kinase 2 Activities of Benzo[e]Pyrimido-[5,4-b]Diazepine-6(11H)-Ones. *Eur J Med Chem* **2013**, 70 (Physiol. Rev. 79 1999), 758–767. <https://doi.org/10.1016/j.ejmech.2013.10.052> .
- (8) Deng, X.; Dzamko, N.; Prescott, A.; Davies, P.; Liu, Q.; Yang, Q.; Lee, J.-D.; Patricelli, M. P.; Nomanbhoy, T. K.; Alessi, D. R.; et al. Characterization of a Selective Inhibitor of the Parkinson's Disease Kinase LRRK2. *Nat Chem Biol* **2011**, 7 (4), 203. <https://doi.org/10.1038/nchembio.538> .
- (9) Finlay, R. M.; Anderton, M.; Ashton, S.; Ballard, P.; Bethel, P. A.; Box, M. R.; Bradbury, R. H.; Brown, S. J.; Butterworth, S.; Campbell, A.; et al. Discovery of a Potent and Selective EGFR Inhibitor (AZD9291) of Both Sensitizing and T790M Resistance Mutations That Spares the Wild Type Form of the Receptor. *J Med Chem* **2014**, 57 (20), 8249–8267. <https://doi.org/10.1021/jm500973a> .

- (10) Galkin, A. V.; Melnick, J. S.; Kim, S.; Hood, T. L.; Li, N.; Li, L.; Xia, G.; Steensma, R.; Chopiuk, G.; Jiang, J.; et al. Identification of NVP-TAE684, a Potent, Selective, and Efficacious Inhibitor of NPM-ALK. *PNAS* **2006**, *104* (1), 270–275.
- (11) Huang, W.-S.; Liu, S.; Zou, D.; Thomas, M.; Wang, Y.; Zhou, T.; Romero, J.; Kohlmann, A.; Li, F.; Qi, J.; et al. Discovery of Brigatinib (AP26113), a Phosphine Oxide-Containing, Potent, Orally Active Inhibitor of Anaplastic Lymphoma Kinase. *J Med Chem* **2016**, *59* (10), 4948–4964. <https://doi.org/10.1021/acs.jmedchem.6b00306> .
- (12) Rudolph, D.; Steegmaier, M.; Hoffmann, M.; Grauert, M.; Baum, A.; Quant, J.; Haslinger, C.; Garin-Chesa, P.; Adolf, G. R. BI 6727, A Polo-like Kinase Inhibitor with Improved Pharmacokinetic Profile and Broad Antitumor Activity. *Clin Cancer Res* **2009**, *15* (9), 3094–3102. <https://doi.org/10.1158/1078-0432.ccr-08-2445> .
- (13) Manser, E.; Leung, T.; Salihuddin, H.; Tan, L.; Lim, L. A Non-Receptor Tyrosine Kinase That Inhibits the GTPase Activity of P21cdc42. *Nature* **1993**, *363* (6427), 364–367–367. <https://doi.org/10.1038/363364a0> .
- (14) Modzelewska, K.; Newman, L. P.; Desai, R.; Keely, P. J. Ack1 Mediates Cdc42-Dependent Cell Migration and Signaling to P130Cas. *J Biol Chem* **2006**, *281* (49), 37527–37535–37535. <https://doi.org/10.1074/jbc.m604342200> .
- (15) van der Horst, E.; Degenhardt, Y. Y.; Strelow, A.; Slavin, A.; Chinn, L.; Orf, J.; Rong, M.; Li, S.; See, L.-H.; Nguyen, K. Q.; et al. Metastatic Properties and Genomic Amplification of the Tyrosine Kinase Gene ACK1. *P Natl Acad Sci Usa* **2005**, *102* (44), 15901–15906–15906. <https://doi.org/10.1073/pnas.0508014102> .
- (16) Jin, M.; Wang, J.; Kleinberg, A.; Kadalbajoo, M.; Siu, K. W.; Cooke, A.; Bittner, M. A.; Yao, Y.; Thelemann, A.; Ji, Q.; et al. Discovery of Potent, Selective and Orally Bioavailable Imidazo[1,5-a]Pyrazine Derived ACK1 Inhibitors. *Bioorg Med Chem Lett* **2013**, *23* (4), 979–984. <https://doi.org/10.1016/j.bmcl.2012.12.042> .
- (17) Kopecky, D. J.; Hao, X.; Chen, Y.; Fu, J.; Jiao, X.; Jaen, J. C.; Cardozo, M. G.; Liu, J.; Wang, Z.; Walker, N.; et al. Identification and Optimization of N3,N6-Diaryl-1H-Pyrazolo[3,4-d]Pyrimidine-3,6-Diamines as a Novel Class of ACK1 Inhibitors. *Bioorg Med Chem Lett* **2008**, *18* (24), 6352–6356. <https://doi.org/10.1016/j.bmcl.2008.10.092> .
- (18) Jiao, X.; Kopecky, D. J.; Liu, J.; Liu, J.; Jaen, J. C.; Cardozo, M. G.; Sharma, R.; Walker, N.; Wesche, H.; Li, S.; et al. Synthesis and Optimization of Substituted Furo[2,3-d]-Pyrimidin-4-Amines and 7H-Pyrrolo[2,3-d]Pyrimidin-4-Amines as ACK1 Inhibitors. *Bioorg Med Chem Lett* **2012**, *22* (19), 6212–6217. <https://doi.org/10.1016/j.bmcl.2012.08.020> .
- (19) Lawrence, H. R.; Mahajan, K.; Luo, Y.; Zhang, D.; Tindall, N.; Huseyin, M.; Gevariya, H.; Kazi, S.; Ozcan, S.; Mahajan, N. P.; et al. Development of Novel ACK1/TNK2 Inhibitors Using a Fragment-Based Approach. *J Med Chem* **2015**, *58* (6), 2746–2763. <https://doi.org/10.1021/jm501929n> .
- (20) Miduturu, C. V.; Deng, X.; Kwiatkowski, N.; Yang, W.; Brault, L.; Filippakopoulos, P.; Chung, E.; Yang, Q.; Schwaller, J.; Knapp, S.; et al. High-Throughput Kinase Profiling: A More Efficient Approach toward the Discovery of New Kinase Inhibitors. *Chem Biol* **2011**, *18* (7), 868–879. <https://doi.org/10.1016/j.chembiol.2011.05.010> .

- (21) Marsilje, T.; Pei, W.; Chen, B.; Lu, W.; Uno, T.; Jin, Y.; Jiang, T.; Kim, S.; Li, N.; Warmuth, M.; et al. Synthesis, Structure-Activity Relationships, and in Vivo Efficacy of the Novel Potent and Selective Anaplastic Lymphoma Kinase (ALK) Inhibitor 5-Chloro-N2-(2-Isopropoxy-5-Methyl-4-(Piperidin-4-Yl)Phenyl)-N4-(2-(Isopropylsulf Onyl)Phenyl)Pyrimidine-2,4-Diamine (LDK378) Currently in Phase 1 and Phase 2 Clinical Trials. *J Med Chem* **2025**, *56* (14), 5675–5690. <https://doi.org/10.1021/jm400402q> .
- (22) Mesaros, E. F.; Thieu, T. V.; Wells, G. J.; Zifcsak, C. A.; Wagner, J. C.; Breslin, H. J.; Tripathy, R.; Diebold, J. L.; McHugh, R. J.; Wohler, A. T.; et al. Strategies to Mitigate the Bioactivation of 2-Anilino-7-Aryl-Pyrrolo[2,1-f][1,2,4]Triazines: Identification of Orally Bioavailable, Efficacious ALK Inhibitors. *J Med Chem* **2012**, *55* (1), 115–125. <https://doi.org/10.1021/jm2010767> .
- (23) Weinberg, L. R.; Albom, M. S.; Angeles, T. S.; Breslin, H. J.; Gingrich, D. E.; Huang, Z.; Lisko, J. G.; Mason, J. L.; Milkiewicz, K. L.; Thieu, T. V.; et al. 2,7-Pyrrolo[2,1-f][1,2,4]Triazines as JAK2 Inhibitors: Modification of Target Structure to Minimize Reactive Metabolite Formation. *Bioorg Med Chem Lett* **2011**, *21* (24), 7325–7330. <https://doi.org/10.1016/j.bmcl.2011.10.032> .
- (24) Achary, R.; Yun, J.; Park, C.; Mathi, G.; Lee, J.; Ha, J.; Chae, C.; Ahn, S.; Park, C.; Lee, C.; et al. Discovery of Novel Tetrahydroisoquinoline-Containing Pyrimidines as ALK Inhibitors. *Bioorgan Med Chem* **2016**, *24* (2), 207–219. <https://doi.org/10.1016/j.bmc.2015.12.004> .
- (25) Wells-Knecht, K. J.; Ott, G. R.; Cheng, M.; Wells, G. J.; Breslin, H. J.; Gingrich, D. E.; Weinberg, L.; Mesaros, E. F.; Huang, Z.; Yazdanian, M.; et al. 2,7-Disubstituted-Pyrrolotriazine Kinase Inhibitors with an Unusually High Degree of Reactive Metabolite Formation. *Chem Res Toxicol* **2011**, *24* (11), 1994–2003. <https://doi.org/10.1021/tx200304r> .

## **Chapter 8: Conclusions and Future Directions**

All of the projects described in this work illustrate the power and versatility of the chemical biologist's toolbox. Combined these projects detail the use of small molecule inhibitors, degraders, and modulators for probing biology and developing lead therapeutic compounds.

**Chapter 2** described the development of the first small molecule degraders of ALK, TL13-12 and TL13-112. These compounds displayed the ability to improve upon the pharmacodynamic properties of their parental inhibitors, especially sustained inhibition of downstream ALK signaling, indicating that degraders are a promising new avenue for targeted ALK therapies. Initial efforts to optimize the potency and selectivity of the lead ALK degraders by basing new degrader compounds on more selective ALK inhibitors, alectinib and JH-VIII-157-02, showed a decrease in ALK degrader potency from the TL13-12 and TL13-112, which were based on the less selective ALK inhibitors TAE684 and LDK378 (ceritinib), respectively. We hypothesize that the strong binding of alectinib and JH-VIII-157-02 to ALK may be preventing compound turnover, resulting in the lower degradation activity. Future studies may benefit from examining the structure-activity relationships around ALK inhibitor warhead binding affinity and ALK degradation. Additionally, although we demonstrated that TL13-12 and TL13-112 had high plasma exposure after IP dosing, with TL13-112 also showing modest oral bioavailability, we have not examined the PD properties of ALK degraders. Future studies should aim to develop a lead ALK degrader for *in vivo* studies that may be used in H3122 xenograft mice. This will help clarify the relationships between the observed *in vitro* characteristics and downstream *in vivo* efficacy, allowing for the development of a lead ALK degrader as a potential therapeutic compound.

**Chapter 3** outlined a screening strategy for identifying potential allosteric ALK inhibitors and demonstrated that we have successfully identified a lead potential allosteric inhibitor. Structural biology efforts are ongoing to validate this compound's mechanism of action. The profiling of this lead allosteric ALK inhibitor is promising and indicates that further screening should be done to target the proposed allosteric pocket adjacent to the ATP binding site. Further screening could involve using the same strategy described here (ALK activity assay run at a high

ATP concentration) against a larger library, or could use an alternative strategy such as a fragment-based screen that focused on allosteric kinase inhibitor like moieties.

**Chapter 4** described the generation of a thalidomide analog library by introducing kinase inhibitor scaffolds to lenalidomide, and the use of a CRBN-dependent antiproliferative screen in order to identify novel CRBN modulators. This screening strategy successfully identified 5 novel CRBN modulators: ZXH-1-084, ZXH-1-161, ZXH-1-167, ZXH-2-160, and ZXH-2-164. These compounds were shown to selectively induce GSPT1 degradation, a previously identified CRBN modulator target that may play a clinical role in acute myeloid leukemia (AML). Molecular modeling allowed for the identification of a nitrogen in the pyrimidine ring of these compounds that confers their GSPT1 activity, and that may help explain their selectivity. Since GSPT1 degradation appears to be highly cytotoxic, it is possible that future screening strategies that use readouts other than antiproliferative activity may identify additional novel functions from this compound library.

**Chapter 5** examined the use of recruiting the CRBN E3 ligase versus the VHL E3 ligase for chemically inducing CRBN degradation. This demonstrated that CRBN-VHL based degraders are much more potent and selective for CRBN degradation than CRBN-CRBN based degraders. This is likely because as CRBN is degraded by a CRBN-CRBN degrader, it reaches a point where the amount of CRBN is lowered to a level where all of the remaining CRBN can be occupied by one end of a degrader compound. In a sense this is a reverse hook effect, where instead of reaching a high dose that leads to complete occupation, protein levels are lowered until complete occupation. This prevents CRBN from being completely degraded by CRBN-CRBN degraders. By recruiting two different E3 ligases we may therefore reach a more complete level of CRBN degradation. From the CRBN-VHL degraders we presented two lead highly selective and potent CRBN degraders, ZXH-4-130 and ZXH-4-137, that may be used as probes for studying CRBN biology. By chemically inducing selective CRBN degradation, these compounds may help validate proposed endogenous CRBN functions in the literature, such as metabolic regulation and

protection against DNA-damage induced apoptosis. Future studies may also potentially use these compounds to discover some novel endogenous function of CRBN.

**Chapter 6** presented the discovery of the first macrocyclic inhibitors of DYRK1A. Macrocyclic compounds are exciting inhibitor scaffolds because they can provide diverse functionality and stereochemical complexity while maintaining a specific conformation. Macrocyclic structures are also associated with improved metabolic stability and blood-brain barrier penetration, a feature that may be of particular use against DYRK1A as it has been shown to play a role in numerous neurological diseases, including Down syndrome, Alzheimer's disease, Parkinson's disease, Huntington's disease, and Pick syndrome. Our lead macrocyclic inhibitor, JH-XIV-68-3, was highly selective for DYRK1A in cellular kinase profiling. This is a potential improvement on current DYRK1A inhibitors, which are notorious for having multiple targets and often have been developed with a primary target that is not DYRK1A. JH-XIV-68-3 also displayed antitumor activity in HNSCC cells, one of the many potential therapeutic applications for DYRK1A inhibition. This indicated that JH-XIV-68-3 may provide a new scaffold for studying DYRK1A biology and developing lead therapeutic compounds.

**Chapter 7** described medicinal chemistry efforts to optimize benzopyrimidodiazepinone inhibitors of TNK2, a potential therapeutic target in AML. Although more work is needed to optimize this series for *in vivo* efficacy, this work does highlight the use of high-throughput chemical biology for exploring structure-activity relationships and developing lead therapeutic compounds.

Overall, this thesis work speaks to the great potential at the intersection of chemistry and biology. Not only have the chemical tools presented here allowed us to modulate biology in order to better understand the nuances of protein functions, they have brought us closer to new therapies for several disease indications, which may in the future have a meaningful impact on how these diseases are treated and managed.